

NATIONAL AERONAUTICS AND SPACE ADMINISTRATION

Technical Memorandum 33-473

*Measured Performance of Silicon Solar Cell
Assemblies Designed for Use at
High Solar Intensities*

Ronald G. Ross, Jr.

Robert K. Yasui

Wiktor Jaworski

Liang-Chi Wen

Edward L. Cleland

FACILITY FORM 602	N71 23780 (ACCESSION NUMBER)	21 (PAGES)	03 (THRU)
	CR-118016 (NASA CR OR TMX OR AD NUMBER)		03 (CODE)
			03 (CATEGORY)

JET PROPULSION LABORATORY
CALIFORNIA INSTITUTE OF TECHNOLOGY
PASADENA, CALIFORNIA

PRICES SUBJECT TO CHANGE

March 15, 1971



NATIONAL AERONAUTICS AND SPACE ADMINISTRATION

Technical Memorandum 33-473

*Measured Performance of Silicon Solar Cell
Assemblies Designed for Use at
High Solar Intensities*

Ronald G. Ross, Jr.

Robert K. Yasui

Wiktor Jaworski

Liang-Chi Wen

Edward L. Cleland

JET PROPULSION LABORATORY
CALIFORNIA INSTITUTE OF TECHNOLOGY
PASADENA, CALIFORNIA

March 15, 1971

Prepared Under Contract No NAS 7-100
National Aeronautics and Space Administration

PREFACE

The work described in this report was performed by the Engineering Mechanics and Guidance and Control Divisions of the Jet Propulsion Laboratory.

CONTENTS

I	Introduction	1
II	Program Definition	2
	A Thermal Control Approaches Considered	2
	B Program Scope	3
III	Solar Cell/Coverglass Configurations Studied	5
	A Standard Production Cells	5
	B Wide-Grid Cells	6
	C Standard Blue and Blue-Red Filters	6
	D Selective Bandpass Filters	6
	E Partially Mirrored Covers	7
IV	Solar Cell Electrical Performance at High Intensities and Temperatures	10
	A Objective	10
	B Experimental Procedure	10
	C Experimental Results and Discussion	11
V	Solar Cell Electrical Performance as Angle of Illumination Changes	113
	A Introduction	113
	B Experimental Procedure	113
	C Data Analysis	114
VI	Solar Cell/Coverglass Thermal Radiation Properties	116
	A Objective	116
	B Experimental Approach	116
	C Experimental Results and Discussion	116
VII	Solar Cell Module Thermal Radiation Properties	125
	A Objective	125
	B Experimental Approach	125
	C Test Apparatus	126
	D System Calibration	127

PRECEDING PAGE BLANK NOT FILMED

CONTENTS (contd)

1.	Calibration of test module temperature measurements	127
2.	Calibration for conductive heat loss	127
3.	Calibration of the solar simulator	127
4.	Calibration of painted surfaces	127
E.	Experimental Procedure	128
F.	Experimental Results and Discussion	128
1.	Emittance measurements	128
2.	Apparent absorptance of contact and intercell space areas	129
3.	Solar absorptance measurements	129
VIII.	Irradiation Effects on Solar Cell Stack Thermo-optical Properties	135
A.	Objective	135
B.	Experimental Approach	135
1.	500-h evaluation test	135
2.	2400-h mission simulation test	135
C.	Test Apparatus	136
D.	Presentation of Results	136
E.	Analysis and Discussion	137
IX.	Solar Cell Adhesive Properties	167
A.	Objective	167
B.	Selected Adhesives	167
C.	Experimental Procedures	167
1.	Lap shear tests	167
2.	Weight-loss and volatile condensable matter tests	168
D.	Experimental Results and Discussion	168
1.	Filter cover adhesives	168
2.	Solar cell to substrate adhesives	168
X.	Performance Comparisons	173
A.	Variable Angle of Incidence Designs	173
B.	Mirror Mosaic Approaches	174
C.	Selective Bandpass Filter Designs	174
References		179
Appendix A. Solar Cell Specifications		181
Appendix B. Solar Cell Electrical Properties Data		187

ABSTRACT

This report presents the results of an experimental program undertaken to evaluate the performance of three solar panel design approaches suitable for use at high solar intensities: the second-surface mirror mosaic approach, the selective bandpass filter approach, and the tilted panel approach. Extensive data are presented on the thermal and electrical characteristics of a number of specific cell/coverglass assemblies representative of these approaches. Included are data on electrical performance at intensities from 1 to 6 suns, data on thermal optical properties both before and after long term-UV and proton radiation exposure, and data on the thermal-mechanical properties of a number of solar cell adhesives.

Solar cell arrays which convert a portion of the incoming solar radiation into electrical power are used to satisfy the power requirements of most interplanetary spacecraft. Because solar cell conversion efficiency and panel structural reliability both decrease rapidly with increasing temperature, solar arrays for use on near-sun missions must be provided with a means for controlling panel temperature. Candidate approaches include decreasing the effective absorptance of the panel front surface through the use of highly reflective coverglasses, tilting the panel surface with respect to the sun axis to decrease the effective intensity, and spinning the panels to decrease the total solar exposure.

The program described in this report was initiated in December 1968 to establish several solar panel approaches suitable for use on the proposed 1973 Venus-Mercury flyby mission and to provide technology readiness with respect to one or more preferred designs. Because of the short time available, the study was limited to designs which represented a minimum deviation from current Mariner solar panel technology. This restriction ruled out the consideration of high-temperature photovoltaics, spinning cylindrical or conical panels, and other approaches requiring a considerable development effort.

Instead, emphasis was placed entirely on flat fold-out panels utilizing either a highly reflective surface or a variable angle of incidence to achieve the required thermal balance.

At the start of the investigation, available data on several key parameters necessary to predict the thermal electrical performance of the candidate designs were quite limited. In particular, the electrical performance of production-type 2 and 10 ohm-cm solar cells at high temperatures and intensities and the thermal radiation characteristics of a variety of solar cell/coverglass combinations were unavailable. As a result, a combined program was undertaken to investigate possible solar panel approaches and, simultaneously, to obtain the needed photovoltaic and thermal radiation characteristics. This report presents the results of this study and provides an extensive set of data on the thermal and electrical characteristics of three solar panel approaches applicable to spacecraft missions between 1.0 and 0.4 AU. These are the second-surface mirror mosaic approach, the selective bandpass interference filter approach, and the tilted panel approach.

Where units of measurement are given in both the metric and the English system, the basic measurements were made in English units.

II. PROGRAM DEFINITION

A. Thermal Control Approaches Considered

Because the equilibrium temperature of a solar panel is determined by the total amount of energy absorbed per unit area, a panel can be cooled by decreasing its solar absorptance while maintaining a high emittance. One technique for achieving this balance, which we refer to as a mirror mosaic, is to cover a percentage of the solar array surface with second-surface mirrors. This arrangement takes advantage of the high emissivity of the quartz ($\epsilon \approx 0.8$) and the low solar absorptivity of the silvered surface ($\alpha_s \approx 0.1$) to maintain a low equilibrium temperature.

The mirror mosaic approach can be implemented in a number of ways. One technique is to place second-surface mirrors between the solar cells as shown in Fig. 1a. However, this approach has the disadvantage of requiring a thick, and therefore heavy, substrate material in order to guarantee adequate lateral conduction between the cell and the cooler mirror areas. In addition it requires the development of unconventional cell interconnecting techniques which could lead to decreased reliability, increased electrical losses, and/or increased magnetic fields.

As an alternative to separate mirrors one can simplify the overall panel construction by using partially mirrored coverglasses. This approach utilizes a conventional filtered coverglass with a second-surface mirror stripe, or other pattern, as shown in Fig. 1b. It has the advantage of using the same cell interconnections as a conventional panel and leads to negligible lateral thermal gradients.

A third technique for achieving a mirror mosaic is to increase the width of the vapor-deposited electrical grid lines on the top surface

of the cell. When the cell is filtered using a conventional quartz coverglass, these areas act as second-surface mirrors. Like the partially mirrored coverglass approach, the wide-grid cells use the same wiring as a conventional solar array and lead to negligible lateral thermal gradients. Both the partially mirrored coverglass and wide grid cell mirror mosaics are treated in this report.

A second thermal control approach considered in this study is the use of a selective bandpass interference filter on the coverglass. Because the spectral response of silicon solar cells is concentrated in the 0.4- to 1.1- μm region of the solar spectrum, it is possible to better the conversion efficiency of a mirror mosaic panel by selectively reflecting the solar energy less useful to the solar cell in its energy conversion process. Figure 2 depicts the bandpass transmission characteristics of a selective filter designed to maximize cell output while maintaining a filtered cell solar absorptance of about 0.3. Like the partially mirrored coverglass and wide-grid cell approaches, selective bandpass filters allow the use of conventional solar array fabrication techniques.

The third thermal control approach investigated is the obvious technique of decreasing the incident solar intensity by tilting the solar array surface with respect to the sun. Although this approach does not require the evaluation of novel solar cell or coverglass designs, it does require data on the performance of conventionally filtered production cells at high solar intensities and temperatures. In addition, supplemental data are required on the thermal and electrical characteristics of solar cell stacks when they are inclined at steep angles relative to the incident solar radiation.

B. Program Scope

The basic aim of the program described herein has been to gather comprehensive data on the thermal and electrical performance characteristics of the three solar array thermal control approaches described above. A secondary objective of the program has been to predict and compare the total mission performance of these designs.

As a first step in the program, a number of wide-grid cells, partially mirrored coverglasses, and selective bandpass filters were procured together with conventional cells and covers to provide several solar cell/coverglass configurations representative of the three thermal control approaches. A detailed description of these components is presented in Section III. Succeeding sections describe the results of the various tests performed on these components.

In particular, Section IV provides extensive data on the electrical performance of the selected

components for temperatures between -140°C and +160°C and solar intensities ranging from 1 to 6 suns. The effect of large tilt angles on the electrical performance is discussed in Section V.

Sections VI and VII provide comprehensive data on the thermal radiation properties of the various solar cell/coverglass assemblies and interconnected solar cell modules, respectively. The stability of these thermal properties under low energy proton and ultraviolet irradiation is described in Section VIII.

Section IX completes the descriptions of the test programs with data on the thermomechanical and outgassing properties of a number of candidate solar cell adhesives.

As a means of summarizing the results of the test programs described in the preceding sections, Section X compares the relative performance of the various solar array design approaches for intensities ranging from 1 to 6 suns.

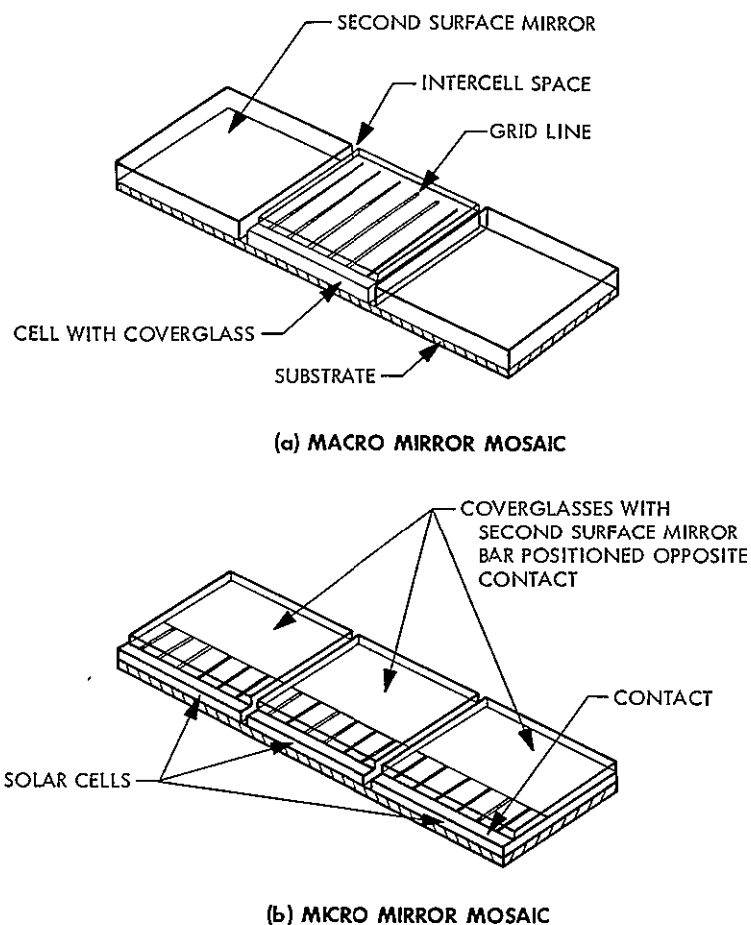


Fig. 1 Two mirror mosaic approaches

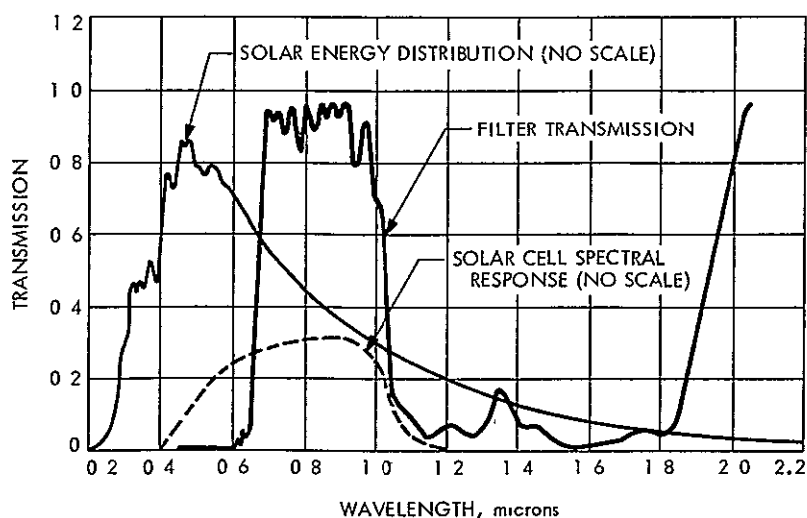


Fig. 2 Spectral transmission of a selective bandpass interference filter designed to give a filtered cell solar absorptance of 0.3

III. SOLAR CELL/COVERGLASS CONFIGURATIONS STUDIED

Six types of solar cells and nine types of coverglass assemblies were selected for electrical and thermal optical property measurements. The samples were chosen so as to provide comprehensive data on a number of solar cell/coverglass configurations representative of the three thermal approaches emphasized in the study. The solar cells were selected in two groups (1) standard 2 and 10 ohm-cm production cells typical of those used on previous Mariner spacecraft, and (2) experimental 2 and 10 ohm-cm wide-grid cells with enlarged grid lines designed to serve as second-surface mirrors. The covers were of three types (1) standard blue and blue-red interference filters and antireflective coatings on fused silica glass, (2) experimental selective bandpass interference filters on fused silica glass, and (3) experimental partially mirrored coverglasses with blue filters and antireflective coatings. Cell assemblies were fabricated by cementing the covers to the cells using General Electric's RTV-602 Adhesive.*

Each of the cells and covers used in the test program is described below in detail. Subsequent reference to these components will be made using the common names, which serve as subheadings in the descriptions which follow. Thus, future reference to a 2 ohm-cm cell with blue filter will imply the 2 ohm-cm cell and blue filter described below, assembled with RTV-602 adhesive.

A. Standard Production Cells

A 2×2 cm by 0.046 cm n/p, 2 ohm-cm solar cell was chosen as the baseline cell for this study because its current use on the Mariner 1969 and

1971 spacecraft made comparison with flight data possible and allowed flight production cells and cell modules to be used in the evaluation program. For comparison purposes, a similar production 10 ohm-cm cell was also included. The two cells are defined below:

(1) 2 ohm-cm cell

Size and type: 2×2 cm $\times 0.046$ cm
n/p, 2 ohm-cm

Grid type: Six Ag-Ti solderless grids terminating in a 0.14-cm-wide ohmic contact strip

Active area: Samples measured had active areas of $3.70 \text{ cm}^2 \pm 1\%$ (including grid area but excluding contact area)

Manufacturer: Heliotek

(2) 10 ohm-cm cell

Size and type: 2×2 cm $\times 0.046$ cm
n/p, 10 ohm-cm

Grid type: Six Ag-Ti solderless grids terminating in a 0.14-cm-wide ohmic contact strip

Active area: 3.70 cm^2

Manufacturer: Centralab

*This is the standard coverglass adhesive used at JPL on past Mariner solar panels. It and other adhesives are compared in Section IX.

B. Wide-Grid Cells

One technique for achieving a second-surface mirror mosaic panel is to increase the width of the vapor-deposited electrical grid lines on the top surface of the cell. In order to establish the electrical and thermal optical properties of wide-grid cells, four representative cells were procured. The cells were manufactured by two different cell manufacturers using both 2 and 10 ohm-cm material and with two different grid patterns. Both grid patterns cover approximately two-thirds of the cell's active area (Fig. 3). Cells are

(1) 2 ohm-cm multiple wide-grid cell

Size and type $2 \times 2 \text{ cm} \times 0.046 \text{ cm}$
n/p, 2 ohm-cm

Grid type: Four 0.326-cm-wide Ag-Ti solderless grids terminating in a 0.070-cm ohmic contact strip

Active area: 65.4% of the available active area (cell area minus contact area) was covered by the Ag-Ti wide grids. The net active cell area was 1.33 cm^2 .

Manufacturer Heliotek

(2) 10 ohm-cm multiple wide-grid cells

These cells were identical to the 2 ohm-cm multiple wide-grid cells except that they were manufactured using 10 ohm-cm material.

(3) 2 ohm-cm single wide-grid cells

Size and type: $2 \times 2 \text{ cm} \times 0.046 \text{ cm}$
n/p, 2 ohm-cm

Grid type: A single 1.310-cm-wide solderless Ag-Ti grid centrally located and terminating in a 0.070-cm-wide ohmic contact strip

Active area: 65.8% of the available active area (cell area minus contact area) was covered by the Ag-Ti wide grid. The net active cell area was 1.31 cm^2 .

Manufacturer: Centralab

(4) 10 ohm-cm single wide-grid cells

These cells were identical to the 2 ohm-cm single wide-grid cells except that they were manufactured using 10 ohm-cm material.

C. Standard Blue and Blue-Red Filters

A fused silica coverglass with a standard blue interference filter and front surface antireflective coating was chosen as the baseline cover. For

comparison purposes, a typical production cover-glass with blue-red filter was also included

(1) Blue filter

Size: $2.00 \times 1.88 \text{ cm} \times 0.05 \text{ cm}$
thick

Material: Corning 7940 fused silica

Ultraviolet rejection: Below $410 \pm 15 \text{ nm} (\text{m}\mu)$

Infrared rejection: None

Antireflective coating: Less than 2% reflection from 575 to 675 nm

Manufacturer: Optical Coating Laboratory, Inc. (OCLI)

(2) Blue-red filter

Size: $2.00 \times 1.88 \text{ cm} \times 0.05 \text{ cm}$
thick

Material: Corning 7940 fused silica

Ultraviolet rejection: Below $400 \pm 5 \text{ nm}$

Infrared rejection: 1050 to 1400 nm

Antireflective coating: Less than 2% reflection from 600 to 800 nm

Manufacturer: OCLI

D. Selective Bandpass Filters

The use of highly reflective bandpass filters on the coverglasses is a second method of decreasing the average solar absorptance of a solar panel. In order to determine the capability of state-of-the-art selective bandpass filters, four representative interference filter designs were developed for JPL by Optical Coating Laboratory, Inc. The four filters had solar reflectances ranging from about 0.5 to 0.7 when mounted on the baseline 2 ohm-cm solar cell, and the bandpass cut-on and cut-off points were chosen so as to maximize the cell output for the particular solar absorptance. The filters were as follows.

(1) 4024 filter

Size: $2.00 \times 1.88 \text{ cm} \times 0.05 \text{ cm}$
thick

Material: Corning 7940 fused silica

Ultraviolet rejection: Below $550 \pm 20 \text{ nm} (\text{m}\mu)$

Infrared rejection: 1000 to $1310 \pm 40 \text{ nm}$

Antireflective coating: None

Manufacturer: OCLI

(2) 4025 filter

Size: 2.00 × 1.88 cm by 0.05 cm thick

Material: Corning 7940 fused silica

Ultraviolet rejection: Below 600 nm

Infrared rejection: 1000 to 1350 nm

Antireflective coating: None

Manufacturer: OCLI

(3) 4026 filter

Size: 2.00 × 1.88 cm by 0.05 cm thick

Material: Corning 7940 fused silica

Ultraviolet rejection: Below 650 ±40 nm

Infrared rejection: 1000 to 1400 ±40 nm

Antireflective coating: None

Manufacturer: OCLI

(4) Modified 4026 filter

This filter has the same bandpass as the 4026 filter but has an additional infrared rejection filter stack.

Size: 2.00 × 1.88 cm by 0.05 cm thick

Material: Corning 7940 fused silica

Ultraviolet rejection: Below 650 ±20 nm

Infrared rejection: 1000 to 1900 ±40 nm

Antireflective coating: None

Manufacturer: OCLI

E. Partially Mirrored Covers

A second technique for achieving a mirror mosaic panel is to apply a second-surface mirror stripe, or other pattern, to the rear surface of each coverglass. In order to establish the electrical and thermal optical characteristics of partially mirrored cells, conventional coverglasses with blue filters were procured with three different second-surface mirror patterns applied over the filter. Each of the patterns covered roughly two-thirds of the cover's surface. The pattern referred to below as mirror stripe was designed to place a mirror stripe over each grid line of the baseline 2 ohm-cm cell. Though expensive to construct, this arrangement maximizes the available active area by placing mirrors over the active area covered by the grids. The mirror bar, on the other hand, was chosen as an inexpensive mirror pattern and was used in two

different arrangements in order to determine the dependence of cell output on the placement of the mirror area. Though the two bars are physically identical, they are referred to as separate patterns because the position of the mirror resulted in somewhat different cell active areas and had a measurable effect on cell performance. The three mirror patterns are shown in Fig. 4 and are as follows.

(1) Mirror stripe

Size: 2.00 × 1.88 by 0.05 cm thick

Material: Corning 7940 fused silica

Filter: Ultraviolet rejection below 410 nm ($\mu\mu$)

Antireflective coating: None

Mirror: OCLI SI-100 metallized coating applied over the blue filter in 6 stripes, each approximately 0.237 cm wide.

Active area: 71.5% of the available active area (cell area minus contact area) is covered with mirror when the cover is assembled onto the baseline 2 ohm-cm cell. The net active cell area is reduced to 1.052 cm².

Manufacturer: OCLI

(2) Mirror bar opposite contact

Sizes: 2.00 × 1.88 cm by 0.05 cm thick

Material: Corning 7940 fused silica

Filter: Ultraviolet rejection below 410 nm

Antireflective coating: None

Mirror: OCLI SI-100 metallized coating applied over the blue filter in a single stripe 1.245 cm wide along one side.

Active area: 67.0% of the available active area (cell area minus contact area) is covered with mirror when the cover is assembled onto the baseline 2 ohm-cm cell with the mirror bar positioned opposite the cell's ohmic contact strip. The mirror reduces the net active cell area to 1.220 cm².

Manufacturer: OCLI

(3) Mirror bar by contact

Size: 2.00 × 1.88 cm by 0.05 cm thick

Material: Corning 7940 fused silica

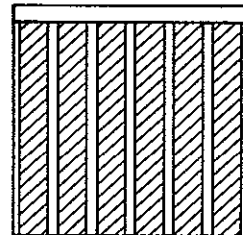
Filter: Ultraviolet rejection below 410 nm

Antireflective coating: None

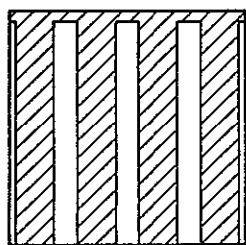
Mirror: OCLI SI-100 metallized coating applied over the blue filter in a single stripe 1.245 cm wide along one side.

Active area 66.0% of the available active area (cell area minus contact area) is covered with mirror when

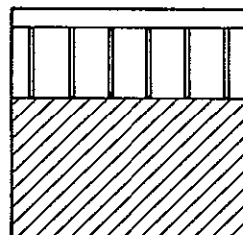
the cover is assembled onto the baseline 2 ohm-cm cell with the mirror bar positioned next to the cell's ohmic contact strip. This is somewhat less mirror area than with the mirror opposite the contact because the edge of the cover overlaps the contact strip slightly. The mirror reduces the net active cell area to 1.255 cm².



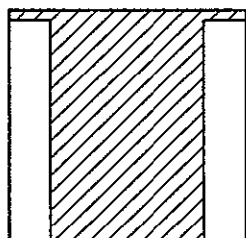
(a) MIRROR STRIPE



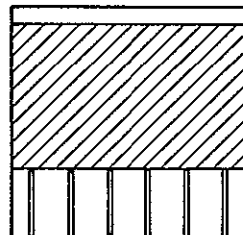
(b) MULTIPLE GRID



(b) MIRROR BAR OPPOSITE CONTACT



(b) SINGLE GRID



(c) MIRROR BAR BY CONTACT

Fig. 3 Wide-grid cells

Fig. 4 Cells filtered with partially mirrored coverglasses

IV. SOLAR CELL ELECTRICAL PERFORMANCE AT HIGH INTENSITIES AND TEMPERATURES

A. Objective

At the start of this investigation, available data on the electrical performance characteristics of production type 2 and 10 ohm-cm silicon solar cells at high solar intensities and temperatures were quite limited. In particular, no high-intensity data were available for the 2 ohm-cm solar cells used at JPL on past Mariner space-craft or for any of the experimental selective bandpass, partially mirrored coverglass, or wide-grid cell assemblies considered in this study. The primary objective of the electrical measurements program described herein was to obtain the needed photovoltaic characteristics. A complete list of the solar cell/coverglass combinations which were evaluated is shown in Table 1. Recall that the detailed description of these cell assemblies is given in Section III.

B. Experimental Procedure

The solar cells used in this measurement program were purchased in pilot production quantities of approximately 200 cells each in accordance with the minimum space acceptance criteria reproduced in Appendix A. Upon delivery, the cells were measured under air-mass-zero solar simulation at an intensity of 140 mW/cm² and a cell temperature of 28°C. Several cells of each type were selected for a close match at maximum power for the above conditions. The cells were then prepared with stress-relieved tin-plated Kovar tabs soldered to the ohmic contacts so that four-wire electrical measurements could be taken. After filtering, the cells were bonded to 3-mm (1/8-in.) thick copper test plates with General Electric's RTV-560 silicone adhesive. Each test plate contained up to 13 test cells plus two cells which had copper constantan thermocouples bonded to their coverglass surfaces. These instrumented cells were not included in the electrical test

circuit but were used for temperature reference purposes. As shown in Fig. 5, there was more than one type of solar cell and coverglass combination on most test plates. This was necessary because of the rather large number (13 types) of cell assemblies investigated.

Figure 6 shows the JPL photovoltaics environmental test facility used to establish the performance of the selected cell assemblies. The multicell testing unit shown in Fig. 7 is built around a special thermal-vacuum chamber which serves to eliminate vapor condensation on the surface of the solar cell assemblies when testing at temperatures below about 10°C. The chamber itself is 33 cm (13 inches) high, 38 cm (15 inches) in diameter, and is equipped with a 20 cm (8-inch) diameter quartz (Corning 7940) window through which the cells are irradiated using a Spectrosun X25 Mark II solar simulator. Intensity and color reference standard cells which have been calibrated as part of the NASA/JPL balloon flight solar cell standardization program (Ref. 1) are used to monitor the intensity level and spectral quality of the solar simulator. The standard cells are mounted inside the test chamber above the main test plate heat sink and are thermally as well as electrically isolated from it. A self-contained, closed water reservoir is used in conjunction with a thermo-electric module for controlling the standard cell and color ratio detector temperatures. The temperature of the test plate heat sink is controlled automatically by a separate controller which references the temperature of the two instrumented cells on the test plate.

After fabrication, the test plates were mounted in the above-described test facility, and the solar cell electrical parameters were obtained in the form of current-voltage (I-V) curves for the matrix of temperatures and intensities shown in Table 2. The I-V curves were obtained in the

conventional manner utilizing a variable resistive load and XY recorder (Ref. 2).

C. Experimental Results and Discussion

After the I-V characteristics of each cell sample had been measured at each of the 25 temperature/intensity combinations noted in Table 2, the short-circuit current, open-circuit voltage, and maximum power point were extracted and reduced with the aid of a computer programmed to average the data for each cell assembly type. In addition, the standard deviations and 95% confidence limits were determined to allow the statistical significance of the data to be noted. Figures 8 - 105 present eight plots for each cell assembly type. Five of each group of plots give the data discussed above, with 95% confidence limits indicated by the tick marks bracketing the average values. Appendix B contains the actual average data values used in these figures. The remaining three plots for each cell type present the dependence of cell efficiency on temperature and intensity and a curve shape factor which expresses the "squareness" of the I-V curve as a function of temperature and intensity.

The functions $\phi(T)$ and $\psi(S)$, which represent the dependence of cell efficiency on temperature T and intensity S , respectively, were determined by minimizing, in a weighted least squares sense, the difference between the maximum power measurements and the power defined by the function

$$P(S, T) = P(1 \text{ sun}, 60^\circ\text{C})\phi(T)\psi(S)S$$

This procedure results in uncoupling the effects of temperature and intensity on maximum power and allows them to be examined separately. Thus, characteristics such as a decrease in cell efficiency at high solar intensity due to a high series resistance are clearly displayed.

The curve shape factor which depicts the "squareness" of the I-V curve is defined as the ratio of maximum power to the product of short-circuit current and open-circuit voltage. Ideally, with a rectangular I-V curve, the curve shape factor will be one. Thus, the extent to which the curve shape factor is less than one indicates the degree of rounding of the knee of the I-V curve.

As may be observed from the various curve factor plots, there was considerably more scatter in the curve shape at high solar intensities and temperatures than there was at conditions approximating those at 1 AU. This is, of course, to be expected since the cells were selected for a close match at 1 sun, 28°C. However, it should be pointed out that the inconsistency noted here could cause serious mismatch problems and a resulting decrease in solar array operating efficiency at high solar intensities. A first approach for solving this problem might be to procure cells based on a specified performance at a higher solar intensity. However, a more positive approach would be to isolate the cause of the variation and to tailor the manufacturing process to decrease or eliminate the effect.

Because the electrical characteristics of the designs are strongly dependent on cell temperature, the thermal properties of the designs must be carefully considered before the electrical performance characteristics can be compared. Since the thermal properties of the selected cell assemblies vary widely, the discussion of the relative attributes of the different designs is delayed until after the thermal characteristics are presented in sections VI and VII. In section X the different operating temperature characteristics of the designs are taken into consideration and the various cell assemblies are compared on an equal thermal performance basis.

Table 1. Solar cell/coverglass assemblies tested

TEST PLATE NUMBER	QUANTITY OF CELLS	CELL ASSEMBLY TYPE
C	13	Blue filter on 2 ohm-cm cell
MV2	8	Blue-red filter on 2 ohm-cm cell
MV2	5	Blue-red filter on 10 ohm-cm cell
MV3	4	4024 bandpass filter on 2 ohm-cm cell
MV3	4	4025 bandpass filter on 2 ohm-cm cell
MV3	4	4026 bandpass filter on 2 ohm-cm cell
MV5	4	Modified 4026 bandpass filter on 2 ohm-cm cell
MV1	5	Mirror stripes on 2 ohm-cm cell
MV1	4	Mirror bar by contact on 2 ohm-cm cell
MV1	4	Mirror bar opposite contact on 2 ohm-cm cell
MV4	6	Blue-red filter on 2 ohm-cm multiple wide grid cell
MV4	6	Blue-red filter on 2 ohm-cm single wide grid cell
MV5	4	Blue-red filter on 10 ohm-cm multiple wide grid cell
MV5	4	Blue-red filter on 10 ohm-cm single wide grid cell

Table 2. Matrix of test temperatures and intensities

		SOLAR INTENSITY						
		mW/cm ²	140	250	400	550	700	850
		°C	-40	-20	0	20	40	60
CELL TEMPERATURE			O					
			O					
			O	O				
			O	O				
			O	O	O			
				O	O	O		
					O	O	O	
						O	O	O
							O	O
							O	O

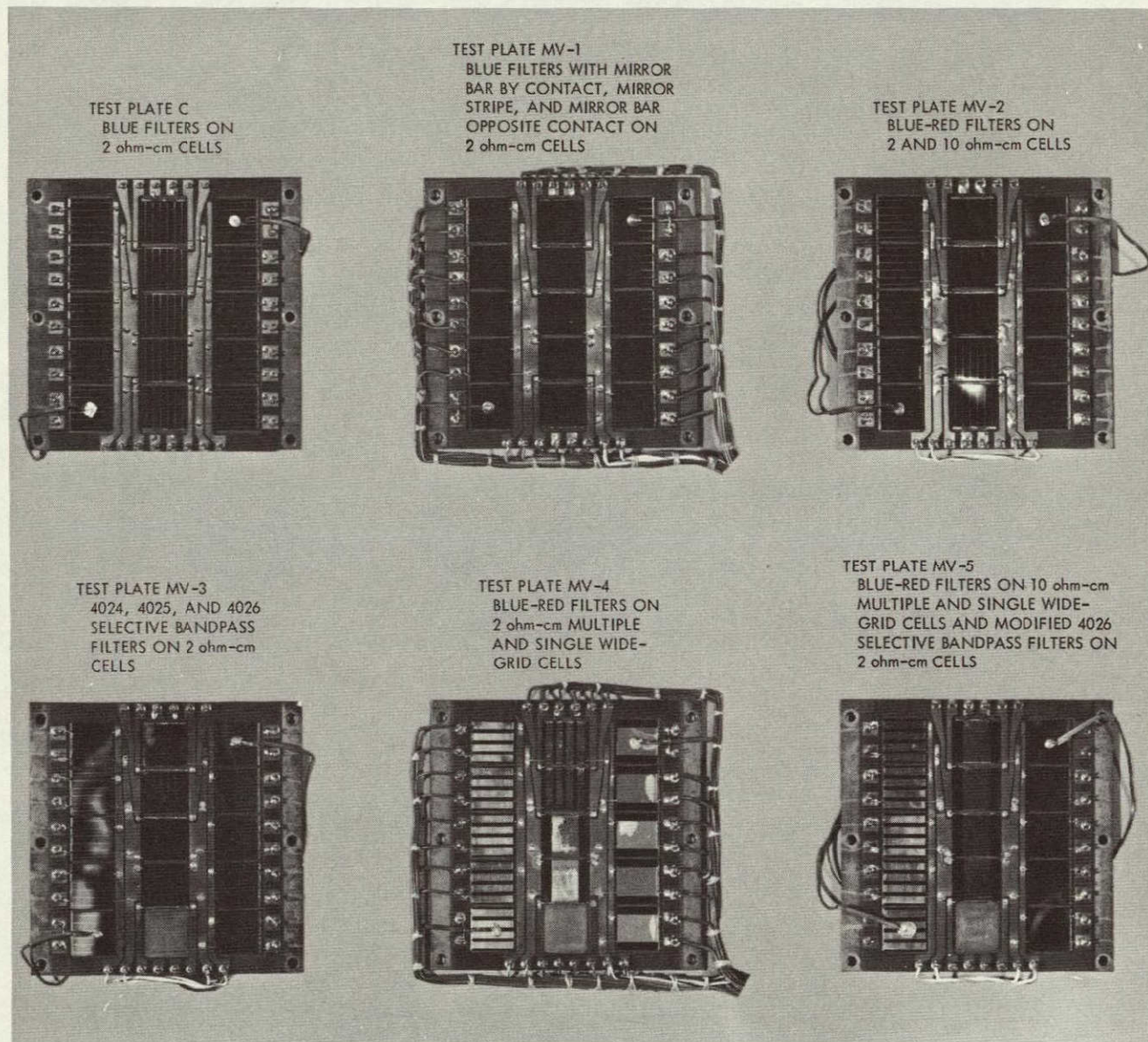


Fig. 5. Various types of solar cell/coverglass combinations mounted onto test plates

NOT REPRODUCIBLE

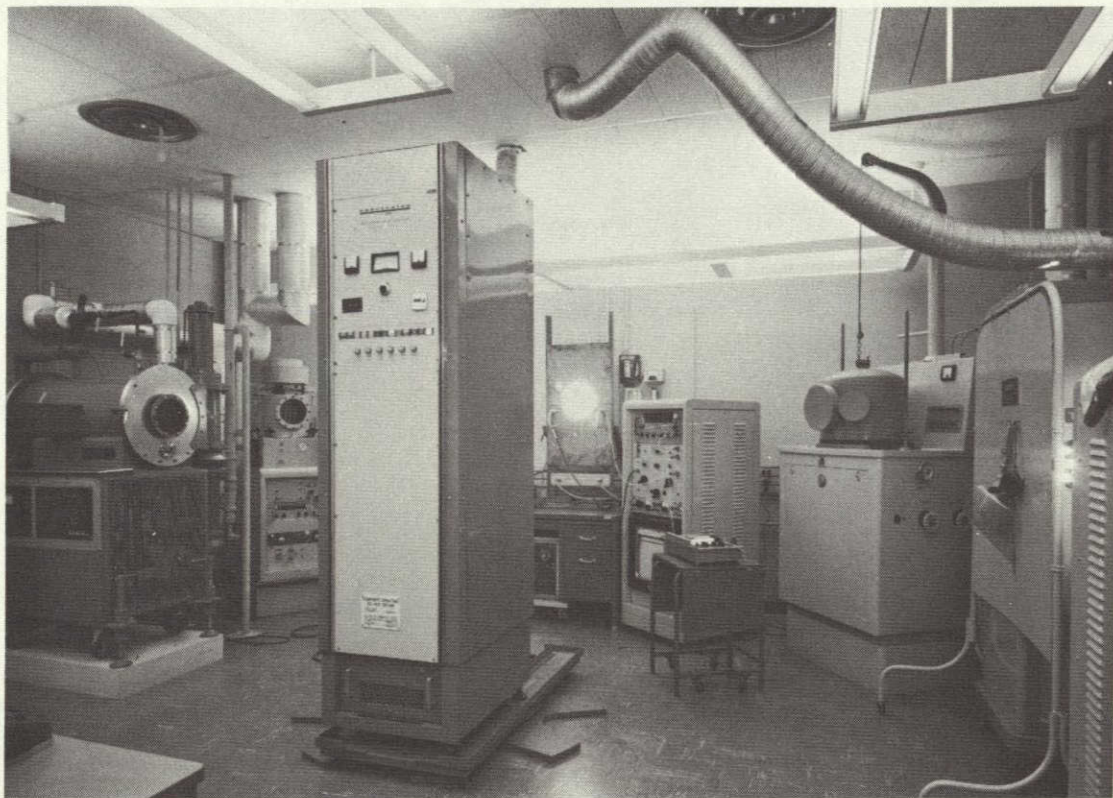


Fig. 6. JPL photovoltaics environmental test facility

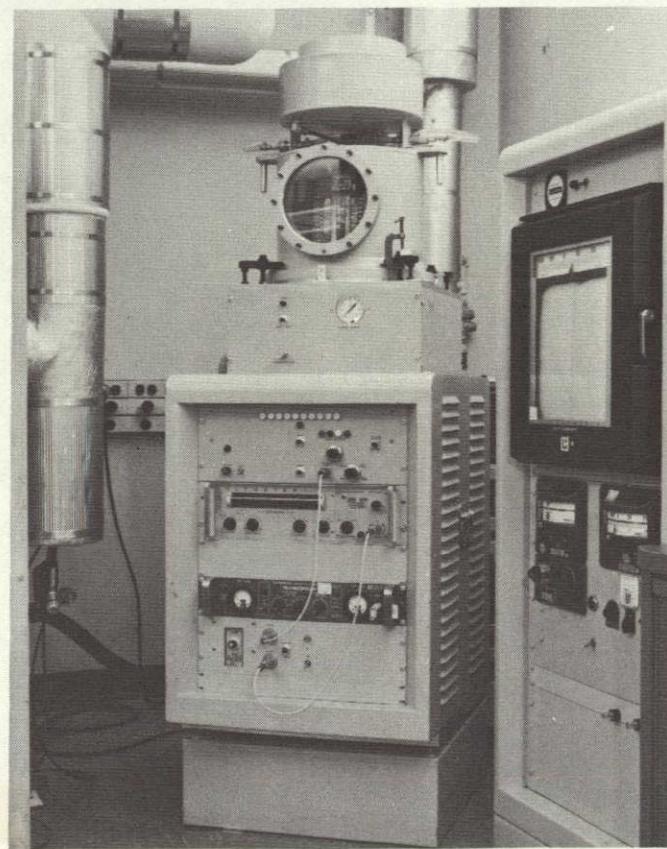


Fig. 7. Solar cell thermal-vacuum test chamber
and associated test equipment

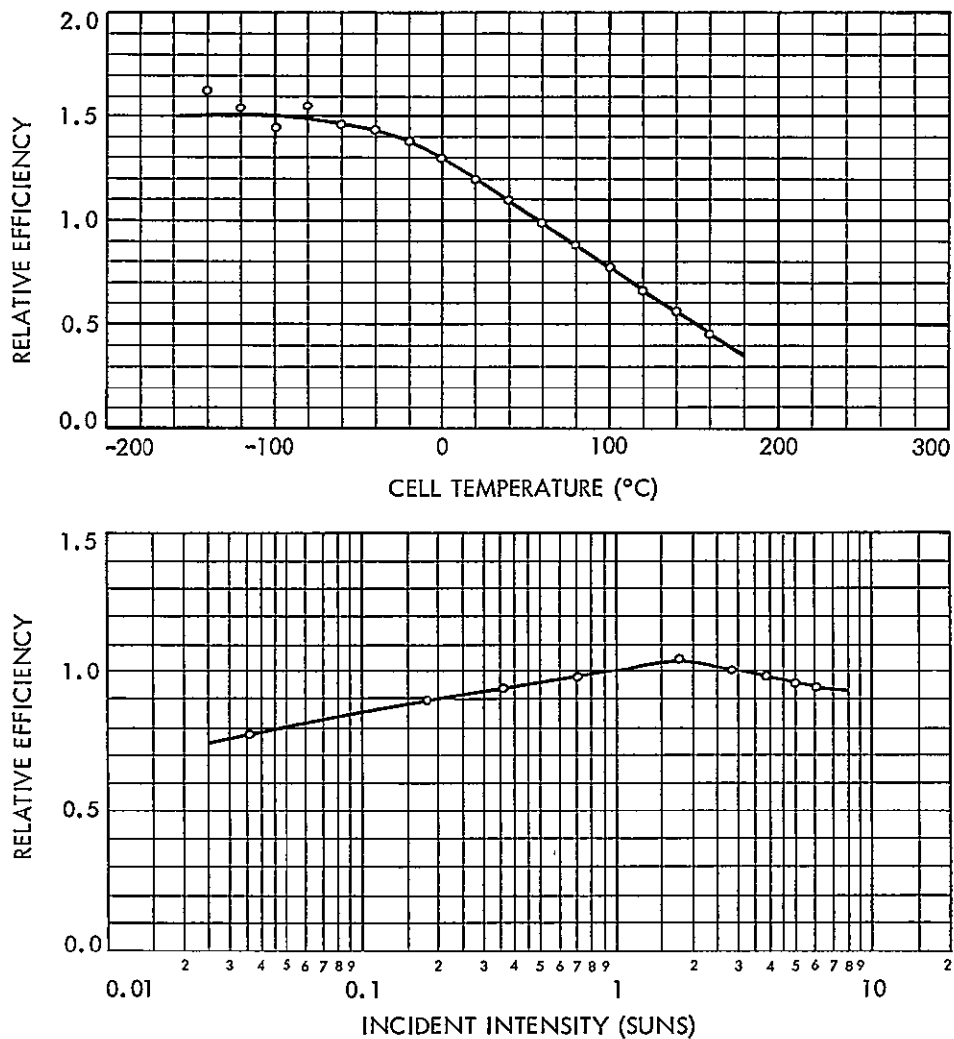


Fig. 8 Cell efficiency vs temperature and intensity, blue filter on
2 ohm-cm cell

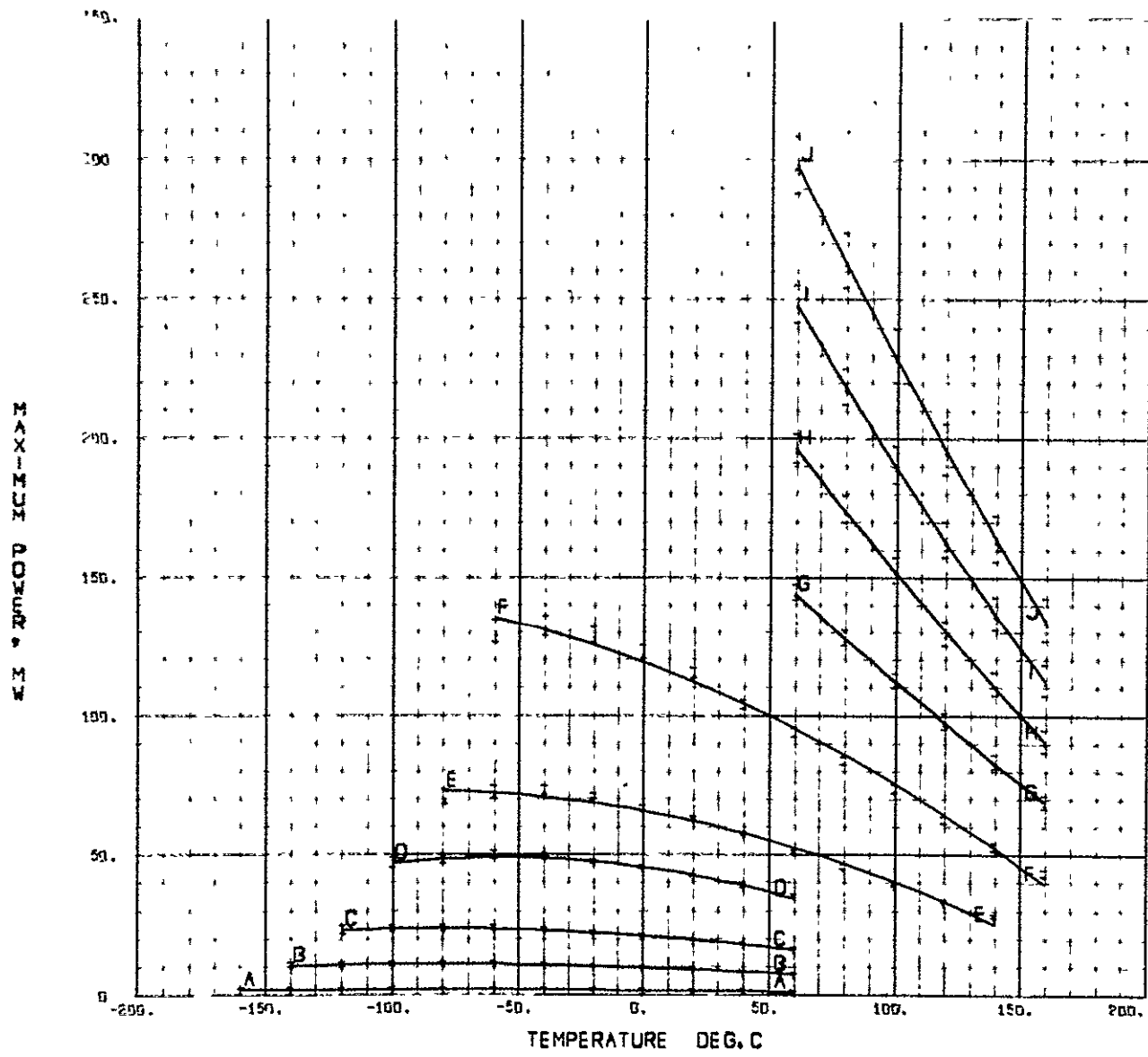


Fig. 9 Maximum power vs temperature, blue filter on 2 ohm-cm cell

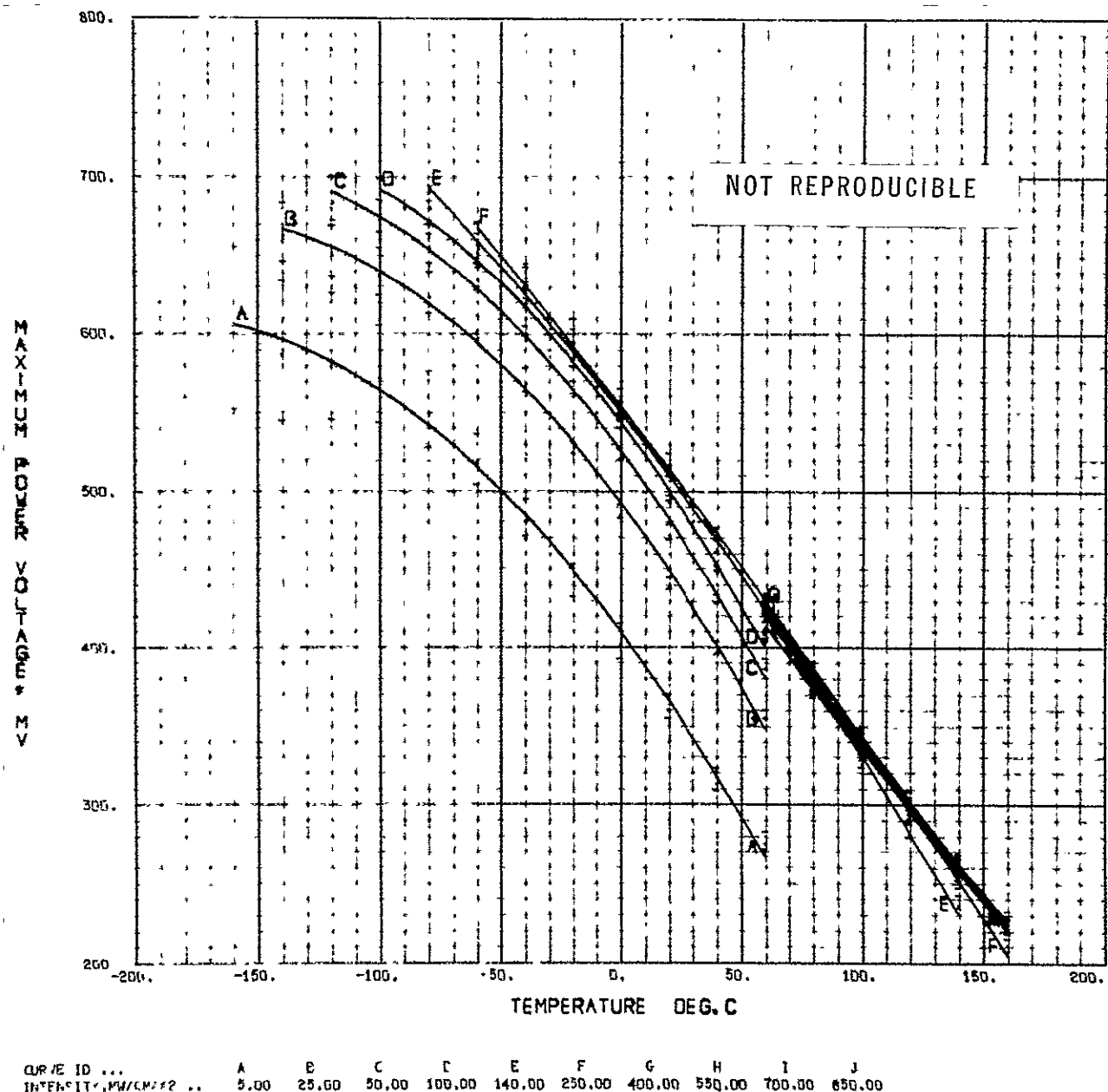


Fig. 10 Maximum-power voltage, blue filter on 2 ohm-cm cell

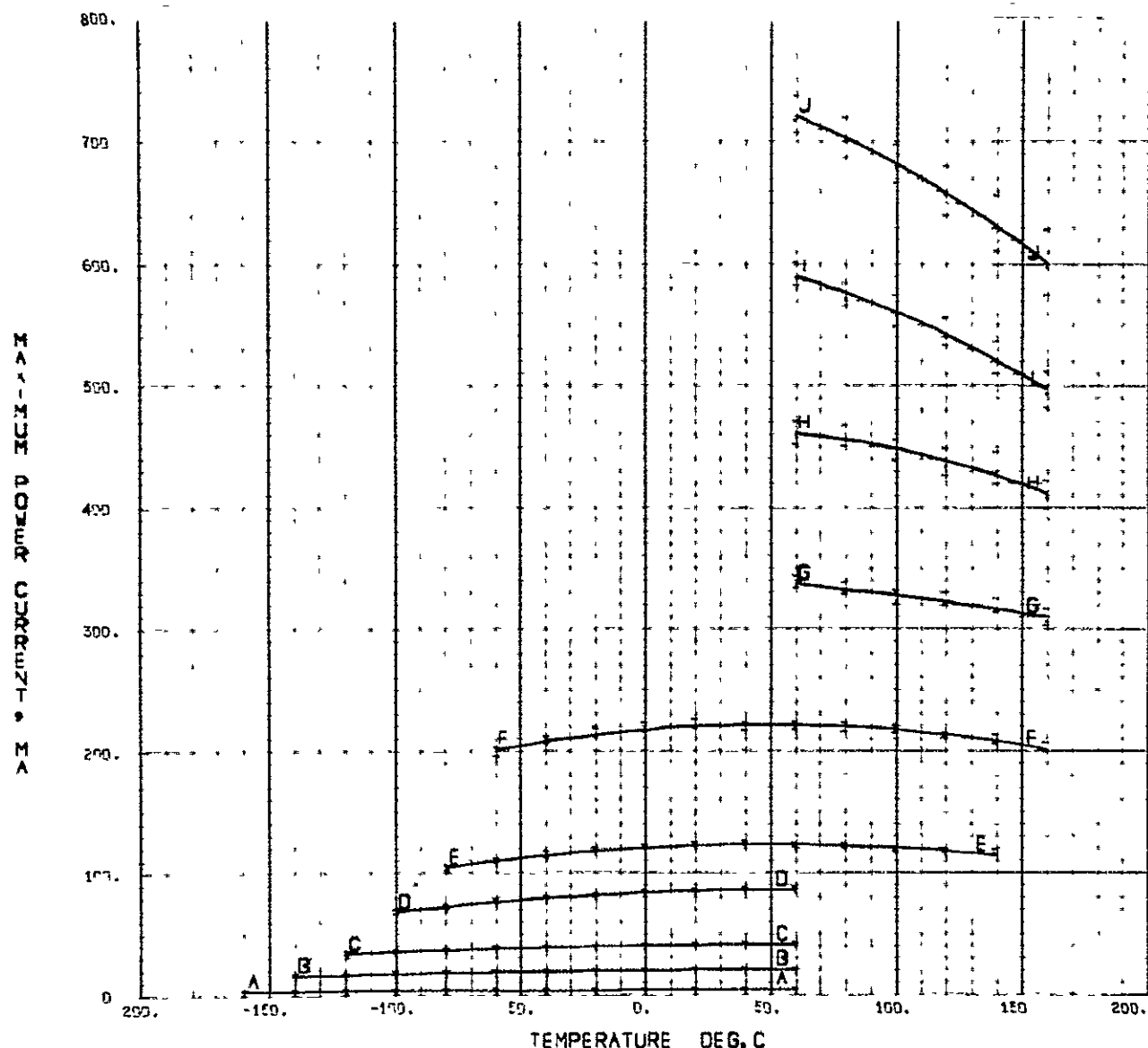


Fig 11. Maximum-power current vs temperature, blue filter on
2 ohm-cm cell

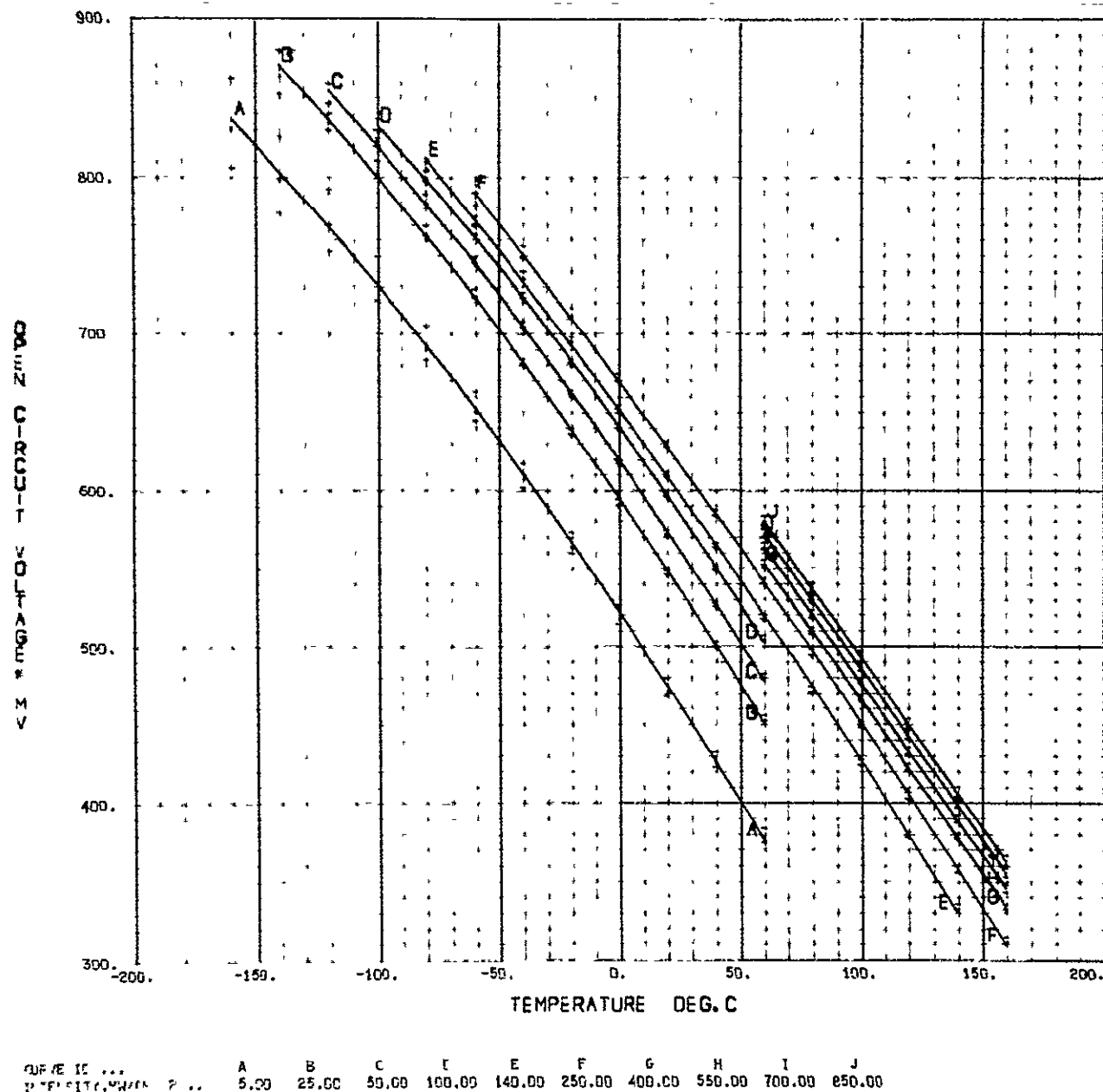


Fig. 12 Open-circuit voltage vs temperature, blue filter on 2 ohm-cm cell

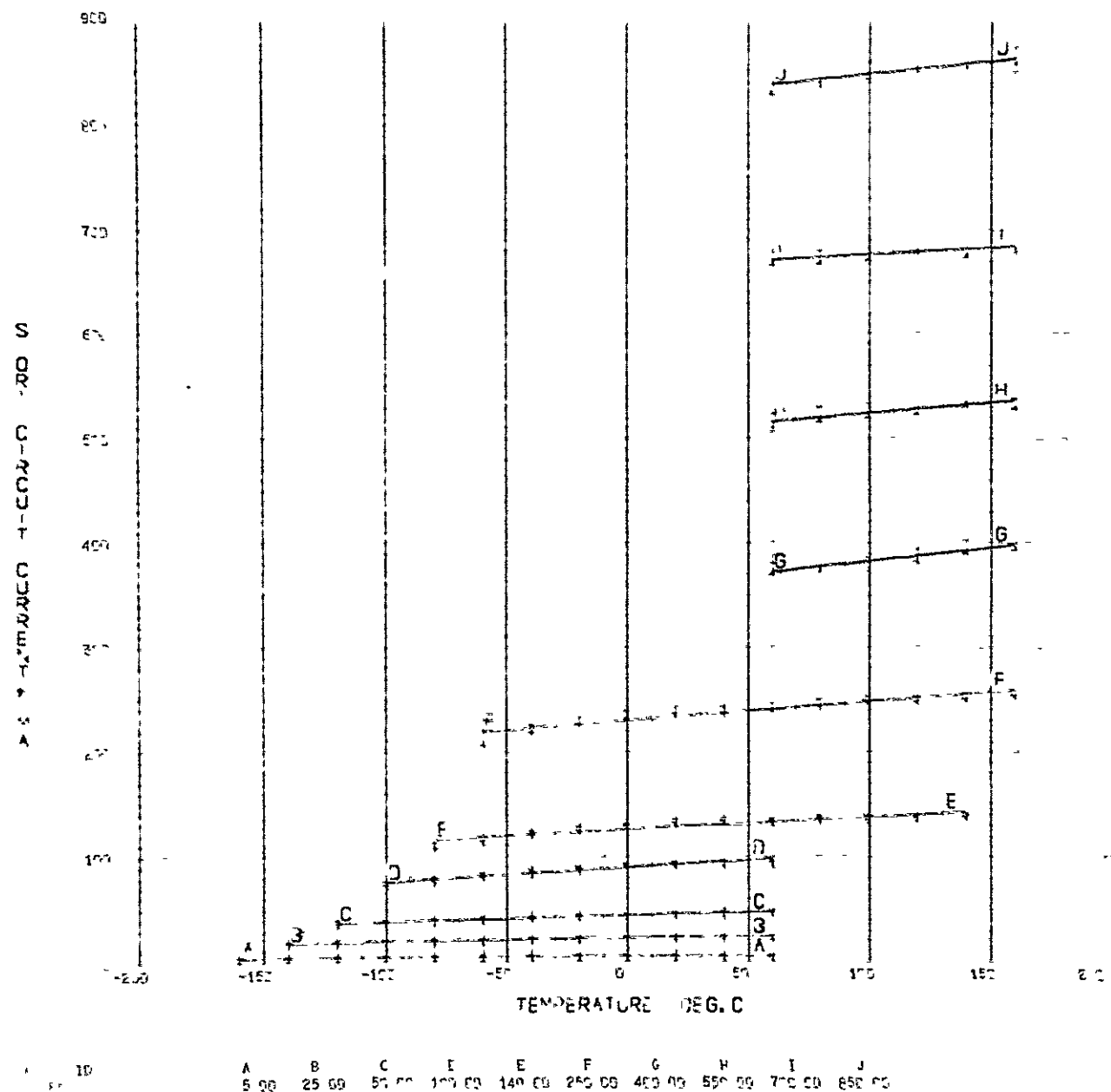


Fig. 13. Short-circuit current vs temperature, blue filter on 2 ohm-cm cell

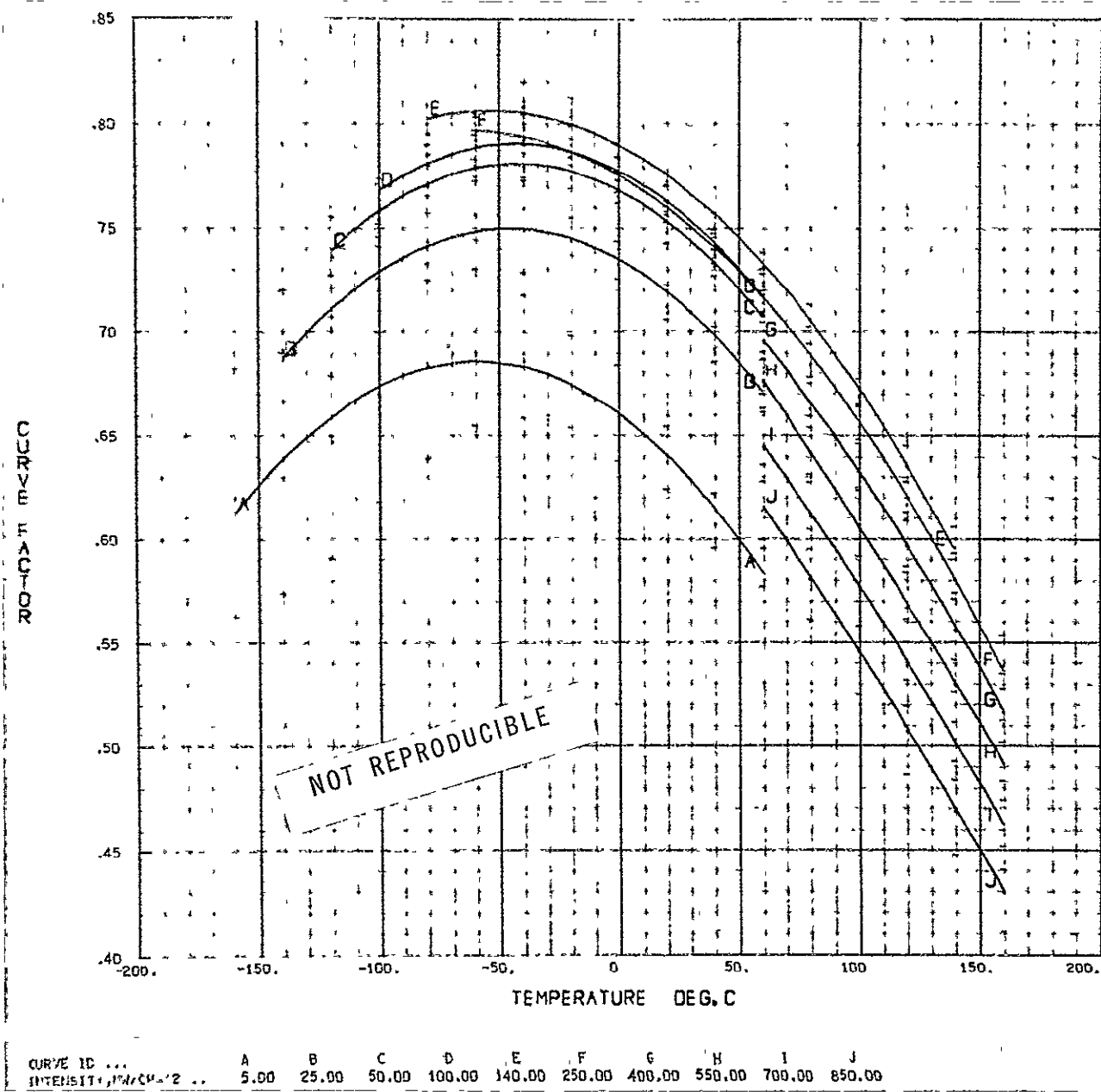


Fig 14. Curve factor vs temperature, blue filter on 2 ohm-cm cell

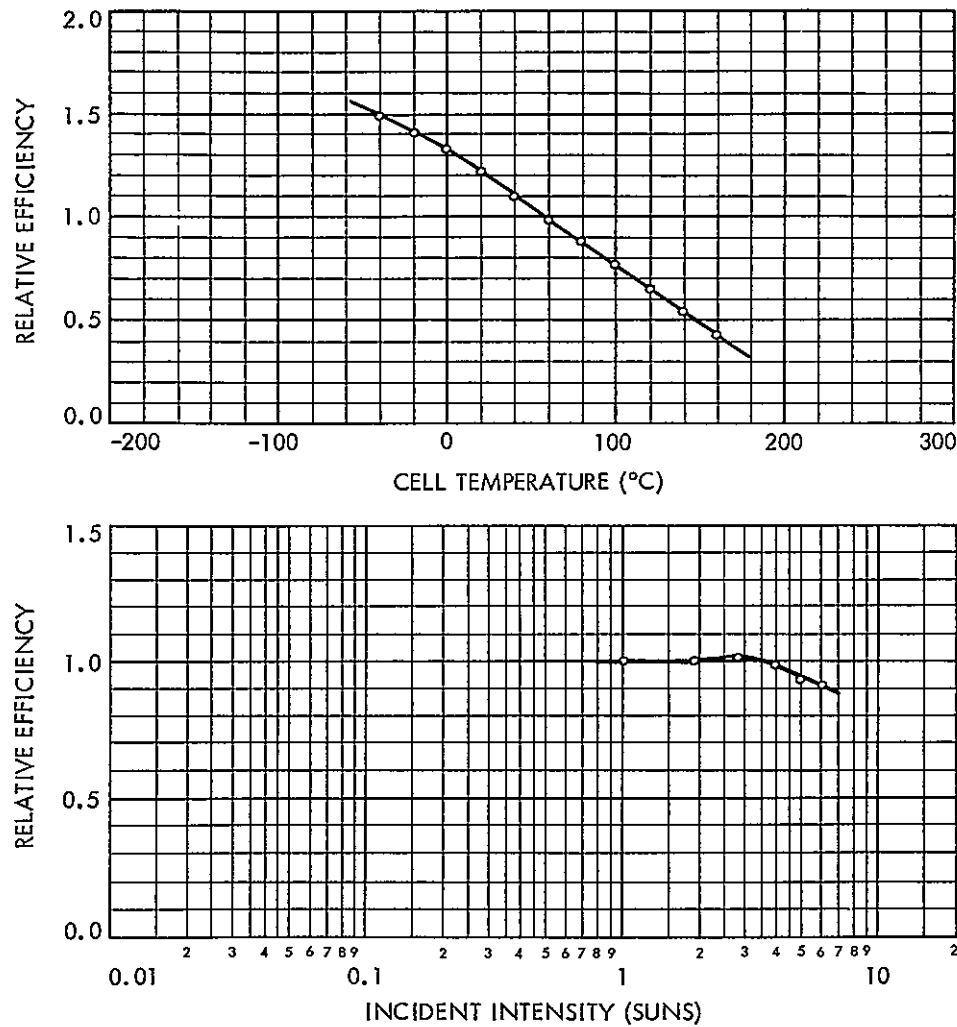


Fig 15 Cell efficiency vs temperature and intensity, blue-red filter on 2 ohm-cm cell

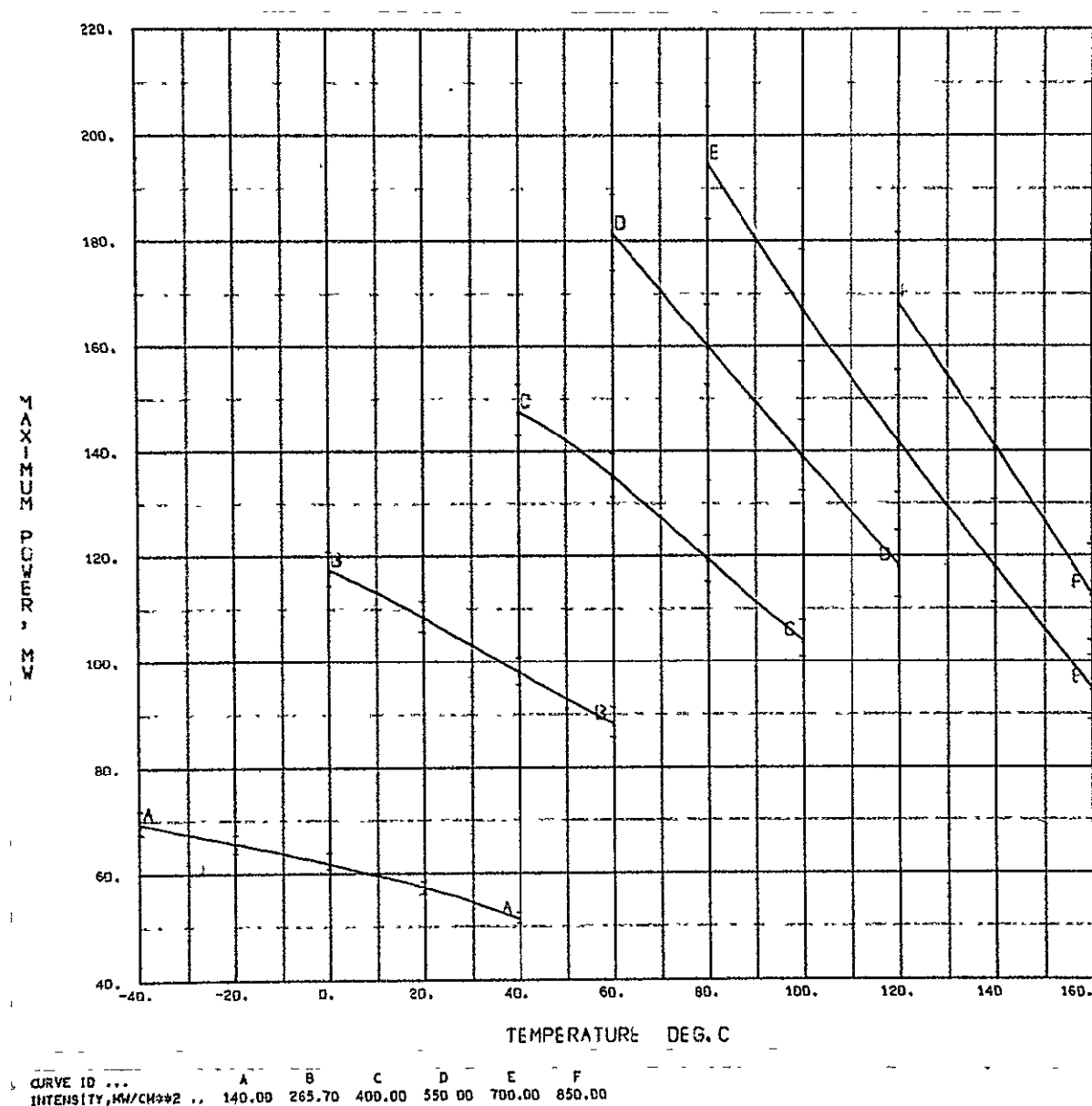


Fig. 16. Maximum power vs temperature, blue-red filter on 2 ohm-cm cell

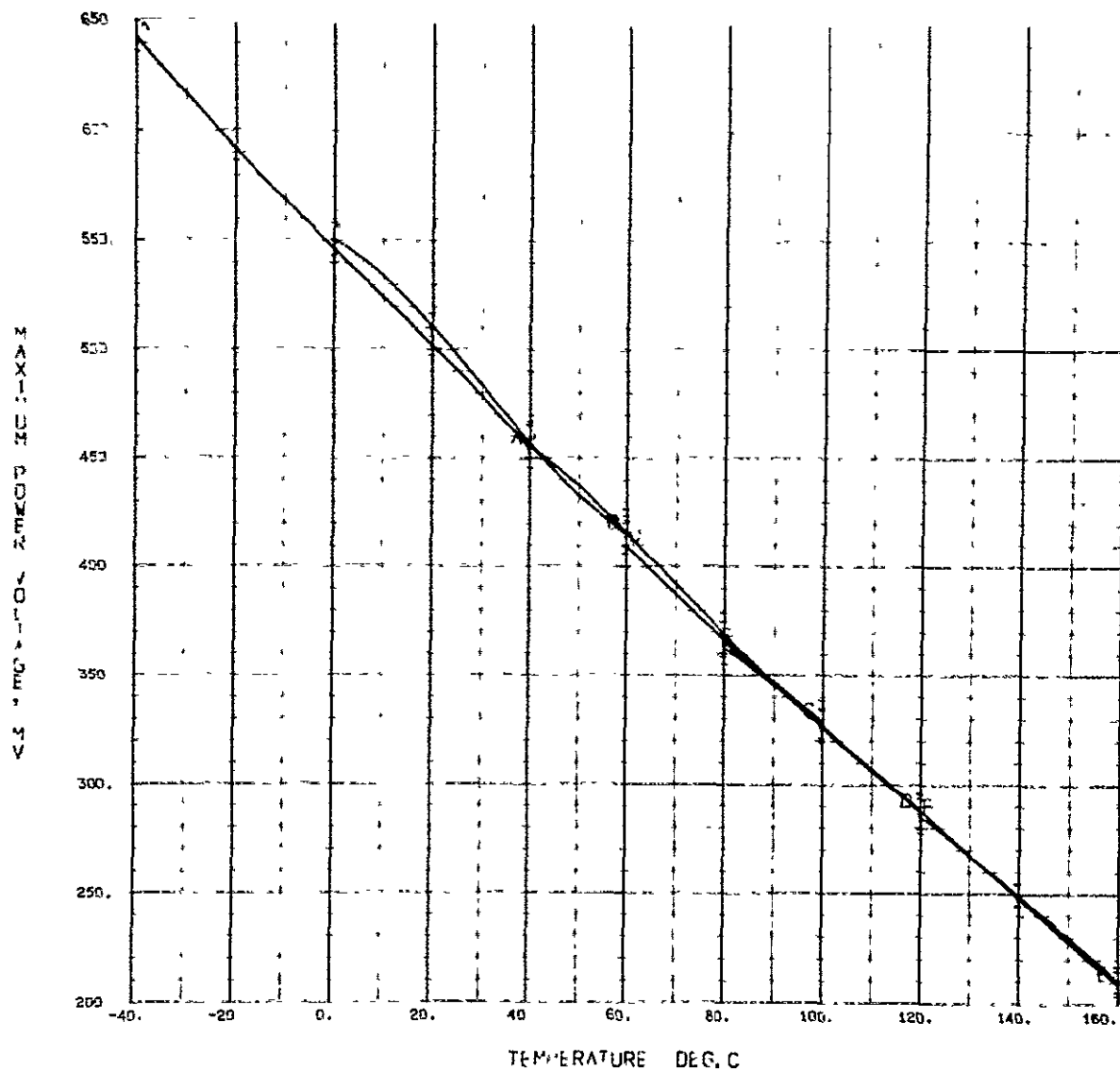


Fig. 17. Maximum-power voltage vs temperature, blue-red filter on 2 ohm-cm cell

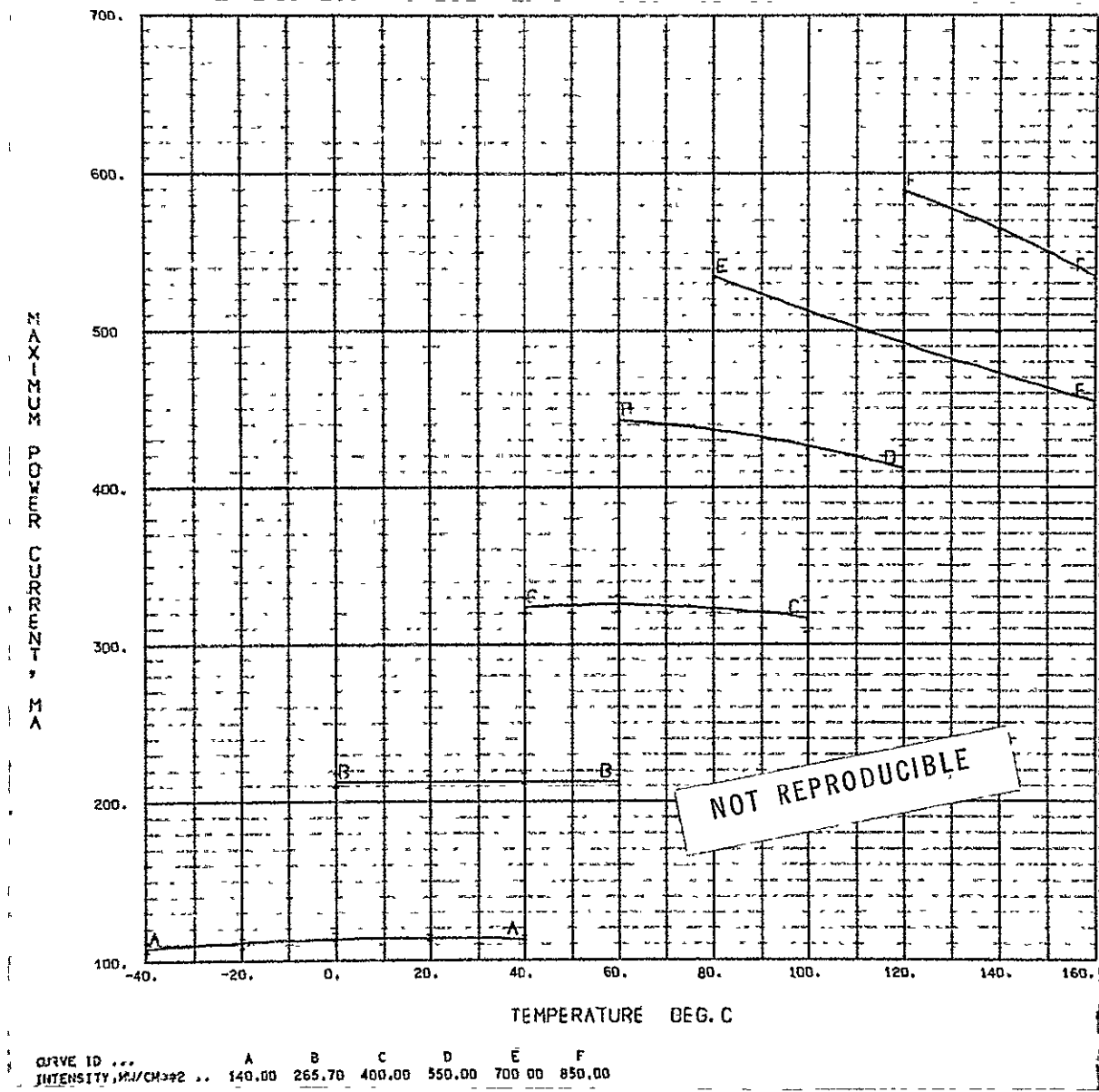


Fig. 18 Maximum-power current vs temperature, blue-red filter on 2 ohm-cm cell

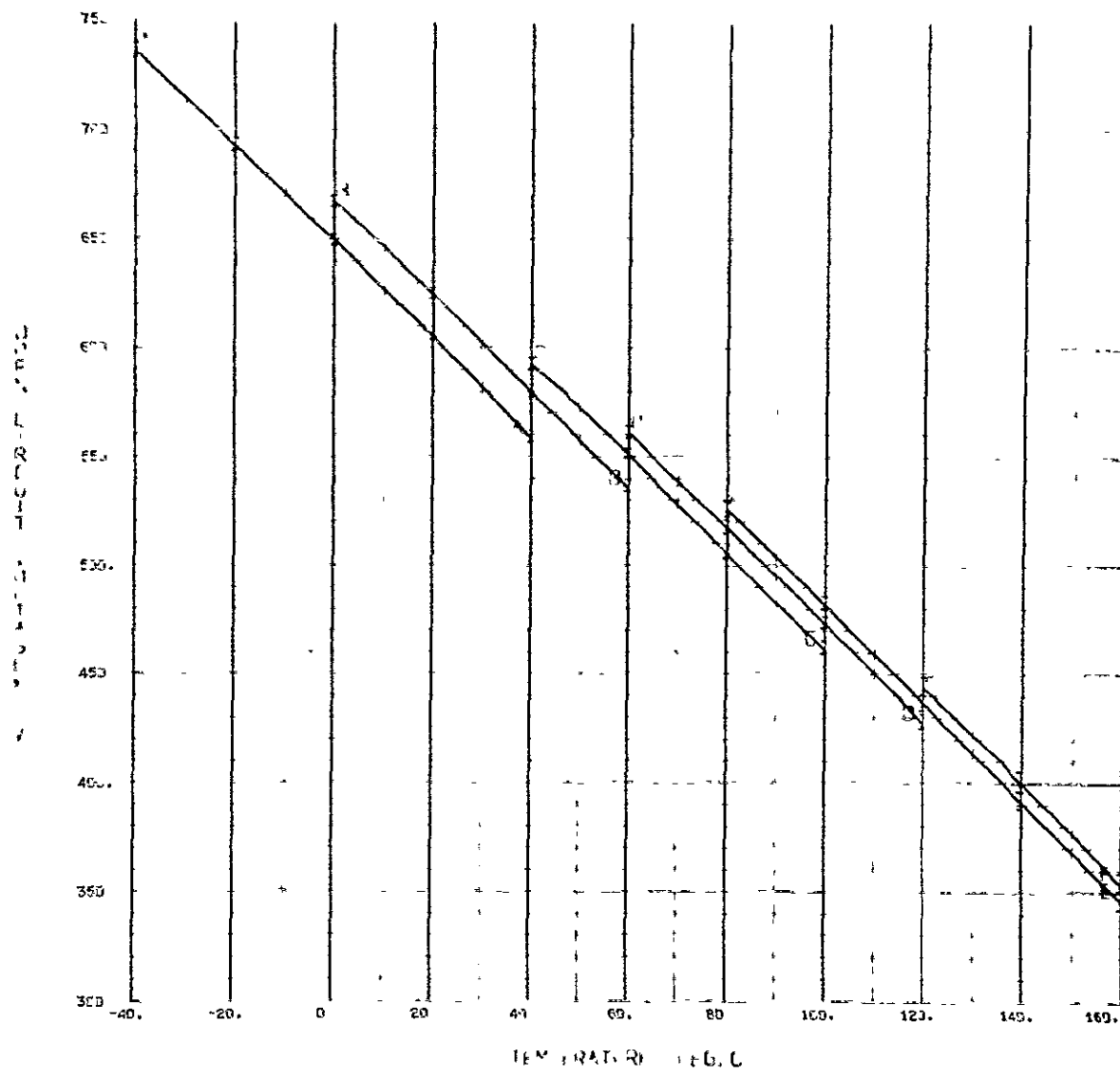


Fig. 19. Open-circuit voltage vs temperature, blue-red filter on
2 ohm-cm cell

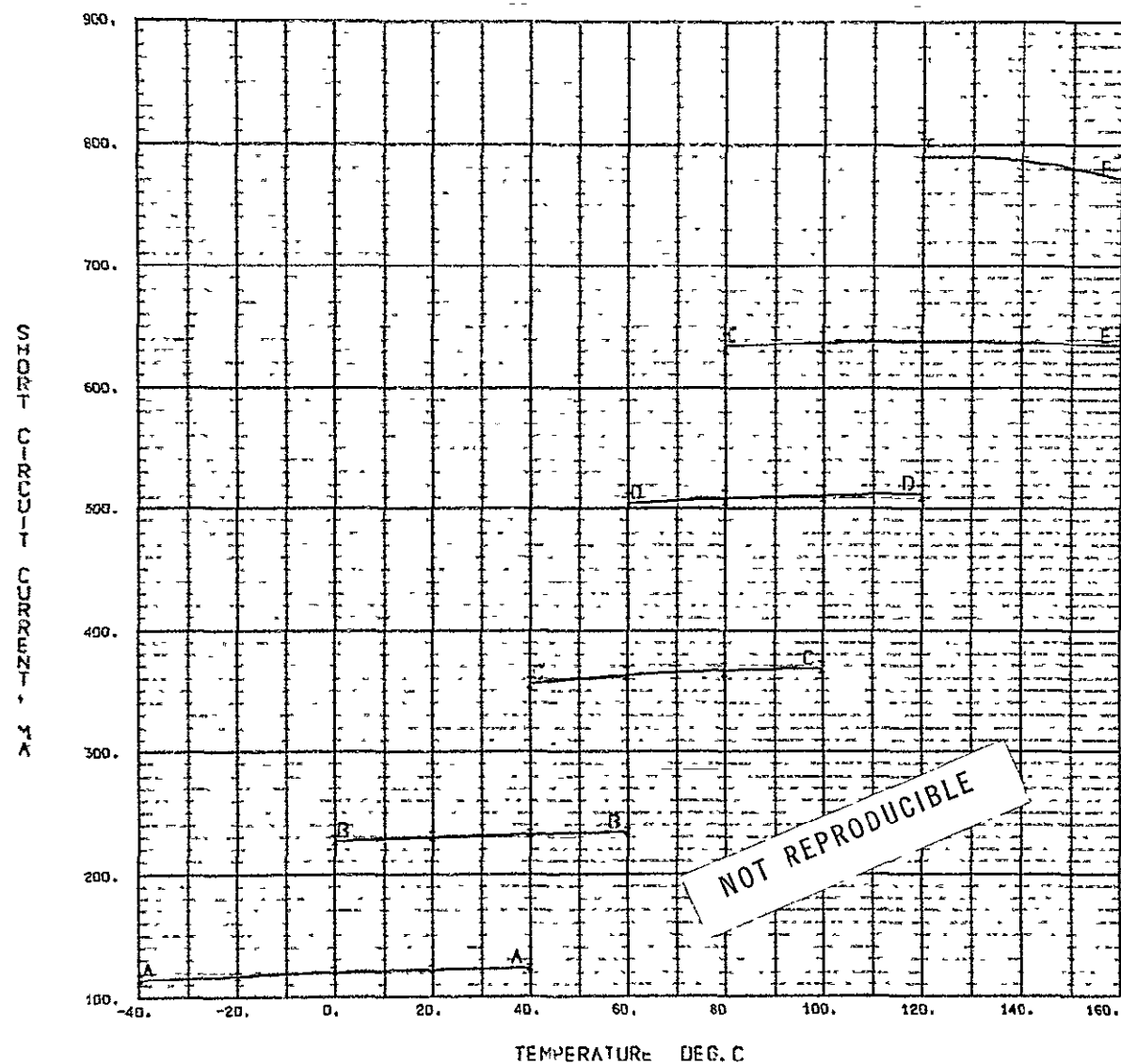


Fig. 20 Short-circuit current vs temperature, blue-red filter on
2 ohm-cm cell

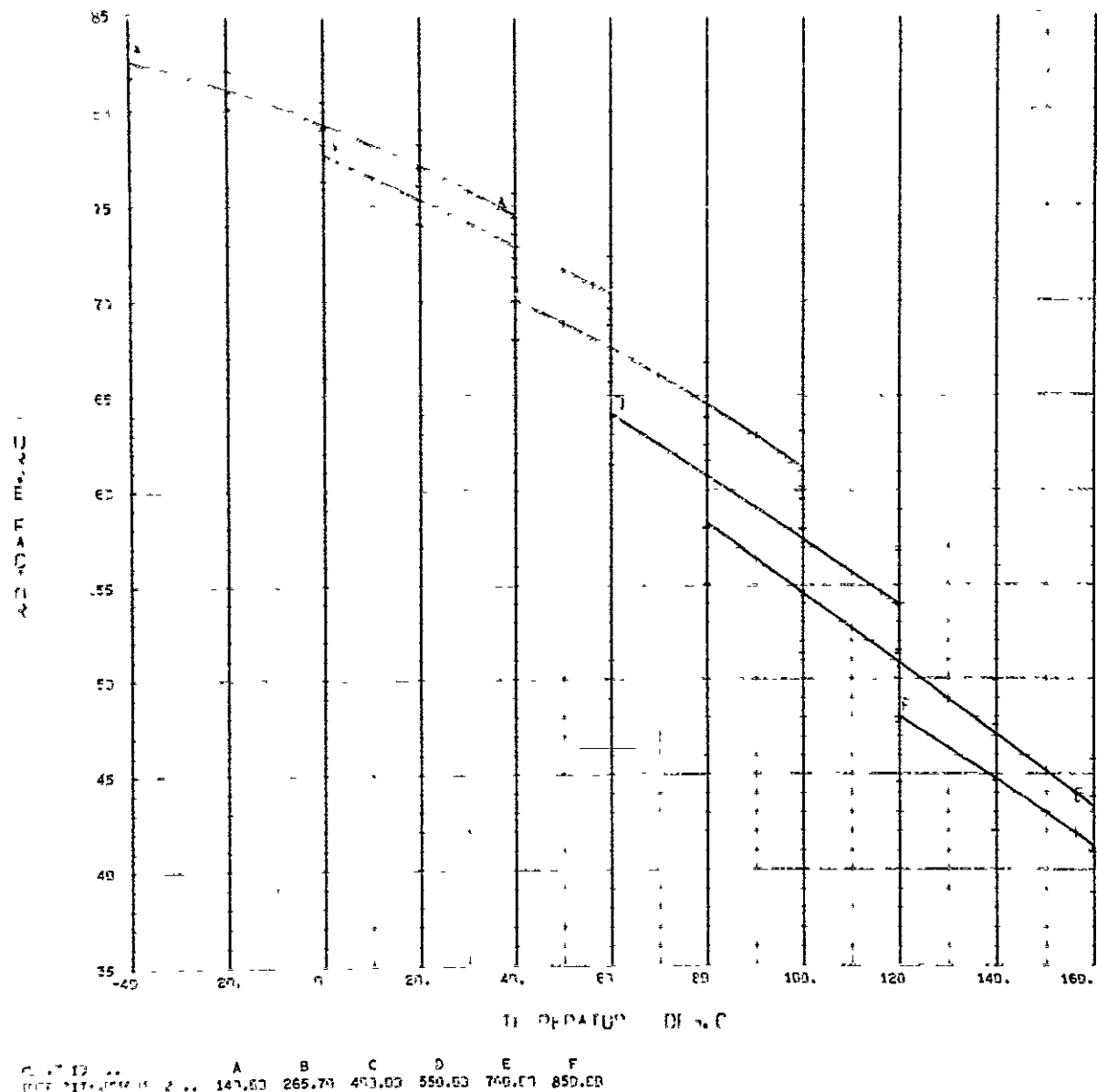


Fig. 21 Curve factor vs temperature, blue-red filter on 2 ohm-cm cell

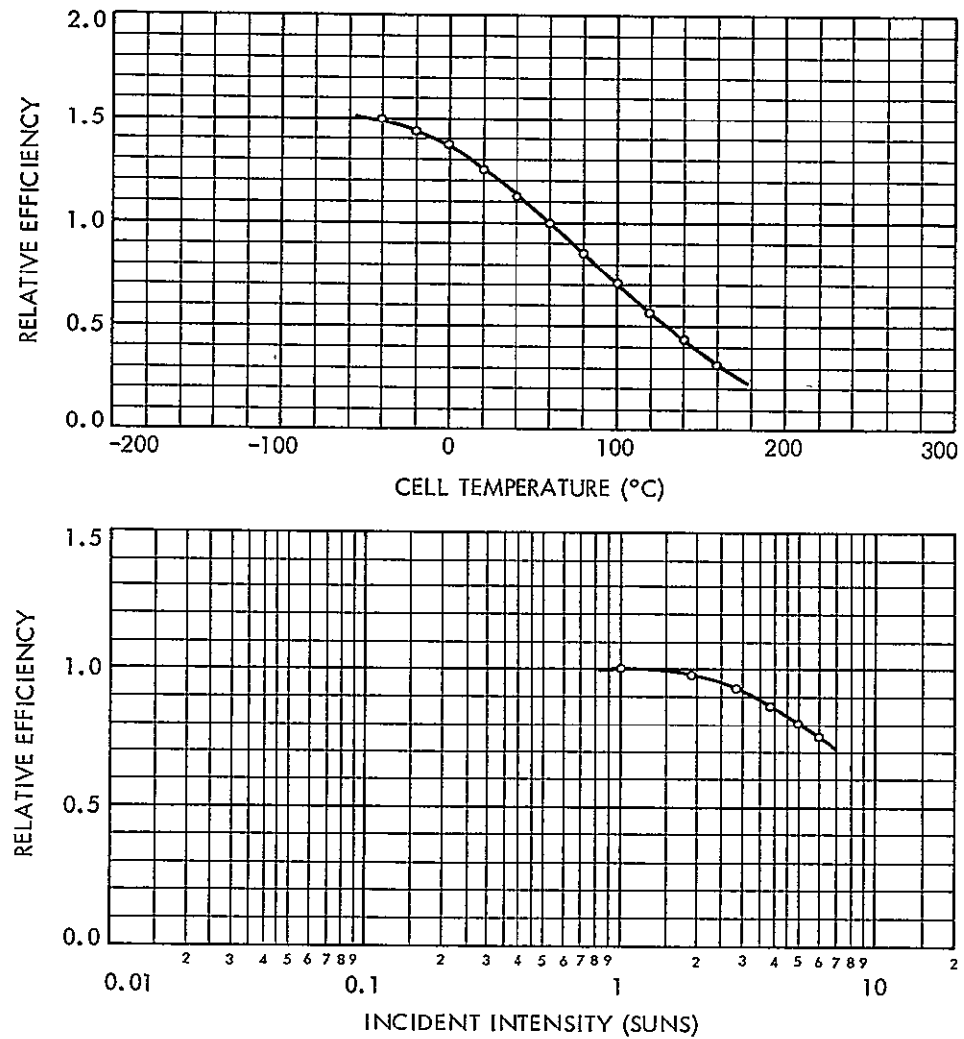


Fig. 22 Cell efficiency vs temperature and intensity, blue-red filter on 10 ohm-cm cell

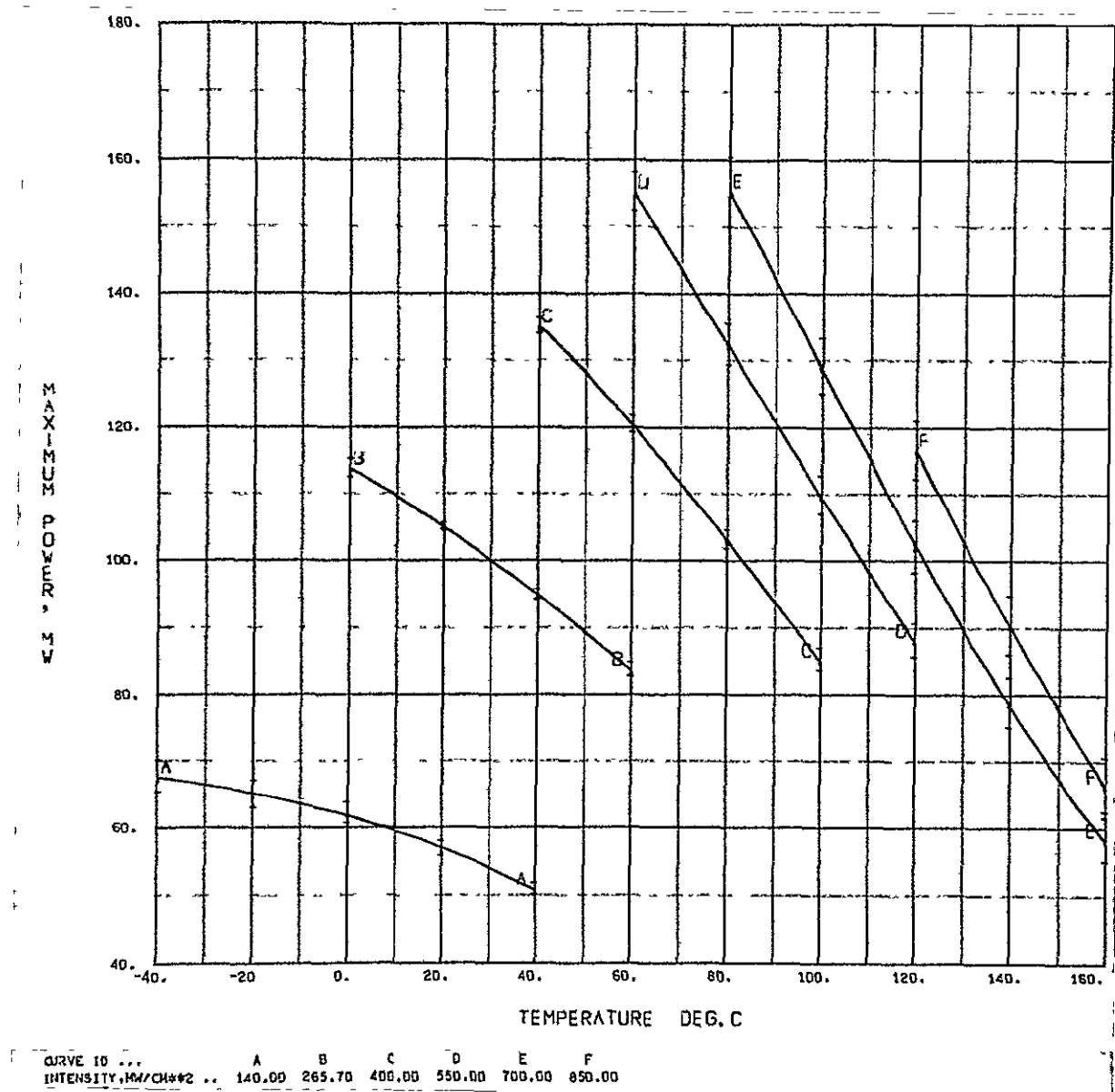


Fig 23 Maximum power vs temperature, blue-red filter on 10 ohm-cm cell

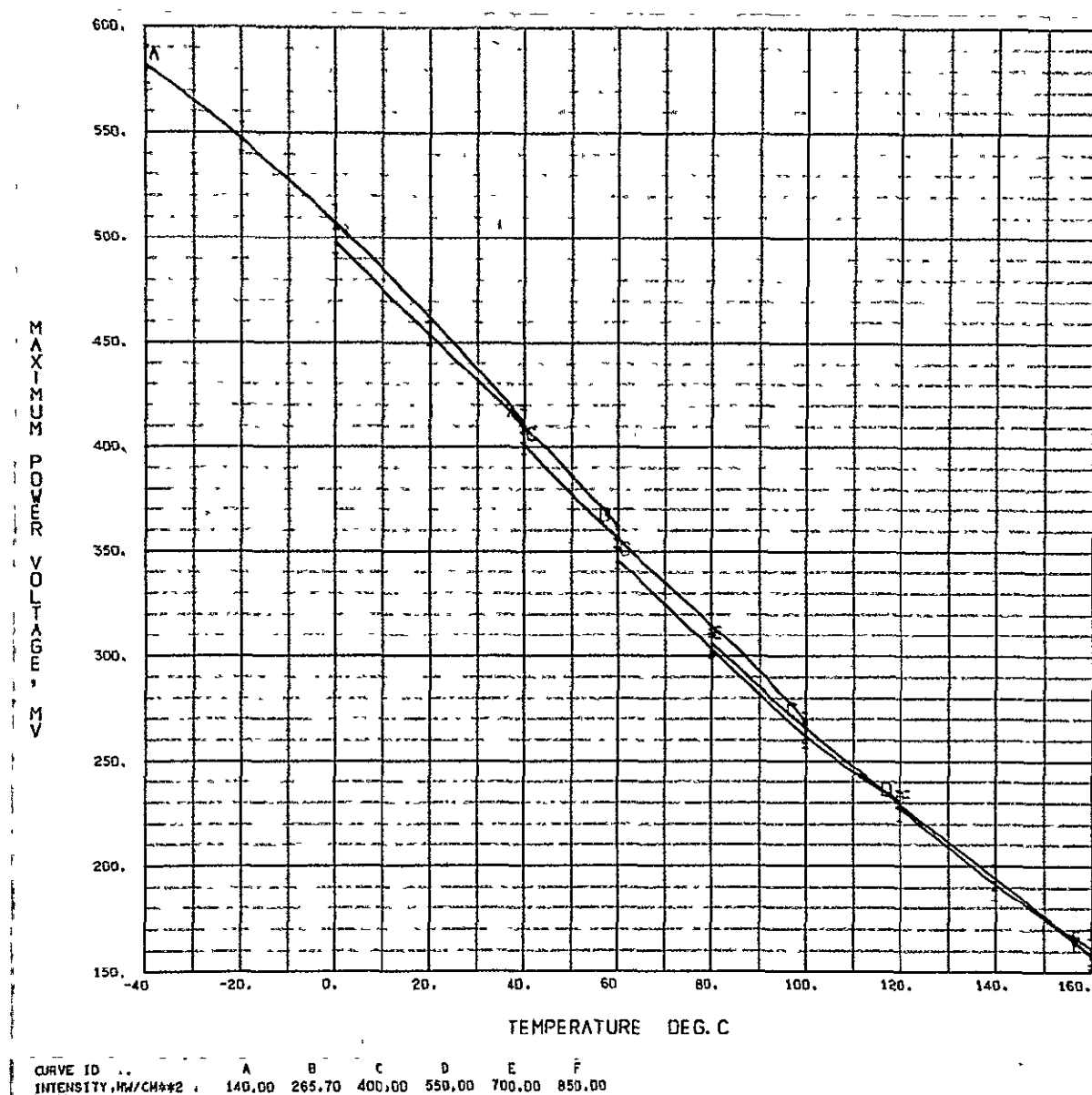


Fig 24. Maximum-power voltage vs temperature, blue-red filter on 10 ohm-cm cell

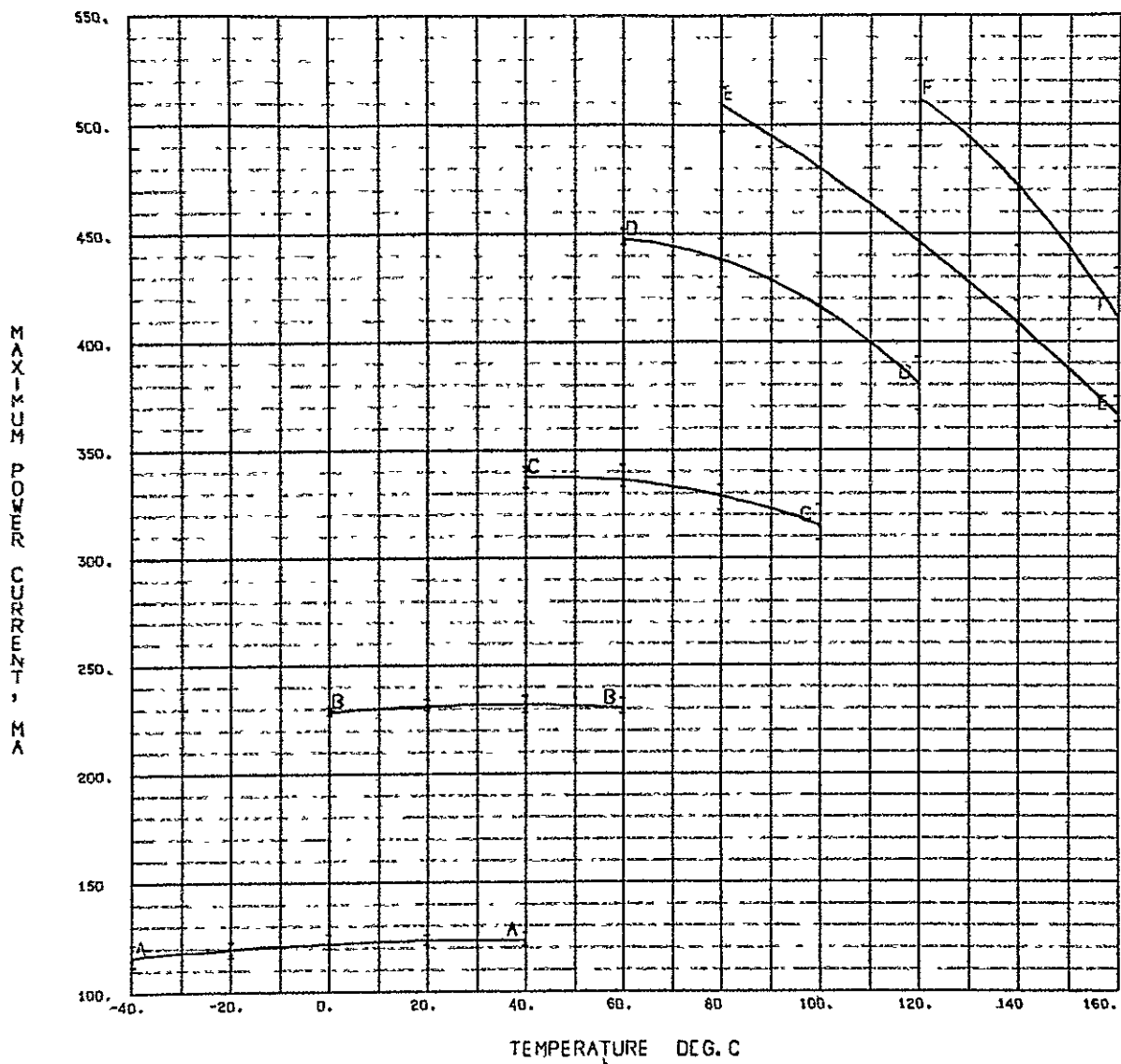


Fig. 25. Maximum-power current vs temperature, blue-red filter on 10 ohm-cm cell

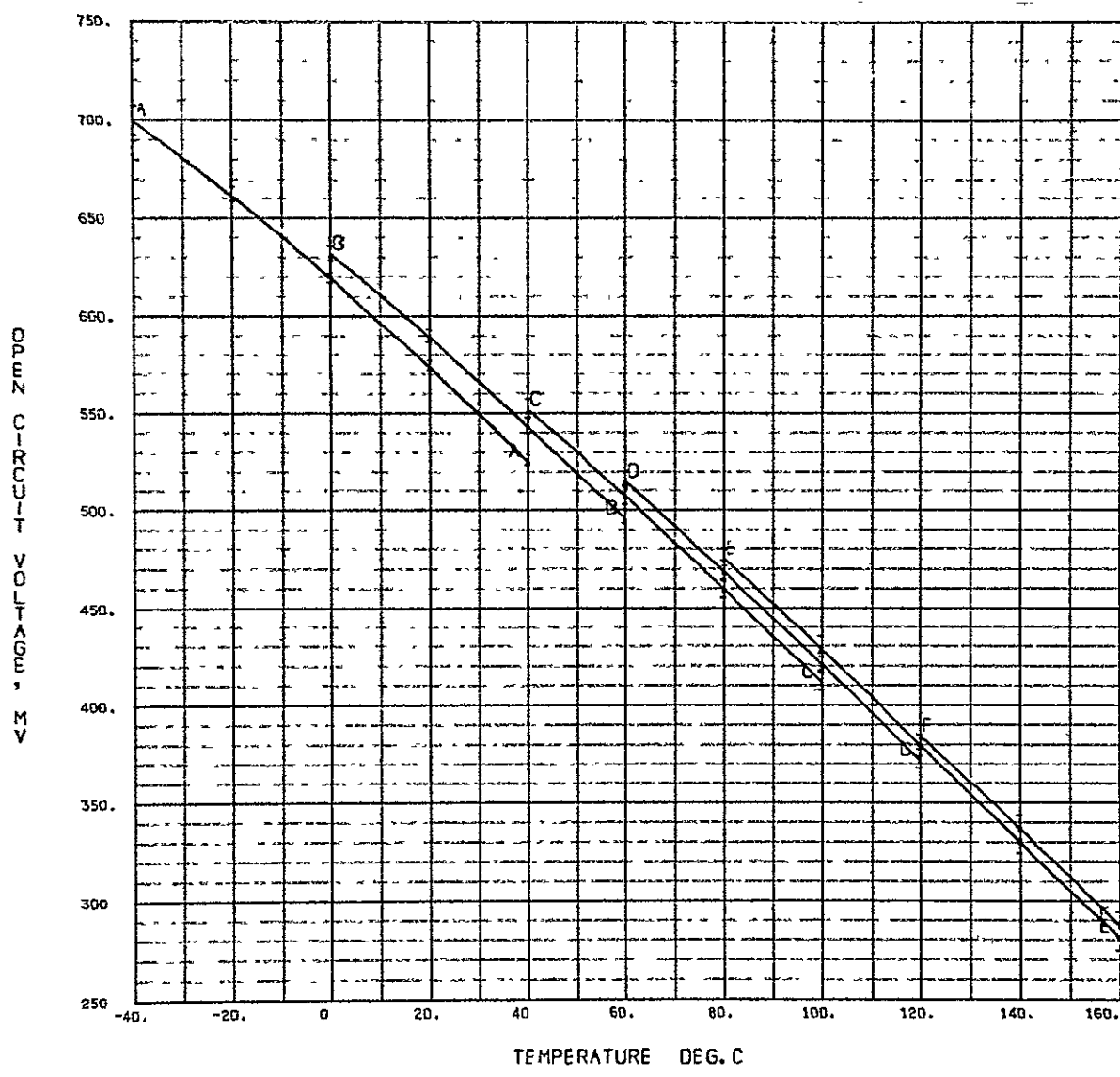


Fig. 26. Open-circuit voltage vs temperature, blue-red filter on 10 ohm-cm cell

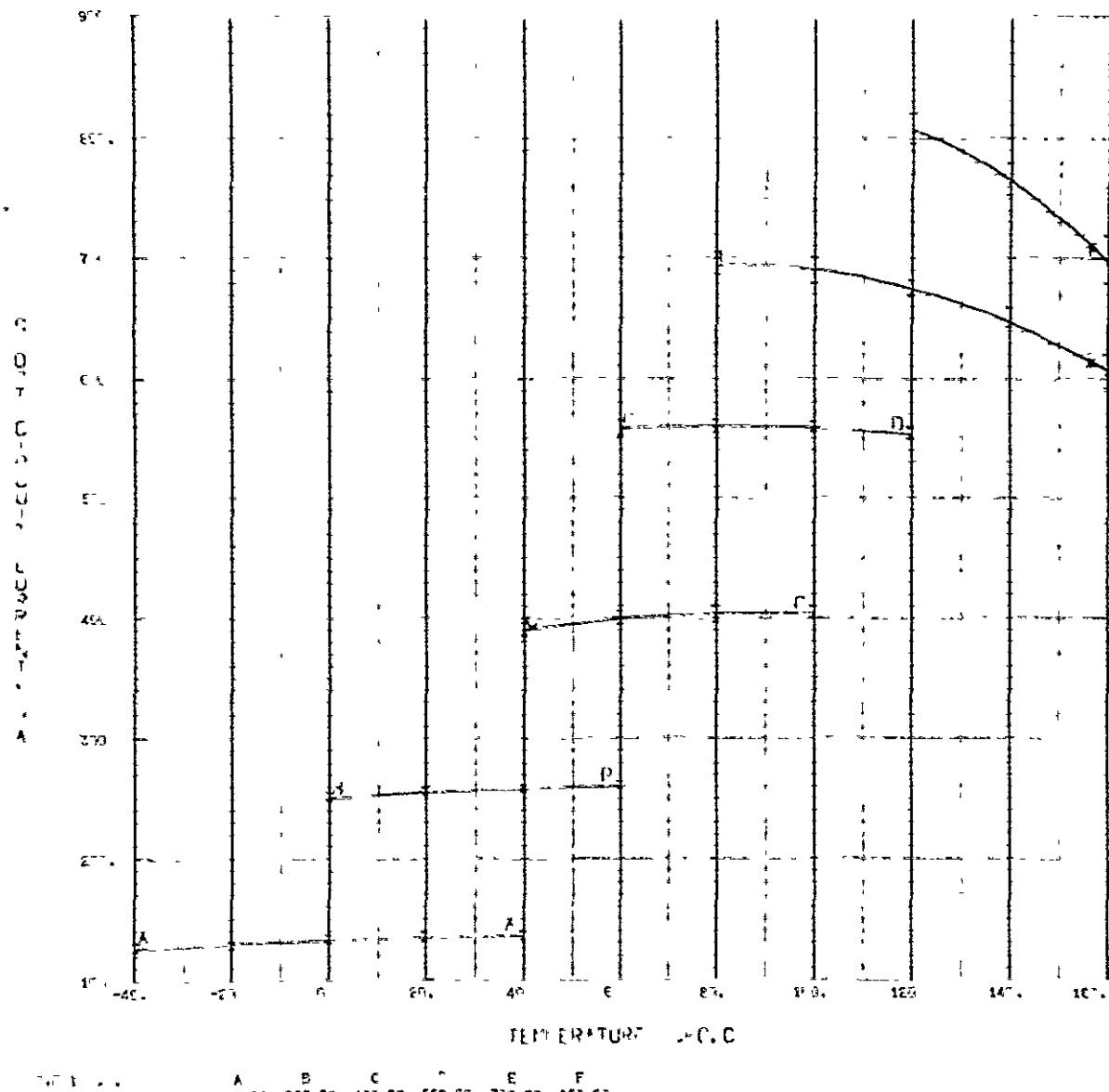


Fig. 27 Short-circuit current vs temperature, blue-red filter on
10 ohm-cm cell

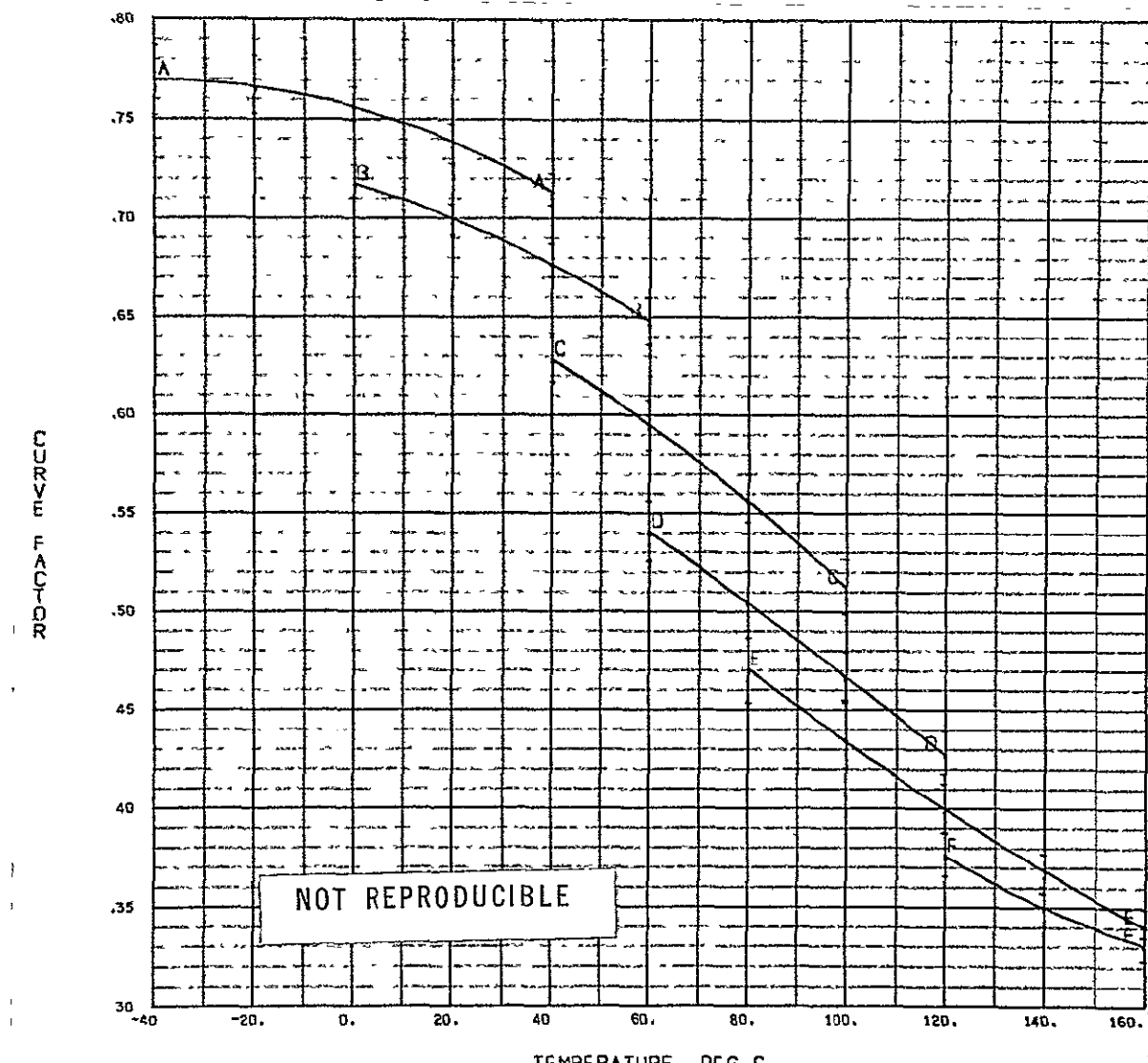


Fig. 28 Curve factor vs temperature, blue-red filter on 10 ohm-cm cell

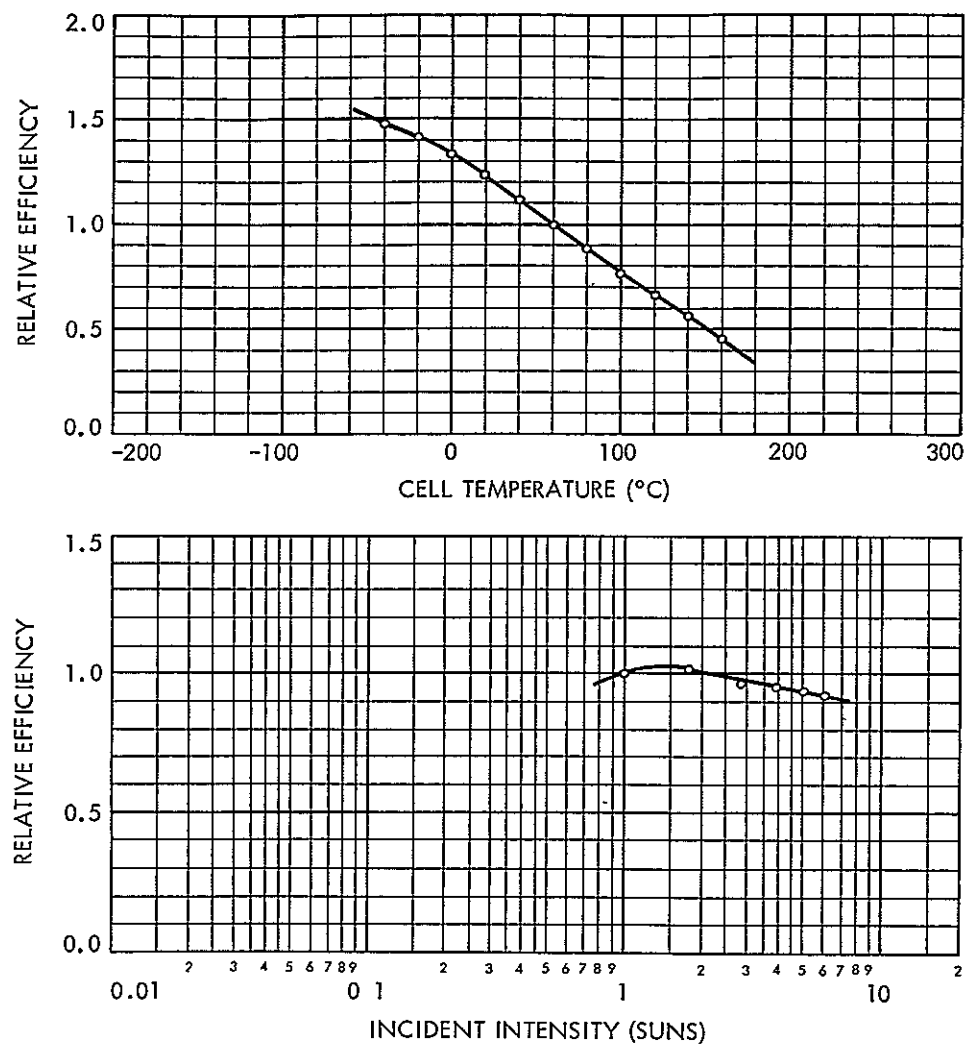


Fig. 29. Cell efficiency vs temperature and intensity, 4024 filter on 2 ohm-cm cell

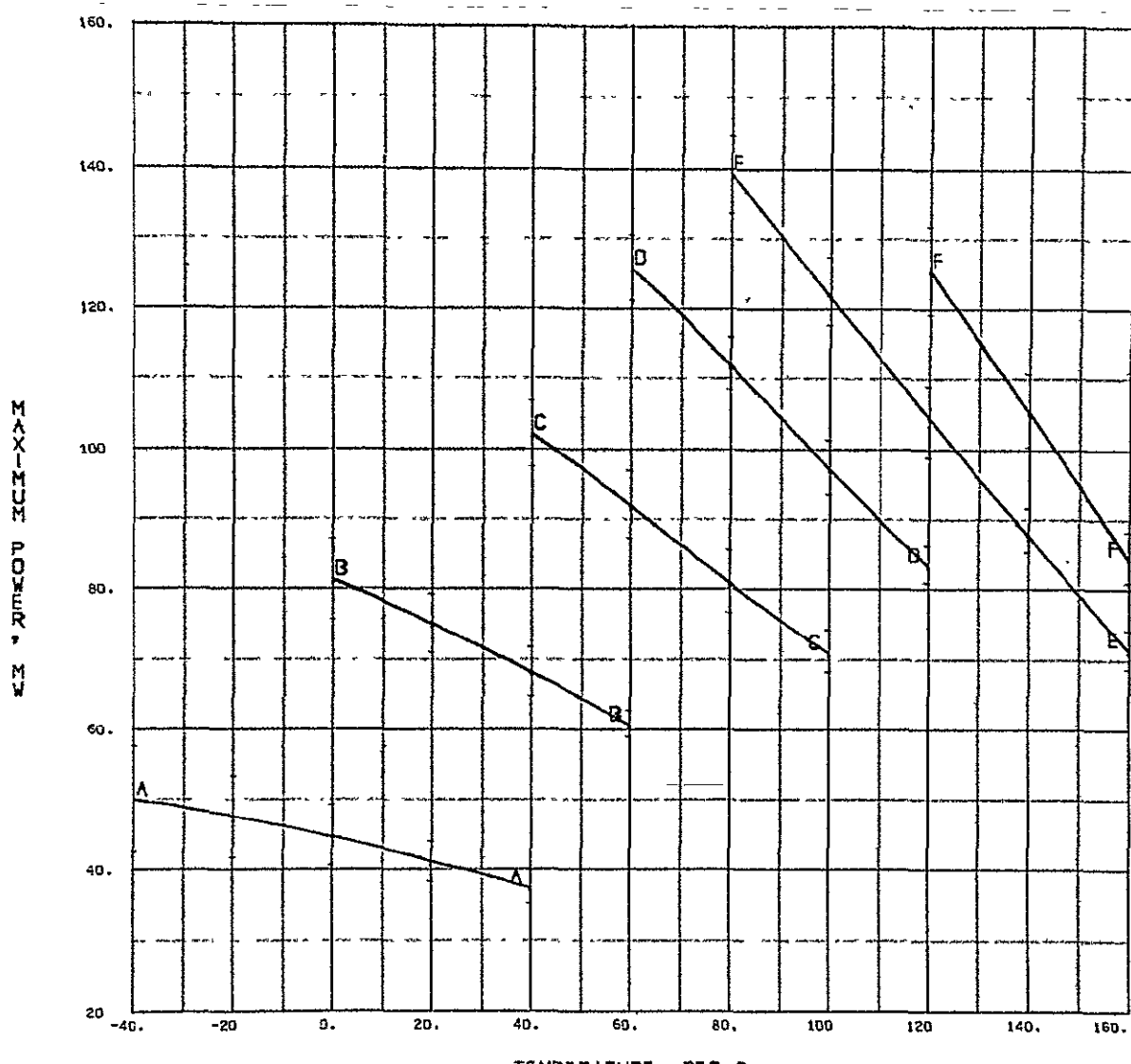


Fig. 30. Maximum power vs temperature, 4024 filter on 2 ohm-cm cell

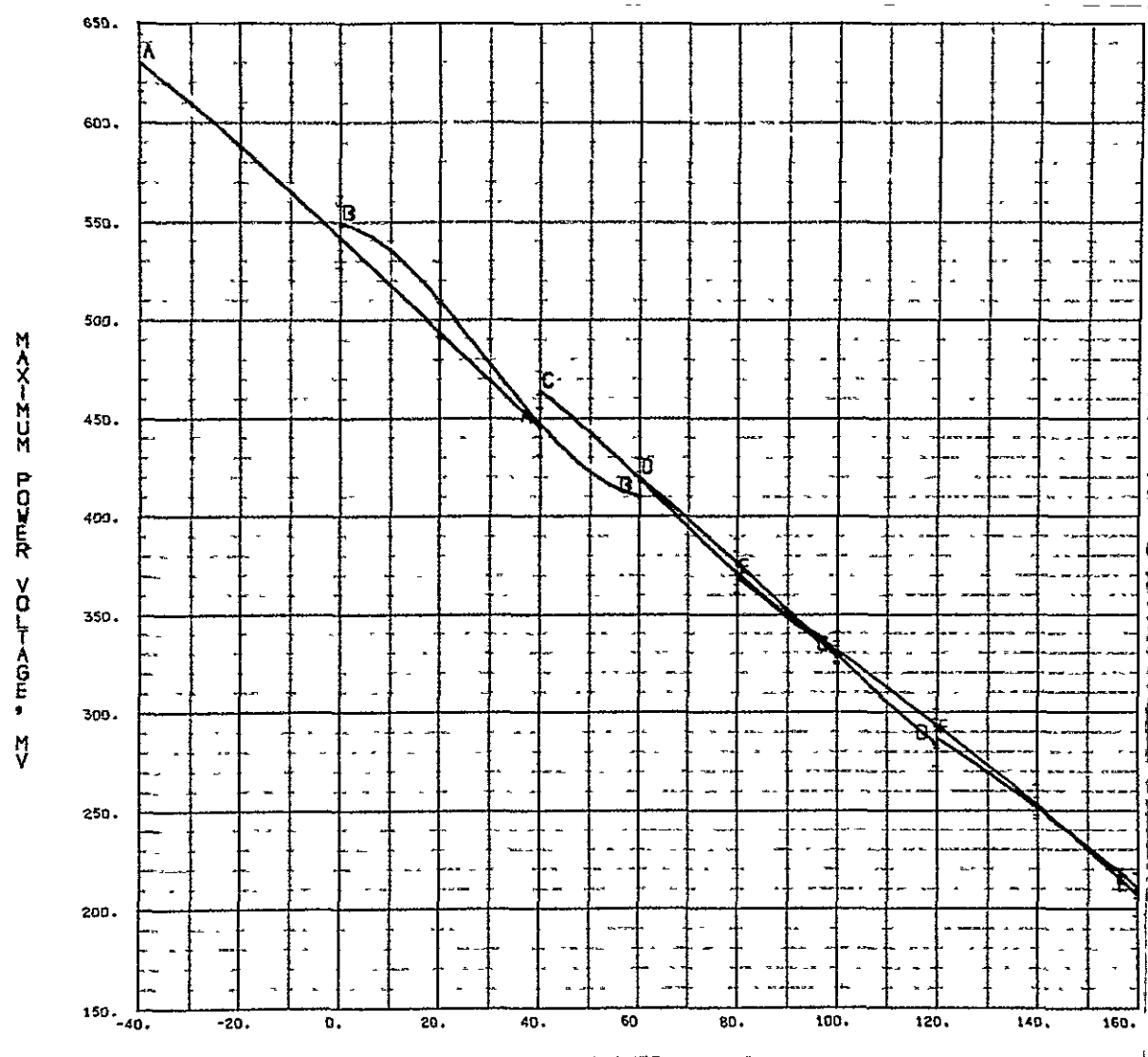


Fig. 31 Maximum-power voltage, 4024 filter on 2 ohm-cm cell

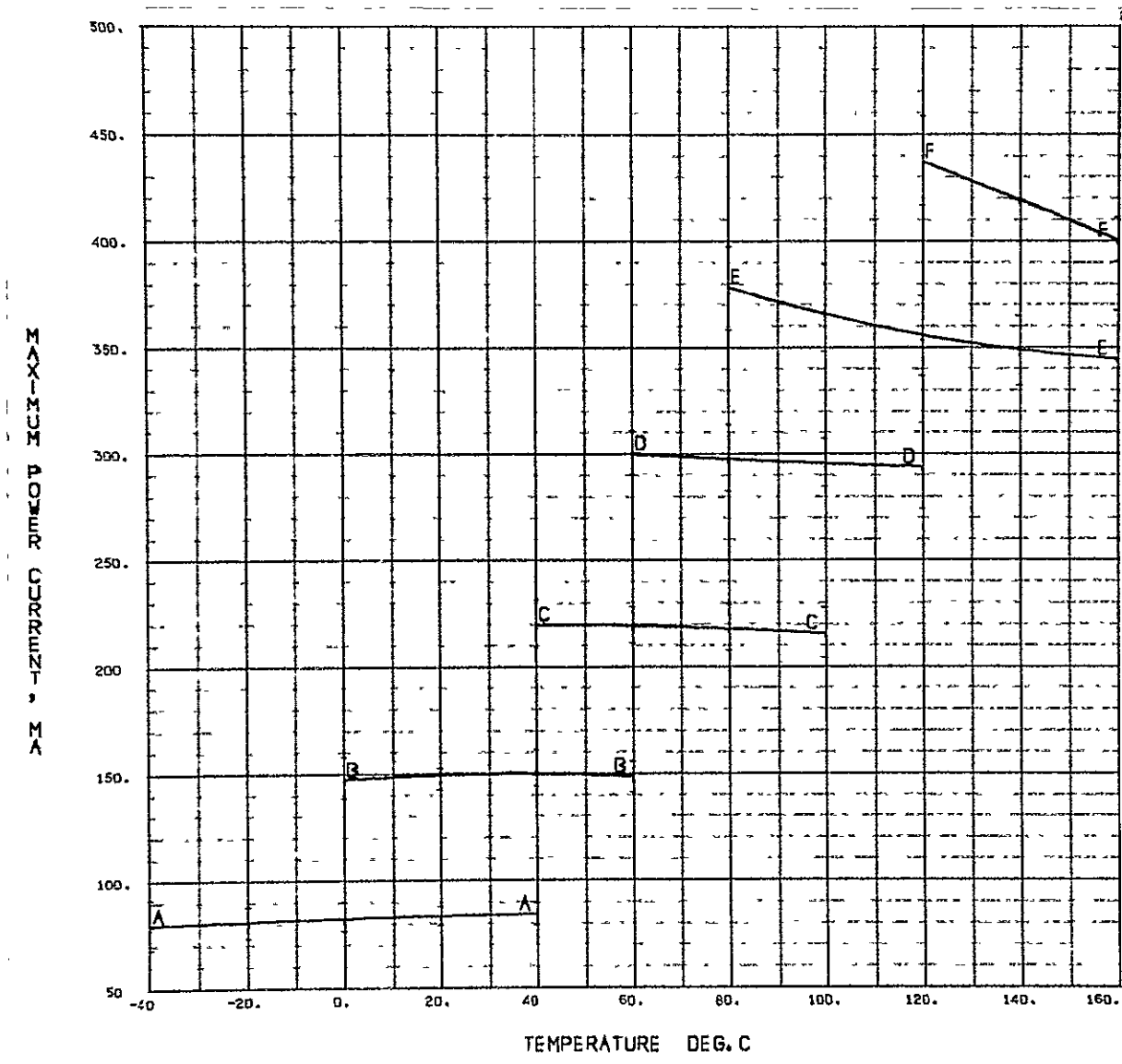


Fig. 32. Maximum-power current vs temperature, 4024 filter on 2 ohm-cm cell

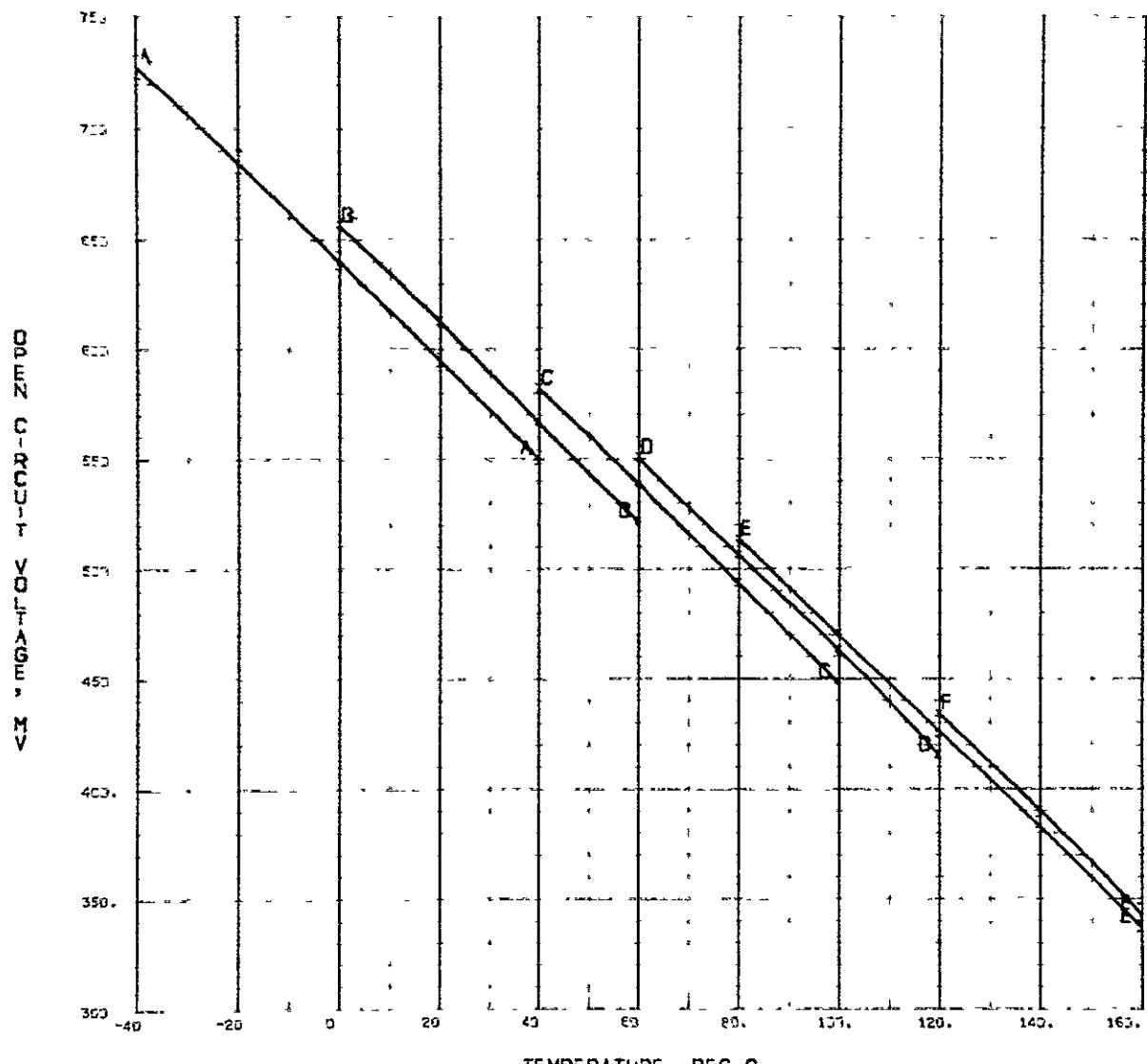


Fig. 33 Open-circuit voltage vs temperature, 4024 filter on 2 ohm-cm cell

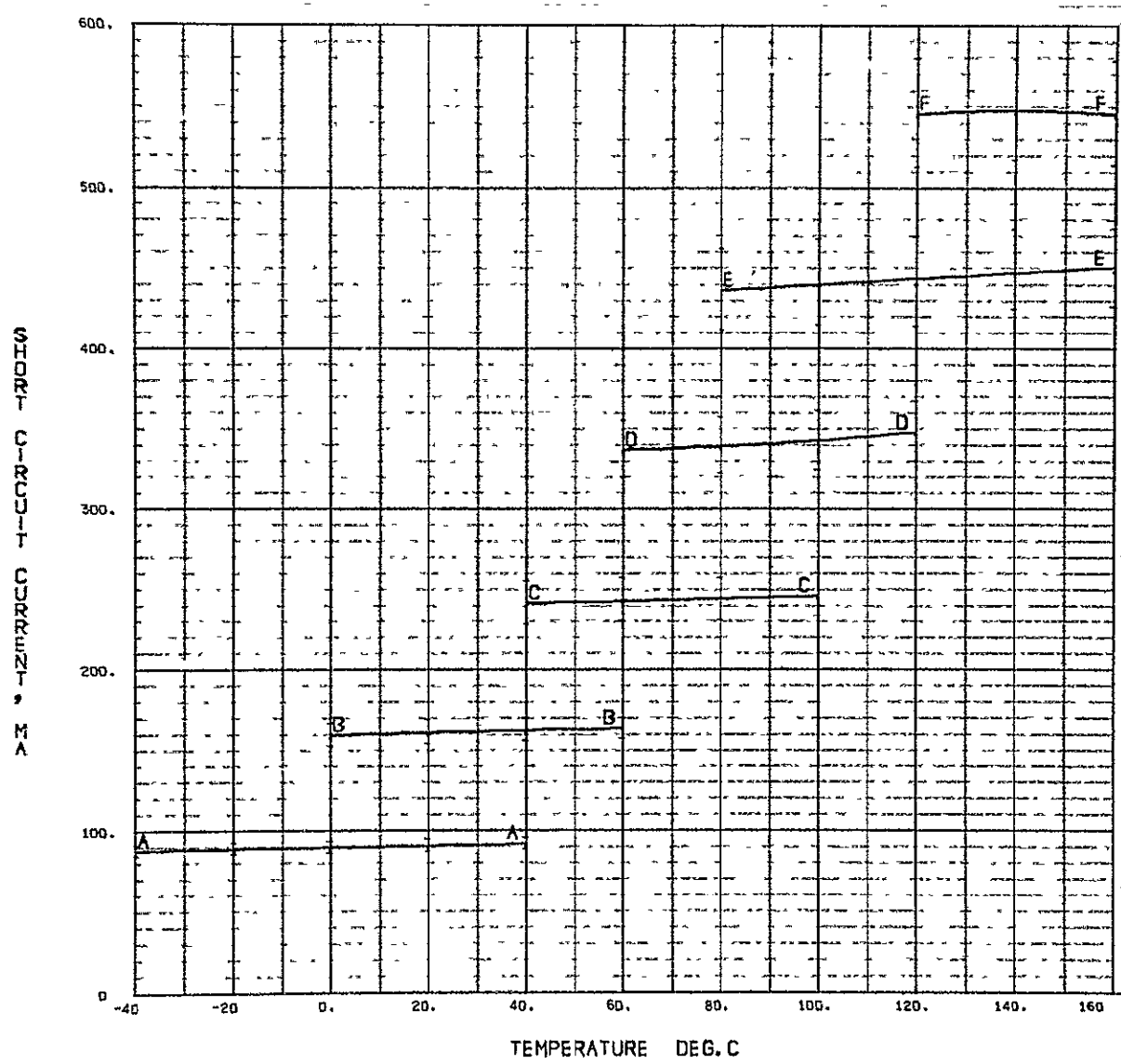


Fig. 34 Short-circuit current vs temperature, 4024 filter on 2 ohm-cm cell

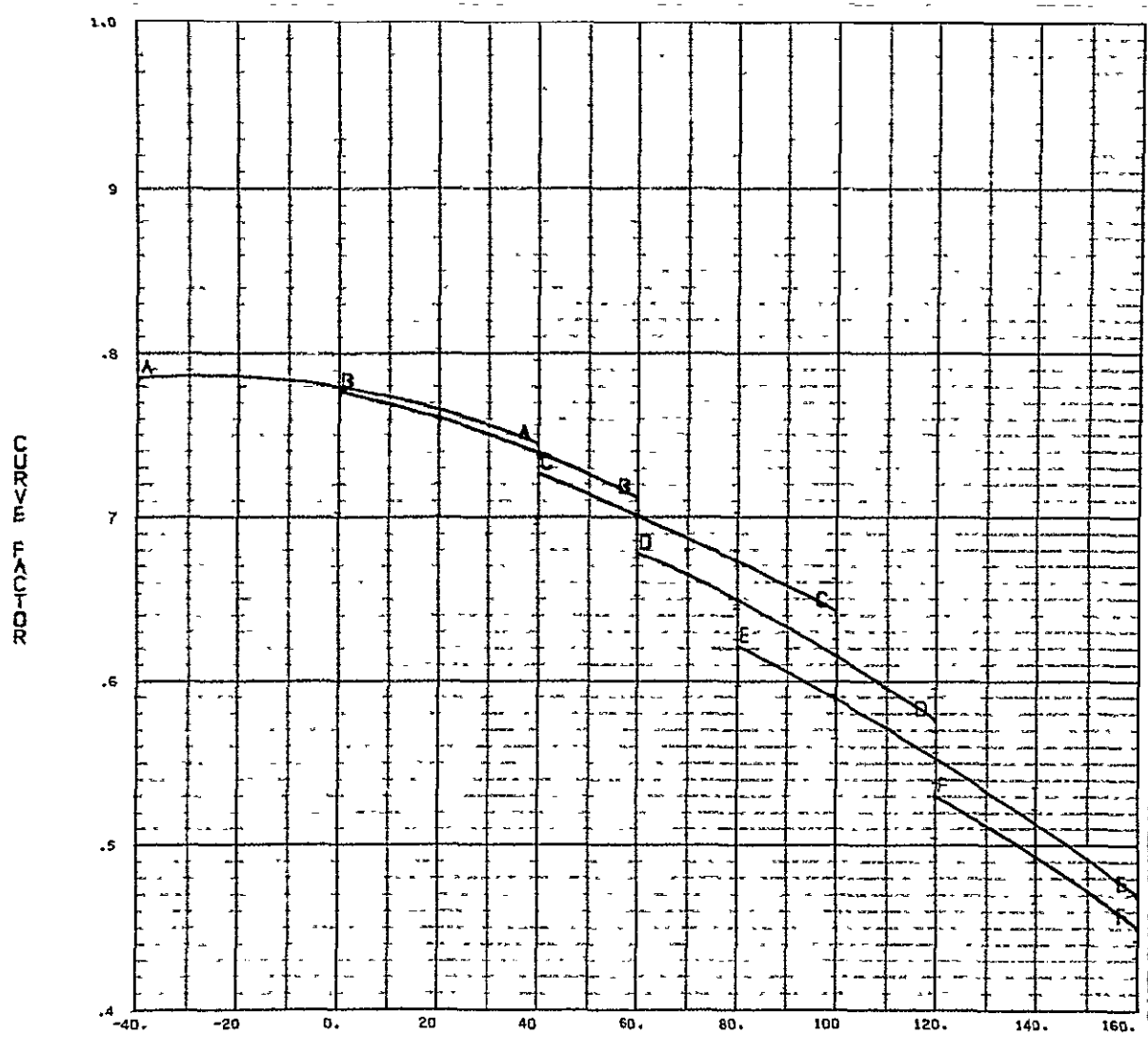


Fig. 35 Curve factor vs temperature, 4024 filter on 2 ohm-cm cell

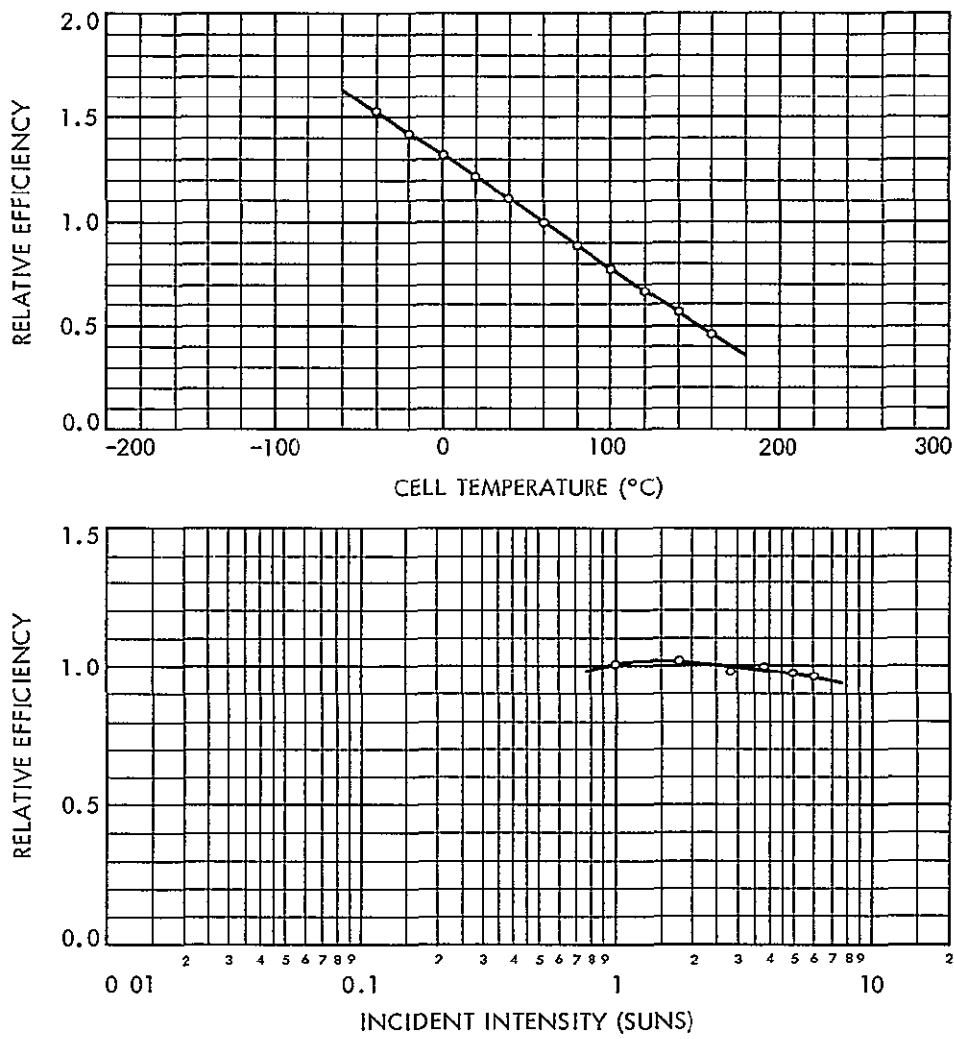


Fig. 36 Cell efficiency vs temperature and intensity, 4025 filter on
2 ohm-cm cell

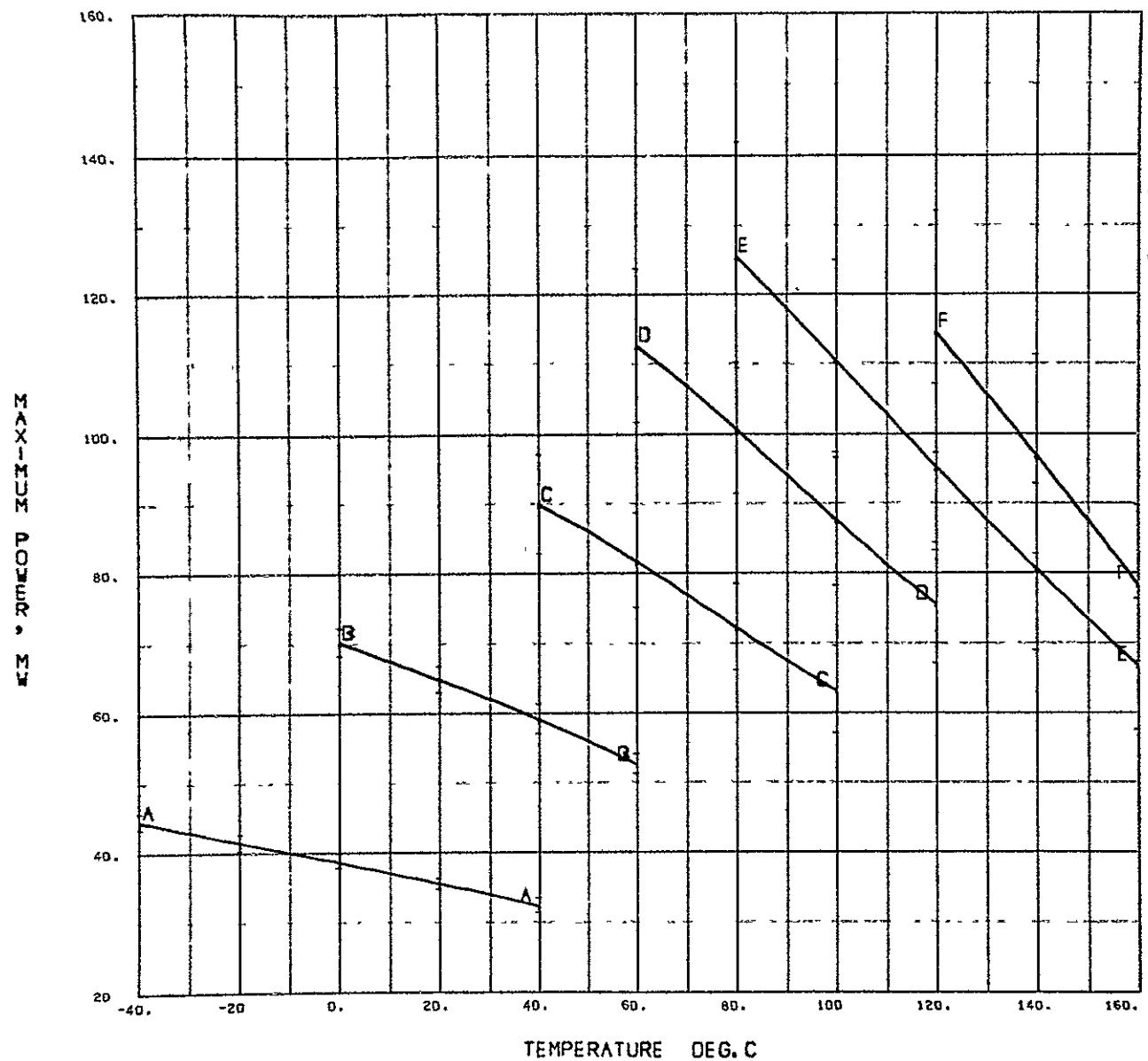


Fig. 37. Maximum power vs temperature, 4025 filter on 2 ohm-cm cell

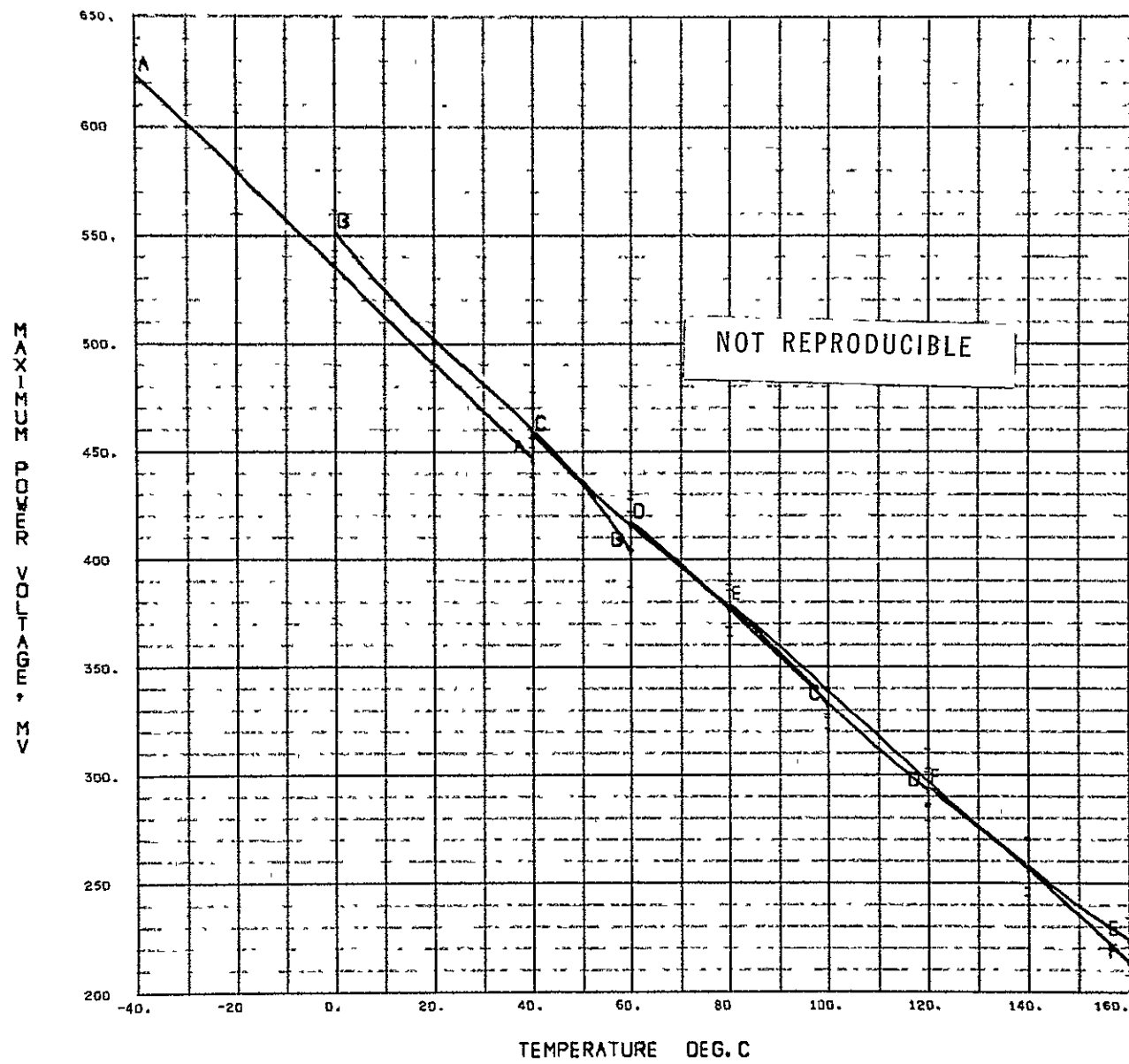
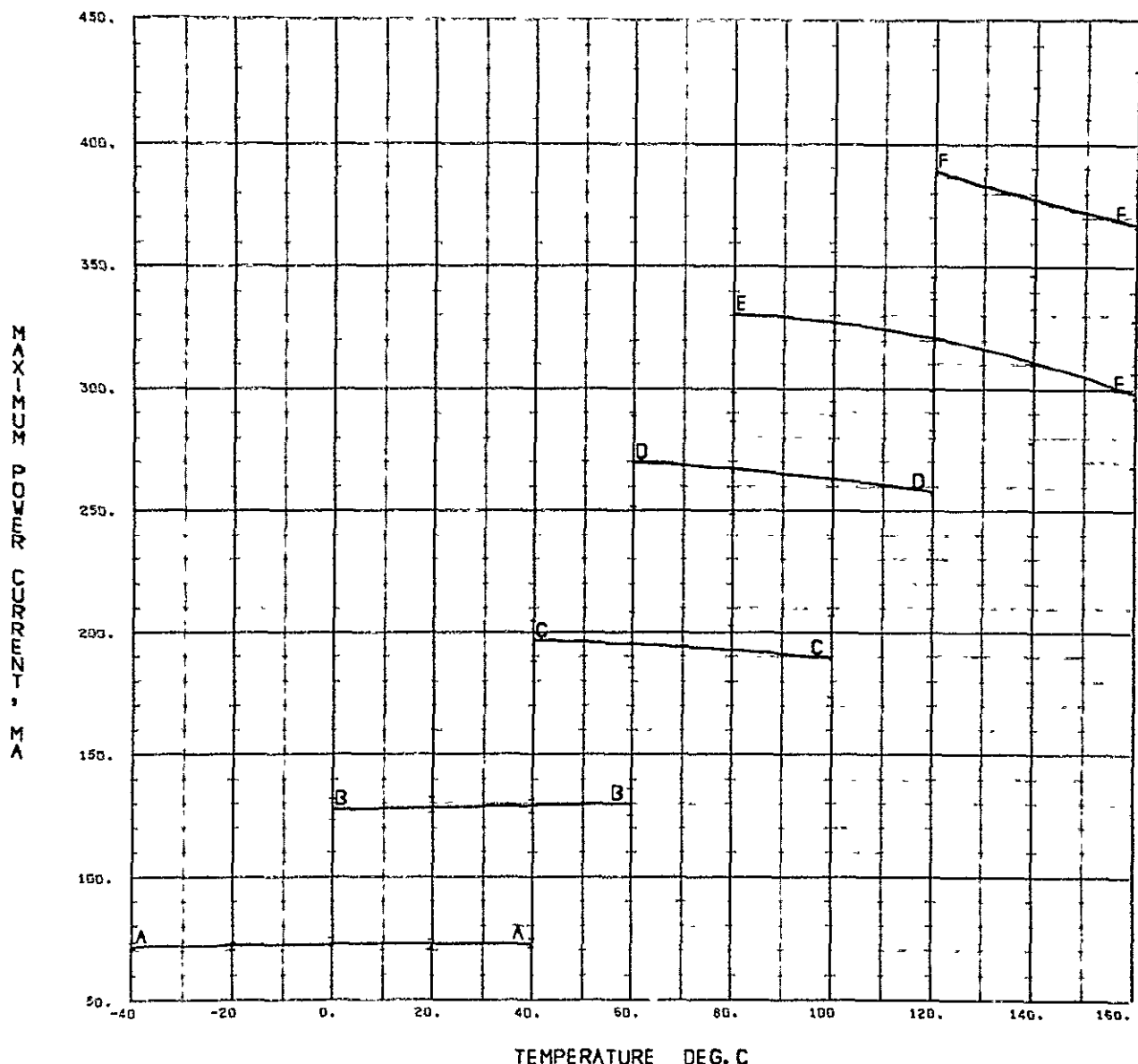
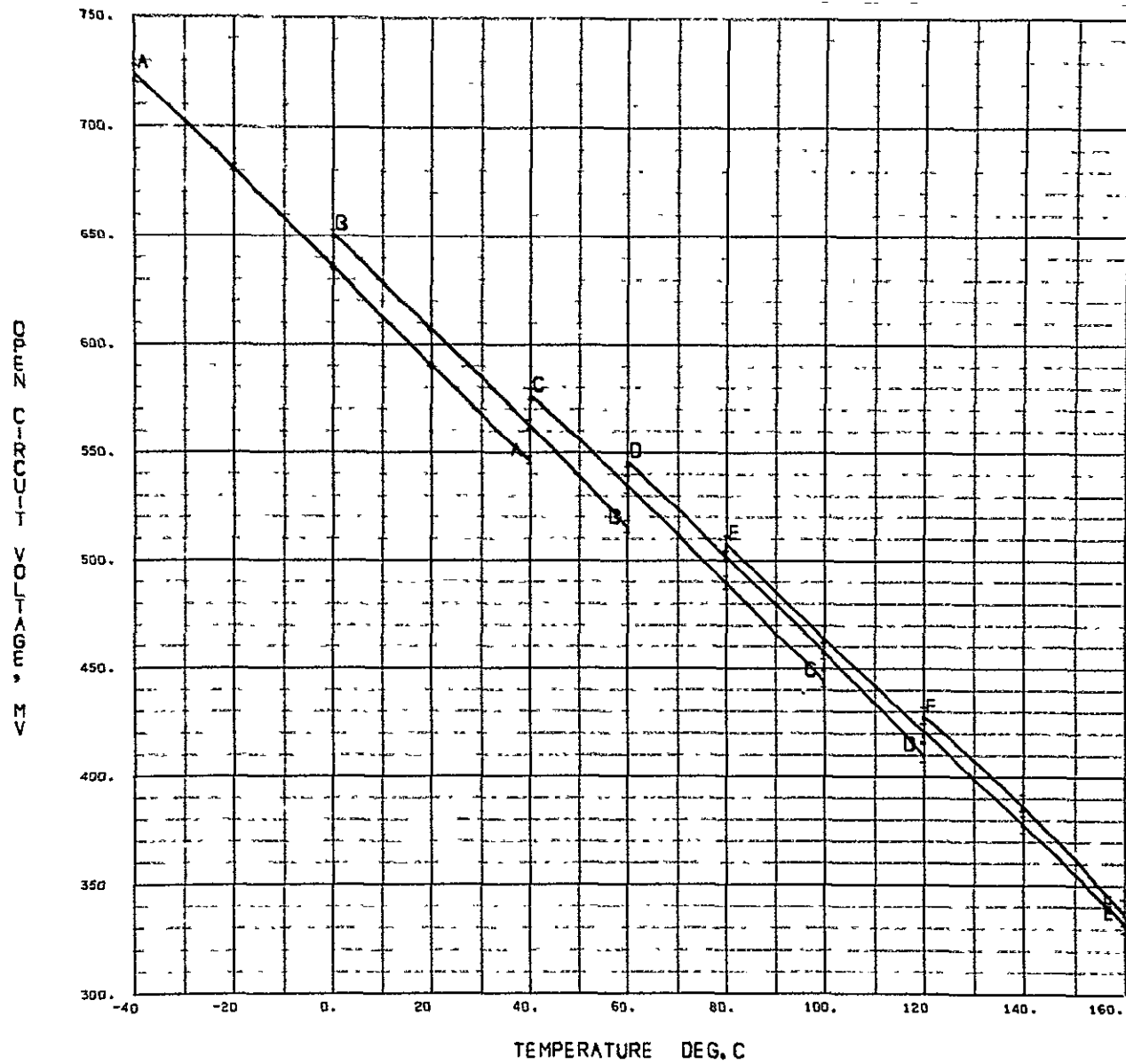


Fig. 38. Maximum-power voltage vs temperature, 4025 filter on 2 ohm-cm cell



CURVE ID . A B C D E F
INTENSITY, HH/CH#2 .. 140.00 250.00 400.00 550.00 700.00 850.00

Fig. 39. Maximum-power current vs temperature, 4025 filter on 2 ohm-cm cell



CURVE ID .. A B C D E F
 INTENSITY, MW/CH#2 . 140.00 250.00 400.00 550.00 700.00 850.00

Fig. 40 Open-circuit voltage vs temperature, 4025 filter on 2 ohm-cm cell

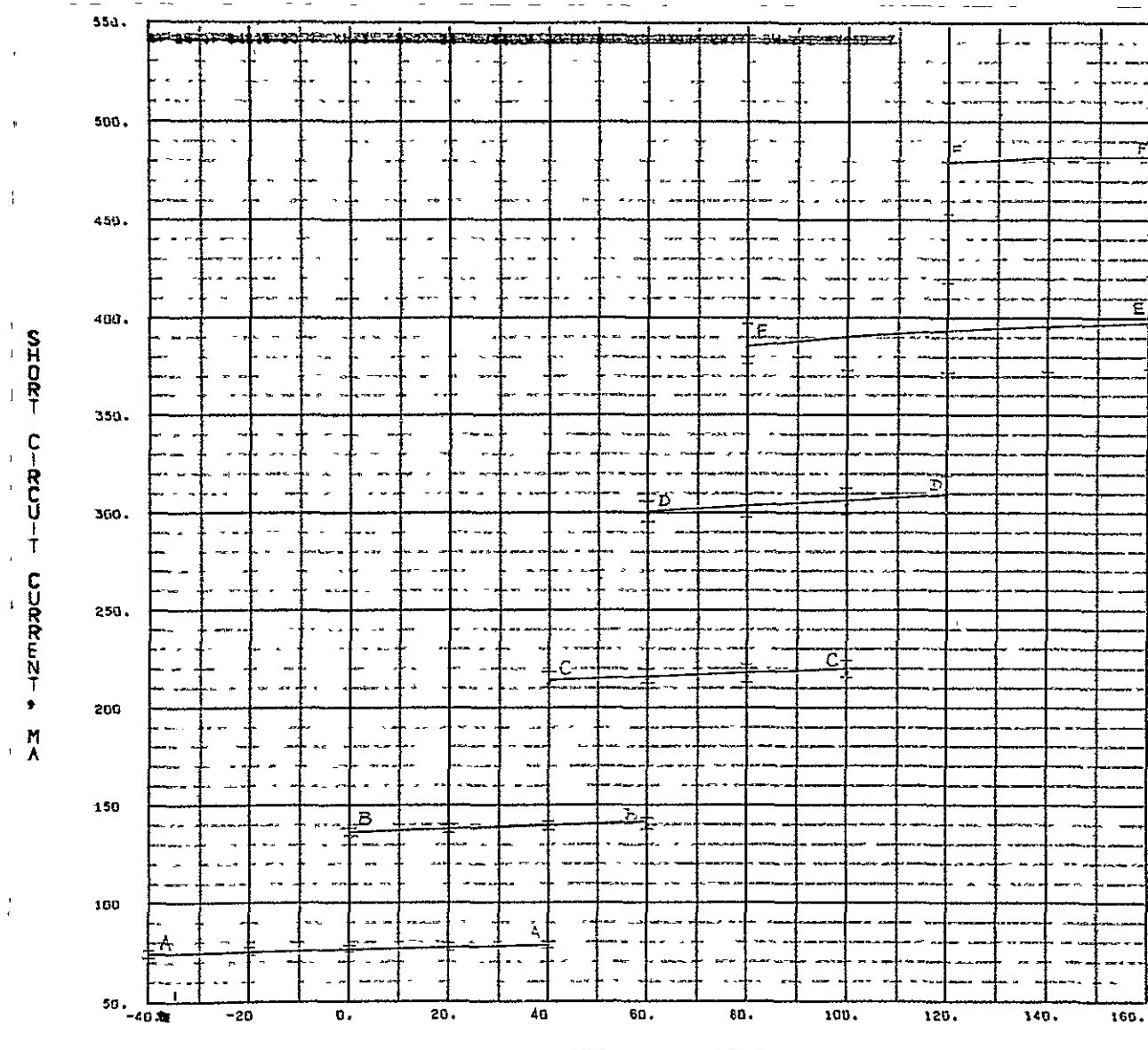


Fig 41. Short-circuit current vs temperature, 4025 filter on 2 ohm-cm cell

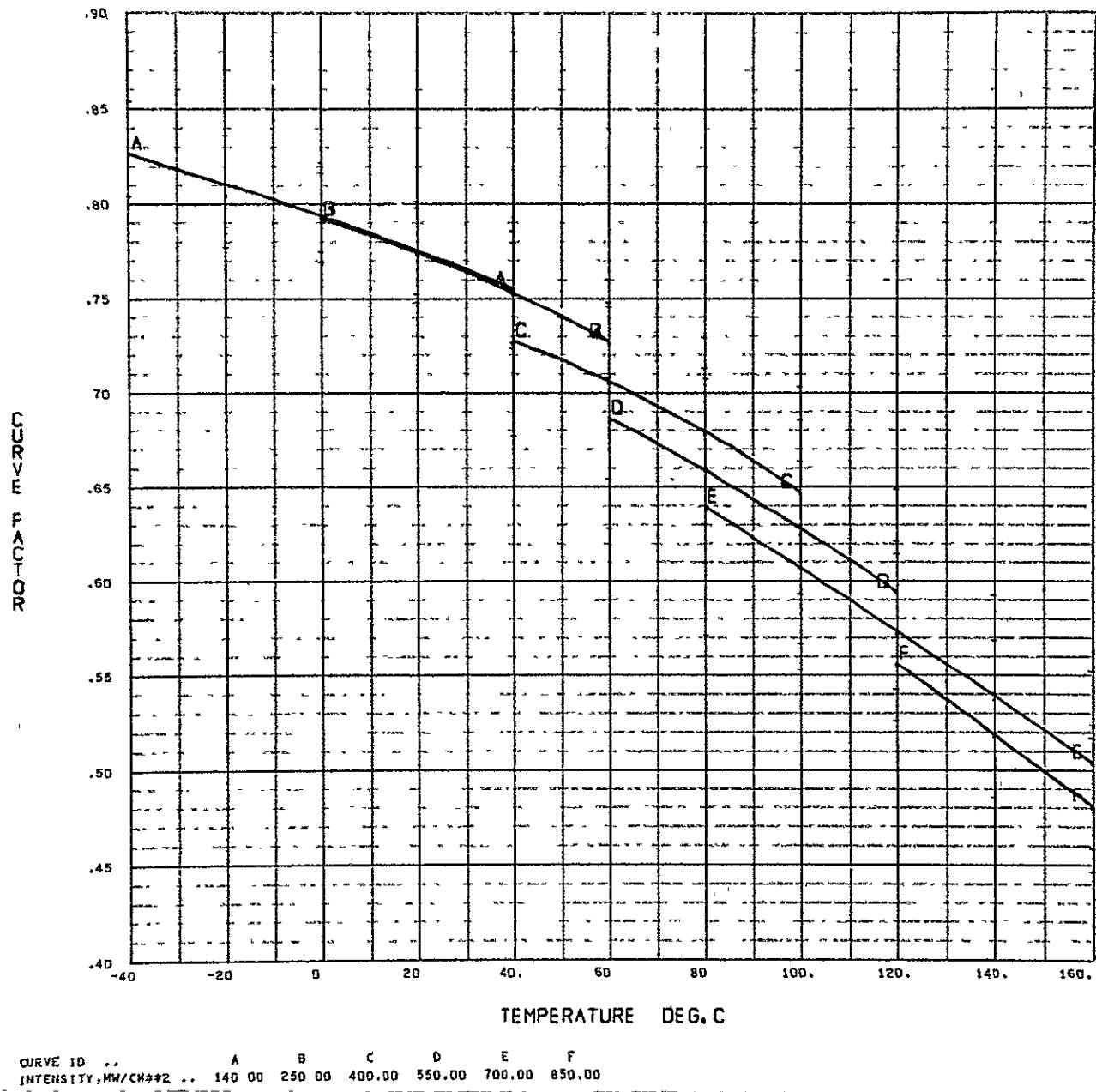


Fig. 42 Curve factor vs temperature, 4025 filter on 2 ohm-cm cell

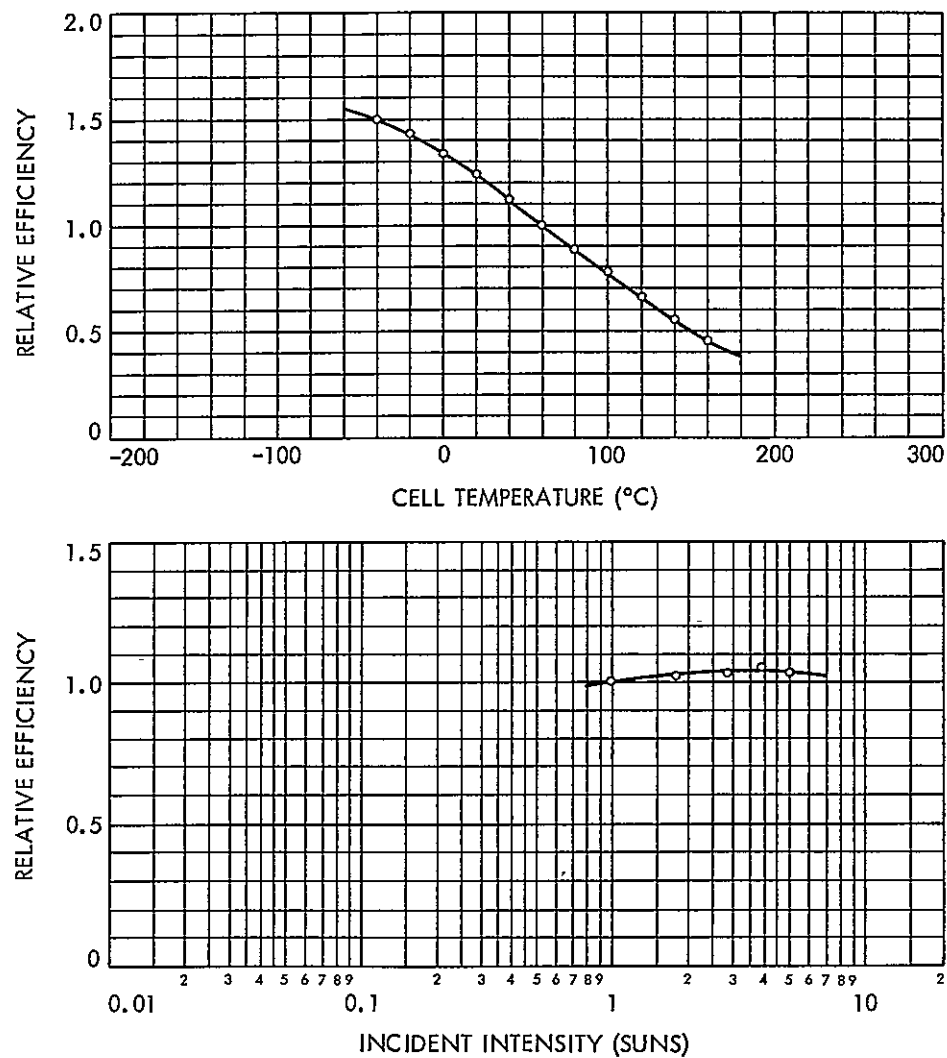


Fig. 43. Cell efficiency vs temperature and intensity, 4026 filter on 2 ohm-cm cell

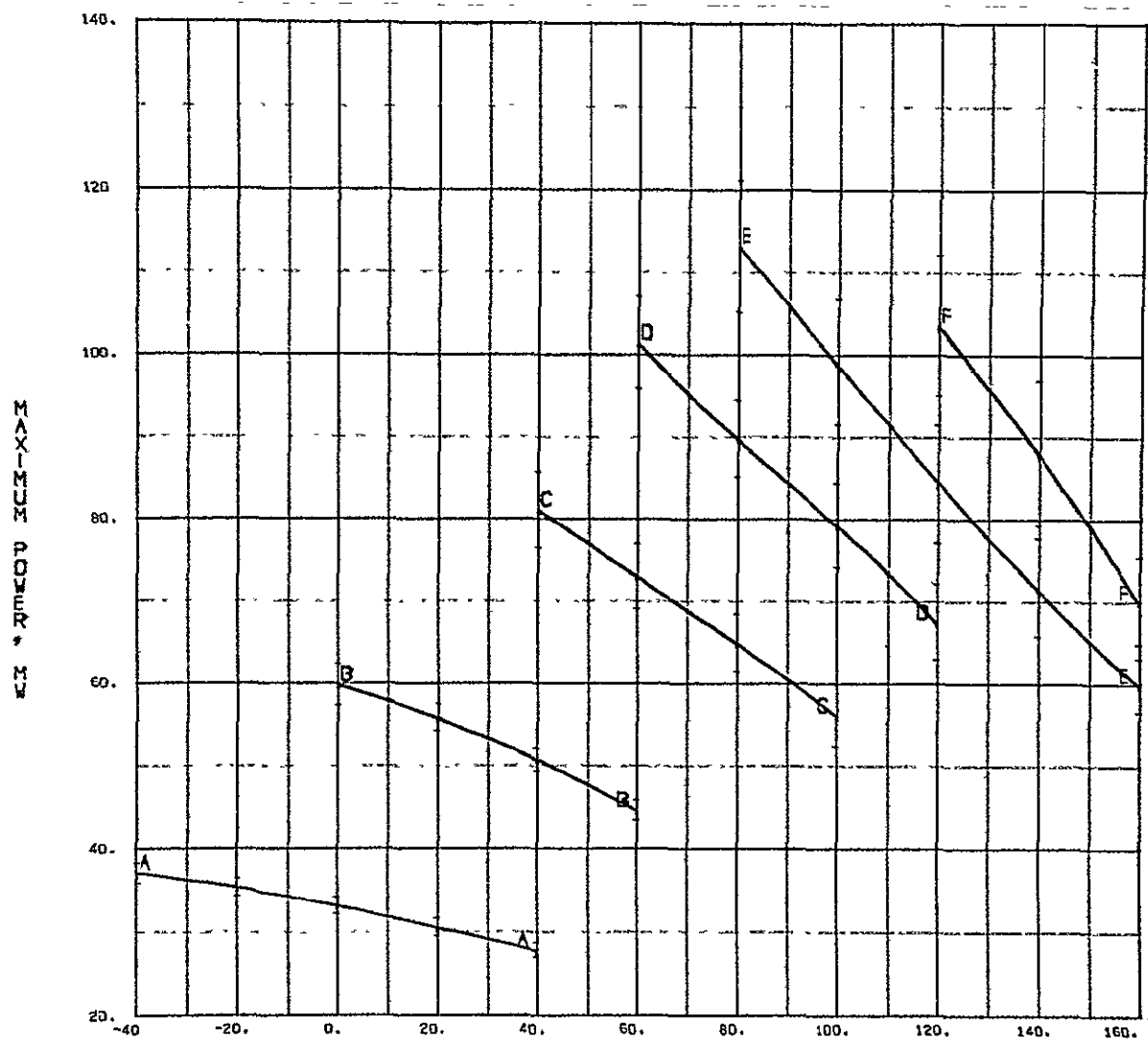


Fig. 44. Maximum power vs temperature, 4026 filter on 2 ohm-cm cell

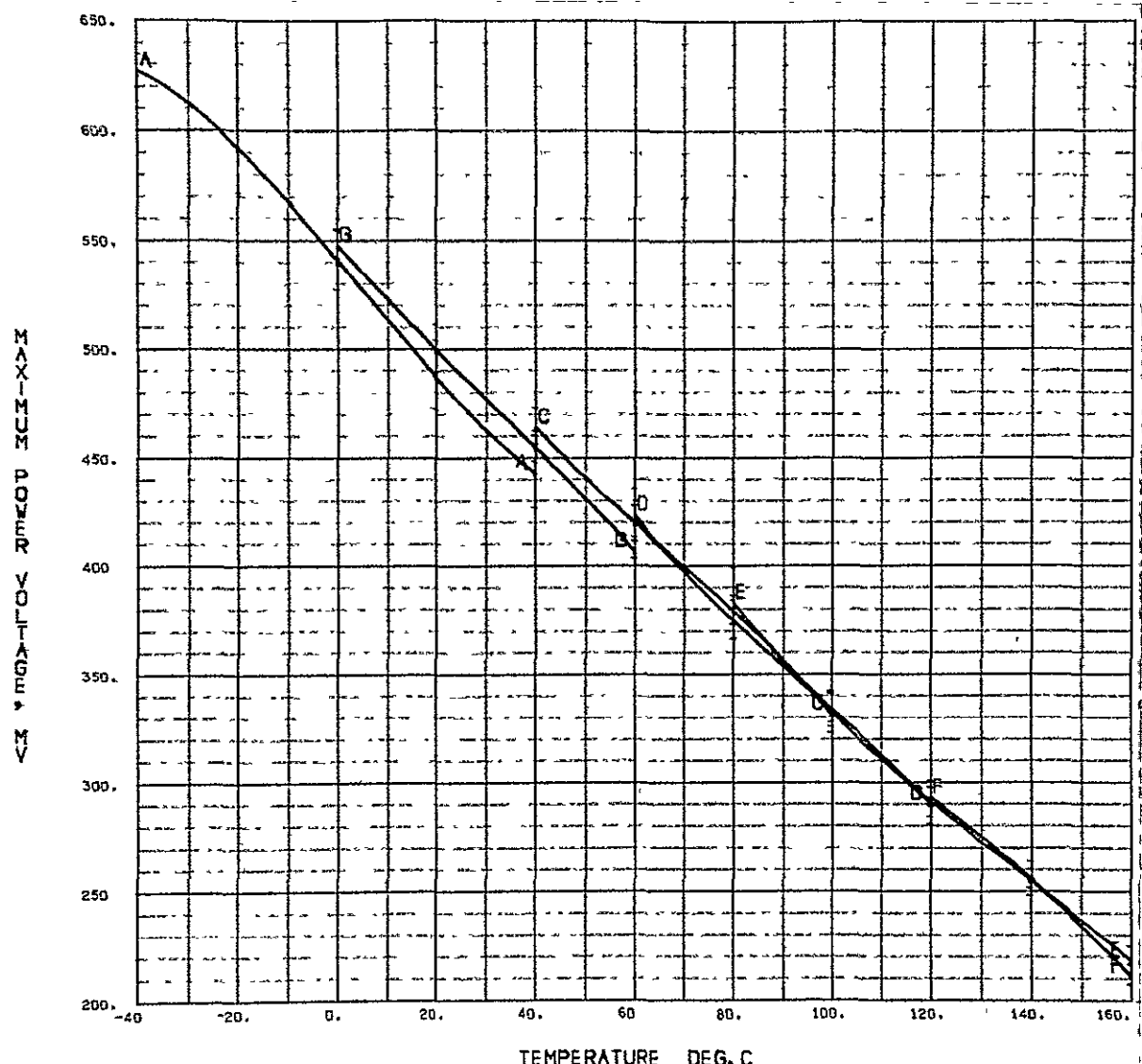
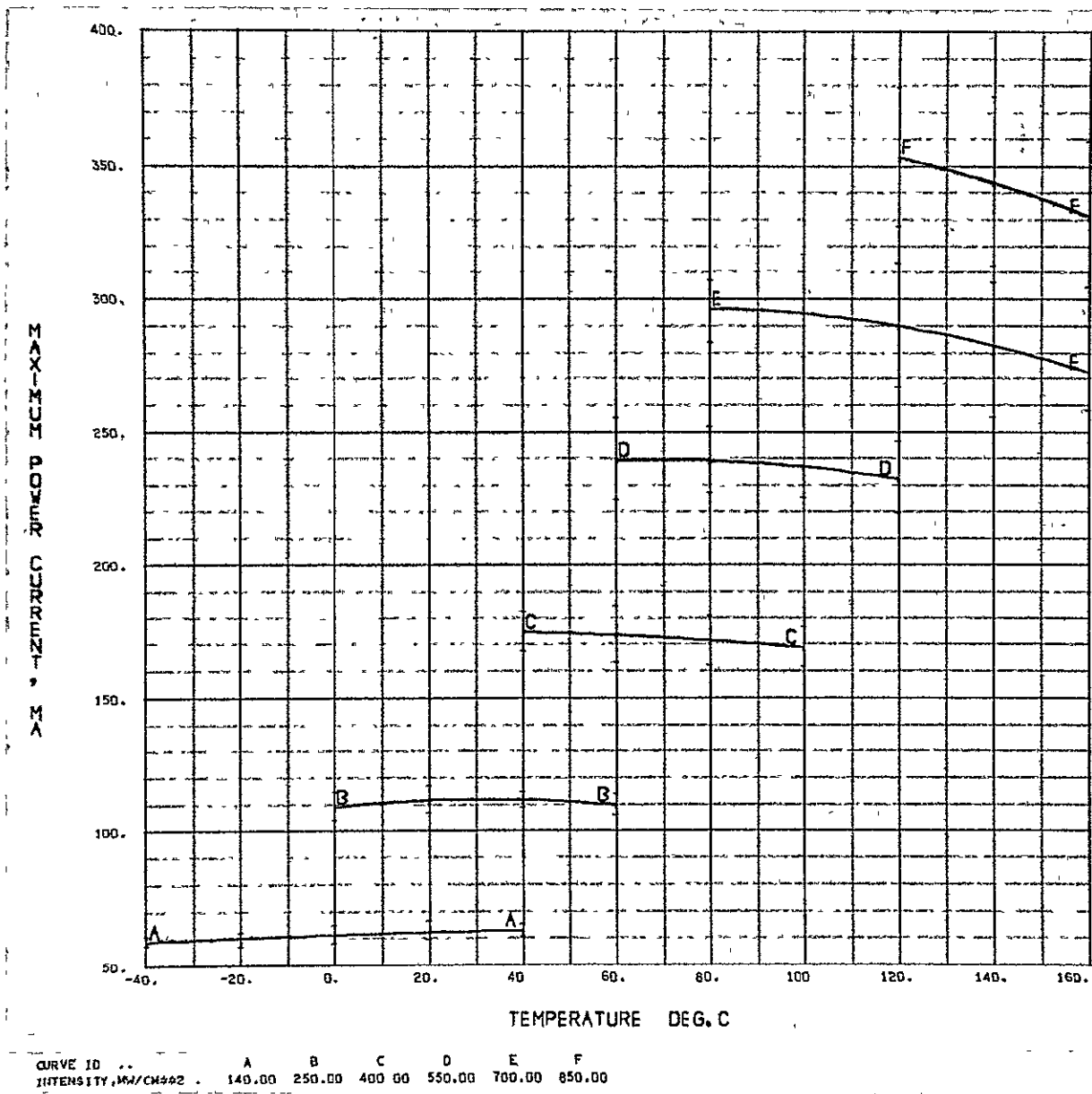


Fig. 45. Maximum-power voltage vs temperature, 4026 filter on 2 ohm-cm cell



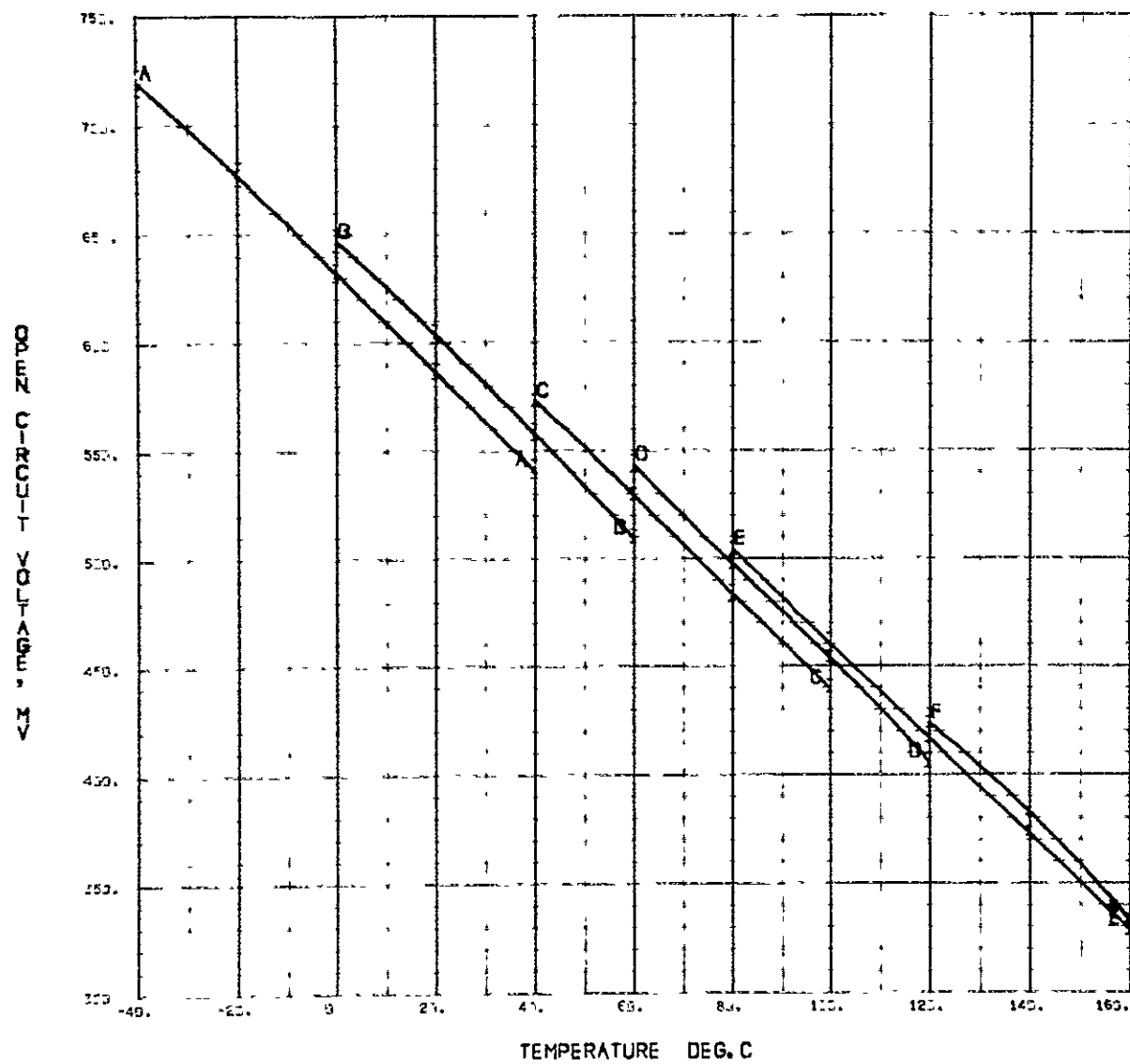


Fig. 47 Open-circuit voltage vs temperature, 4026 filter on 2 ohm-cm cell

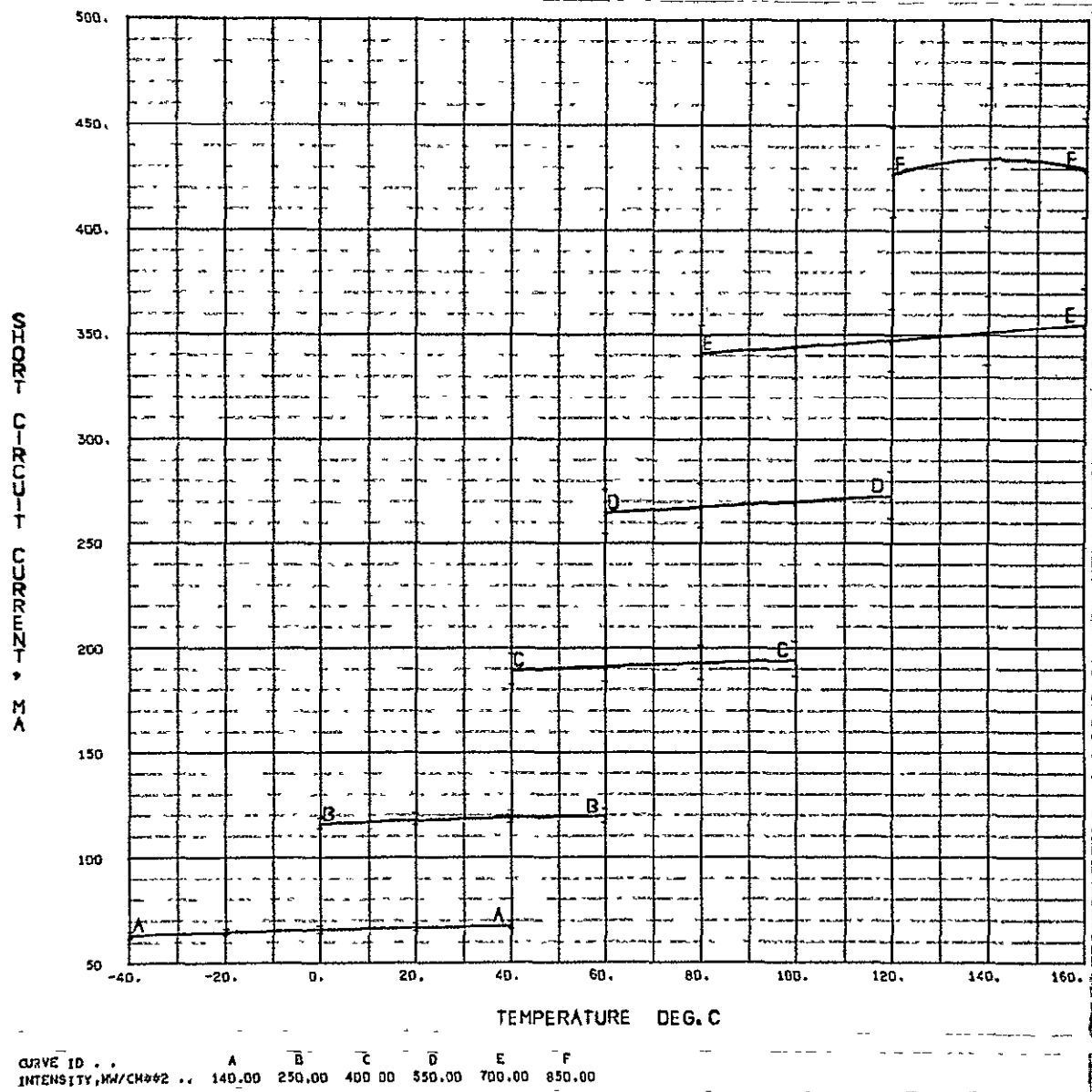


Fig. 48. Short-circuit current vs temperature, 4026 filter on 2 ohm-cm cell

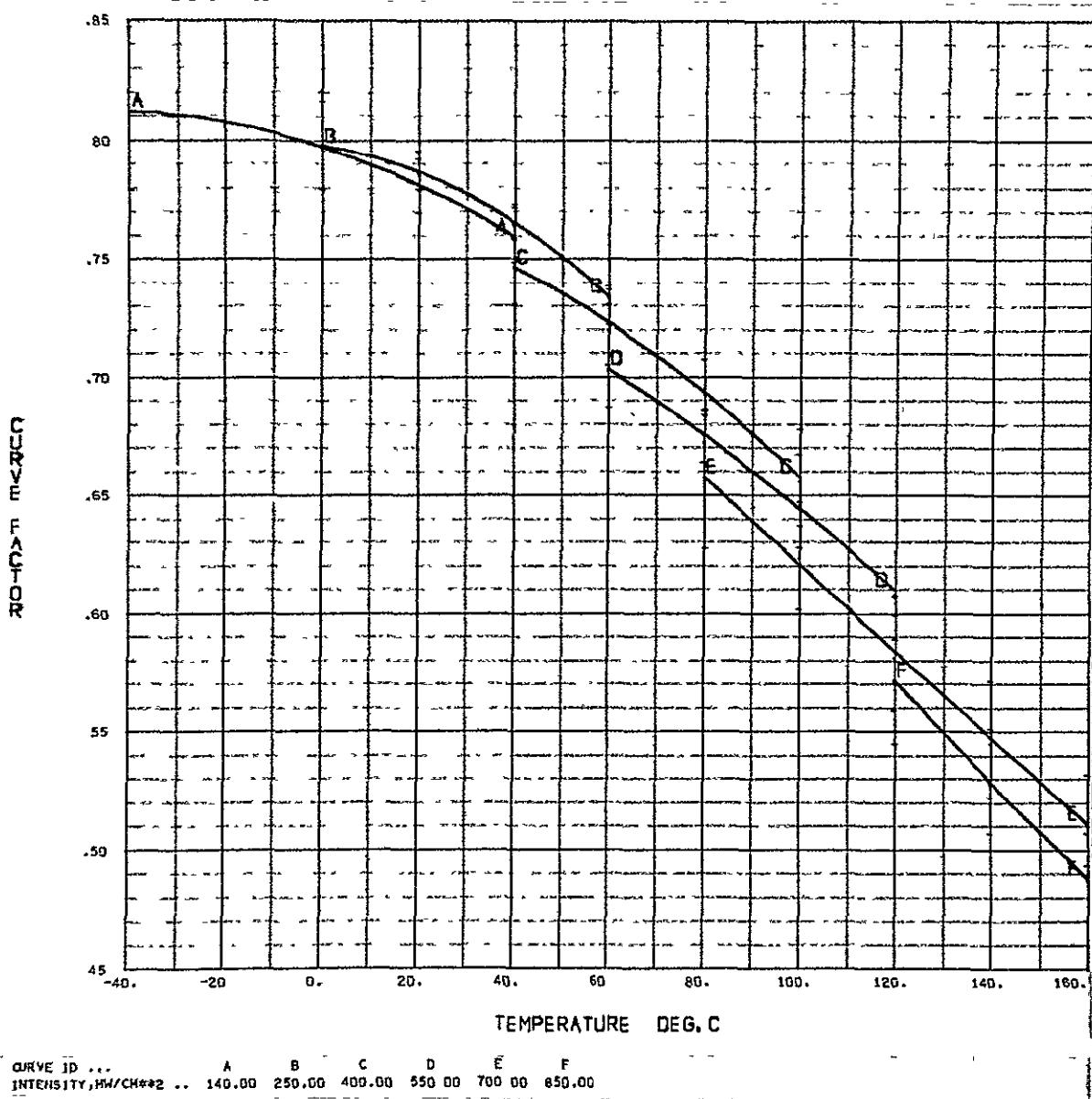


Fig. 49. Curve factor vs temperature, 4026 filter on 2 ohm-cm cell

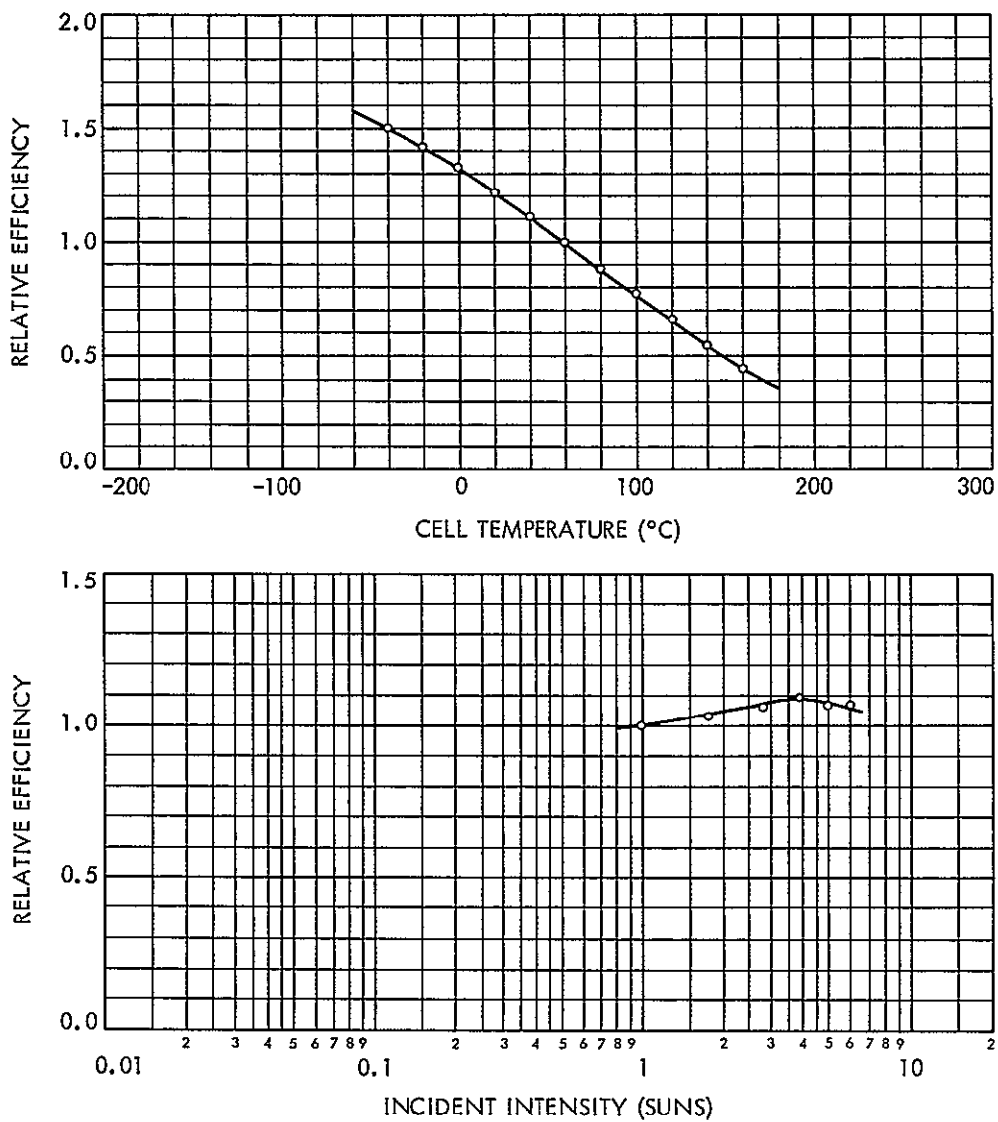


Fig. 50. Cell efficiency vs temperature and intensity, modified 4026 filter on 2 ohm-cm cell

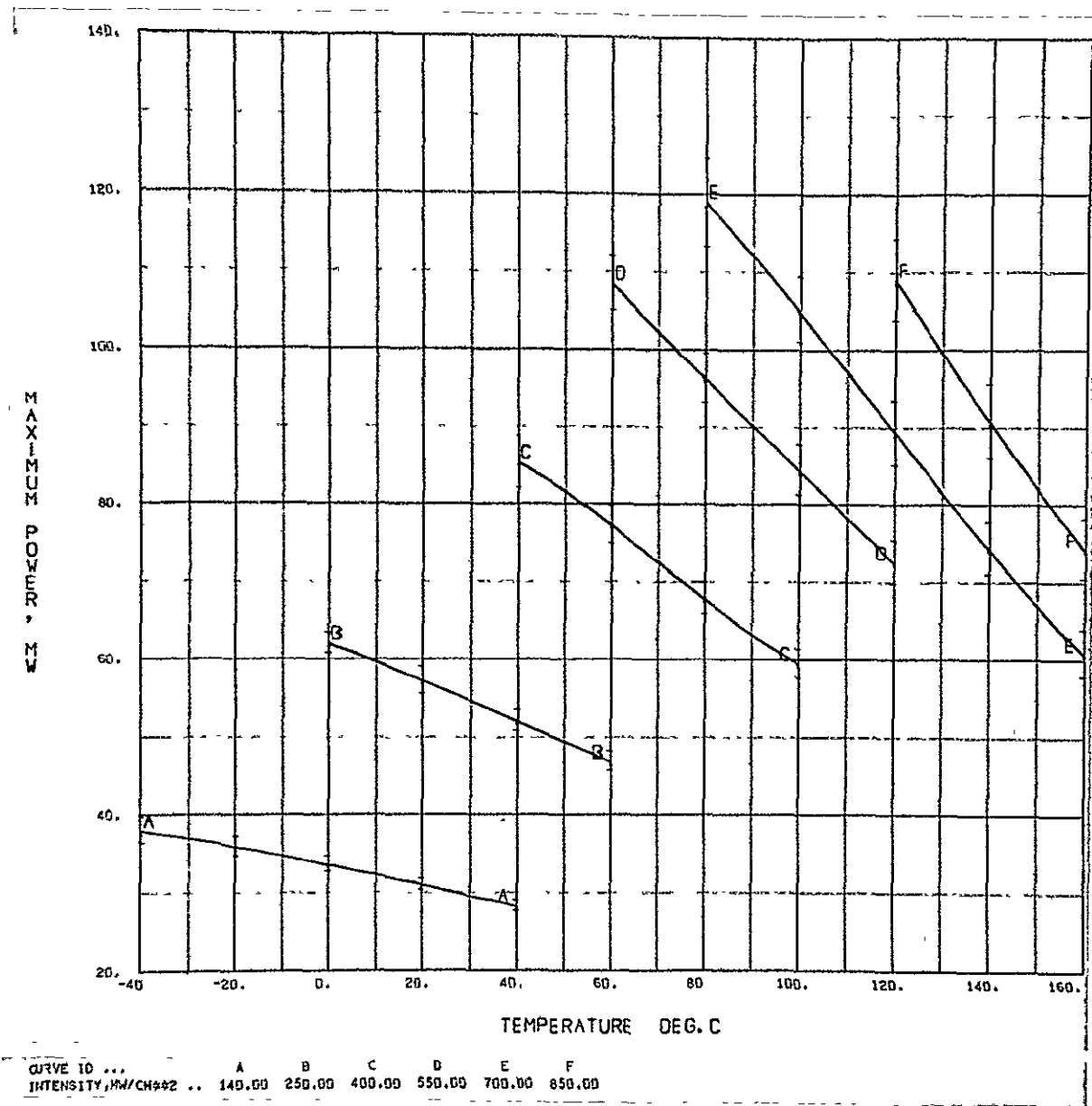


Fig 51. Maximum power vs temperature, modified 4026 filter on 2 ohm-cm cell

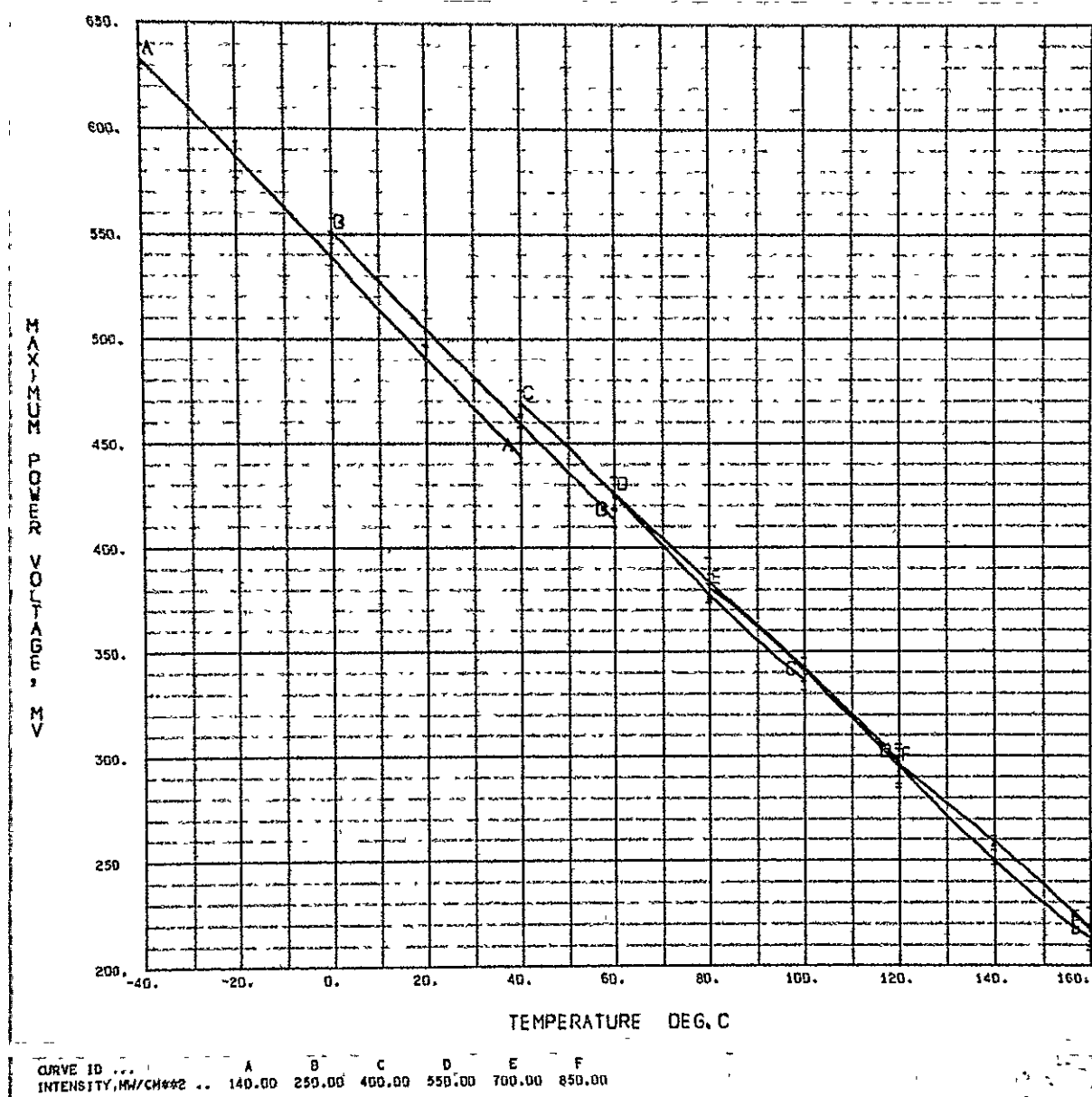


Fig. 52. Maximum-power voltage vs temperature, modified 4026 filter on 2 ohm-cm cell

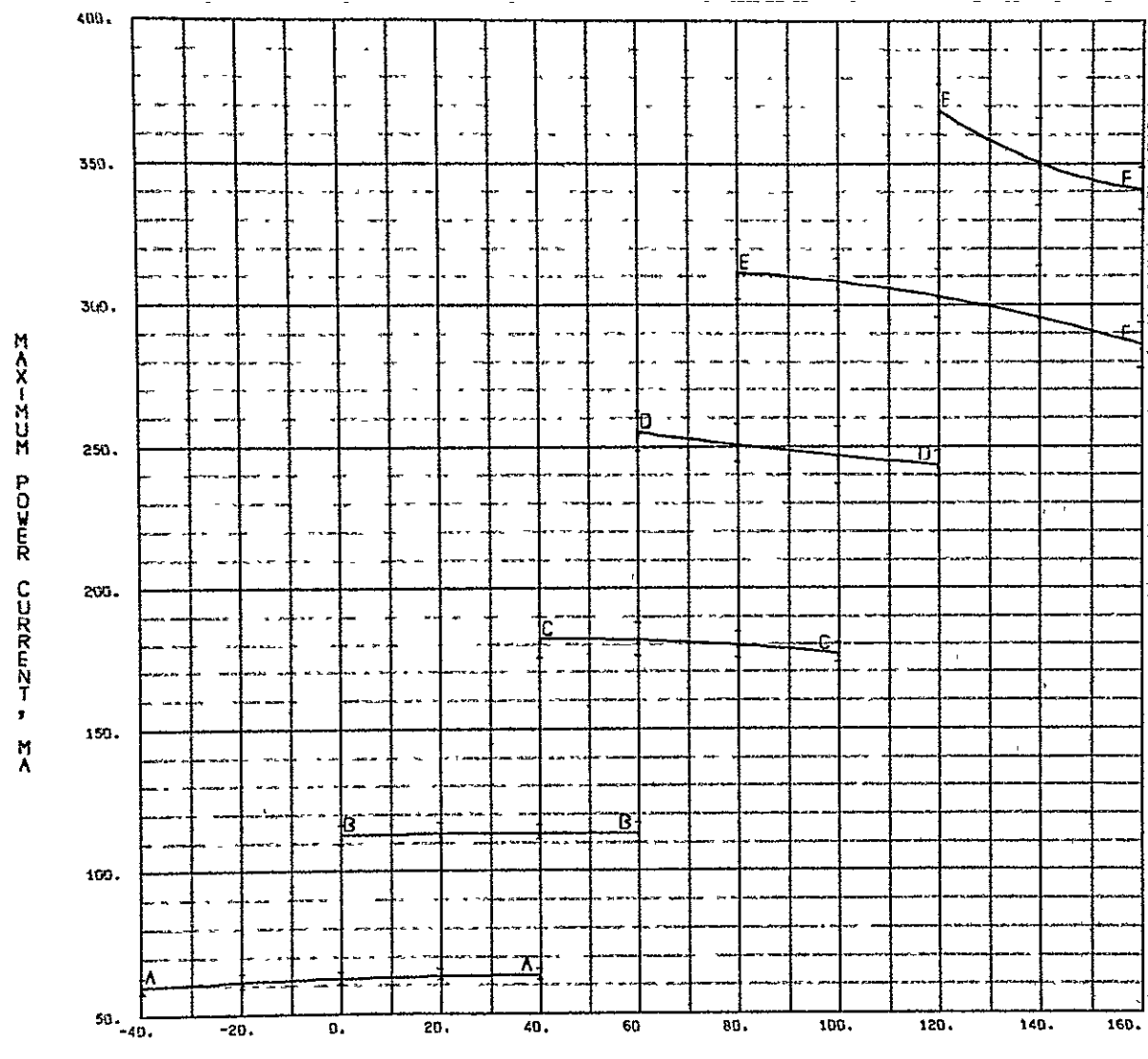


Fig 53 Maximum-power current vs temperature, modified 4026 filter on 2 ohm-cm cell

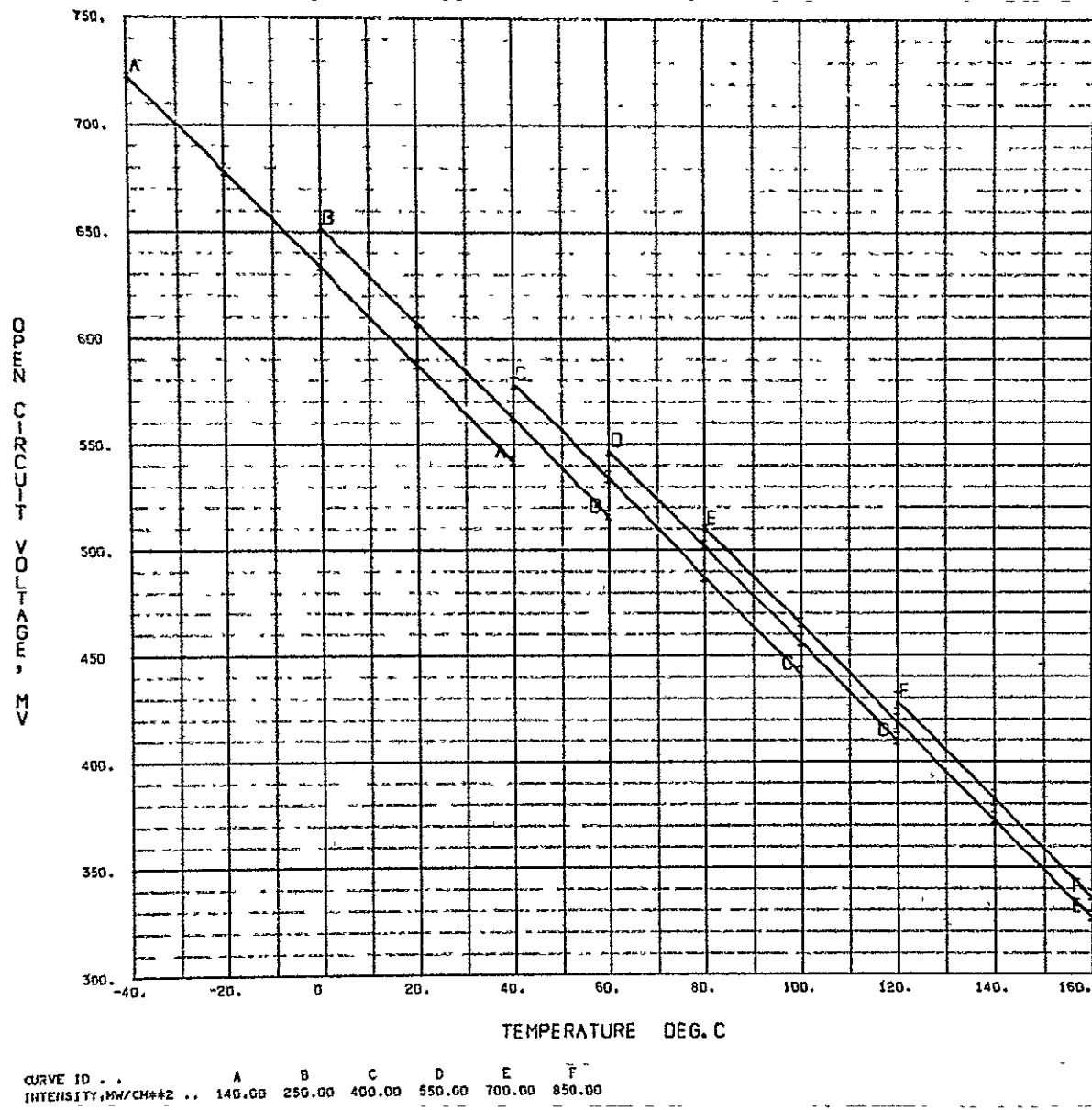


Fig 54. Open-circuit voltage vs temperature, modified 4026 filter on 2 ohm-cm cell

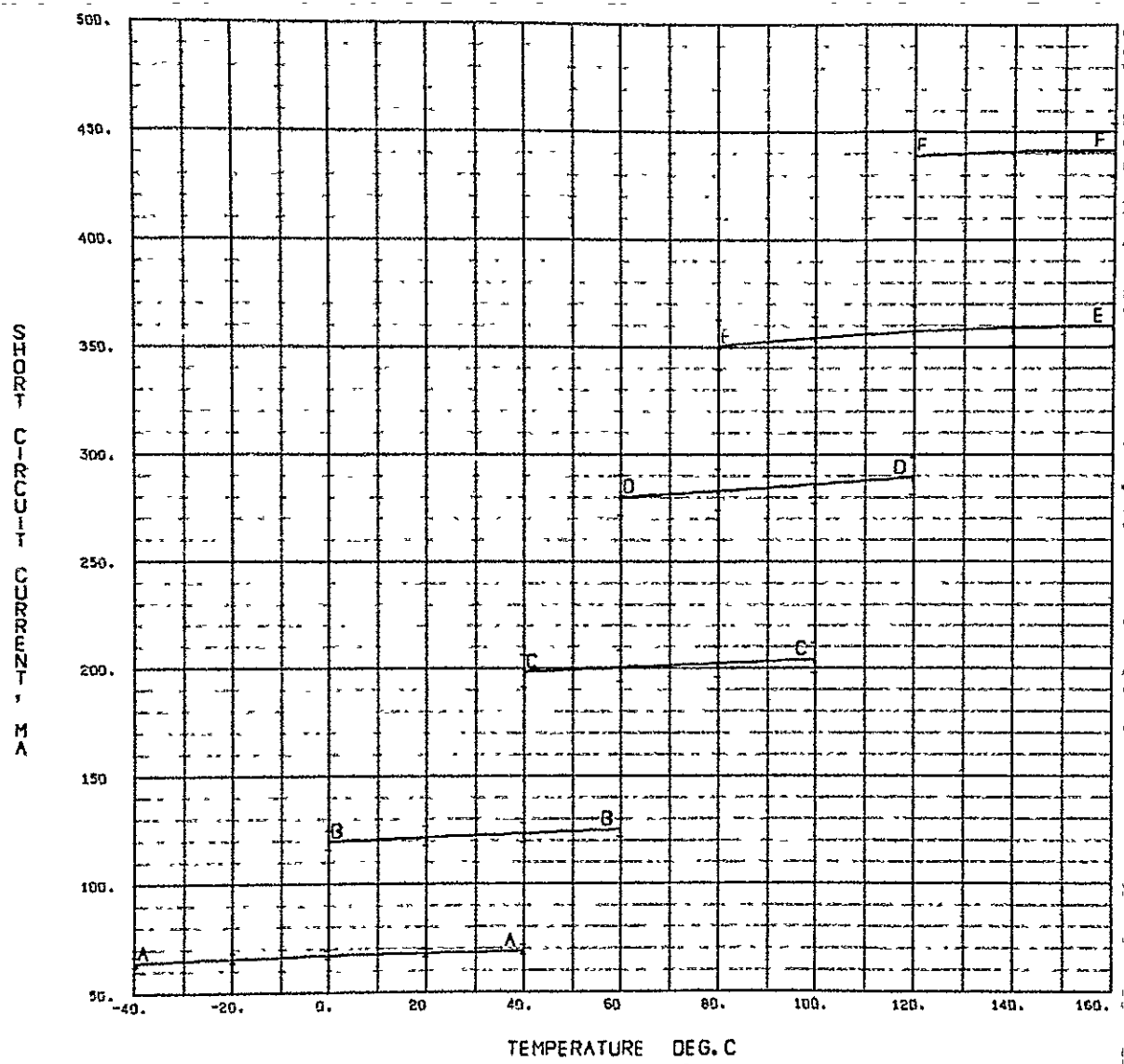


Fig. 55 Short-circuit current vs temperature, modified 4026 filter on 2 ohm-cm cell

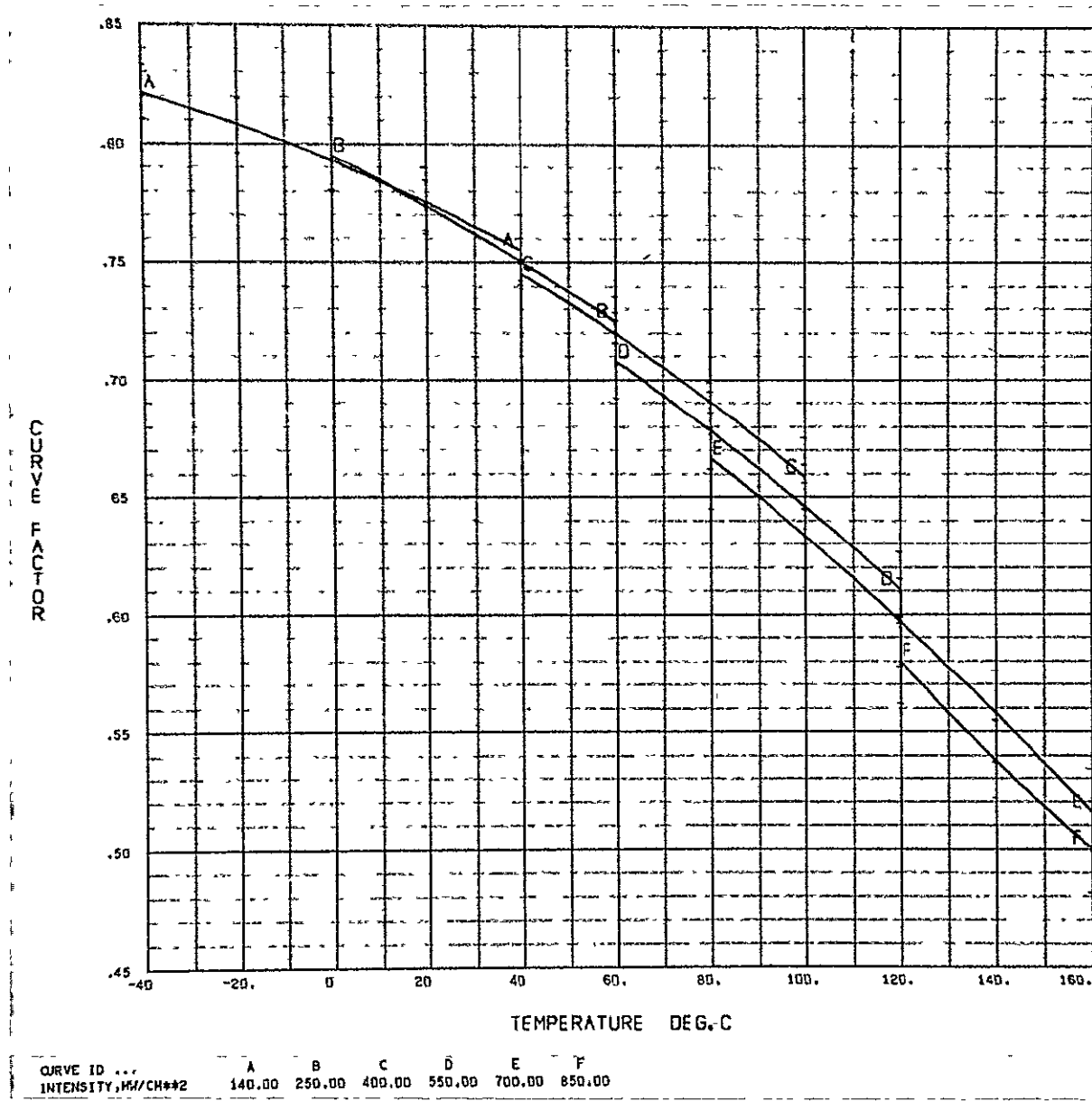


Fig. 56 Curve factor vs temperature, modified 4026 filter on 2 ohm-cm cell

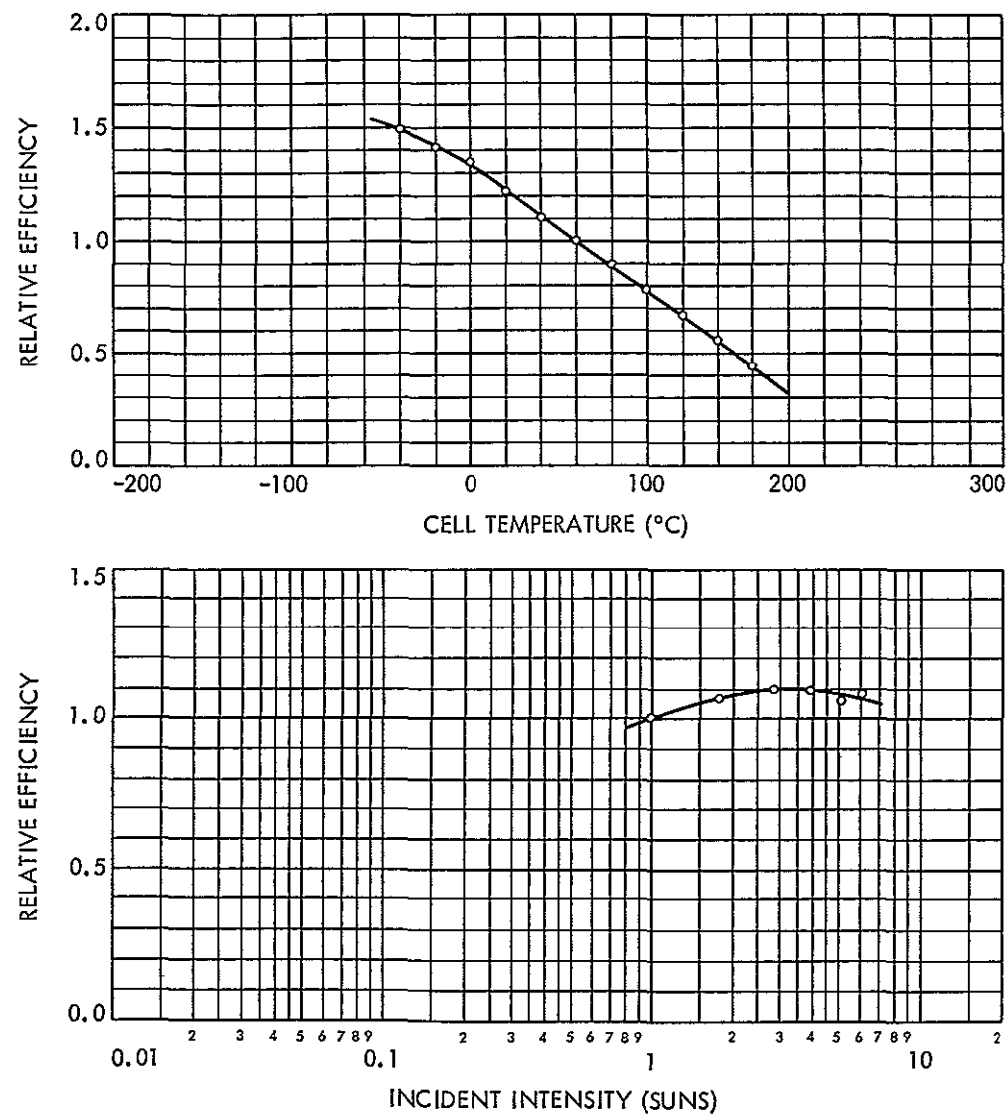


Fig. 57. Cell efficiency vs temperature and intensity, blue filter with mirror stripes on 2 ohm-cm cell

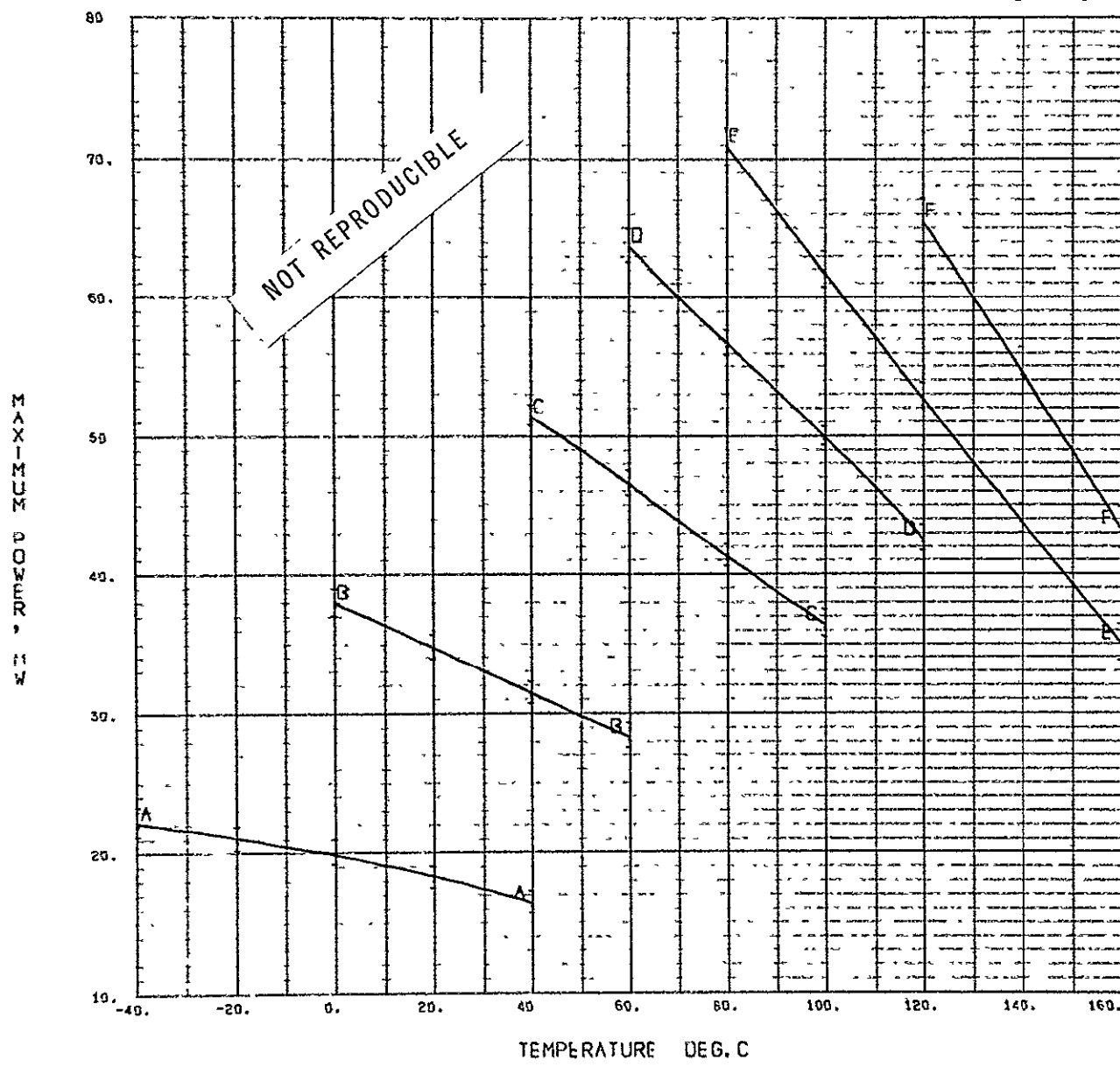


Fig. 58 Maximum power vs temperature, blue filter with mirror stripes on 2 ohm-cm cell

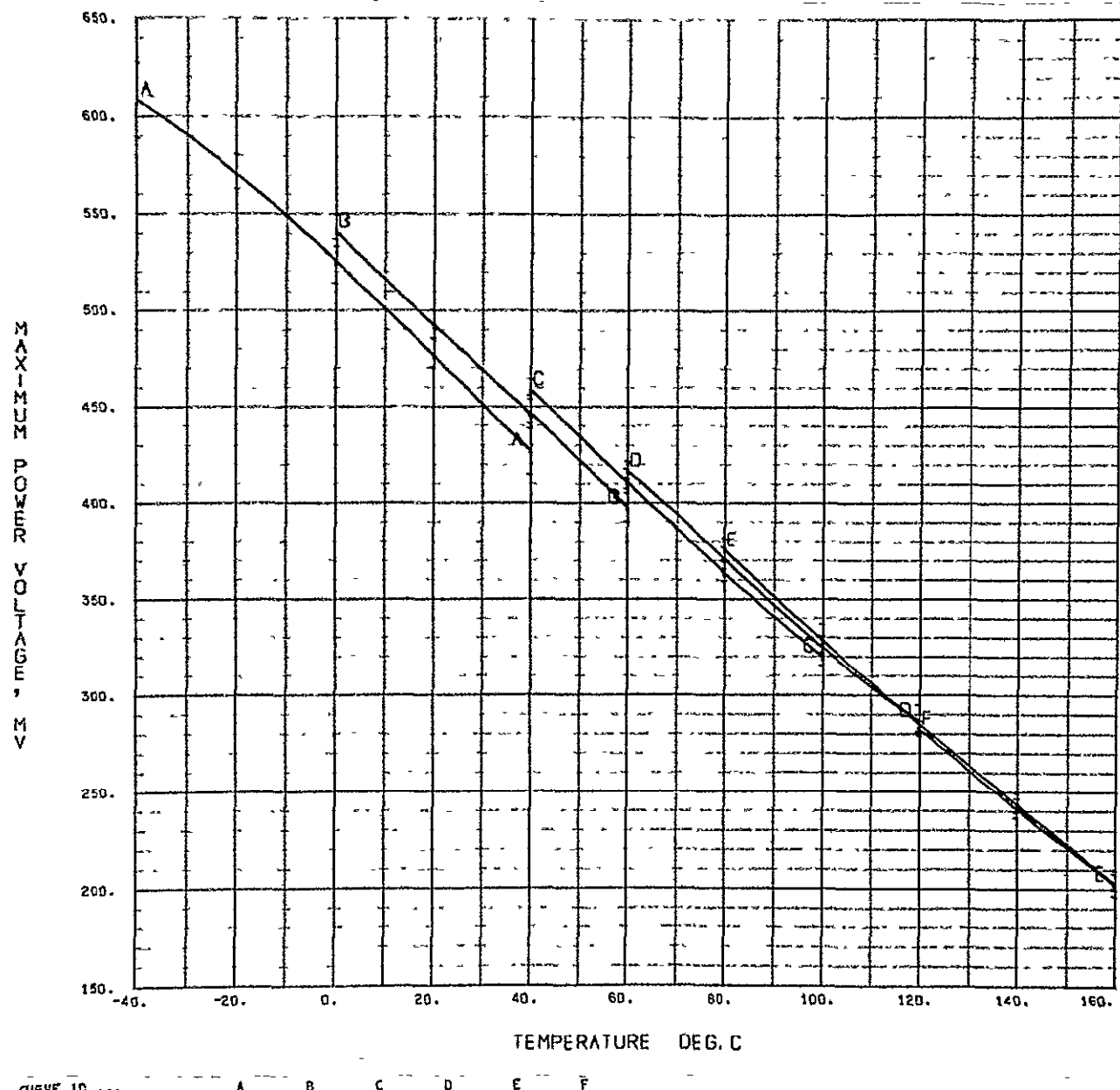


Fig. 59. Maximum-power voltage vs temperature, blue filter with mirror stripes on 2 ohm-cm cell

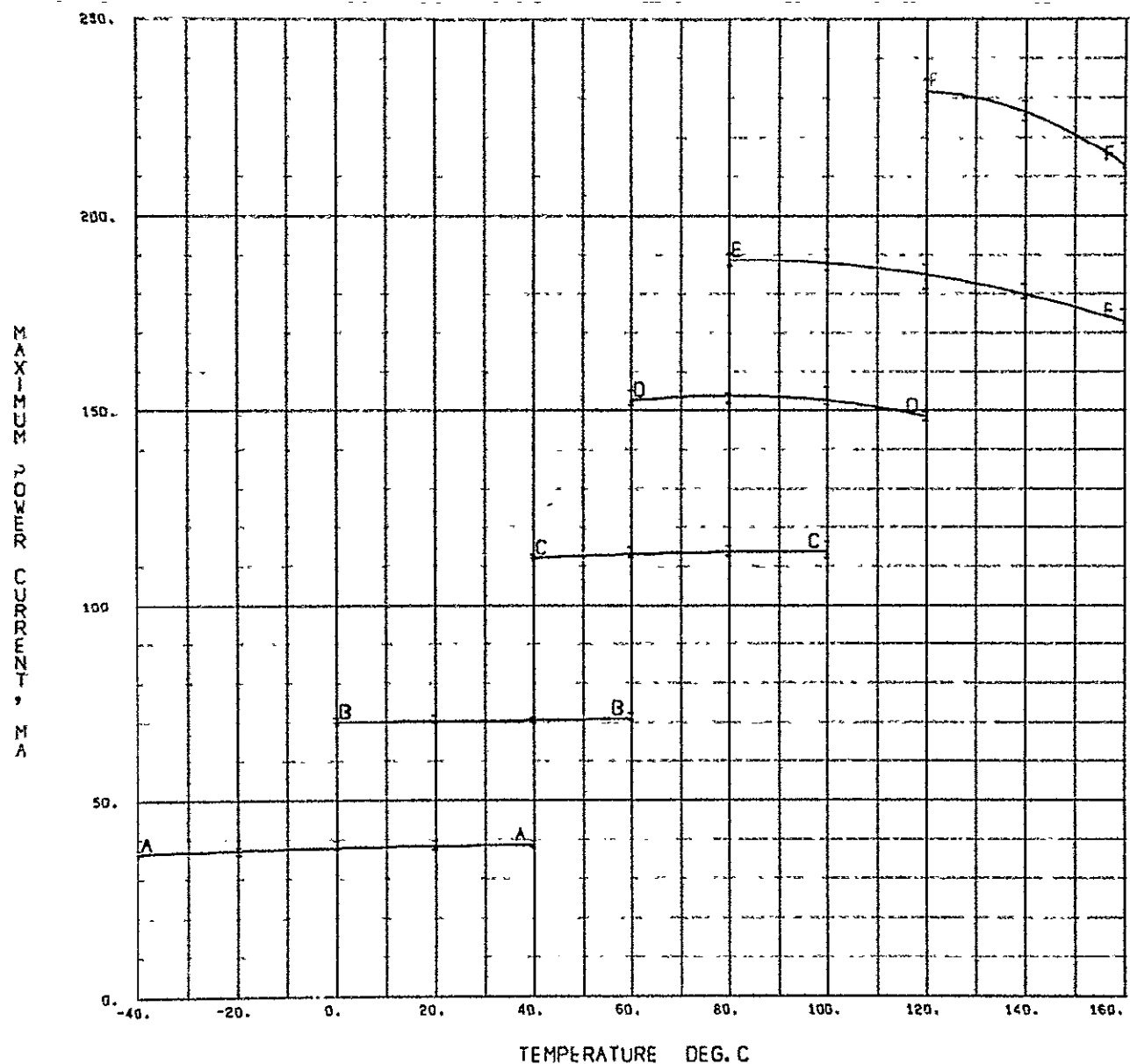


Fig. 60. Maximum-power current vs temperature, blue filter with mirror stripes on 2 ohm-cm cell

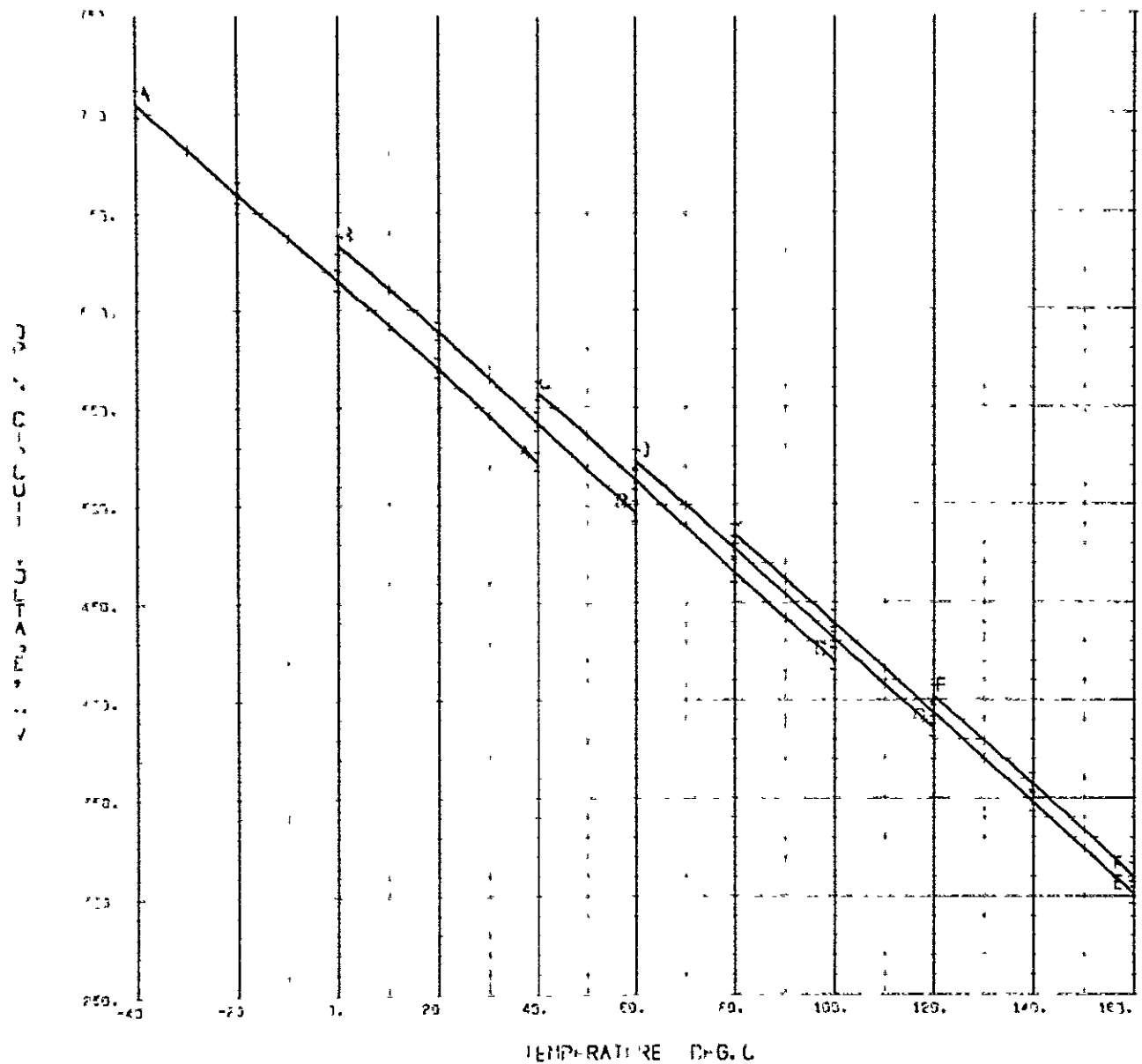


Fig. 61. Open-circuit voltage vs temperature, blue filter with mirror stripes on 2 ohm-cm cell

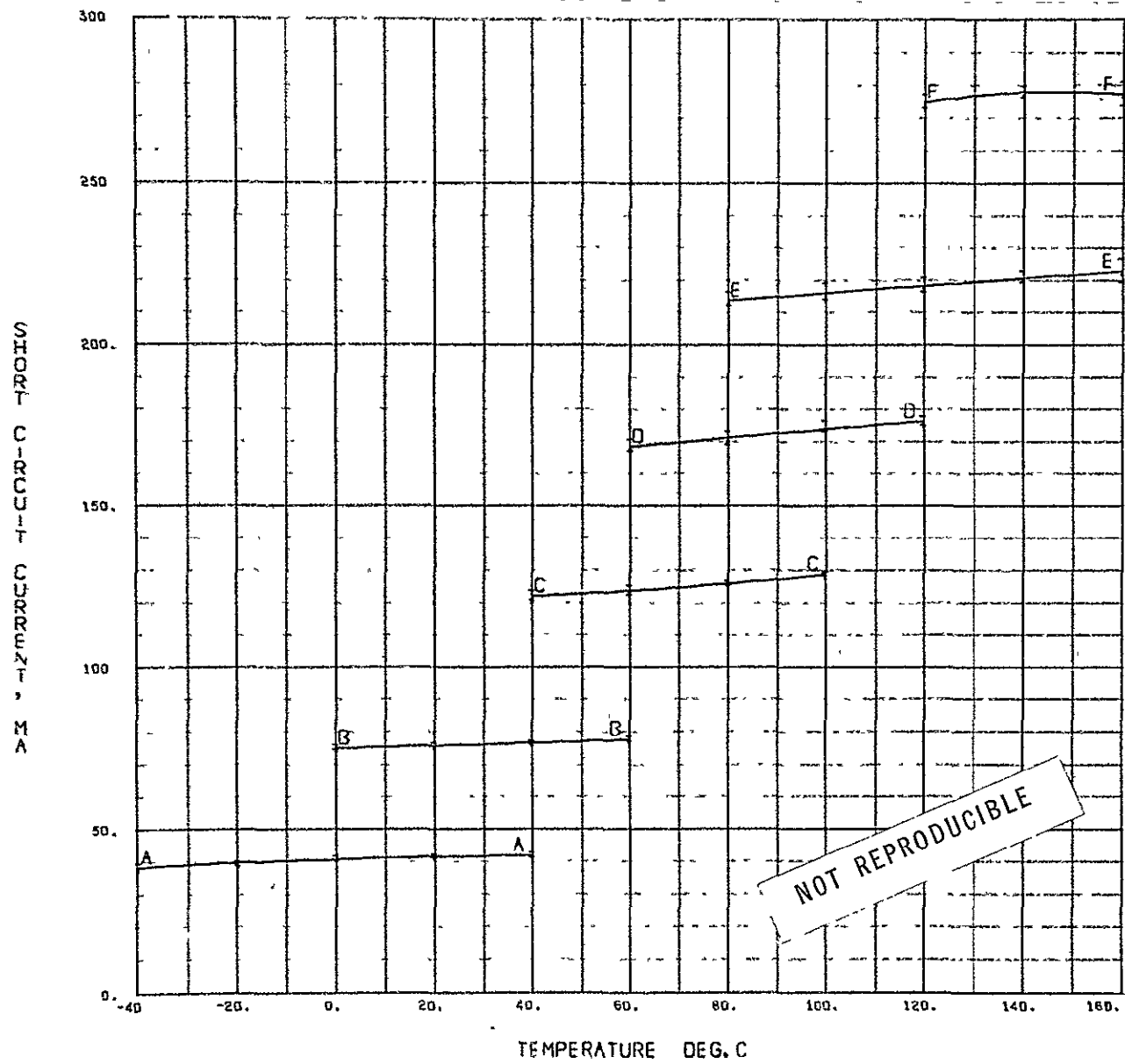


Fig. 62. Short-circuit current vs temperature, blue filter with mirror stripes on 2 ohm-cm cell

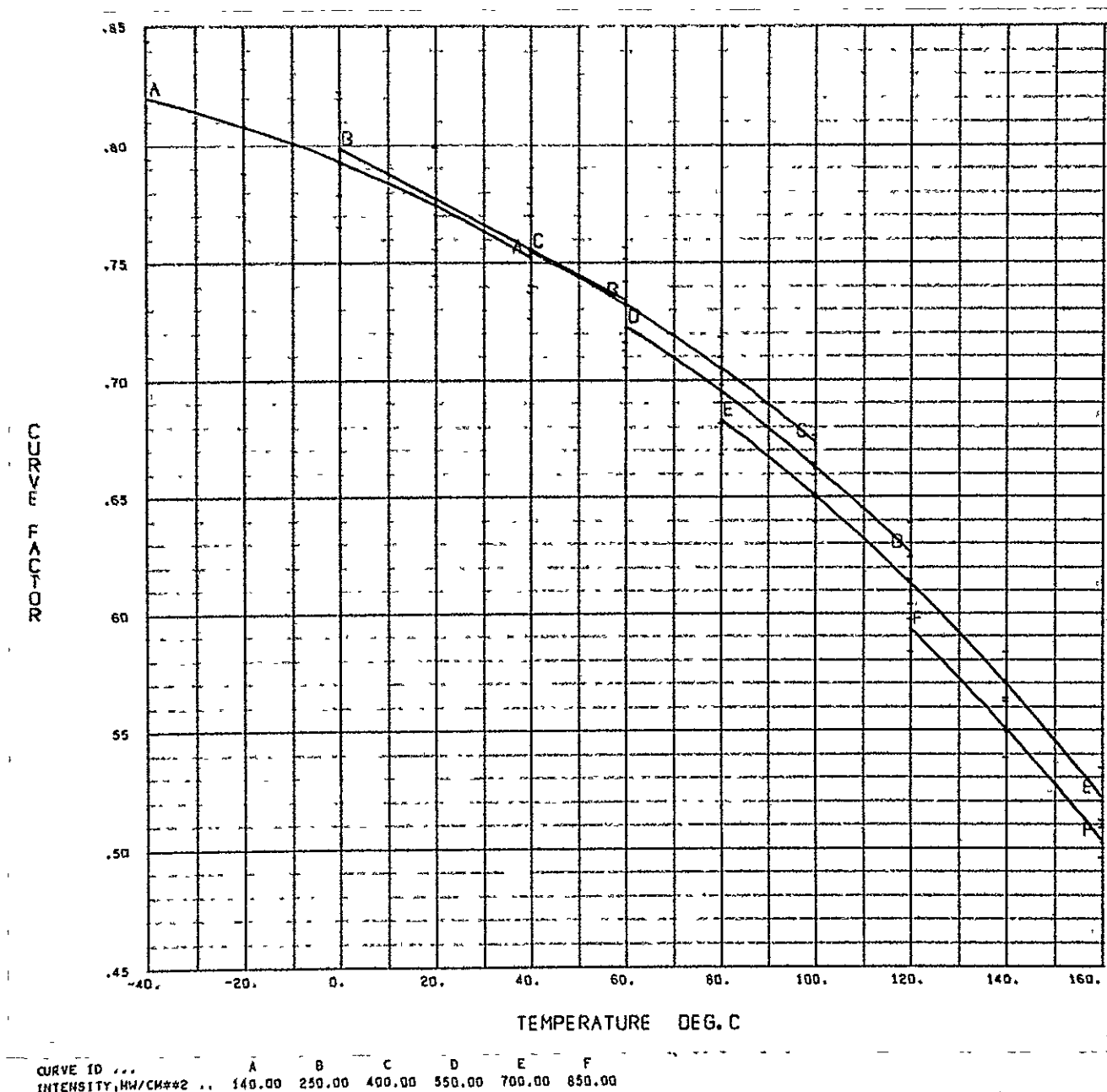


Fig. 63. Curve factor vs temperature, blue filter with mirror stripes on 2 ohm-cm cell

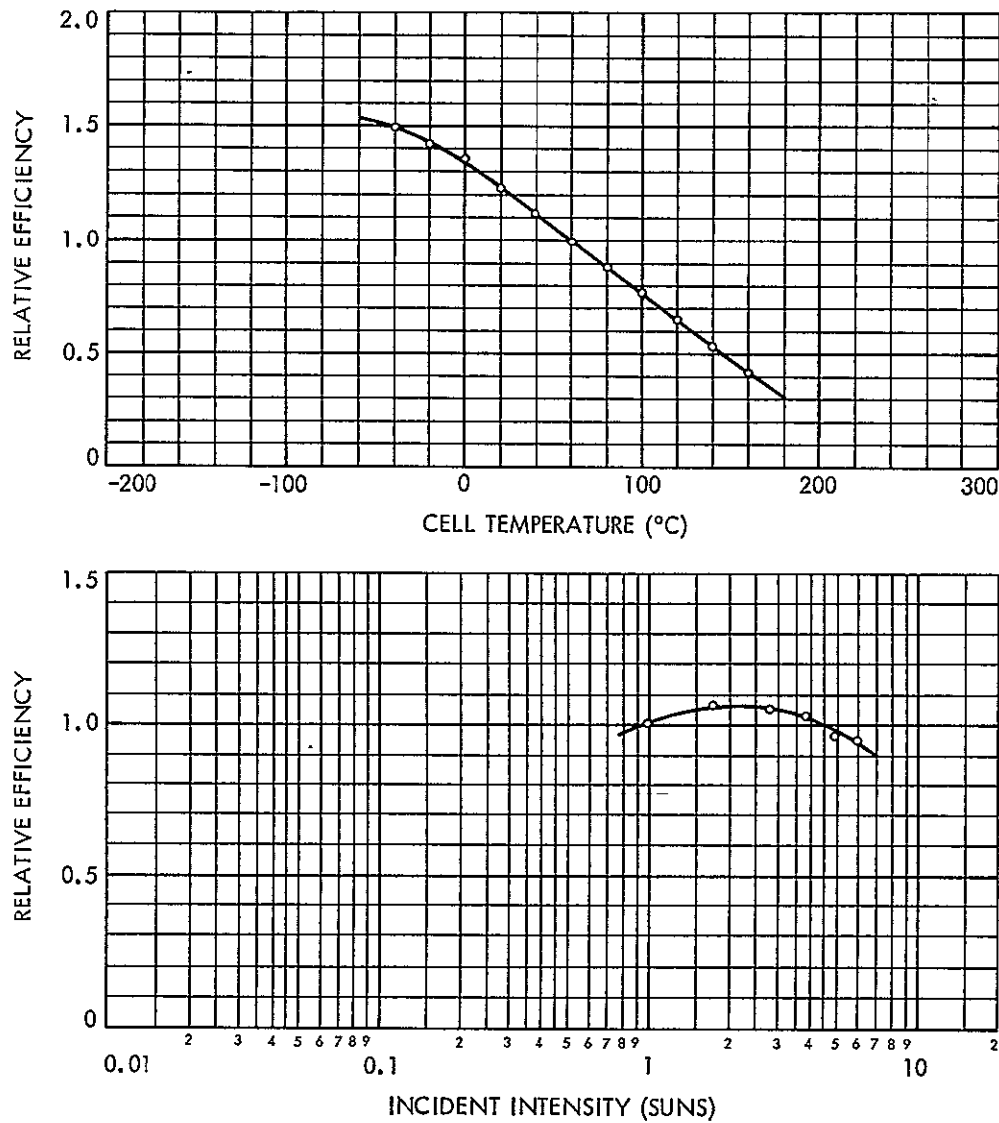


Fig. 64. Cell efficiency vs temperature and intensity, blue filter with mirror bar by contact on 2 ohm-cm cell

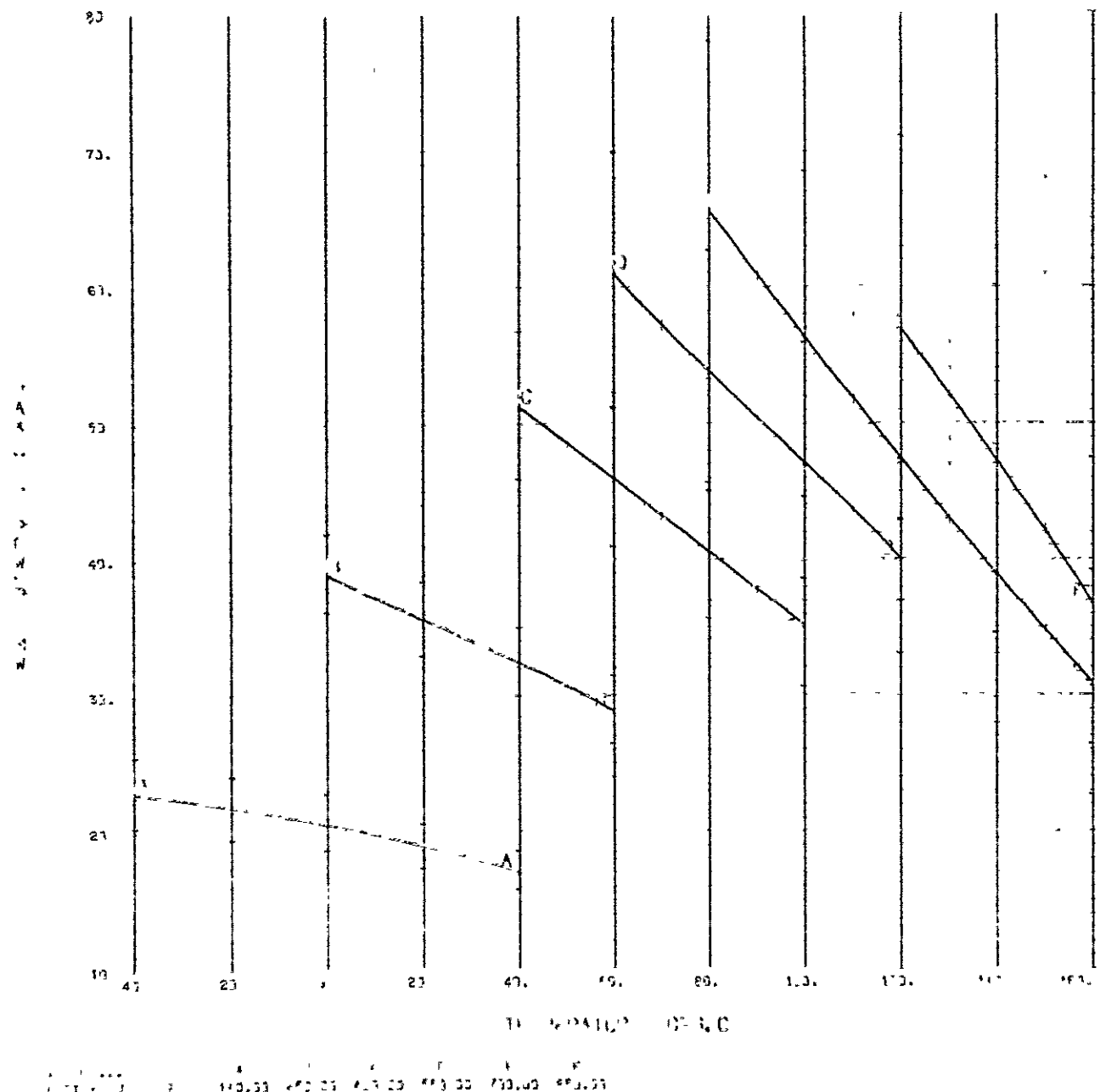


Fig. 65. Maximum power vs temperature, blue filter with mirror bar by contact on 2 ohm-cm cell

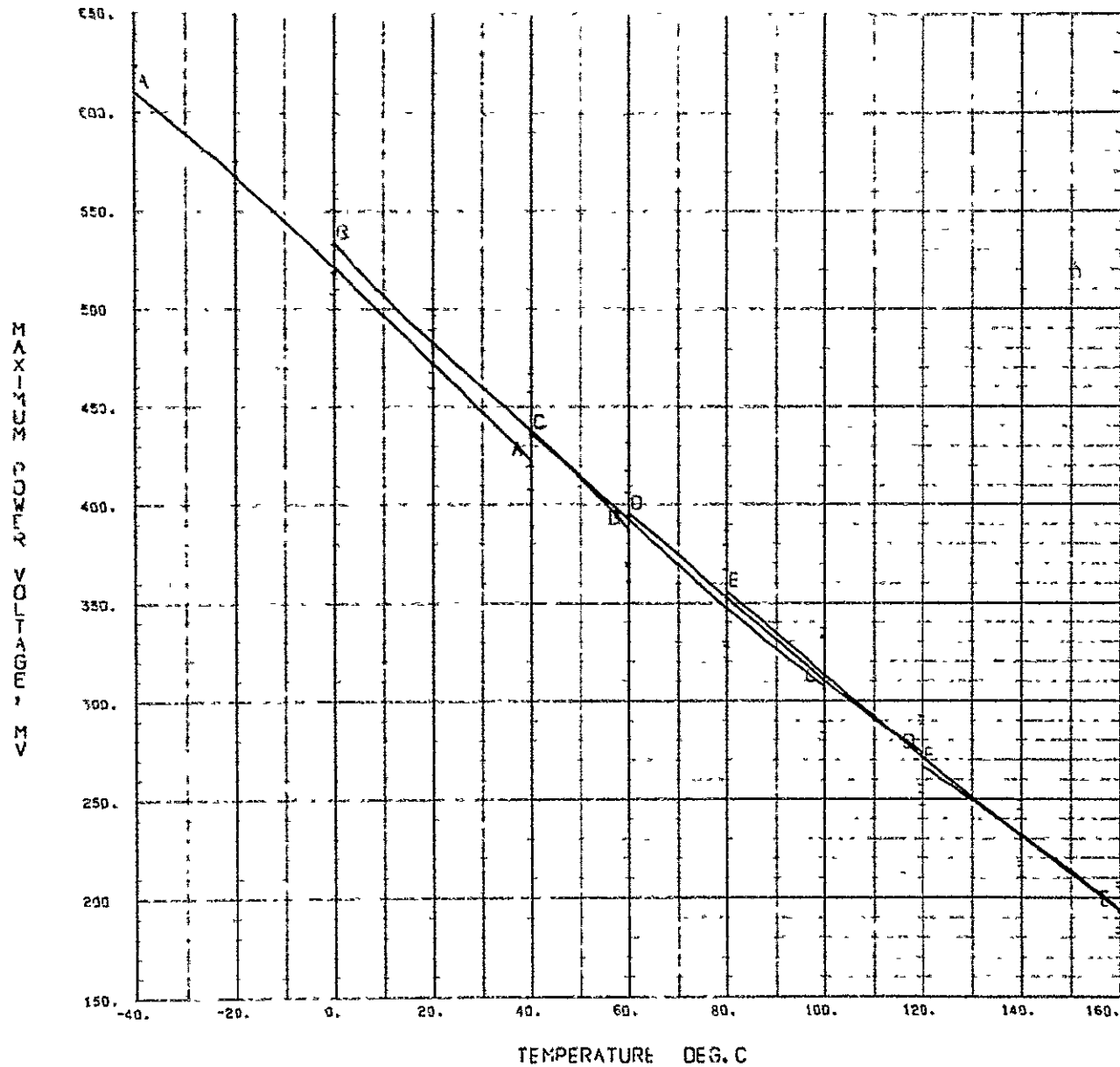


Fig. 66. Maximum-power voltage vs temperature, blue filter with mirror bar by contact on 2 ohm-cm cell

NOT REPRODUCIBLE

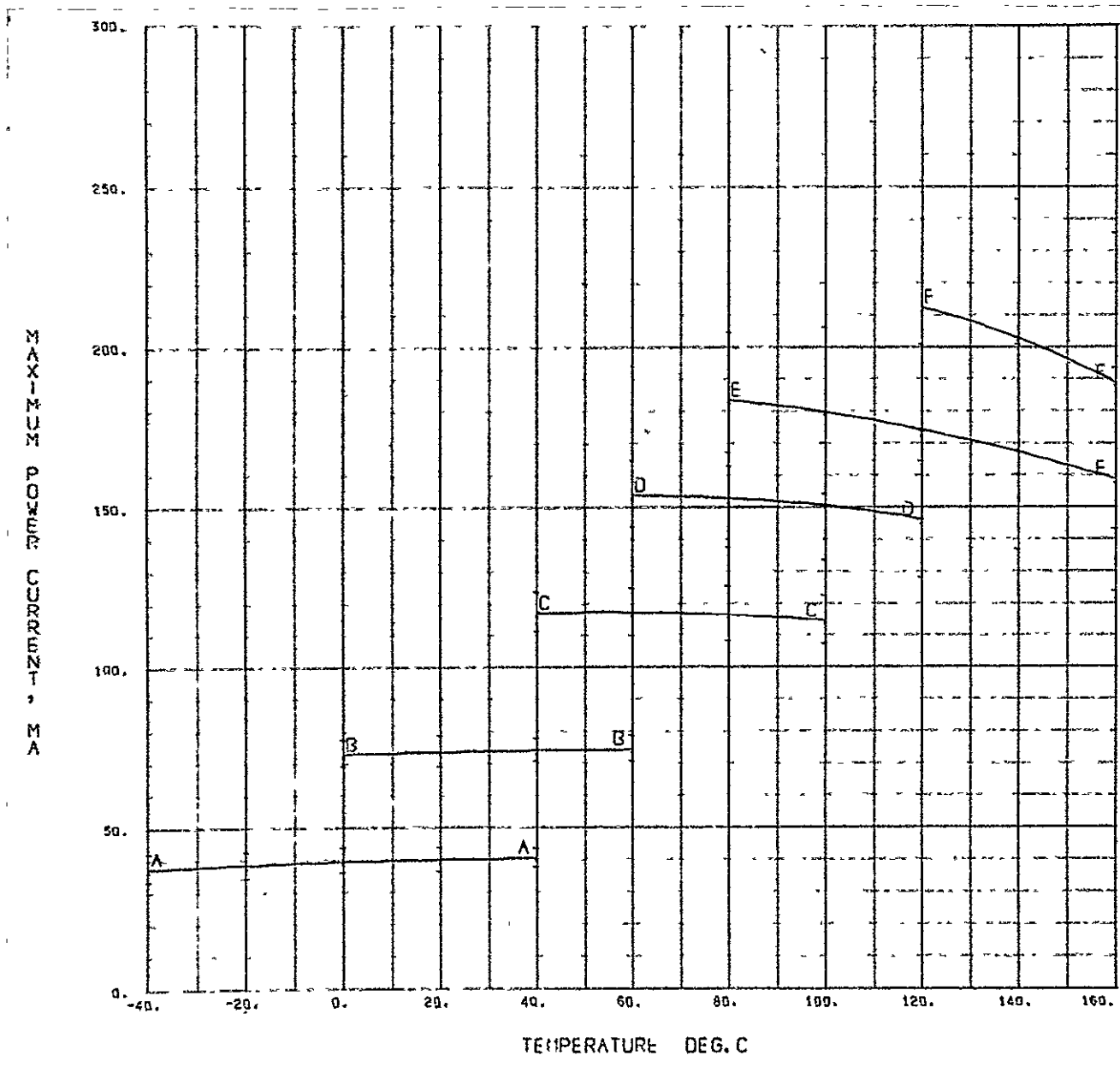
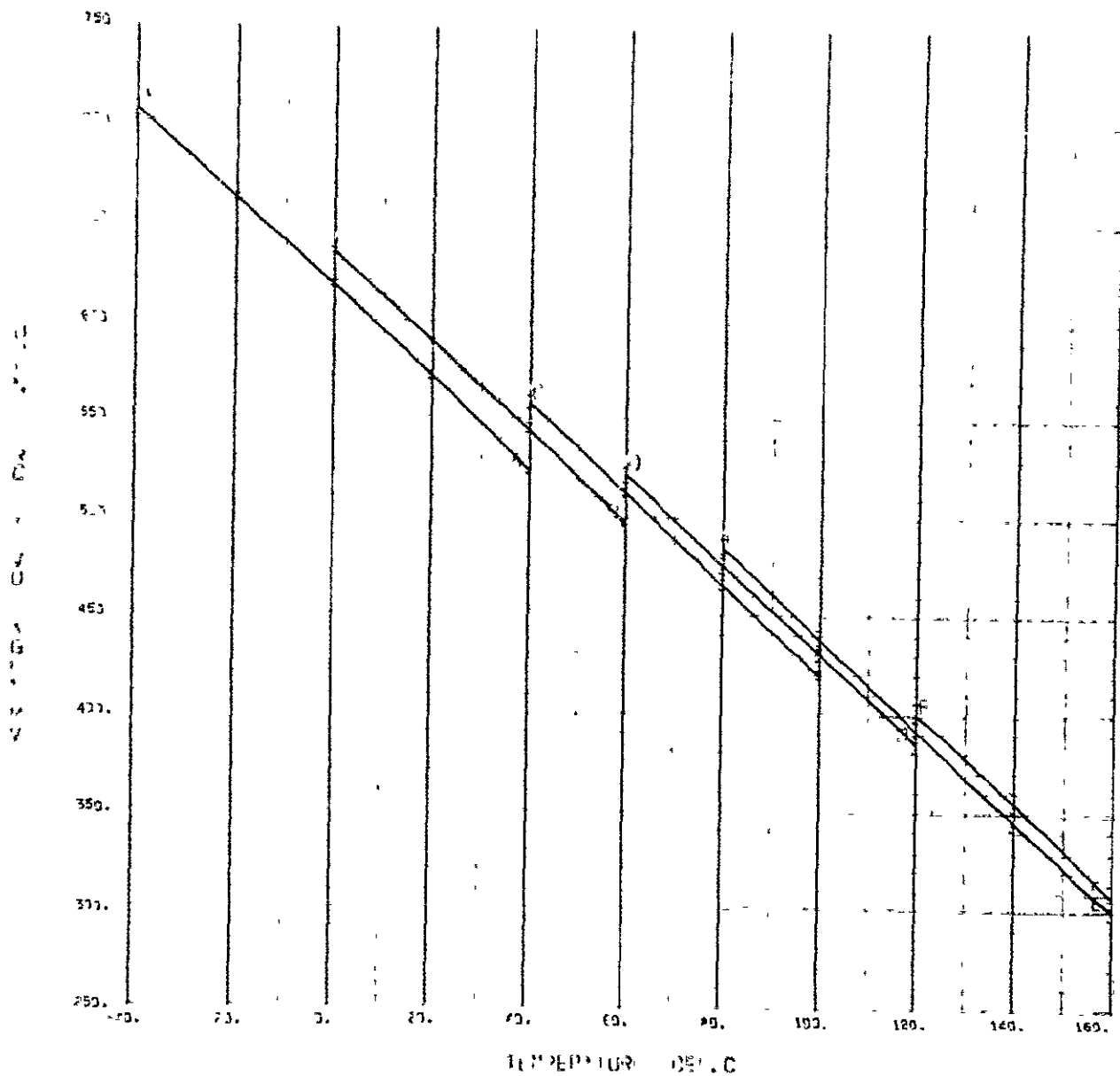


Fig. 67. Maximum-power current vs temperature, blue filter with mirror bar by contact on 2 ohm-cm cell



1.9xE 10 .. A 8 C D E F
1.9E 11T7.5x10⁻² .. 140.00 250.00 439.00 553.00 700.00 854.00

Fig. 68. Open-circuit voltage vs temperature, blue filter with mirror bar by contact on 2 ohm-cm cell

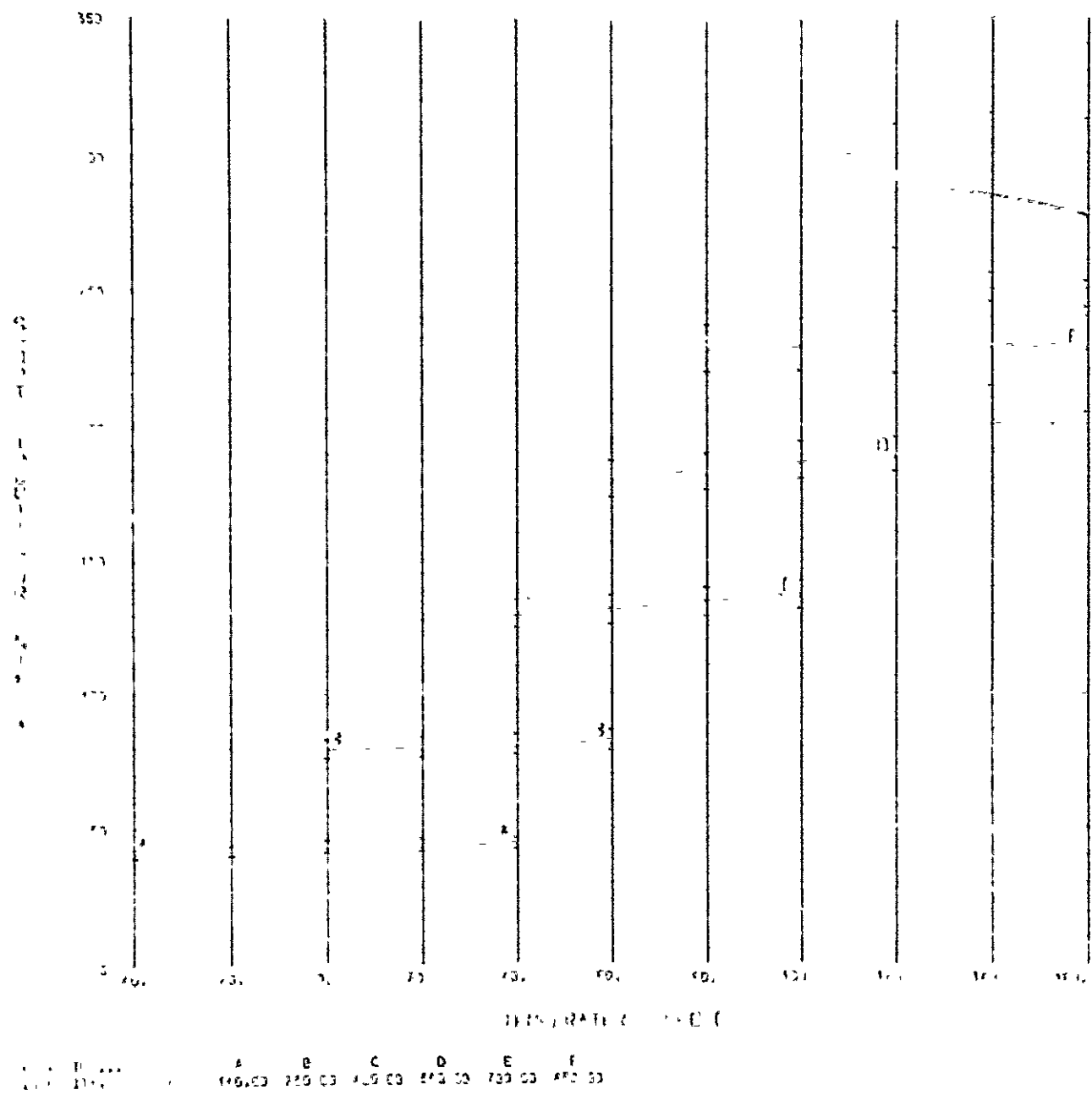


Fig. 69. Short-circuit current vs temperature, blue filter with mirror bar by contact on 2 ohm-cm cell

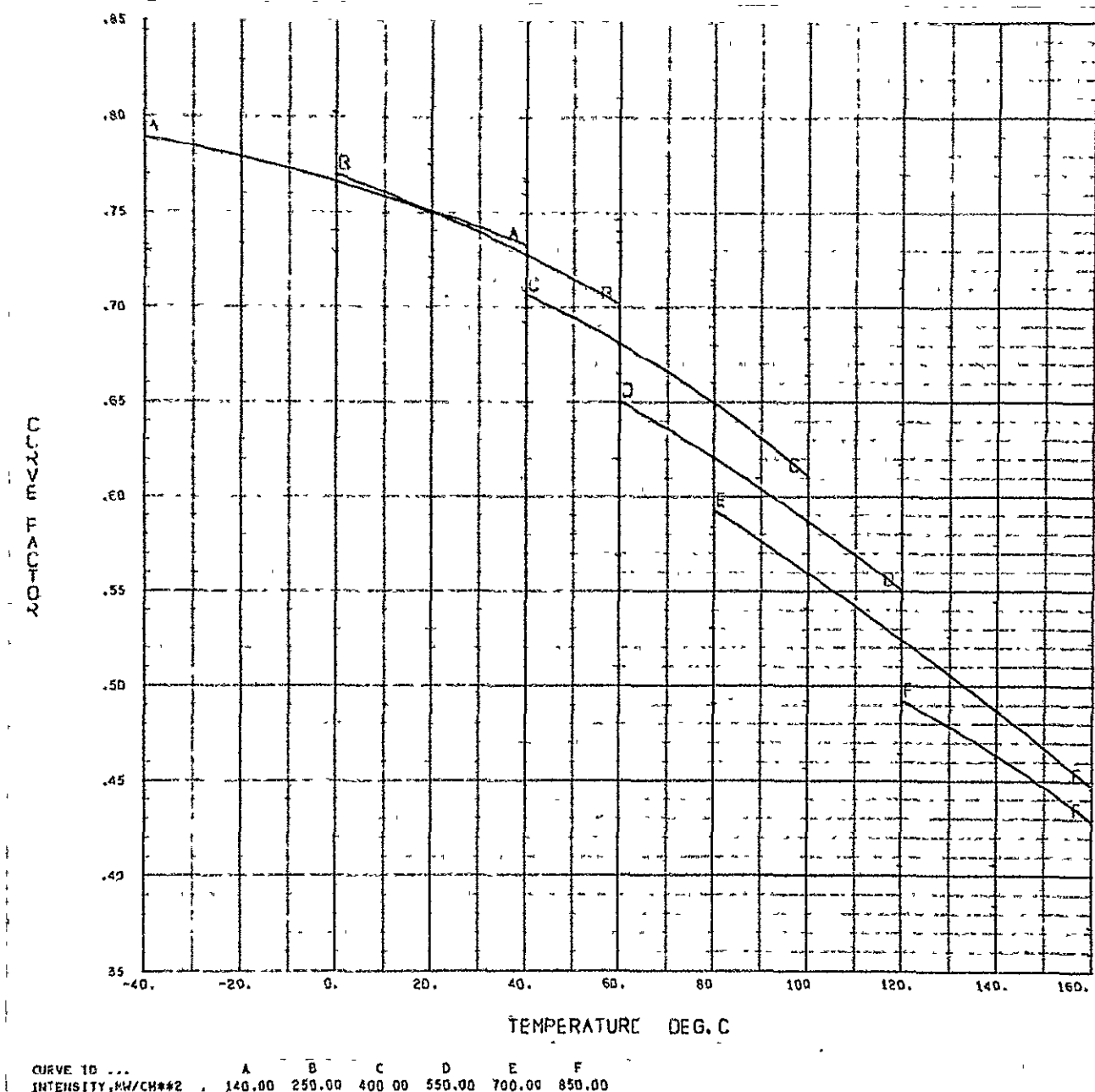


Fig. 70. Curve factor vs temperature, blue filter with mirror bar by contact on 2 ohm-cm cell

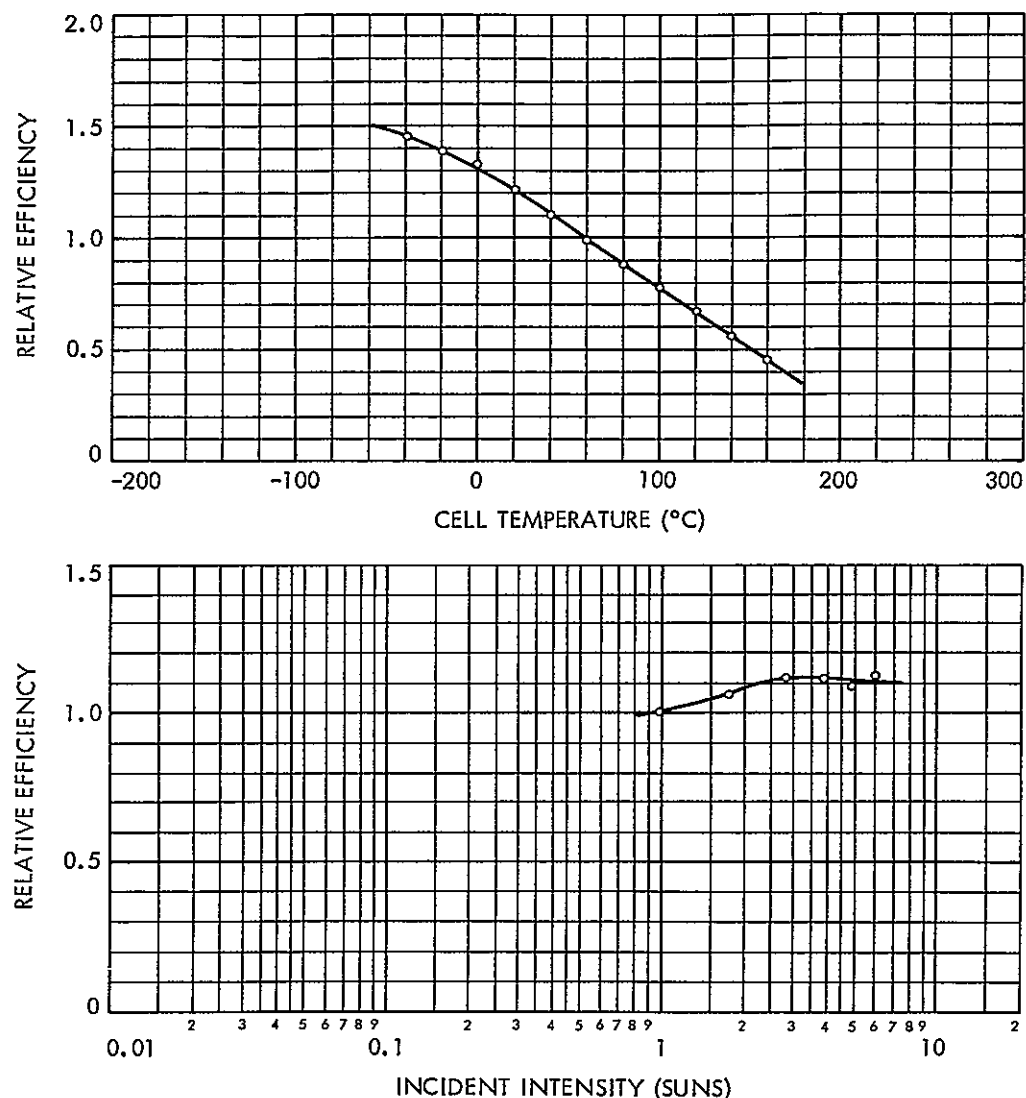
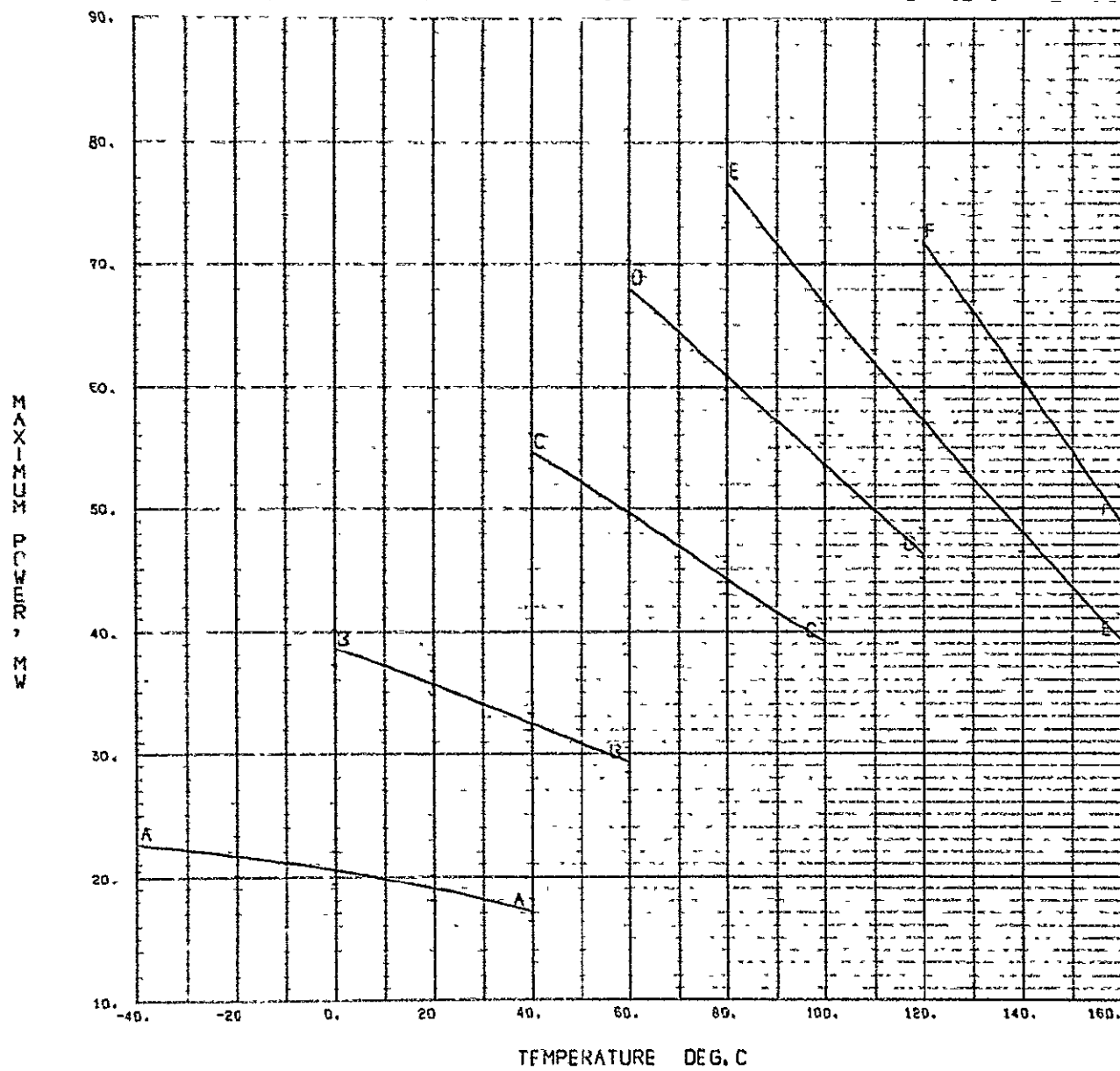


Fig. 71. Cell efficiency vs temperature and intensity, blue filter with mirror bar opposite contact on 2 ohm-cm cell



CURVE 10 ... A B C D E F
 INTENSITY, MW/CH4#2 .. 140.00 250.00 400.00 550.00 700.00 850.00

Fig. 72. Maximum power vs temperature, blue filter with mirror bar opposite contact on 2 ohm-cm cell

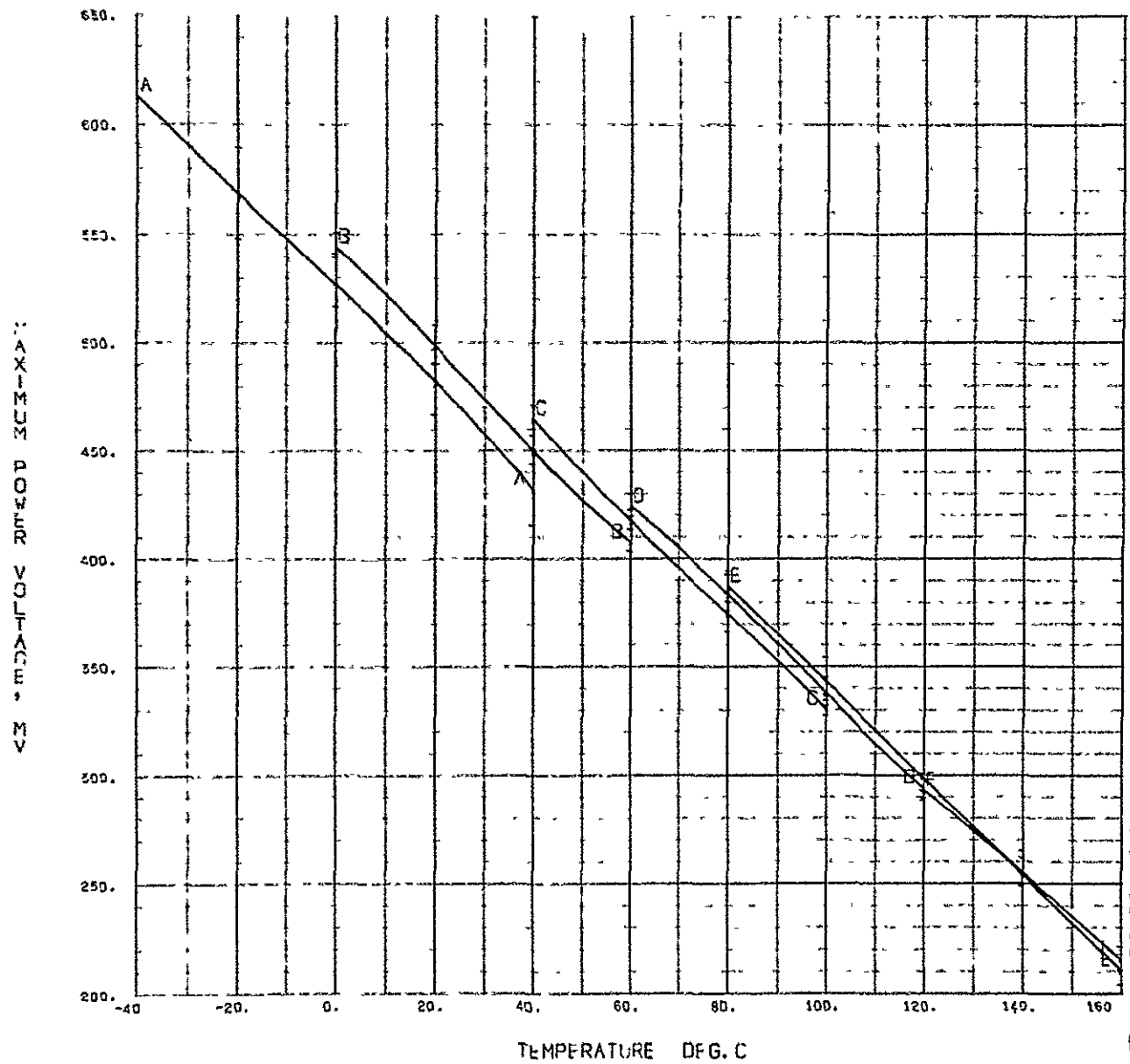


Fig. 73. Maximum-power voltage vs temperature, blue filter with mirror bar opposite contact on 2 ohm-cm cell

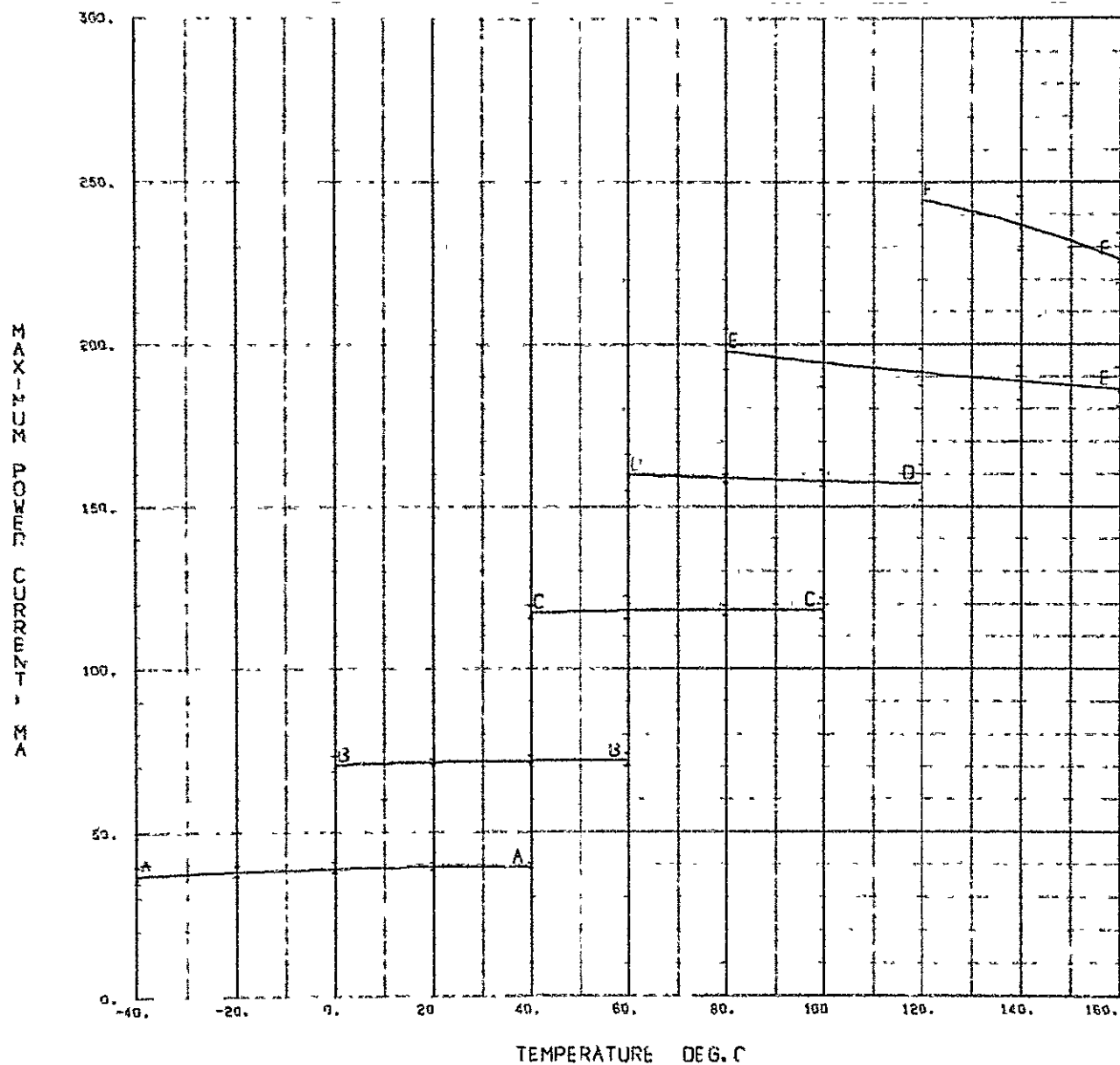


Fig. 74 Maximum-power current vs temperature, blue filter with mirror bar opposite contact on 2 ohm-cm cell

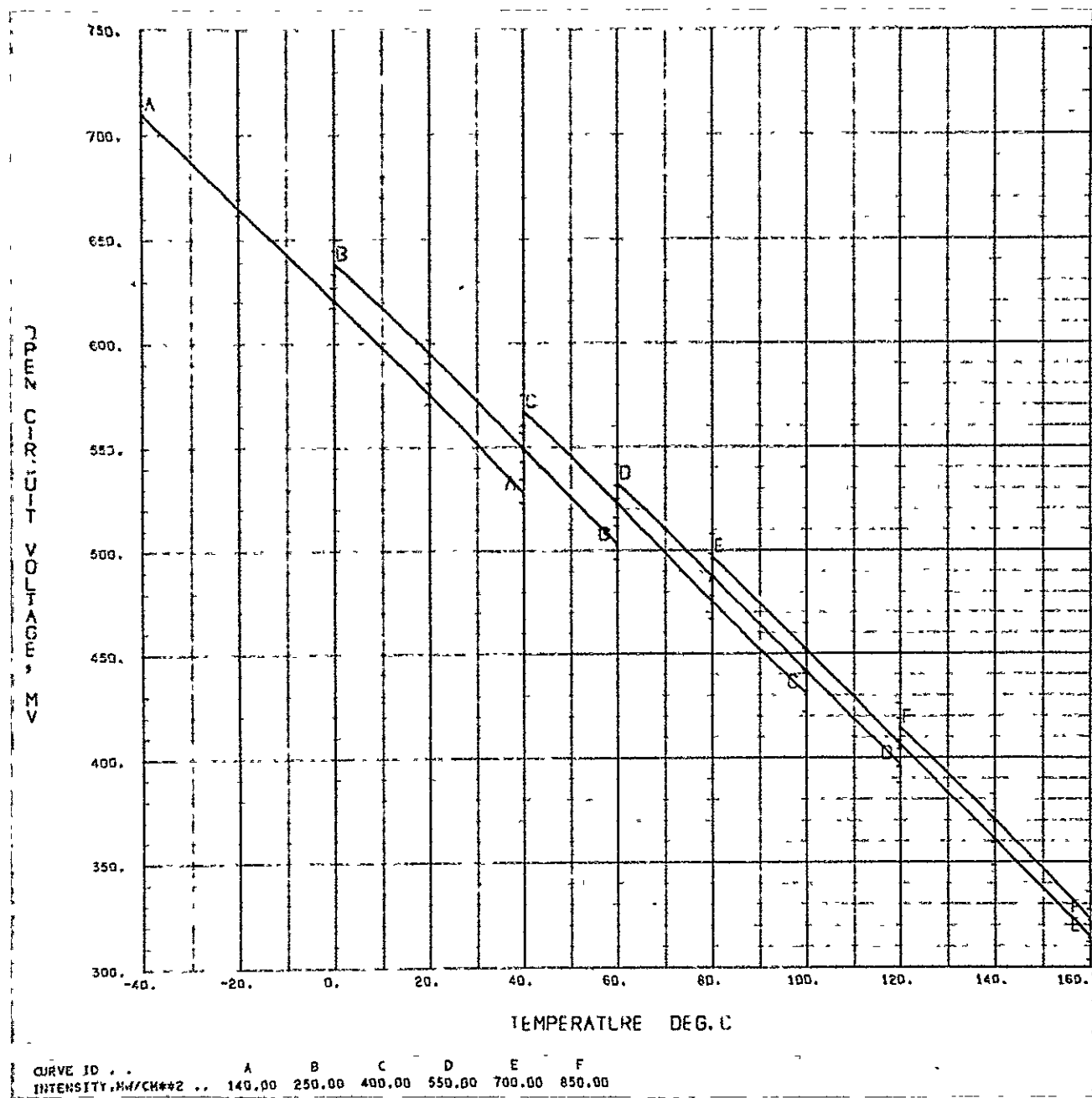


Fig. 75. Open-circuit voltage vs temperature, blue filter with mirror bar opposite contact on 2 ohm-cm cell

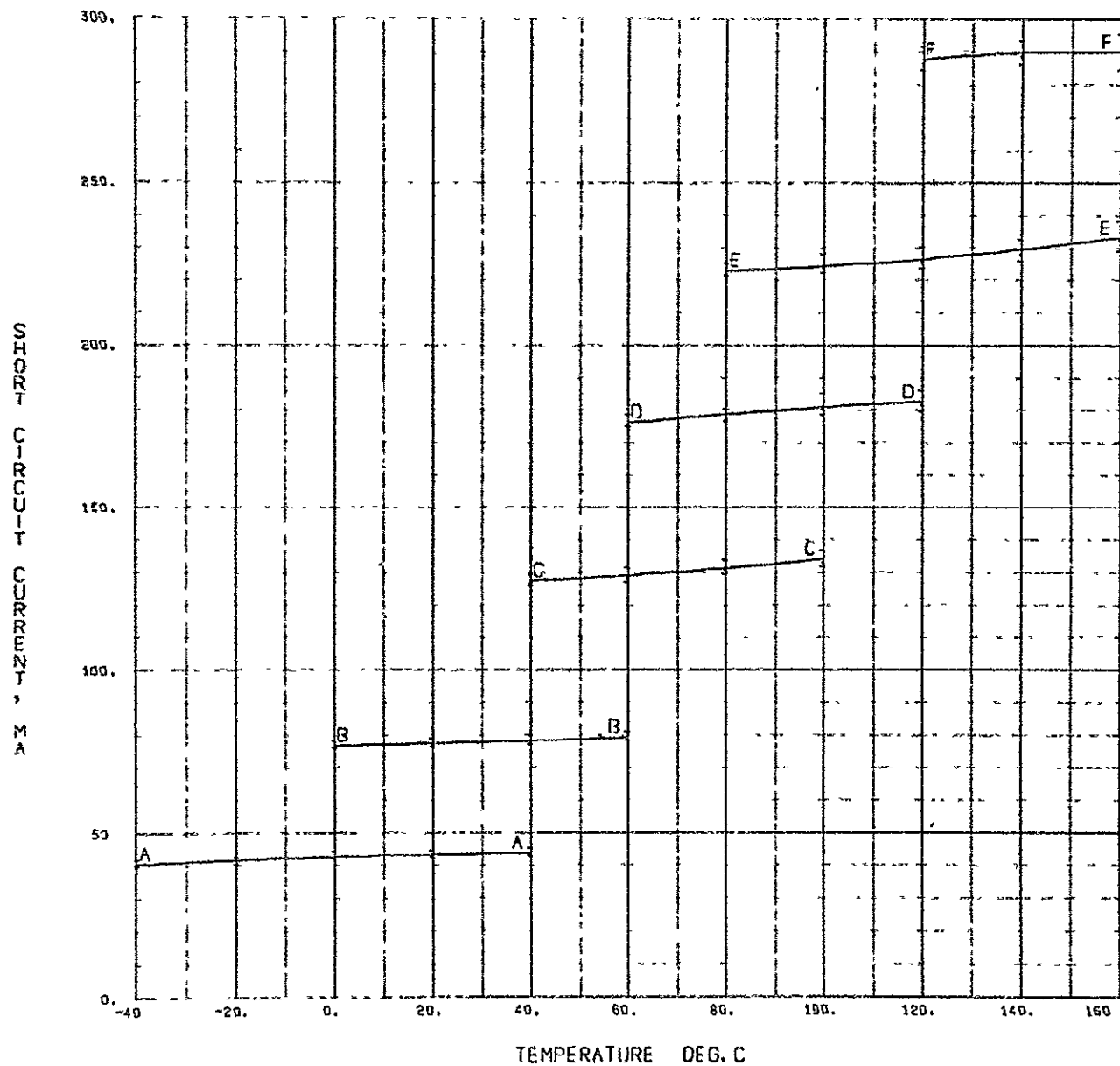
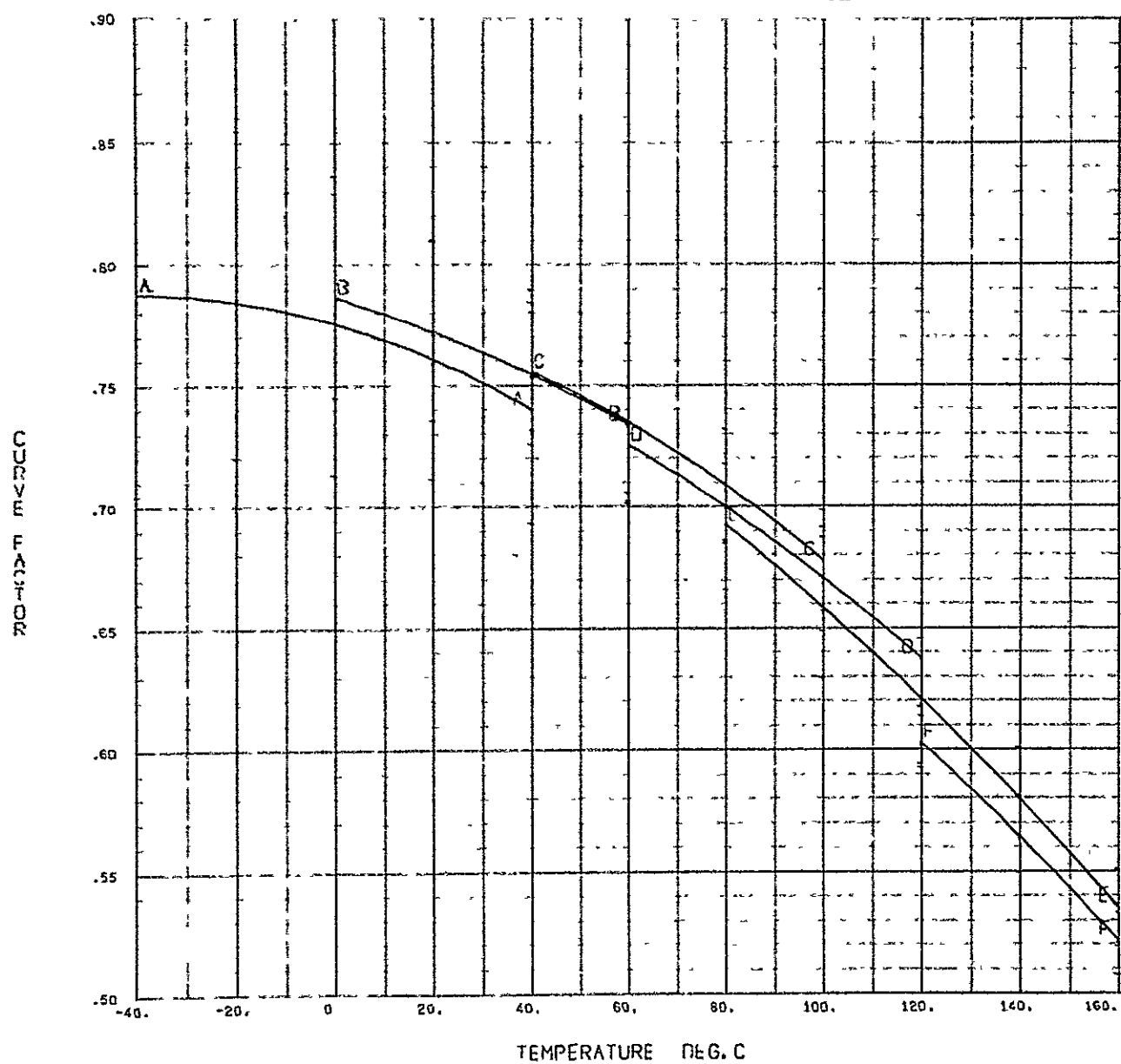


Fig. 76. Short-circuit current vs temperature, blue filter with mirror bar opposite contact on 2 ohm-cm cell

NOT REPRODUCIBLE



CURVE ID ... A B C D E F
 INTENSITY, MH/CH**2 , 140.00 250.00 400.00 550.00 700.00 850.00

Fig. 77 Curve factor vs temperature, blue filter with mirror bar opposite contact on 2 ohm-cm cell

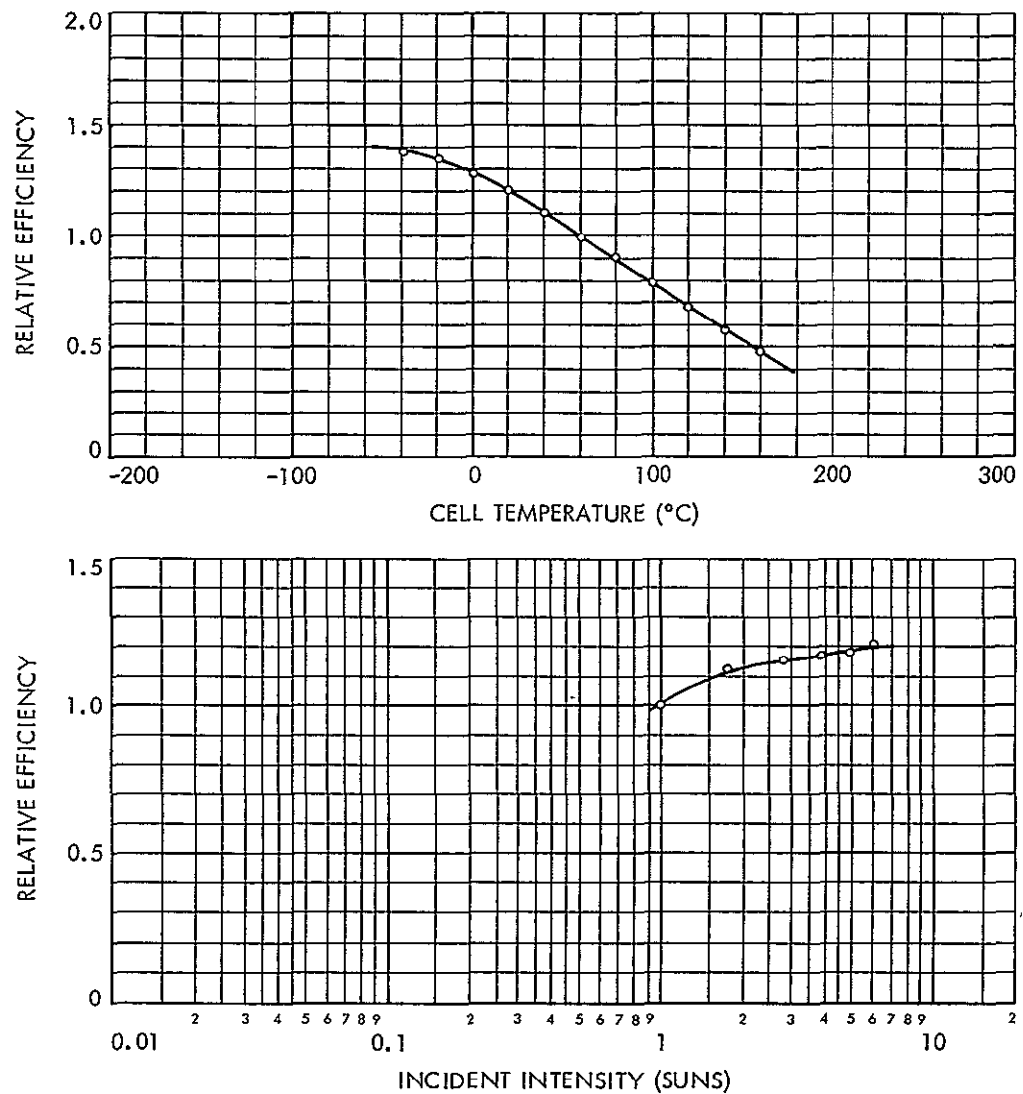


Fig 78 Cell efficiency vs temperature and intensity, blue-red filter on
2 ohm-cm multiple wide-grid cell

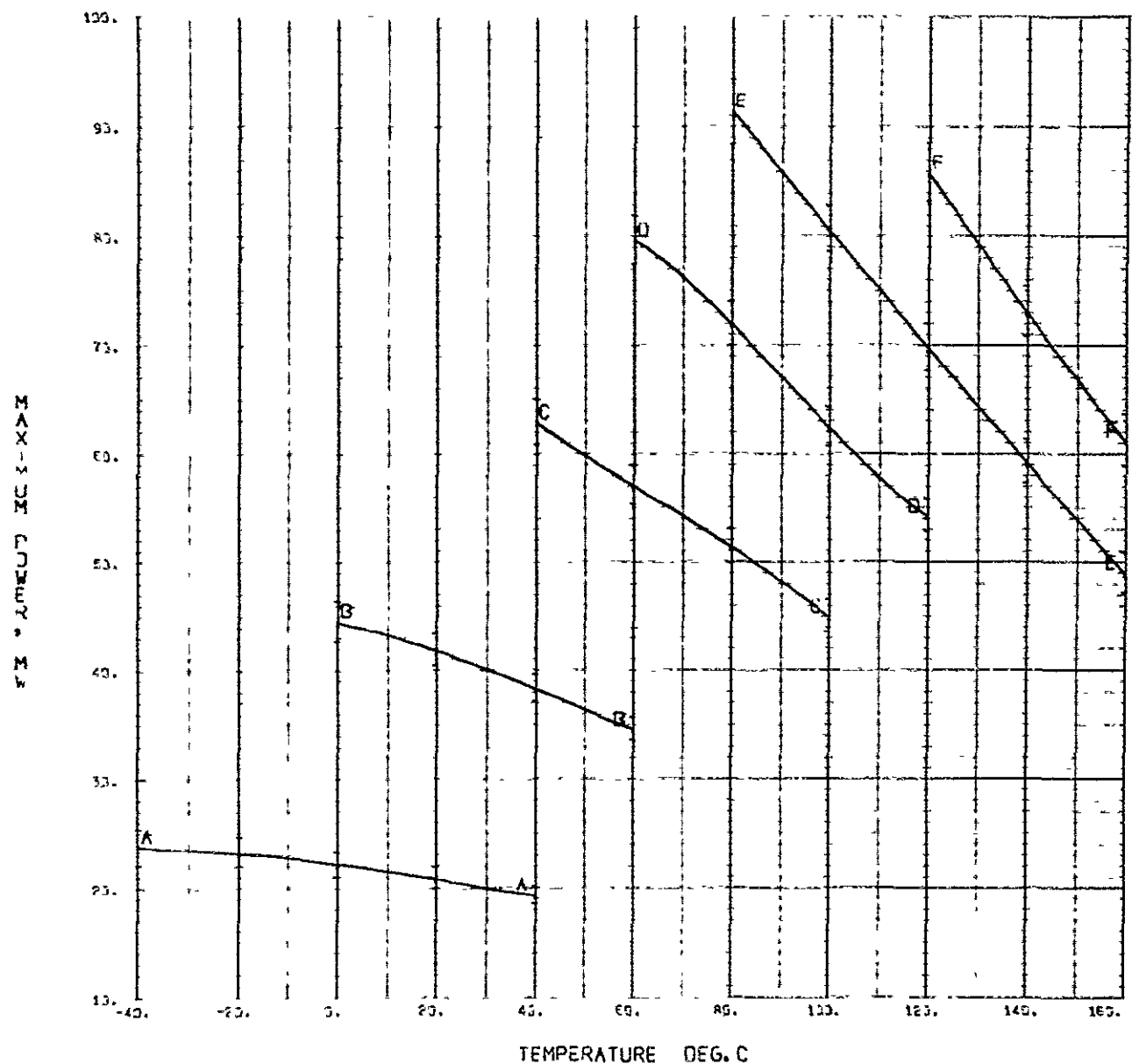


Fig. 79. Maximum power vs temperature, blue-red filter on 2 ohm-cm multiple wide-grid cell

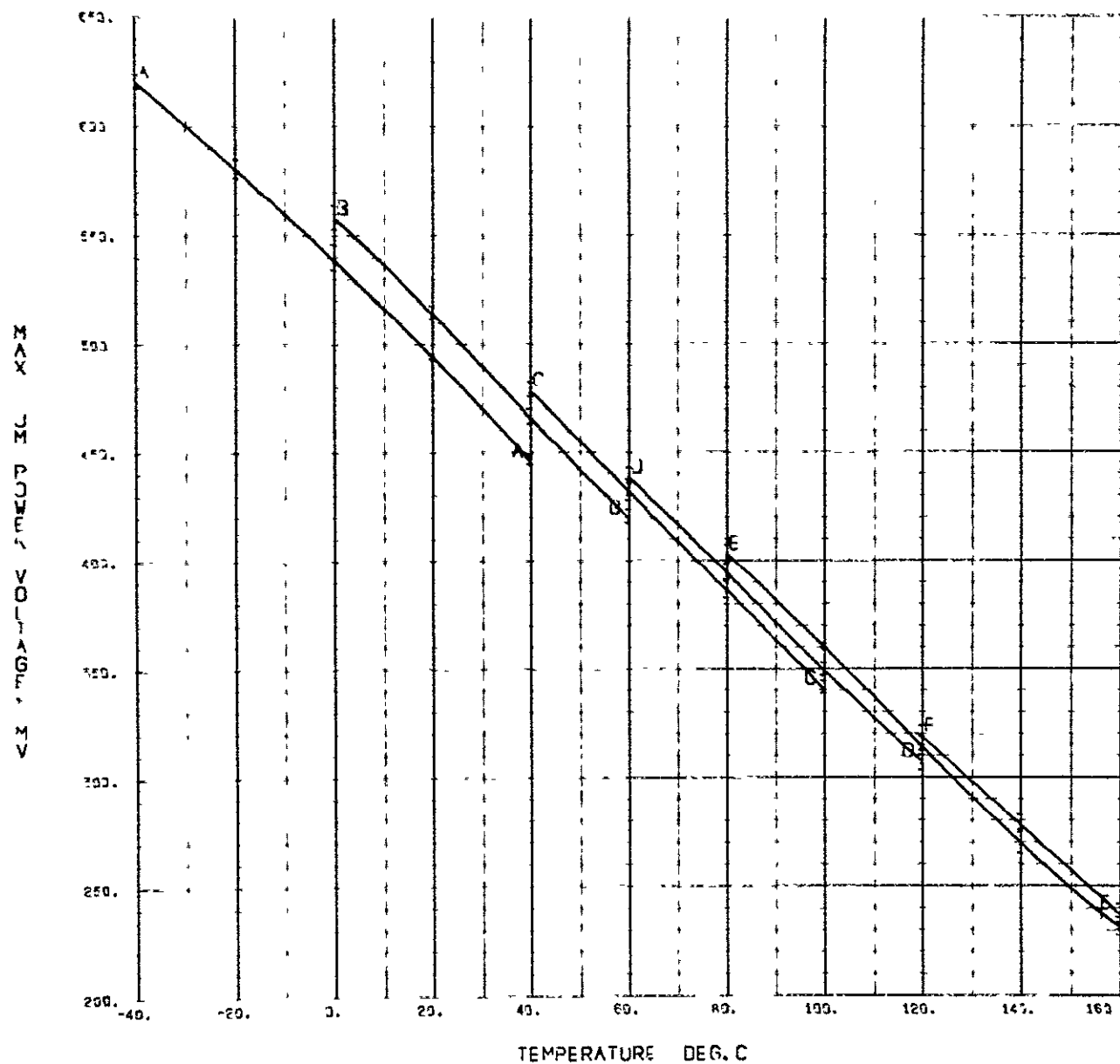


Fig. 80. Maximum-power voltage vs temperature, blue-red filter on 2 ohm-cm multiple wide-grid cell

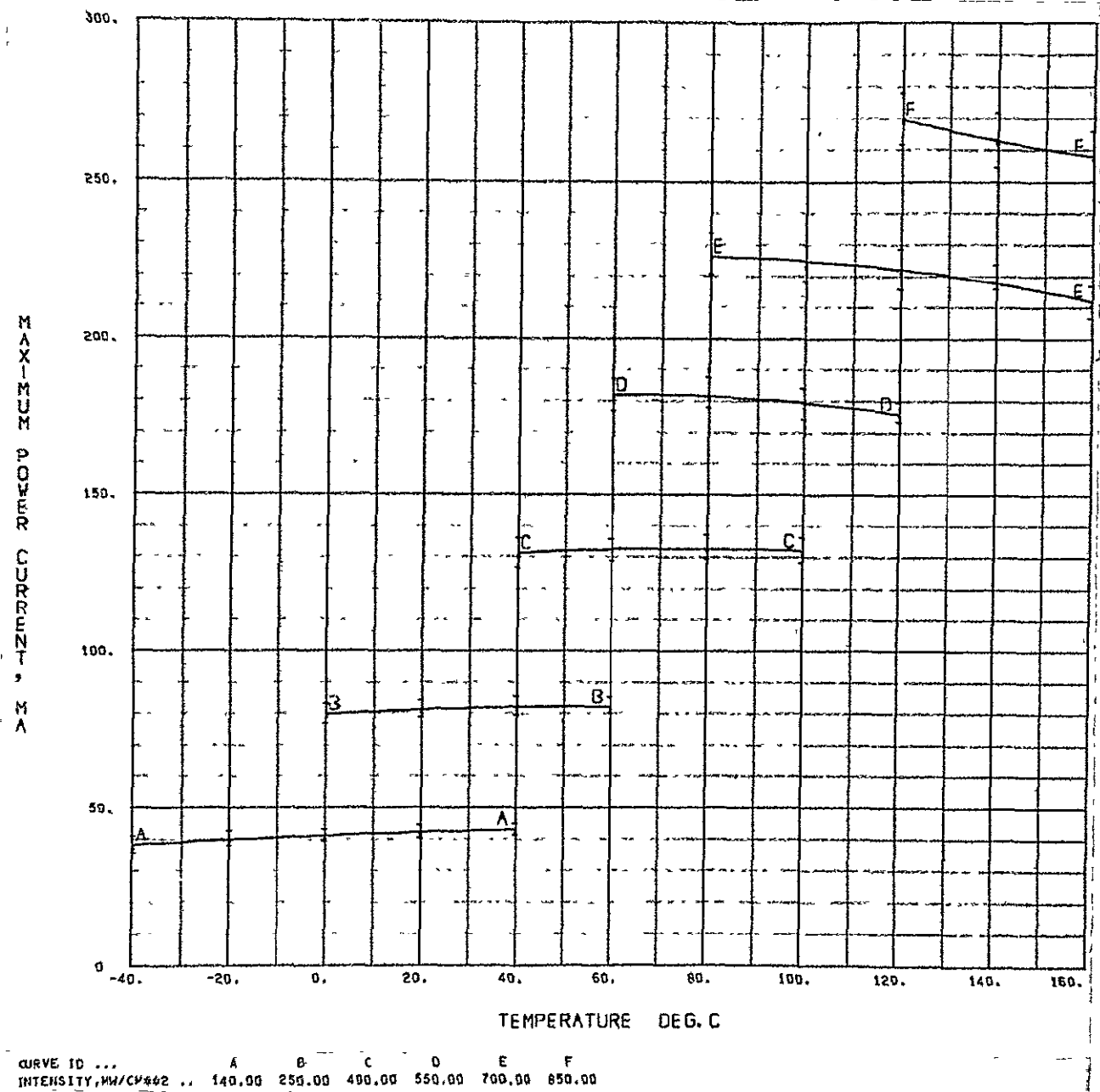


Fig. 81. Maximum-power current vs temperature, blue-red filter on 2 ohm-cm multiple wide-grid cell

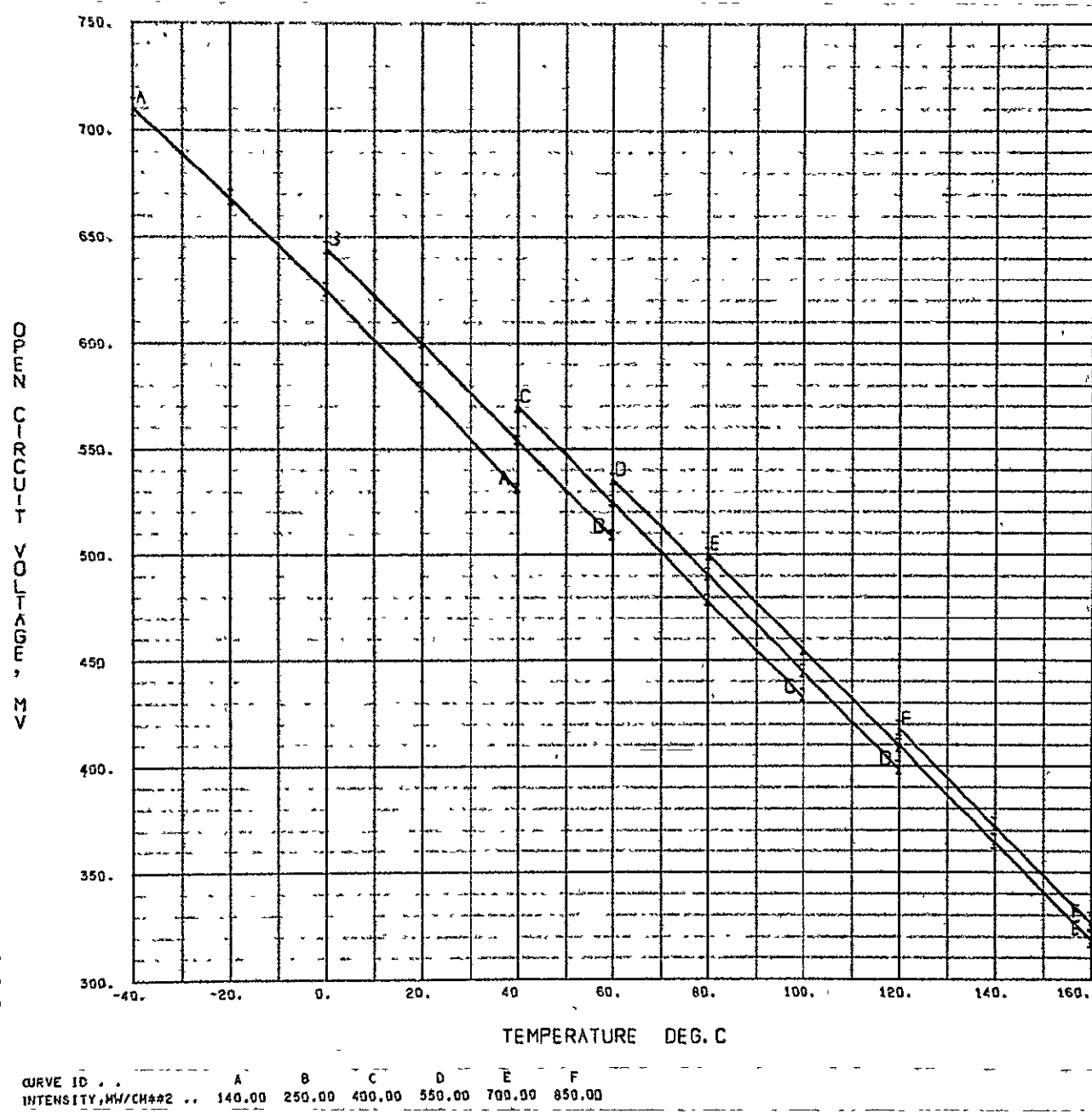


Fig. 82. Open-circuit voltage vs temperature, blue-red filter on 2 ohm-cm multiple wide-grid cell

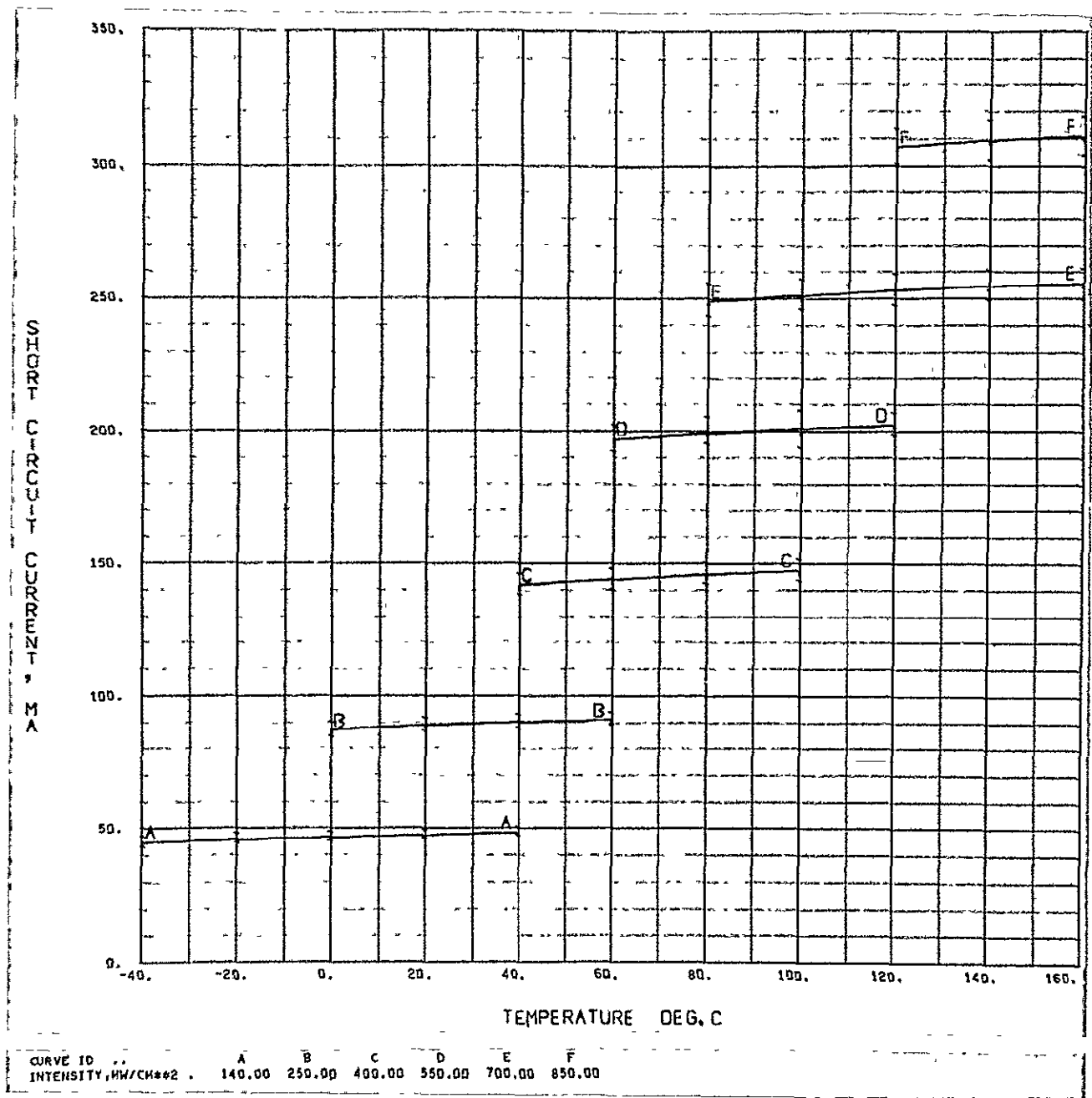


Fig. 83. Short-circuit current vs temperature, blue-red filter on 2 ohm-cm multiple wide-grid cell

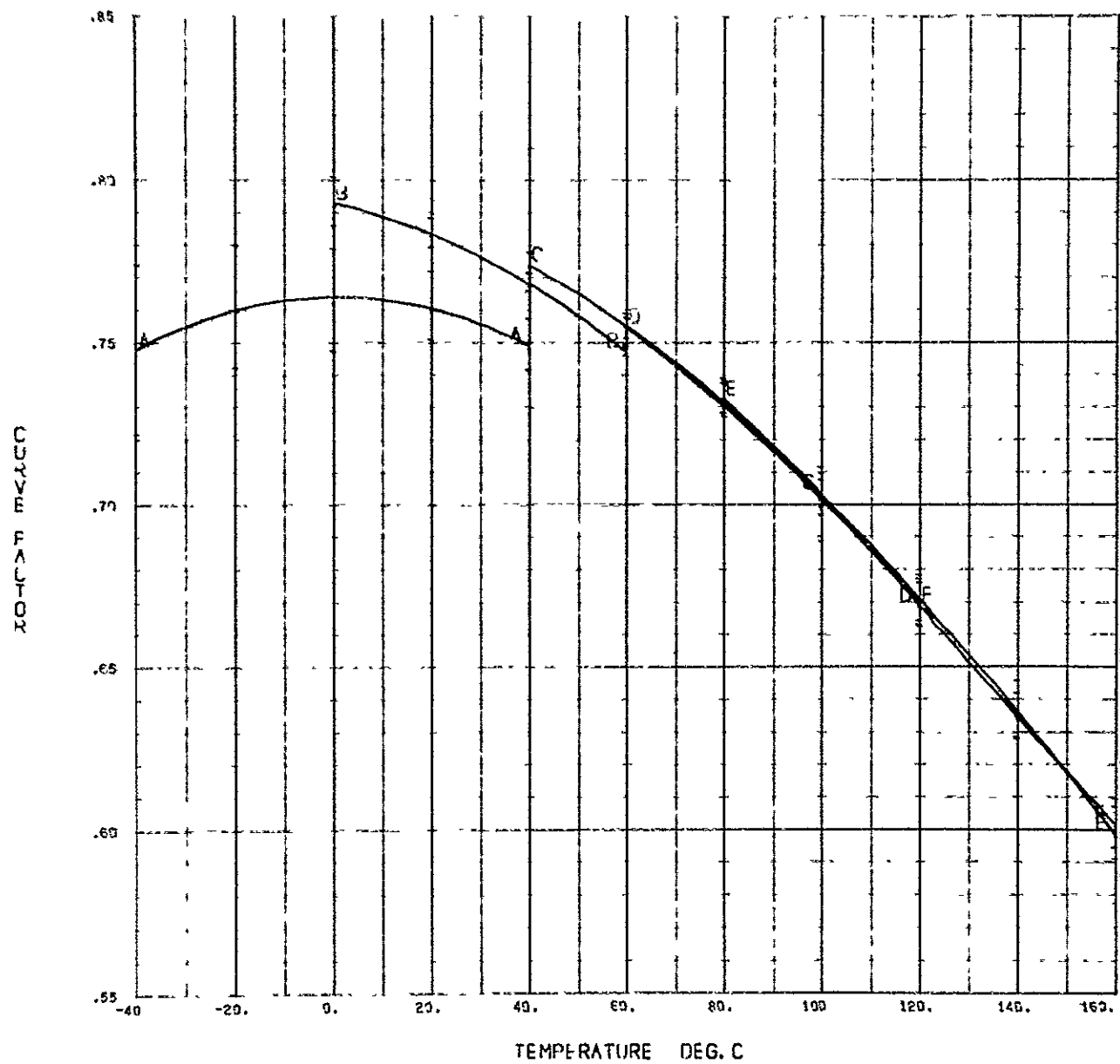


Fig. 84. Curve factor vs temperature, blue-red filter on 2 ohm-cm multiple wide-grid cell

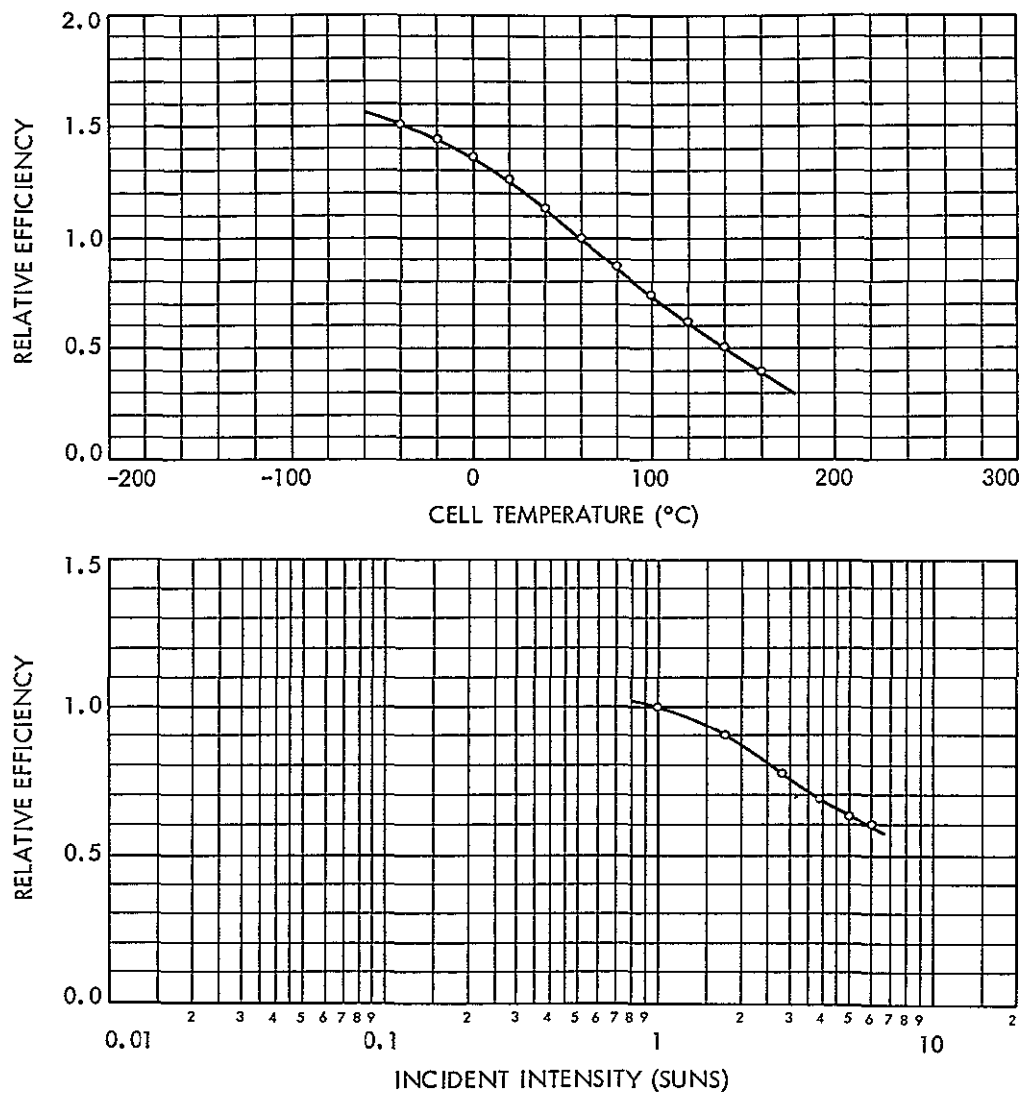


Fig. 85. Cell efficiency vs temperature and intensity, blue-red filter on 2 ohm-cm single wide-grid cell

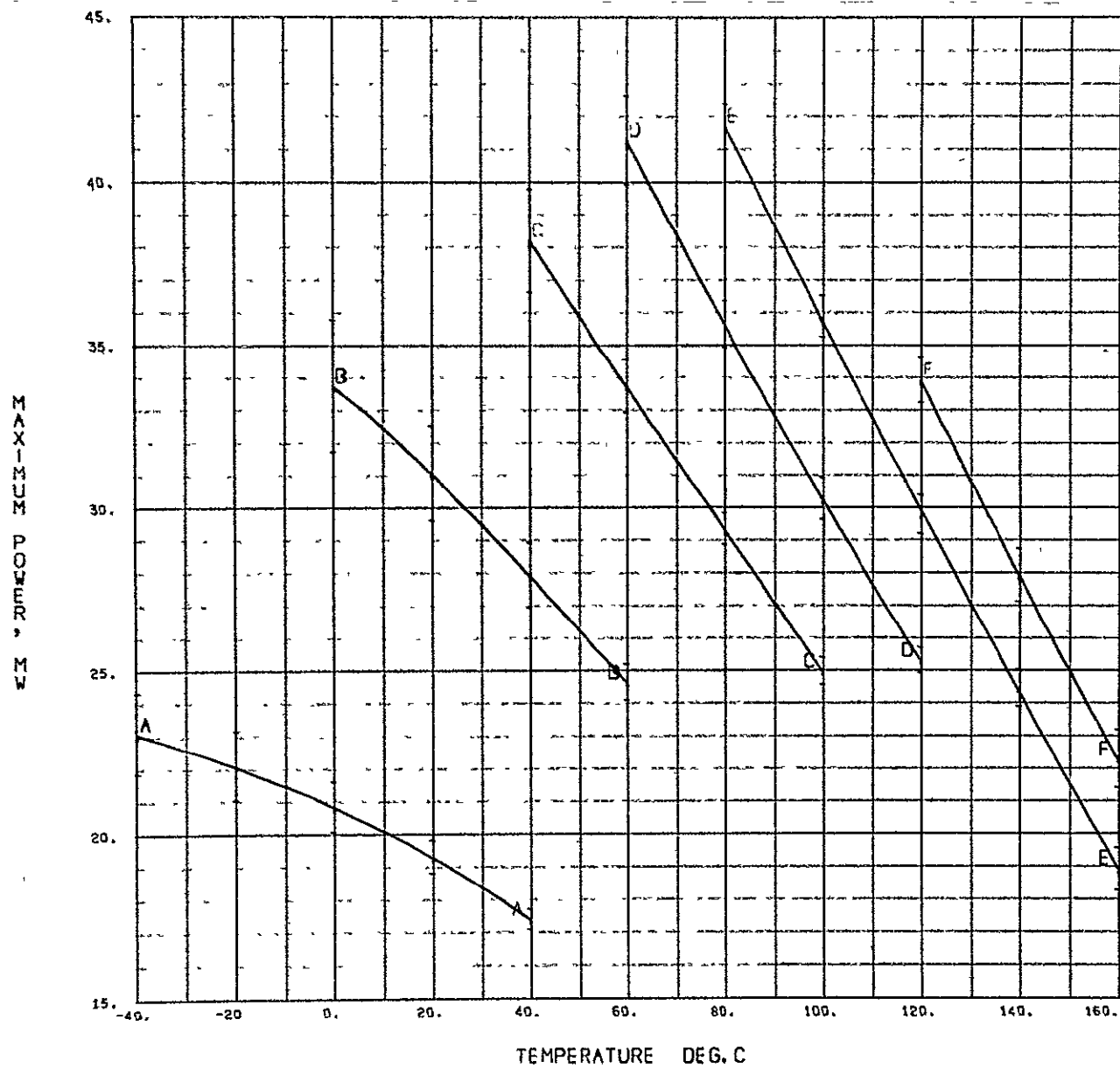


Fig. 86. Maximum power vs temperature, blue-red filter on 2 ohm-cm single wide-grid cell

NOT REPRODUCIBLE

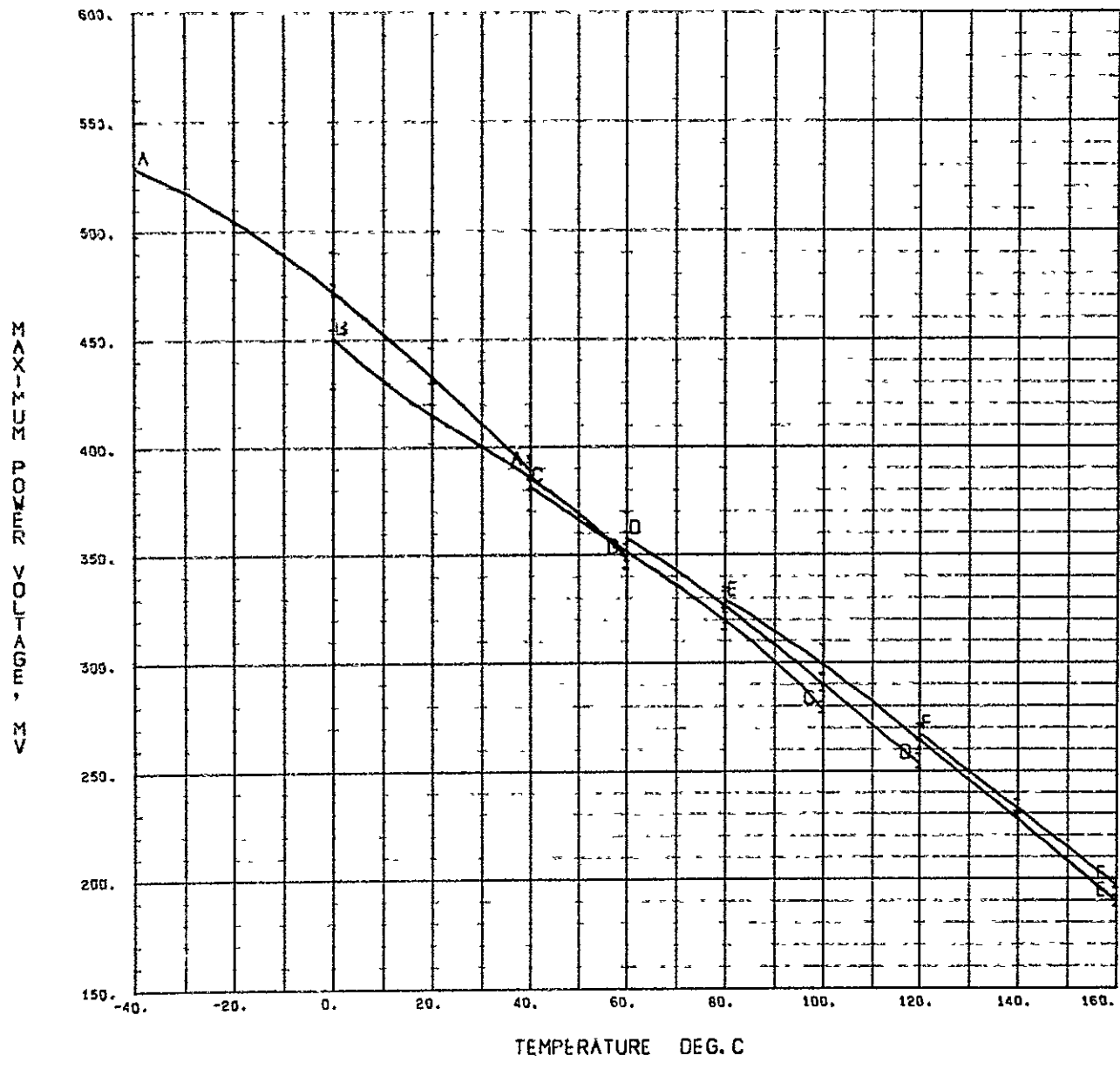
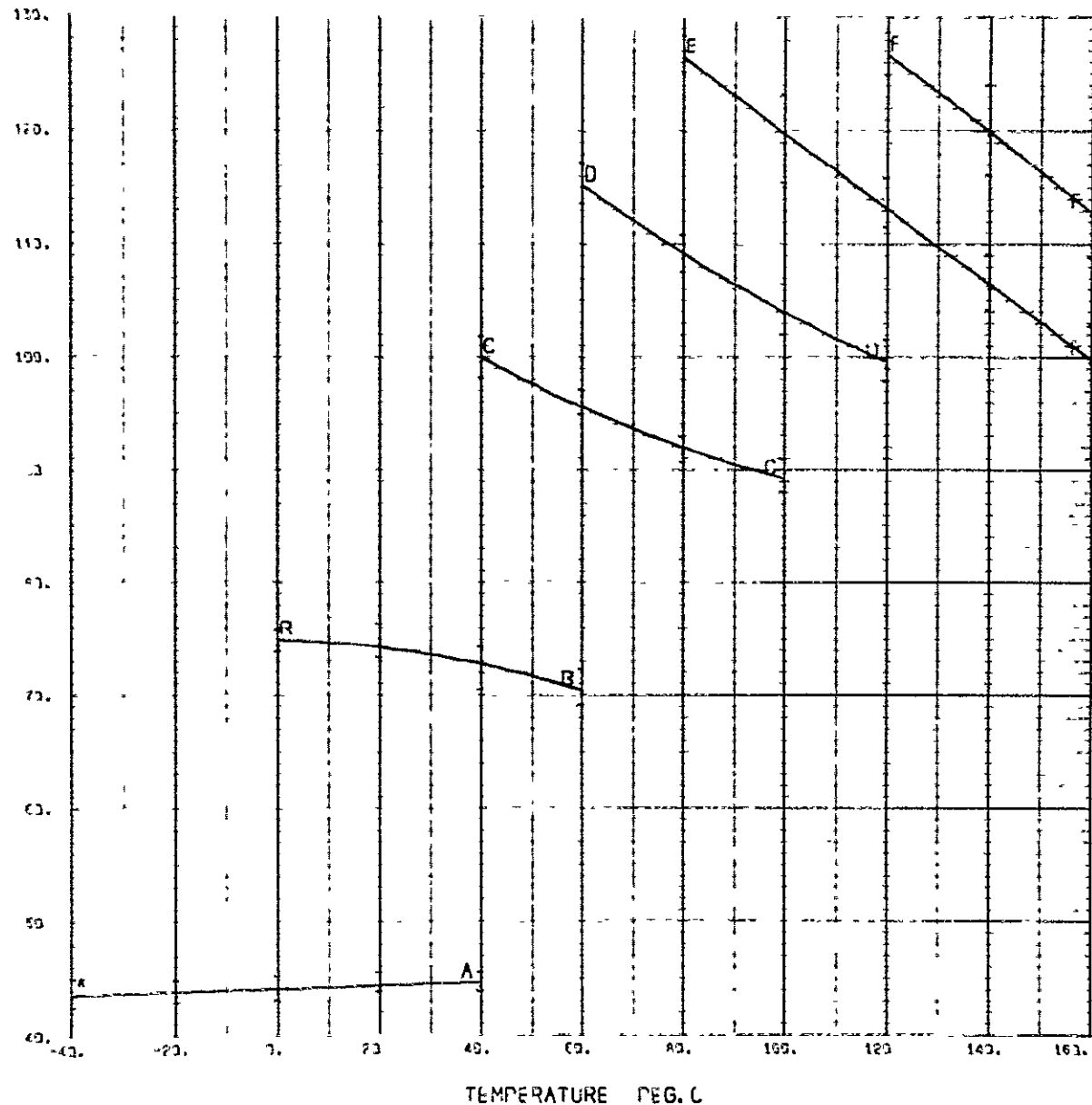


Fig. 87. Maximum-power voltage vs temperature, blue-red filter on 2 ohm-cm single wide-grid cell

MAXIMUM POWER CURRENT



DATA FOR
INTENSITy, MA/100°C², A E C D E F
140.00 250.00 400.00 550.00 700.00 450.00

Fig. 88. Maximum-power current vs temperature, blue-red filter on 2 ohm-cm single wide-grid cell

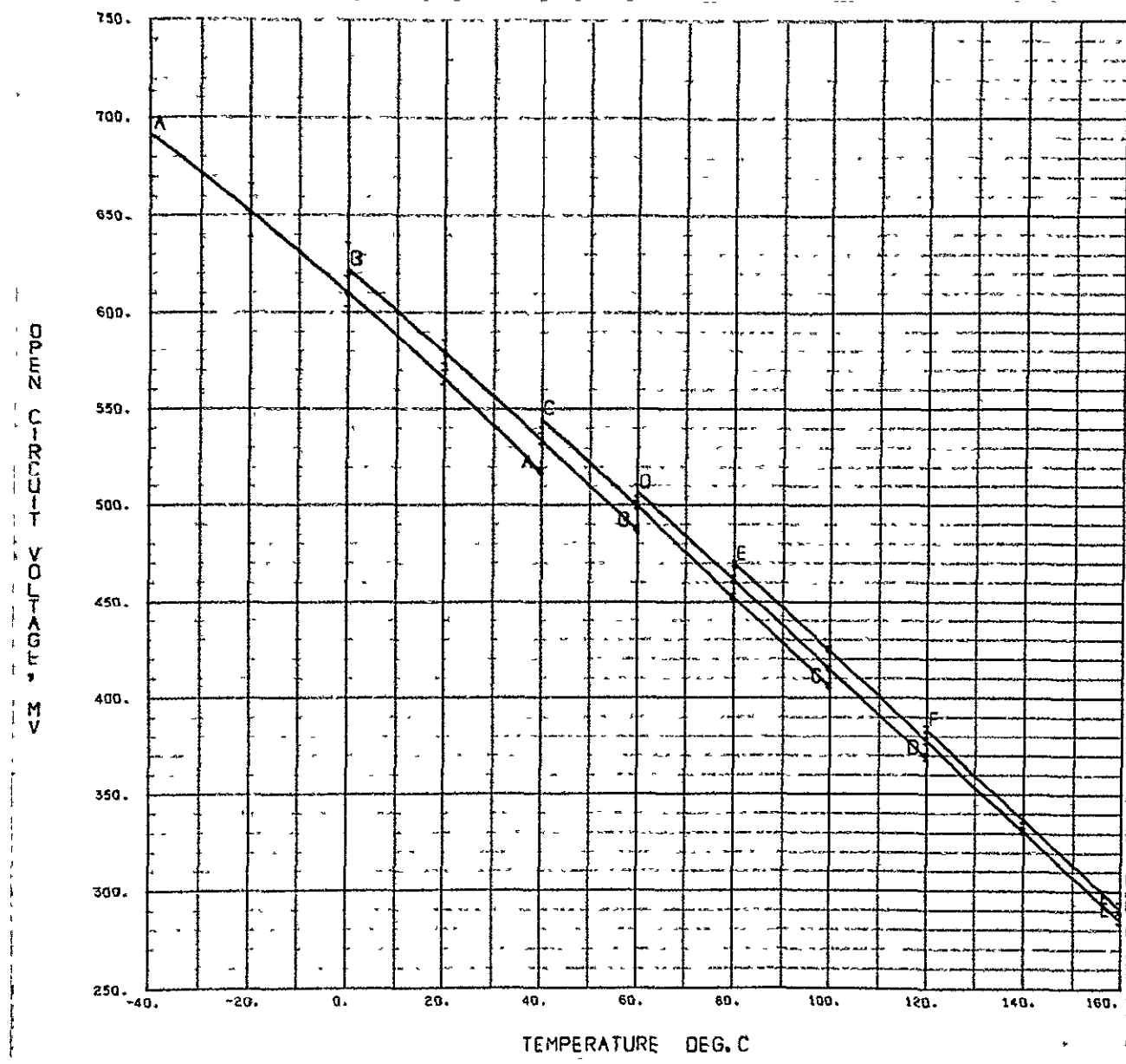


Fig. 89. Open-circuit voltage vs temperature, blue-red filter on 2 ohm-cm single wide-grid cell

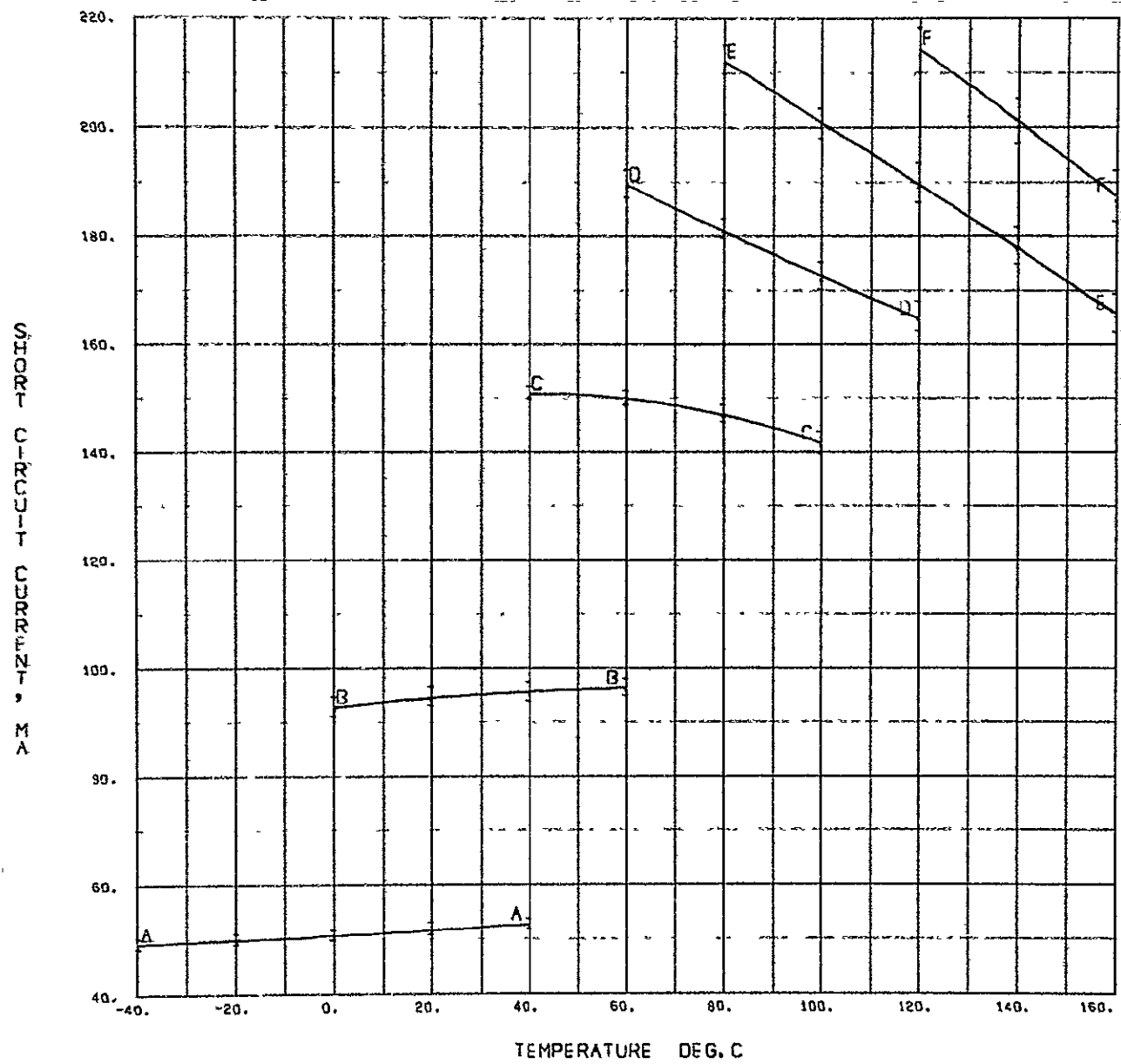


Fig. 90. Short-circuit current vs temperature, blue-red filter on 2 ohm-cm single wide-grid cell

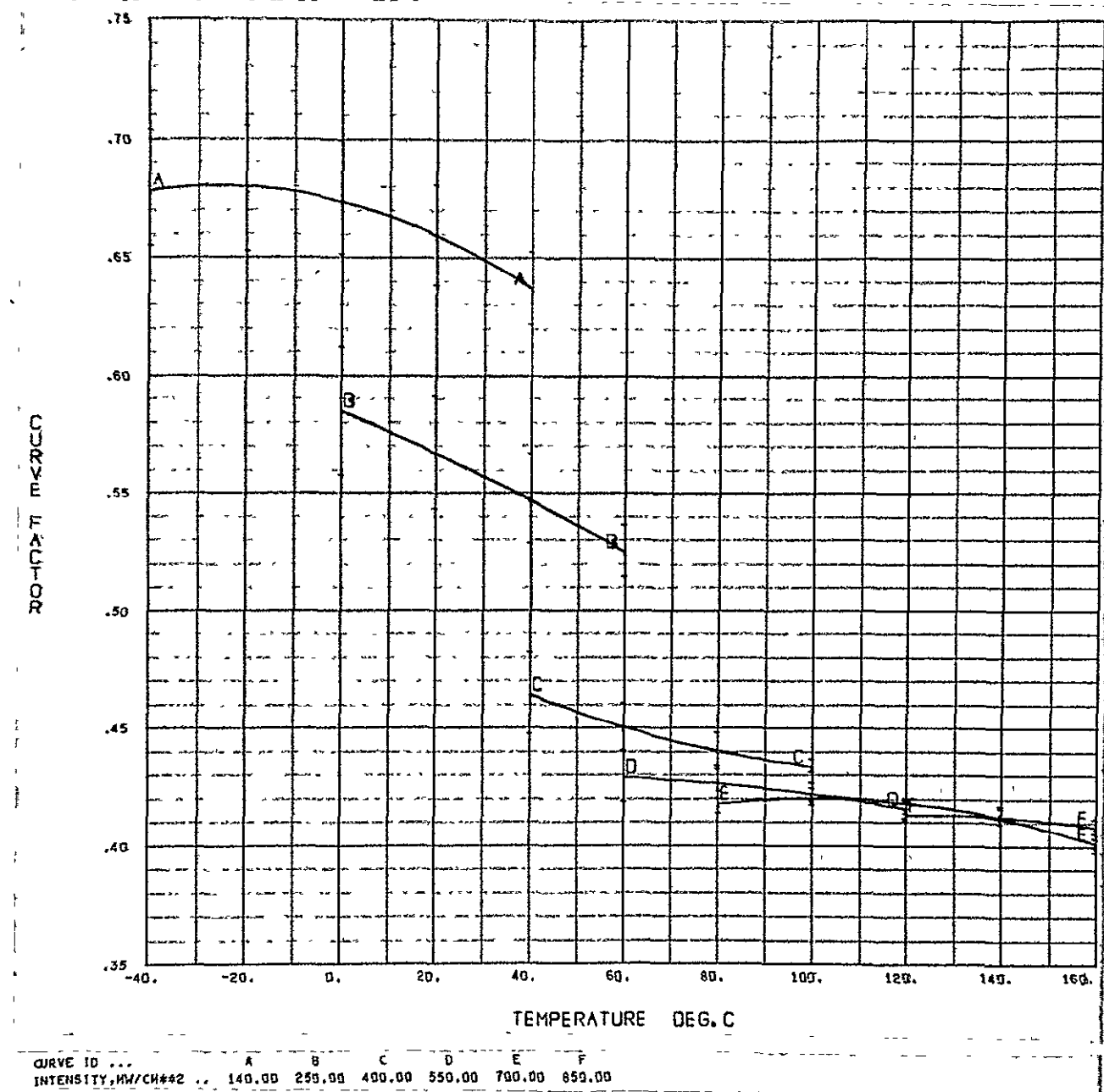


Fig. 91. Curve factor vs temperature, blue-red filter on 2 ohm-cm single wide-grid cell

NOT REPRODUCIBLE

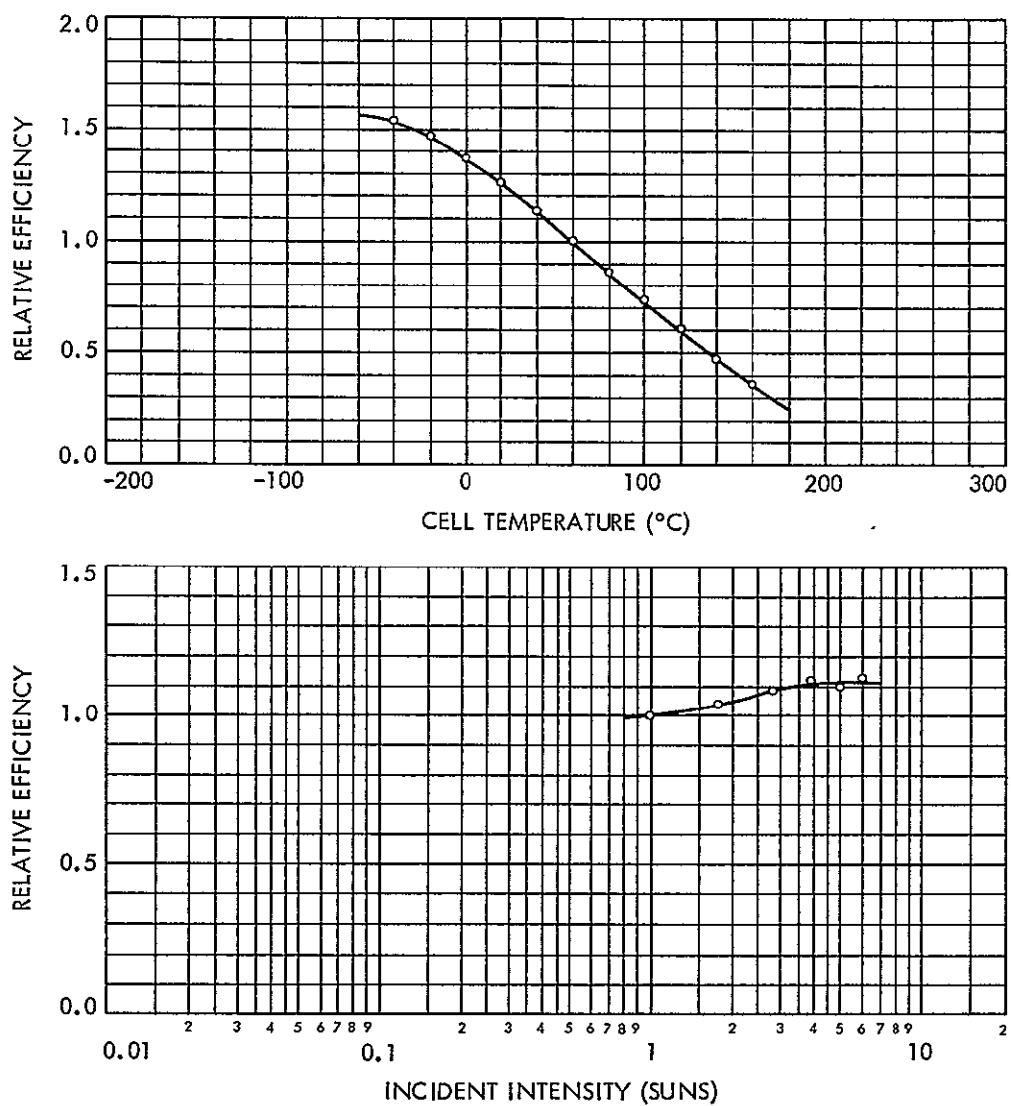


Fig. 92. Cell efficiency vs temperature and intensity, blue-red filter on 10 ohm-cm multiple wide-grid cell

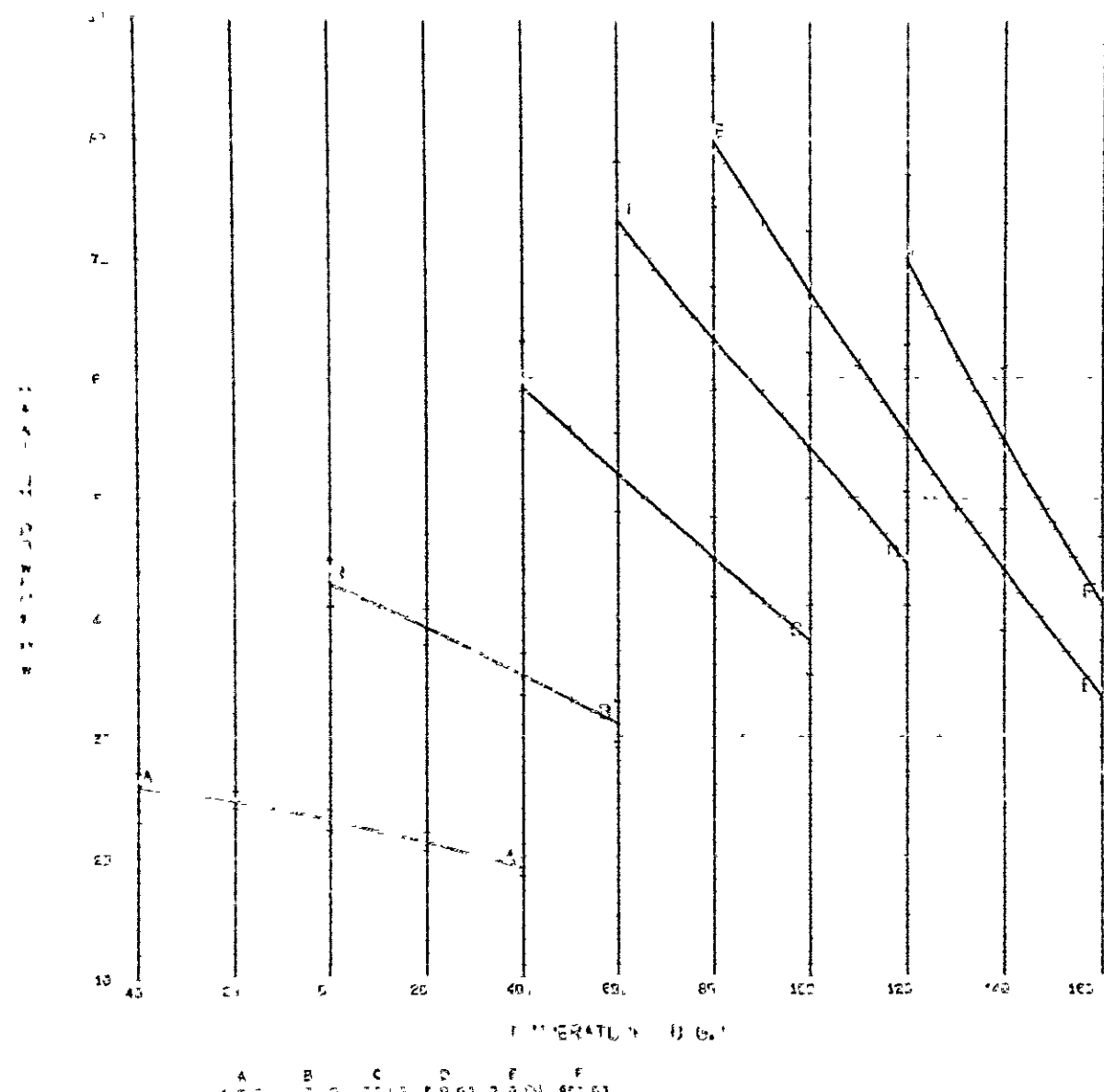


Fig. 93. Maximum power vs temperature, blue-red filter on 10 ohm-cm multiple wide-grid cell

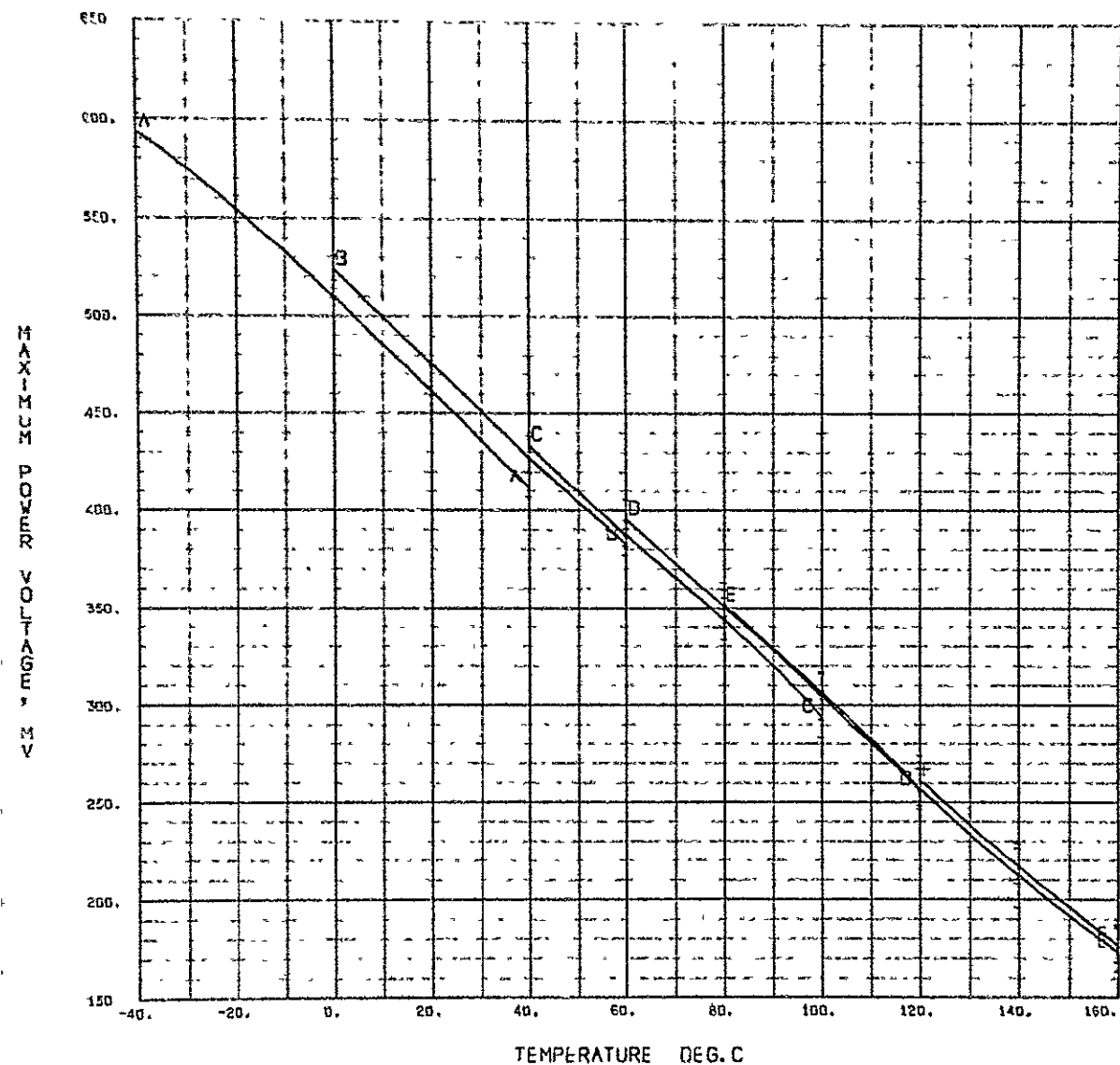
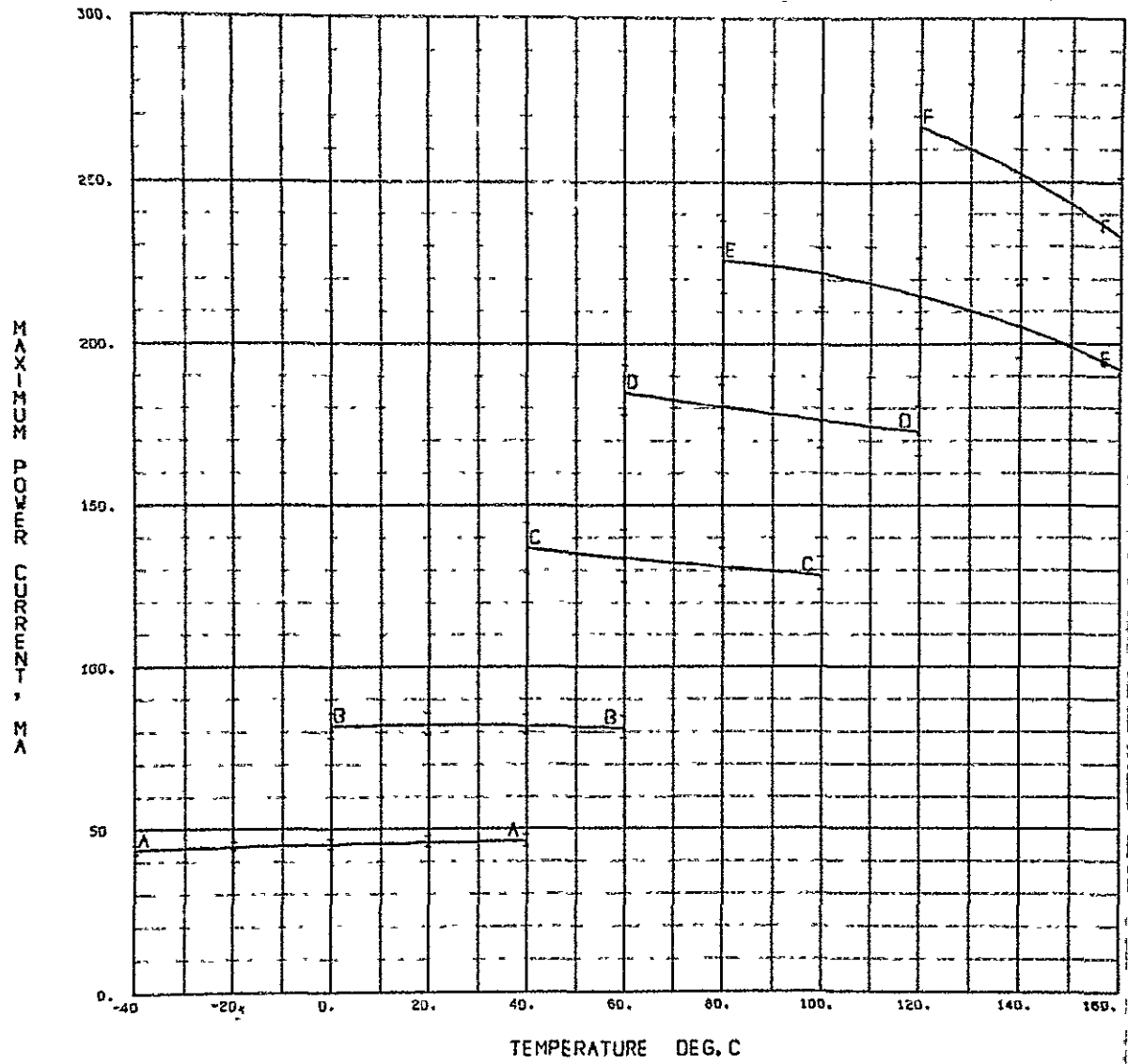


Fig. 94. Maximum-power voltage vs temperature, blue-red filter on 10 ohm-cm multiple wide-grid cell



CURVE ID ... A B C D E F
 INTENSITY, MW/CH#42 . 140.00 250.00 400.00 550.00 700.00 850.00

Fig. 95 Maximum-power current vs temperature, blue-red filter on 10 ohm-cm multiple wide-grid cell

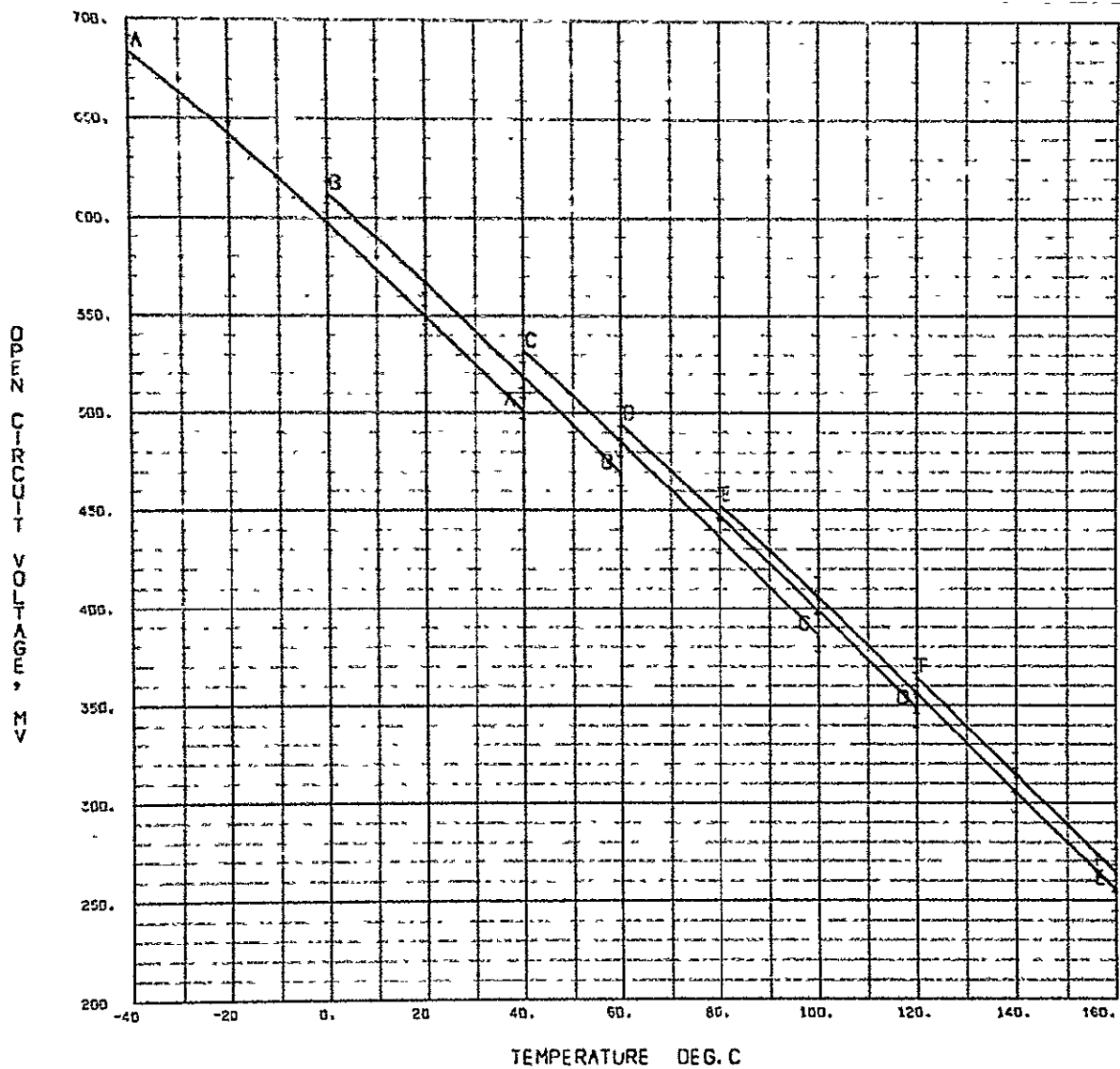
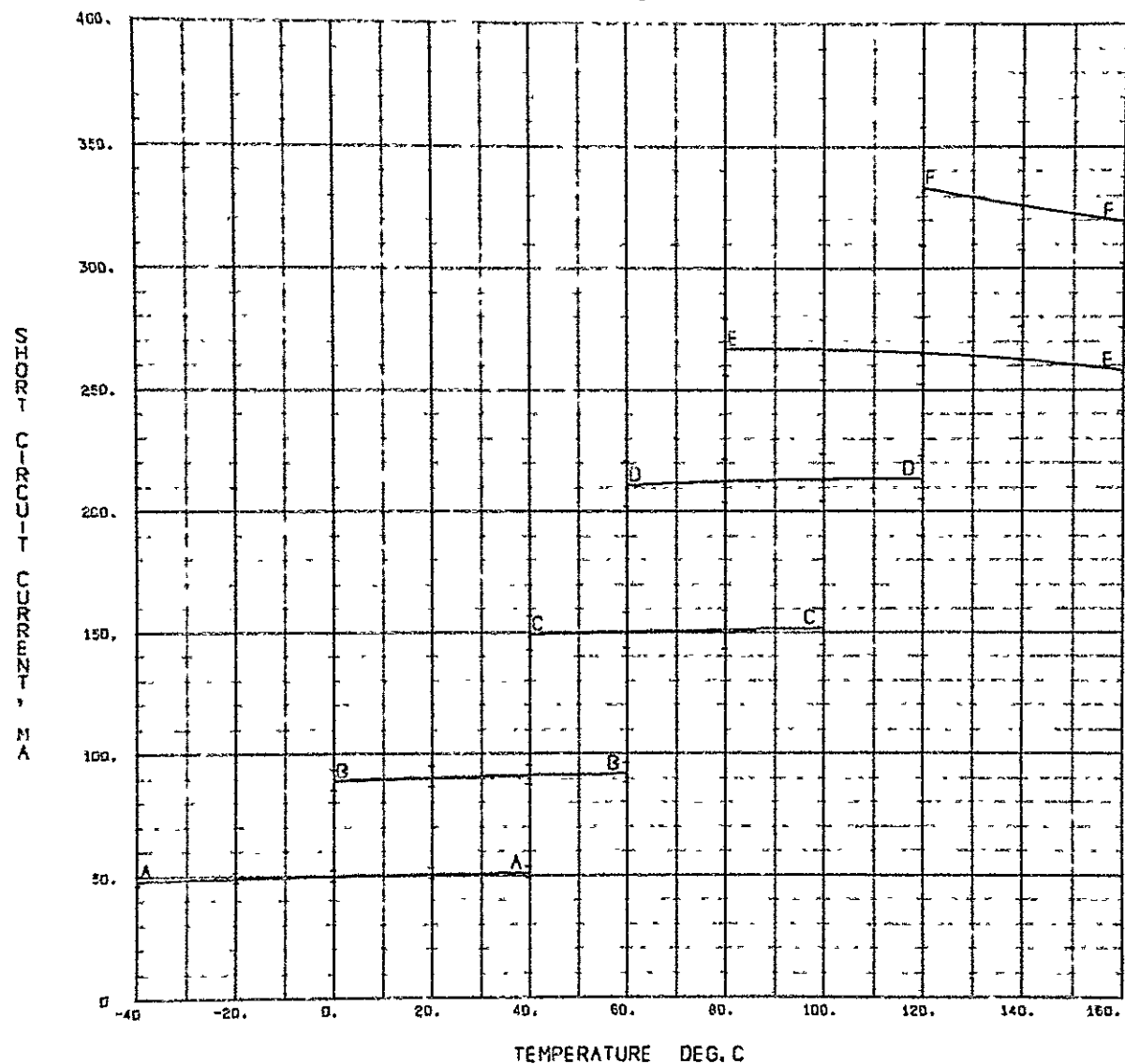


Fig. 96. Open-circuit voltage vs temperature, blue-red filter on 10 ohm-cm multiple wide-grid cell

NOT REPRODUCIBLE



CURVE ID ... A B C D E F
 INTENSITY, MW/CM² .. 140.00 250.00 400.00 550.00 700.00 850.00

Fig. 97. Short-circuit current vs temperature, blue-red filter on 10 ohm-cm multiple wide-grid cell

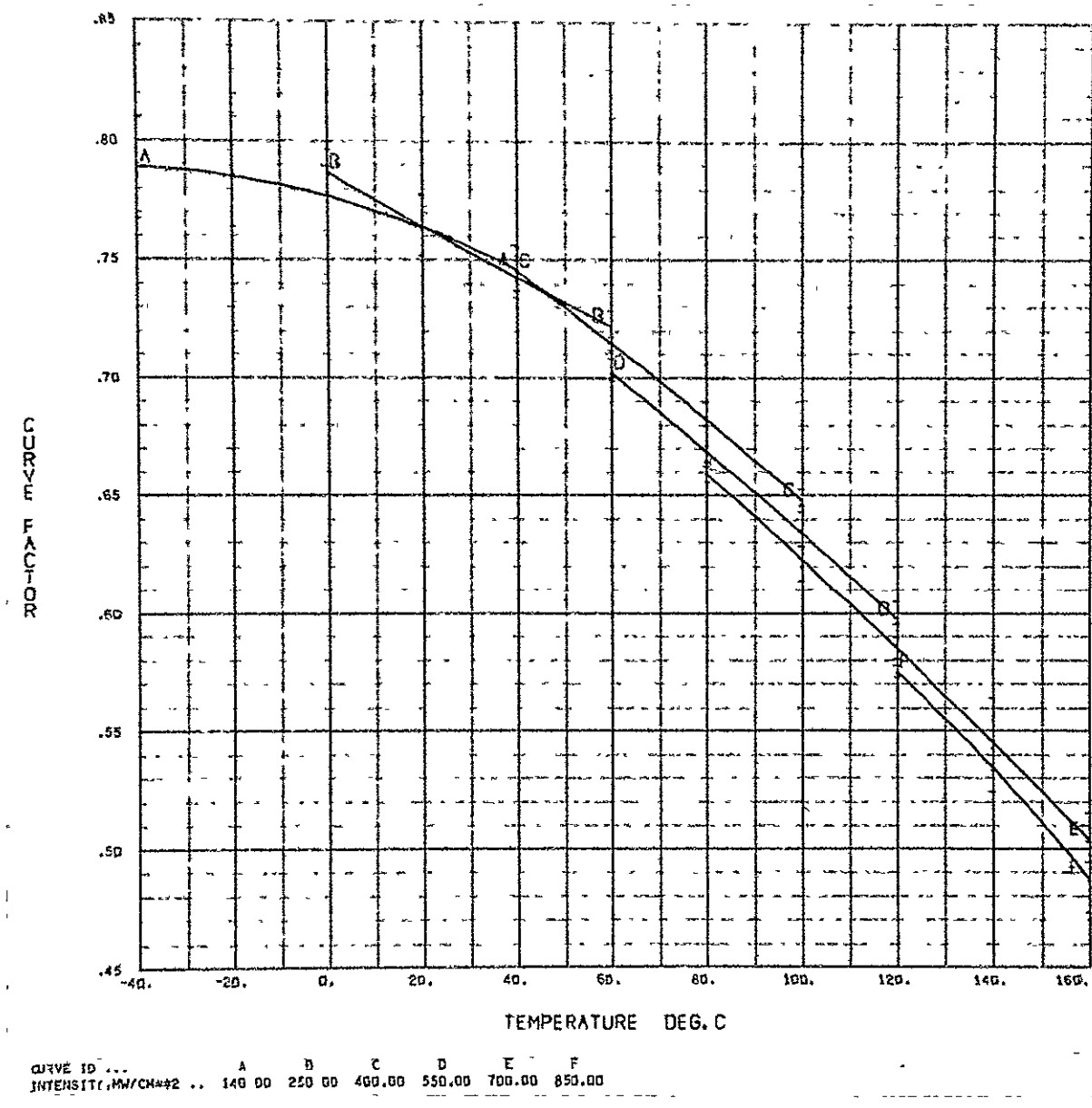


Fig. 98. Curve factor vs temperature, blue-red filter on 10 ohm-cm multiple wide-grid cell

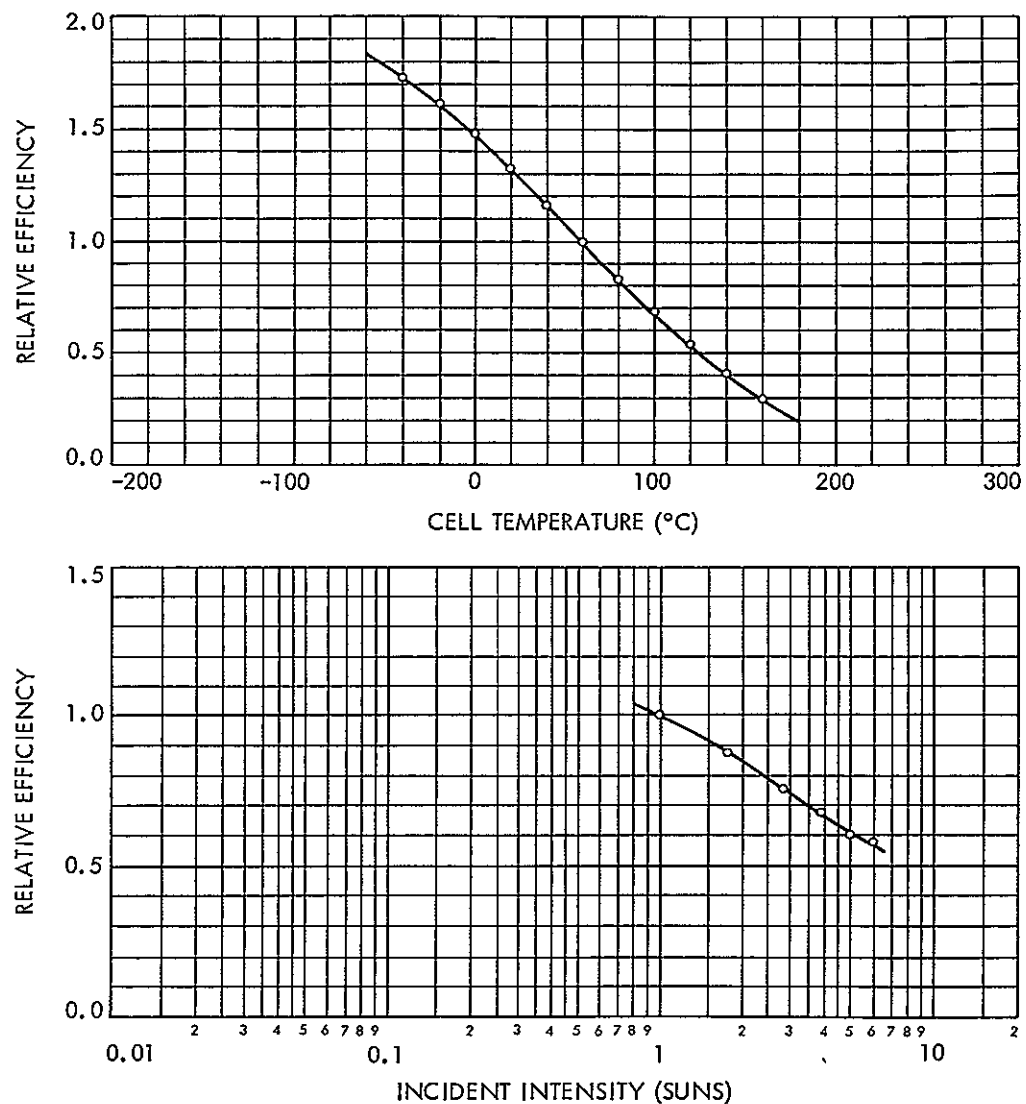
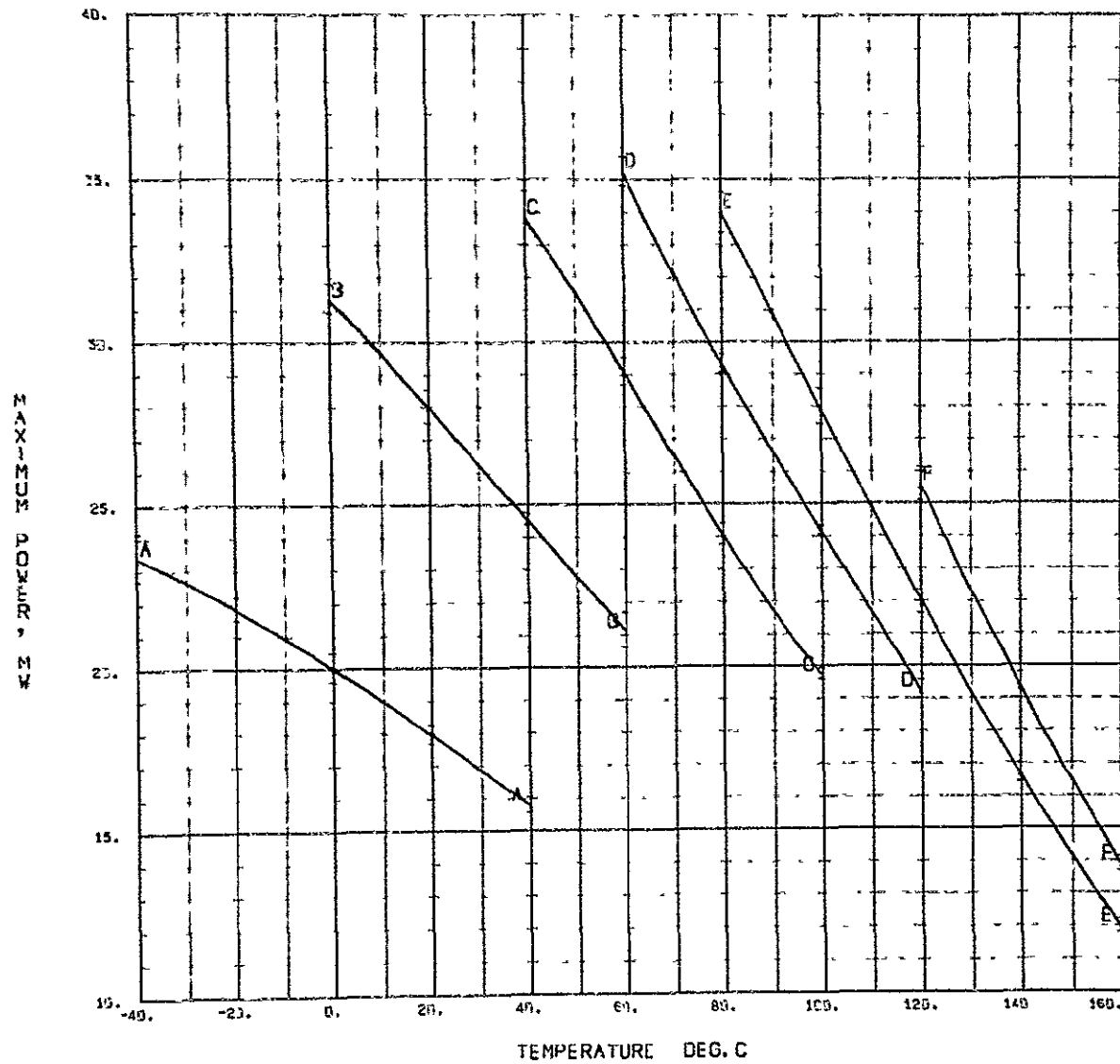


Fig. 99. Cell efficiency vs temperature and intensity for blue-red filter on 10 ohm-cm single wide-grid cell



CURVE ID ... A B C D E F
 INTENSITY, MW/CM² ... 140.00 250.00 460.00 550.00 760.00 850.00

Fig. 100. Maximum power vs temperature, blue-red filter on 10 ohm-cm single wide-grid cell

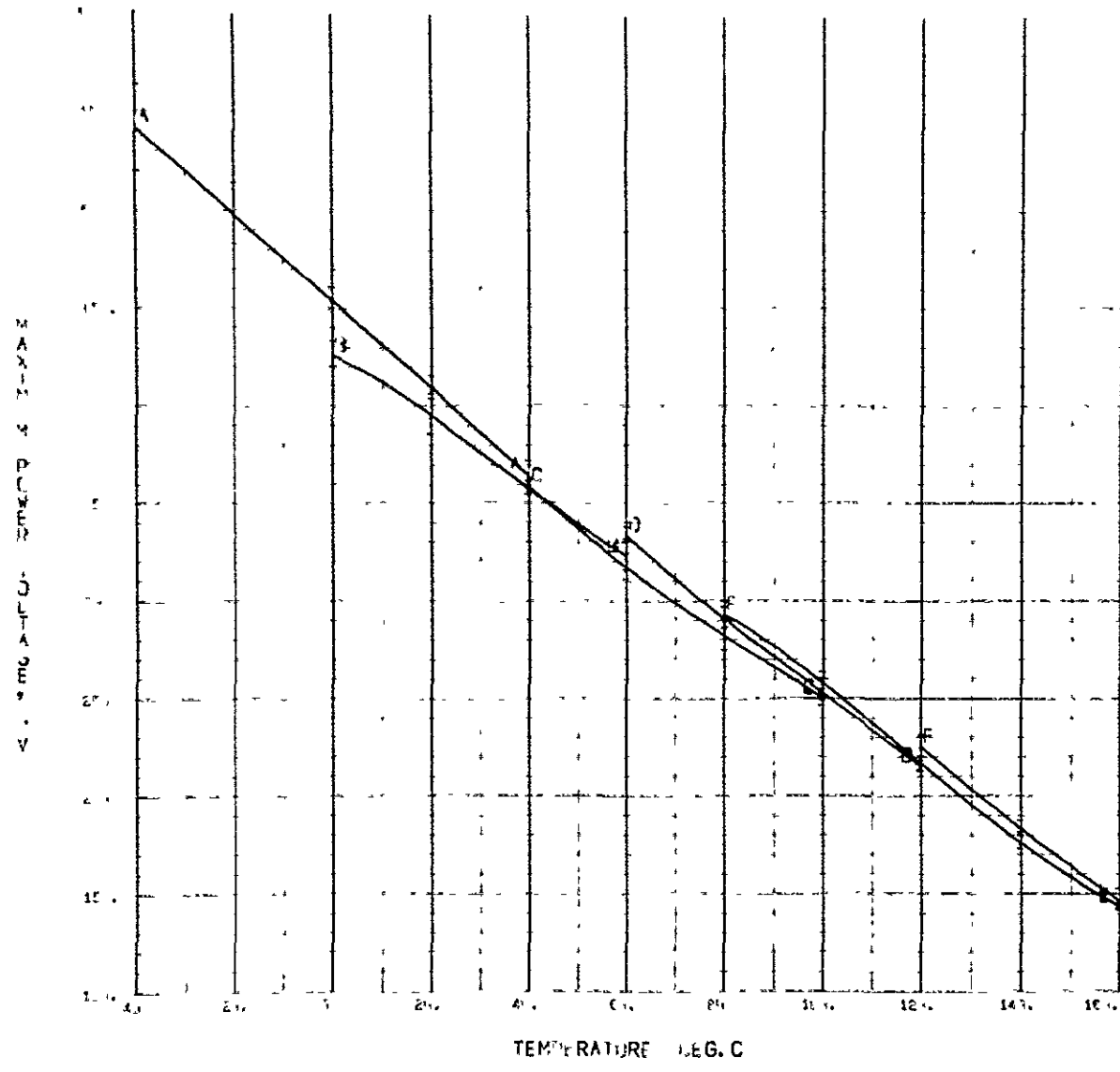
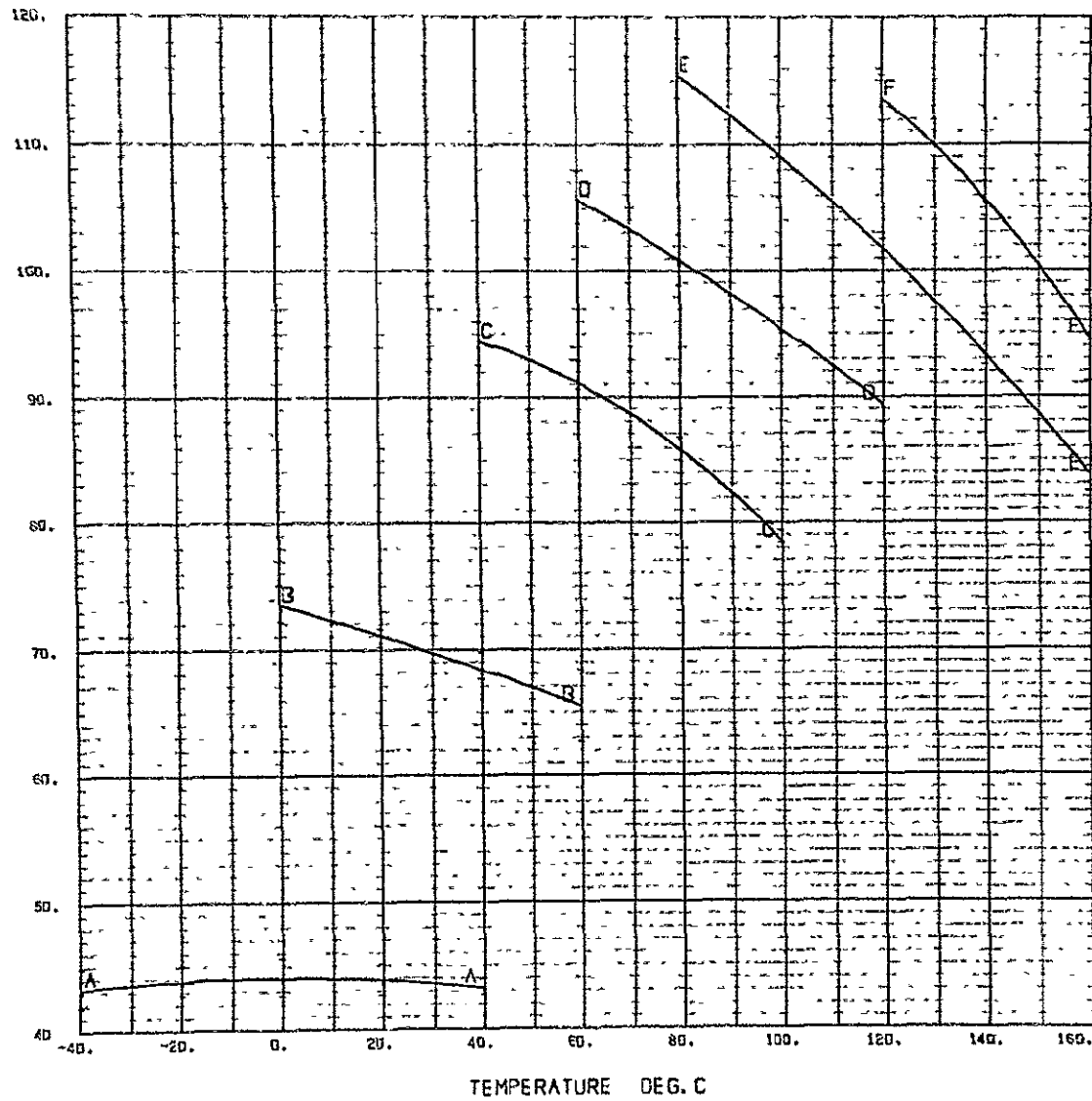


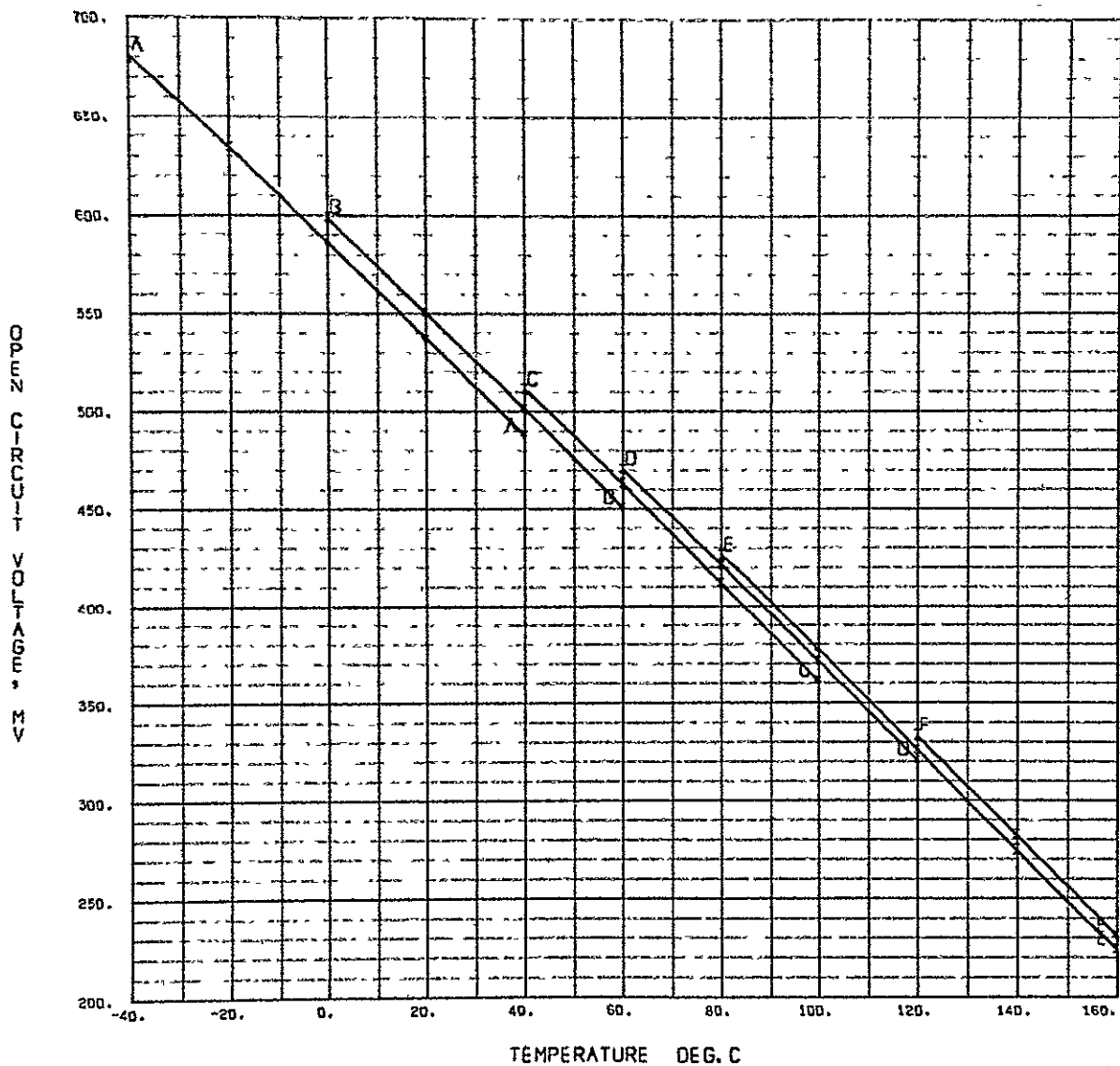
Fig. 101. Maximum-power voltage vs temperature, blue-red filter on 10 ohm-cm single wide-grid cell

MAXIMUM POWER CURRENT, MA



DRIVE ID ... A B C D E F
INTENSITY, M.I./CM² .. 140.00 250.00 450.00 550.00 700.00 850.00

Fig. 102 Maximum-power current vs temperature, blue-red filter on 10 ohm-cm single wide-grid cell



CURVE ID ... A B C D E F
 INTENSITY, MW/CH#2 . 140.00 250.00 400.00 550.00 700.00 850.00

Fig. 103. Open-circuit voltage vs temperature, blue-red filter on 10 ohm-cm single wide-grid cell

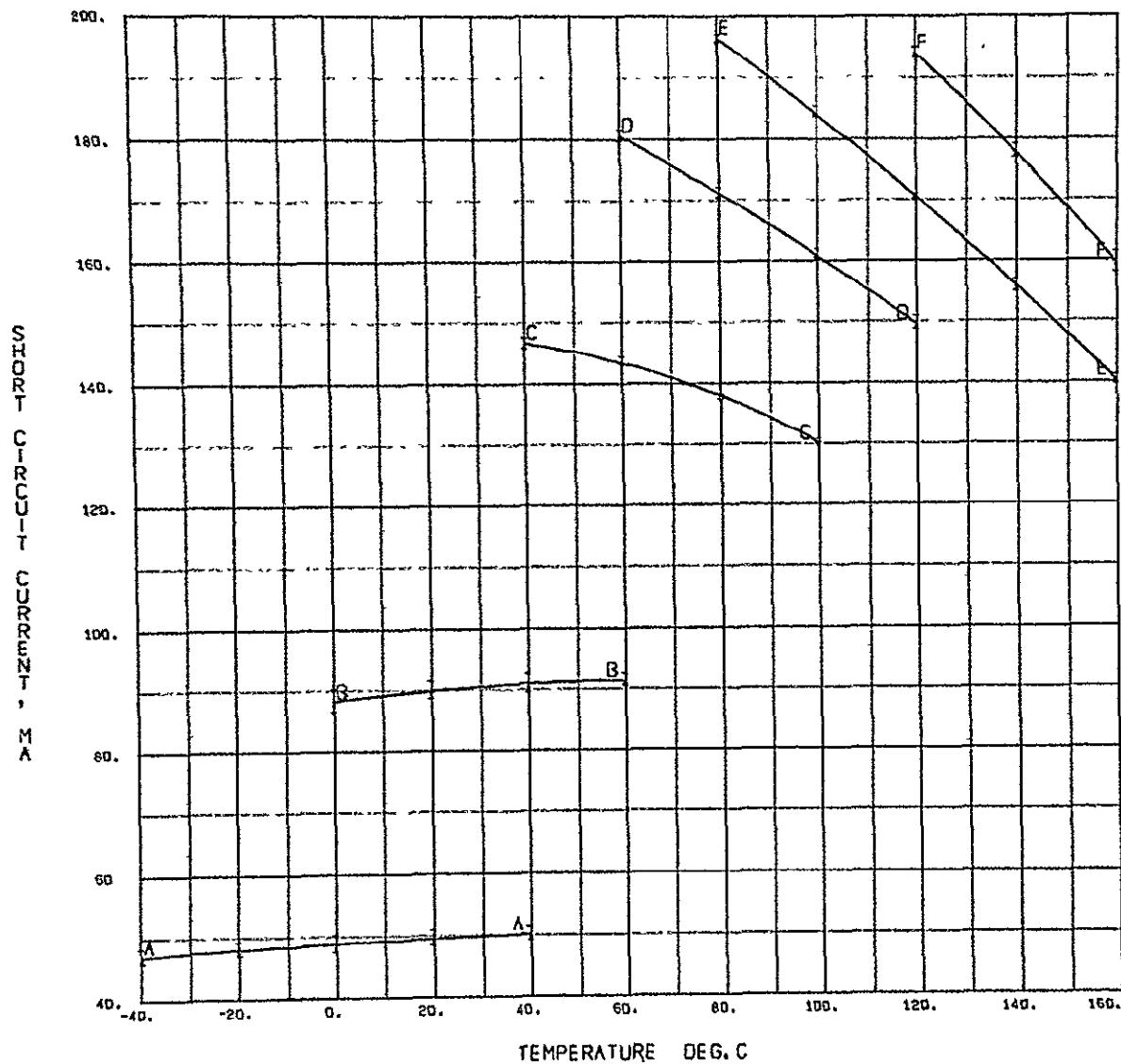


Fig. 104 Short-circuit current vs temperature, blue-red filter on 10 ohm-cm single wide-grid cell

NOT REPRODUCIBLE

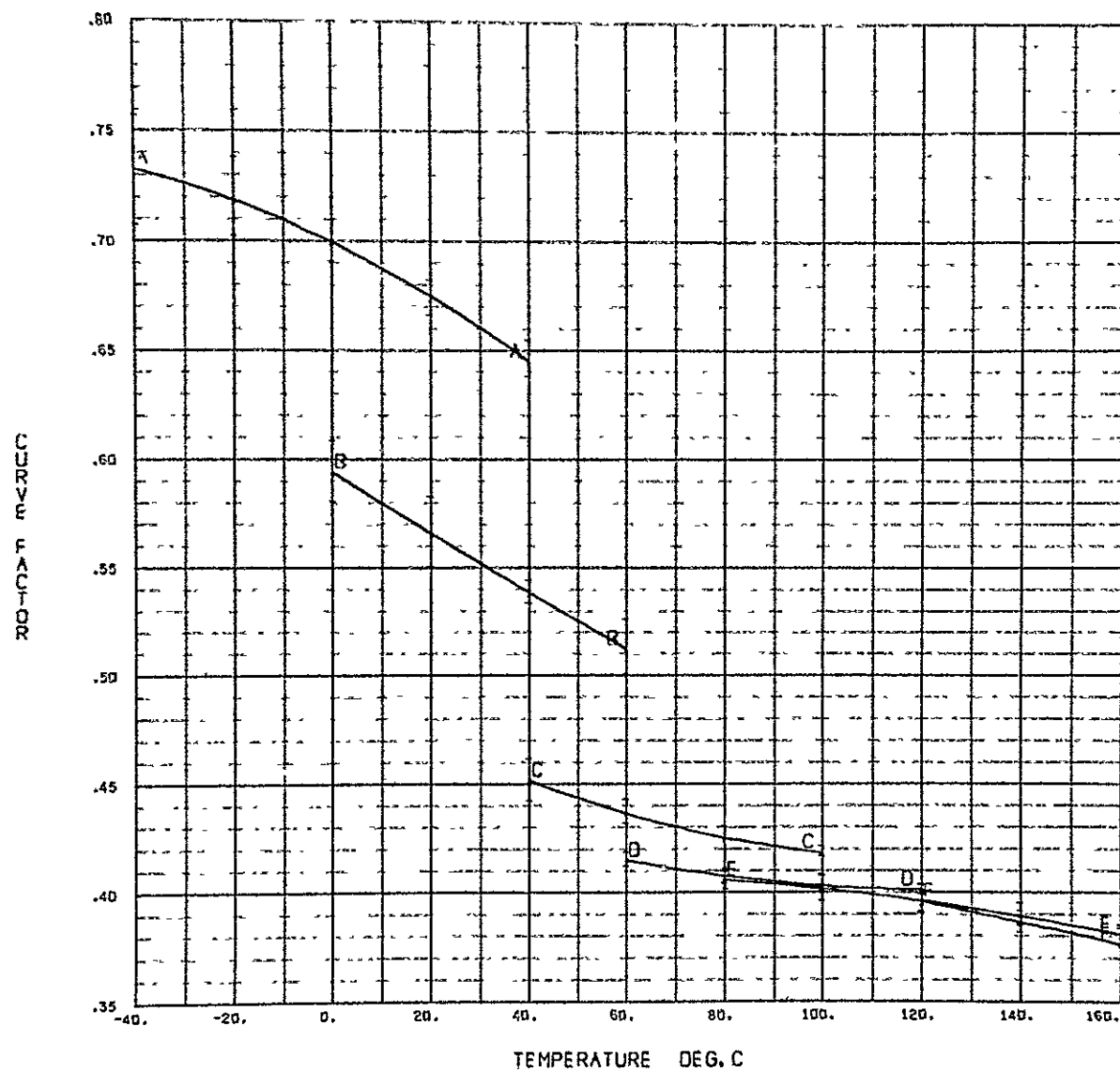


Fig. 105. Curve factor vs temperature, blue-red filter on 10 ohm-cm single wide-grid cell

V SOLAR CELL ELECTRICAL PERFORMANCE AS ANGLE OF ILLUMINATION CHANGES

A. Introduction

Because the solar intensity incident upon a solar panel surface decreases as the cosine of the angle of incidence, solar panel temperature can be lowered by tilting the panel surface with respect to the sun. However, at large tilt angles, it has been observed that the relationship between solar cell output and angle of incidence departs from this cosine behavior. The majority of the departure from the cosine law appears to be attributable to a variation in cell stack reflectance with angle of incidence. Ross (Ref. 3), for example, has found excellent agreement between the deviation from the cosine measured by Johnson (Ref. 4) and that predicted by assuming the variation in cell stack reflectance is proportional to the variation in front surface reflectance described by the Fresnel formulas.

During recent tilted panel tests conducted by Anspaugh* as part of the calibration of the experimental solar panels flown on the ATS-E Spacecraft, further data has been obtained which supports the variation in solar intensity predicted by the Fresnel formulas. In these experiments, the test panels were mounted in a solar beam of parallel rays in the JPL Celestarium, and solar cell output was measured as a function of the angle of incidence for angles of 0, 30, 45, 60, and 75 deg. There were 13 types of solar cell/coverglass configurations encompassing coverglass thicknesses ranging from 0.152 mm (6 mils) to 1.52 mm (60 mils). Each configuration was represented by a sample size of 5 cells. Data for three of the solar cell/coverglass configurations are reported here: 10 ohm-cm, 0.305-mm (12-mil) cells with 0.508-mm (20-mil) coverglasses, 10 ohm-cm, 0.305-mm (12-mil) cells with 0.152-mm (6-mil) coverglasses, and 2 ohm-cm, 0.203-mm (8-mil)

cells with 0.152-mm (6-mil) coverglasses. The 2 ohm-cm cells were solderless cells of Heliotek manufacture. The other two were solder-dipped cells manufactured by Centralab. Coverglass material was Corning 7940 fused silica with ultraviolet filter and antireflective coating, and the coverglasses were mounted on the cells with RTV-602 silicone adhesive.

B. Experimental Procedure

During the photovoltaic measurements, the test panels were mounted in the 60-cm (24-in.) diameter beam of sunlight produced by the heliostat in JPL's Celestarium facility. The heliostat consists of a set of mirrors which automatically track the sun and produce a bundle of rays which is perpendicular to the test area within ± 6 s and uniform in intensity $\pm 1.5\%$.

The panels were mounted to a dividing head capable of rotation about two axes, and fixtures were constructed to allow the panels to be accurately adjusted perpendicular to the beam. Though the panels were rotated about only one axis for the measurements reported here, it was established that the axis of rotation made no difference in cell short-circuit current output (a function which varies linearly with light intensity) for rotation about either of the dividing head axes.

Current-voltage (I-V) curves were taken for each cell using a variable resistive load and an XY plotter. Open-circuit voltage was read out separately on a digital voltmeter. Solar cell temperature was not controlled during these measurements but was noted by monitoring the output of thermistors mounted behind the cells. The intensity of the normally incident sunlight varied as the day progressed and was monitored by a JPL

*Anspaugh, Bruce, Jet Propulsion Laboratory, Pasadena Calif., private communications.

Balloon Flight standard cell. During the measurements the solar intensity ranged from 68 mW/cm² to 74 mW/cm², and the cell temperature varied from 32.2 to 41.7°C.

C. Data Analysis

As noted above, the effective intensity incident on the solar cell surface decreases as the cosine of the angle of incidence except at large angles, where a significant amount of energy is apparently lost due to increased reflection from the solar cell stack. If we neglect the effect of the antireflective coating on the coverglass, the variation in front surface reflectance with angle of incidence is described by the Fresnel formulas as

$$p(\theta) = \frac{1}{2} \left[\frac{\tan^2(\theta - \theta')}{\tan^2(\theta + \theta')} + \frac{\sin^2(\theta - \theta')}{\sin^2(\theta + \theta')} \right] \quad (1)$$

where θ and θ' are the angles of incidence and refraction, respectively (Ref. 5). Snell's Law defines θ' in terms of θ by

$$\theta' = \text{arc sin} \left(\frac{\sin \theta}{n} \right)$$

where n is the index of refraction of the reflecting surface. For fused silica, $n = 1.46$.

Assuming that the total reflectance varies with angle according to Eq. (1), the energy $S(\theta)$ transmitted to the cell can be described in terms of the energy transmitted at $\theta = 0$ by

$$S(\theta) = S(0) \left[\frac{1 - p(\theta)}{1 - p(0)} \right] \cos \theta \quad (2)$$

Figure 106 depicts the variation in reflectance $p(\theta)$ and the effective tilt intensity $S(\theta)/S(\theta = 0)$ as a function of θ for $n = 1.46$. Cosine θ is also shown for comparison.

In order to establish the effect of angle of incidence on cell output, data were taken from the I-V curves and processed with the aid of a computer. Statistical parameters were calculated for maximum power, short-circuit current, current at maximum power, voltage at maximum power, and open-circuit voltage. In addition, the average characteristics of each cell assembly type were determined.

Since short-circuit current I_{sc} and current at maximum power I_{mp} vary linearly with intensity and are slowly varying functions of temperature, the variation in these parameters provides a dependable measure of the effective intensity transmitted to the cell at any angle of incidence. On the other hand, the use of the variation in maximum power as an indication of the variation in effective intensity is complicated by the fact that solar cell maximum power is not linearly related to incident intensity and is a strong function of temperature (Ref. 3). For this reason, the variation in I_{sc} and I_{mp} was used to measure the variation in effective intensity transmitted to the cell as a function of angle of incidence. Figure 107 compares the measured variation in I_{sc} and I_{mp} with the cosine function and with the function defined by Eq. (2), which accounts for the increase in cell stack reflectance with increasing angle of incidence. As can be seen from this figure, the variation in effective intensity described by Eq. (2) correlates very well with the variations indicated by the short-circuit current and maximum-power current measurements. In addition, there appears to be no significant difference in off-axis solar cell performance between cells covered by 0.152-mm (6-mil) coverglasses and cells covered by 0.508-mm (20-mil) coverglasses.

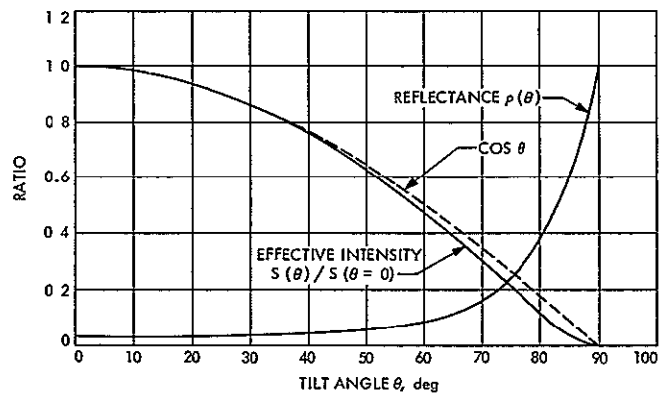


Fig. 106. First-surface reflection for fused silica and predicted effective intensity reaching the cell, vs angle of incidence

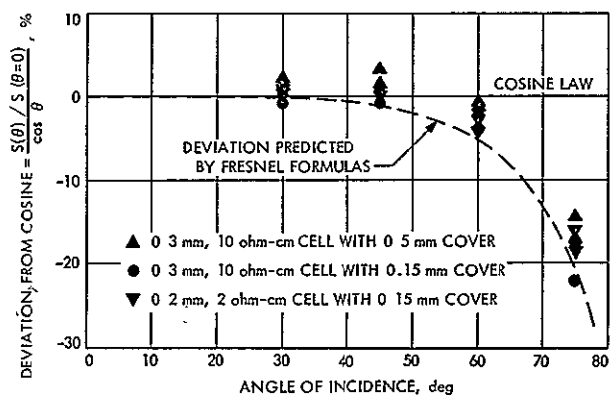


Fig. 107. Relative intensity reaching the cell vs angle of incidence as indicated by solar cell short-circuit current and maximum-power current

VI. SOLAR CELL/COVERGLASS THERMAL RADIATION PROPERTIES

The thermal radiation properties measurements described herein were performed at TRW Space Systems, Redondo Beach, California, under JPL Contract No. 952308.

A. Objective

At the start of this investigation, data on the thermal radiation characteristics of the selected solar cell/coverglass components and assemblies were quite limited. In particular, no data were available for the reflectance of cell assemblies utilizing the specially procured selective bandpass filters, or for the reflectance of the Ag-Ti wide-grid or SI-100/blue filter second-surface mirror surfaces. In addition, the properties of cell assemblies using the standard blue and blue-red filters contained large uncertainties.

The measurement program described herein was established to provide these necessary thermal radiation properties. Data, not necessarily required for solar array performance analyses but desirable for interpretation of the results of the irradiation stability tests, were also obtained for bare fused silica and two different coverglass adhesives (RTV-602 and XR6-3489).

B Experimental Approach

Except for the adhesive measurements, the testing was conducted in a routine manner using TRW's standard laboratory equipment as described in Ref. 6. The equipment consisted of a Gier-Dunkle (Edwards type) integrating sphere reflectometer, a Beckman DK-2A spectrophotometer, a TRW-constructed integrating sphere attachment for the Beckman DK-2A spectrophotometer, and a heated-cavity absolute reflectometer.

Two types of measurements were made: spectral reflectance and spectral transmittance. The

spectral reflectance for wavelengths between 0.28 and 2.5 μm was determined with the integrating sphere reflectometer (Ref. 7). The monochromatic source of light was provided by the Beckman DK-2A spectrophotometer (Ref. 8), which also did the actual reflectance reading. When measurements between 2.5 and 7.0 μm were required, the heated cavity absolute reflectometer (Ref. 9) was used. Transmittance was measured by placing the test sample at the entrance port of the integrating sphere reflectometer.

Because the absorptance α_λ of the samples was of primary interest, it was obtained from the reflectance r_λ and transmittance t_λ measurements using the relation

$$\alpha_\lambda = 1 - (r_\lambda + t_\lambda) \quad (3)$$

Solar absorptance α_s was then obtained by integrating the spectral absorptance over the Johnson solar energy spectrum (Ref. 10).

Although all but the adhesive measurements were made at laboratory atmospheric conditions and mostly at room temperature, the results for all practical purposes should be equal to those made in vacuum. For the adhesive measurements, the temperature was controlled by varying the temperature of a circulated inert gas (nitrogen).

C. Experimental Results and Discussion

The number and description of the samples tested are listed in Table 3. The last column indicates the type of spectral measurements made and, if determined, the integrated solar absorptance of the sample. For opaque samples, the spectral data are limited to the spectral reflectance or derived spectral absorptance obtained

from Eq. (3) by assuming $\tau_\lambda = 0$. In the case of transparent samples, the spectral data consist of spectral transmittance and combined spectral reflectance plus transmittance.

Figures 108-112 provide spectral data for a bare 2 ohm-cm cell, a blue filter, and cell assemblies using both the blue and blue-red filters. Figures 113-116 present the spectral reflectance of solar cell assemblies made with the four selective bandpass filters supplied by OCLI. The spectral properties of the modified 4026 filter alone are given in Figs. 117 and 118.

Figures 119 and 120 present the spectral data for two SI 100/blue filter second-surface mirror samples. This mirror surface, which was constructed by applying a conventional OCLI SI-100 mirror coating on top of the standard blue filter, is the one used on the mirror bar and mirror stripe coverglasses investigated in this study. The two samples were chosen from a group of approximately 200 and represent visual extremes. The one with the lower absorptance appeared silver, whereas the other appeared slightly yellow and was selected as representative of the most yellowish-looking mirrors. Figure 121 represents the characteristics of a similar mirror made on an earlier program by applying the SI-100 mirror on top of a conventional blue-red filter. The wide variation in solar absorptance (from 0.088 to 0.138) indicates that the use of partially mirrored coverglasses of this type may require stringent quality control measures or necessitate

the masking of the filter away from the mirror area.

As indicated in Table 3, the solar absorptance of the Ag-Ti wide-grid mirror surface also exhibited considerable variation. The wide-grid spectral reflectance properties are presented in Figs. 122 and 123 for both the bare Ag-Ti-SiO surface and for the surface covered with a conventional coverglass and blue filter. At least some of the variation in the solar absorptance of these samples can be attributed to a slight amount of oxidation which occurred due to voids in the SiO protective coating. Of particular significance is the fact that the reflectance of the wide grid is approximately the same as that for the SI-100/blue filter mirror.

The spectral thermal radiation characteristics of bare fused silica and two different cover-glass adhesives (RTV-602 and XR6-3489) are shown in Figs. 124-129. These were obtained primarily to aid the interpretation of the irradiation test results presented in Section VIII. Figure 130 shows the test setup with nitrogen circulation system and the detail of the sample mounting used in the adhesive tests. The adhesive samples were made by first casting strips approximately 1.25 mm thick and then cutting them to sample holder size. Both adhesives tested appear to have almost identical thermo-optical properties and display an excellent stability at higher temperatures in the normal laboratory environment. In the visible wavelength range, the absorptance is only about 1%.

Table 3. Thermo-optical properties measured

No. of Samples	Sample Description	Type of Measurement
3	2 Ω cm Bare Solar Cell	ρ_λ ; $\alpha_s = 0.794 - 0.823$
5	Blue Filter	ρ_λ ; τ_λ ; $\rho_\lambda + \tau_\lambda$
2	Blue Filter on 2 Ω cm Cell	ρ_λ ; $\alpha_s = 0.774 - 0.777$
1	Blue-Red Filter on 2 Ω cm Cell	ρ_λ ; $\alpha_s = 0.675$
1	4024 Filter on 2 Ω cm Cell	ρ_λ ; $\alpha_s = 0.470$
1	4025 Filter on 2 Ω cm Cell	ρ_λ ; $\alpha_s = 0.430$
1	4026 Filter on 2 Ω cm Cell	ρ_λ ; $\alpha_s = 0.384$
2	Modified 4026 Filter	τ_λ ; $\rho_\lambda + \tau_\lambda$; $\alpha_3 = 0.03$
2	Modified 4026 Filter on 2 Ω cm Cell	ρ_λ ; $\alpha_s = 0.296 - 0.311$
1	Blue Filter on Mirror Surface (Sample A)	α_λ ; $\alpha_s = 0.106$
1	Blue Filter on Mirror Surface (Sample B)	α_λ ; $\alpha_s = 0.138$
1	Blue-Red Filter on Mirror Surface	ρ_λ ; $\alpha_s = 0.088$
5	"Wide Grid" (Ti/Ag/SiO) Surface	ρ_λ ; $\alpha_s = 0.125 - 0.137$
2	Blue Filter on "Wide Grid" (Ti/Ag/SiO) Surface	ρ_λ ; $\alpha_s = 0.121 - 0.141$
2	Fused Silica Cover	τ_λ ; $\rho_\lambda + \tau_\lambda$
2	RTV-602 Adhesive	τ_λ and $\rho_\lambda + \tau_\lambda$ as $f(T)$
2	XR6-3489 Adhesive	τ_λ and $\rho_\lambda + \tau_\lambda$ as $f(T)$

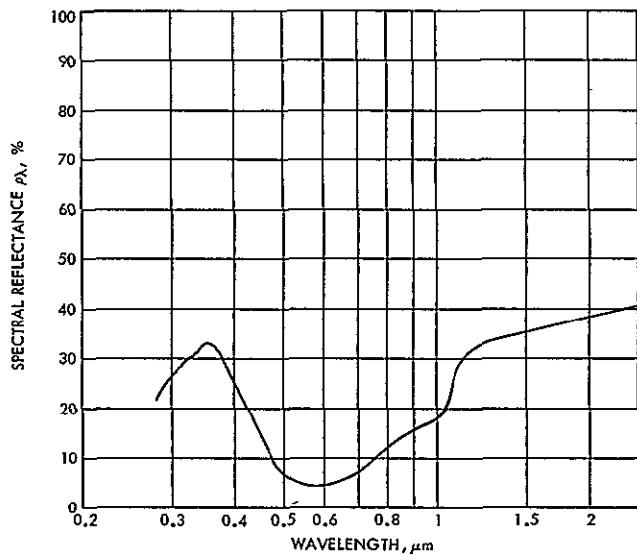


Fig. 108 Spectral reflectance of 2 ohm-cm bare solar cell

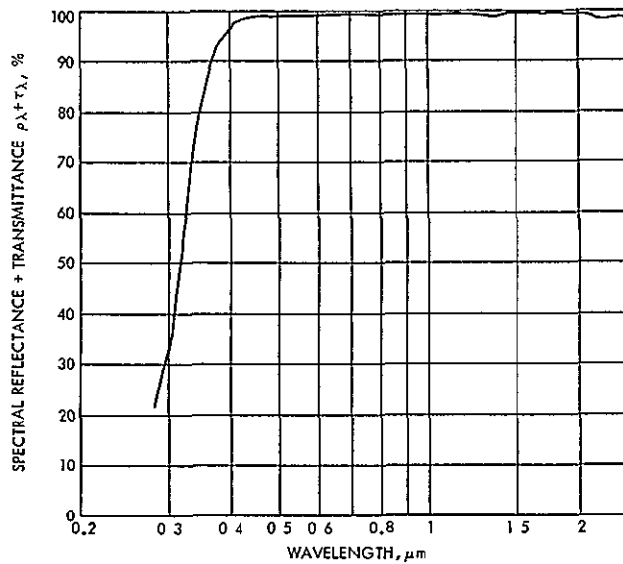


Fig. 110. Spectral reflectance plus transmittance of blue filter

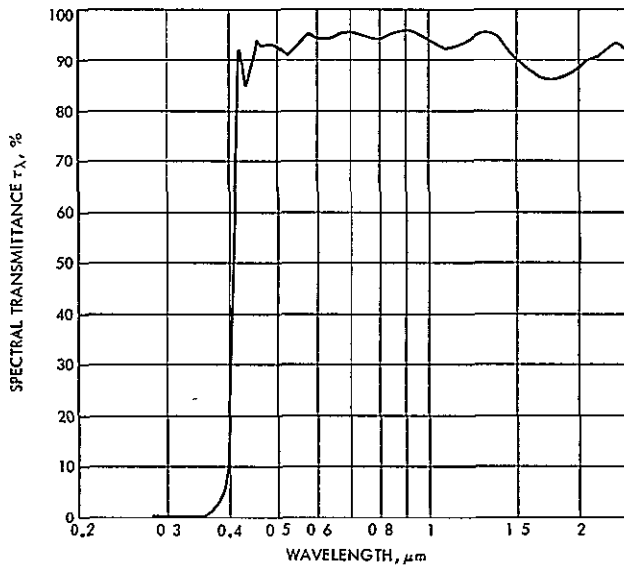


Fig. 109 Spectral transmittance of blue filter

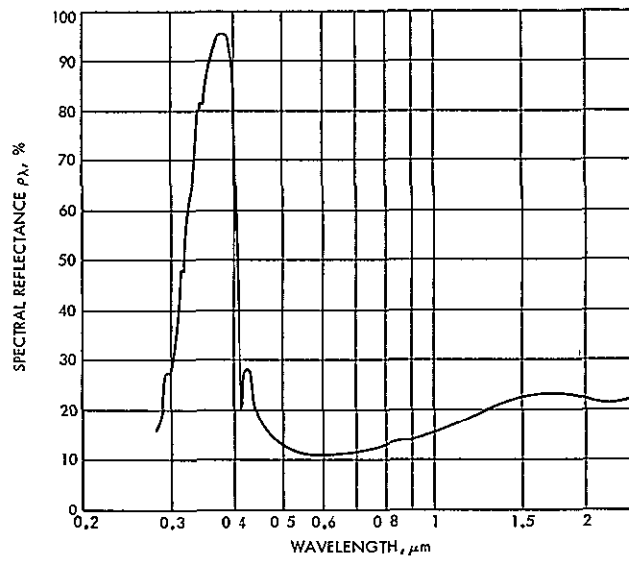


Fig. 111. Spectral reflectance of blue filter on 2 ohm-cm solar cell

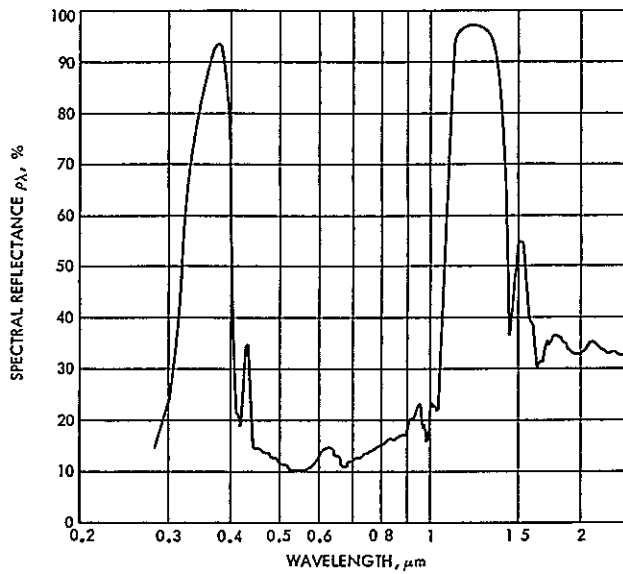


Fig. 112. Spectral reflectance of blue-red filter on 2 ohm-cm solar cell

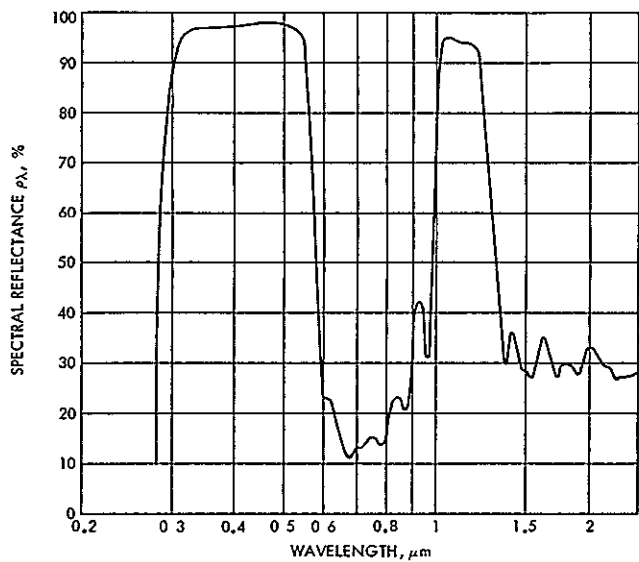


Fig. 114. Spectral reflectance of 4025 filter on 2 ohm-cm solar cell

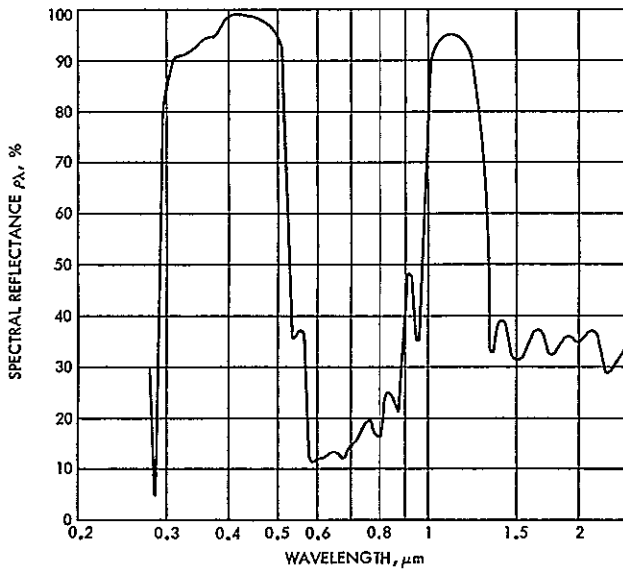


Fig. 113. Spectral reflectance of 4024 filter on 2 ohm-cm solar cell

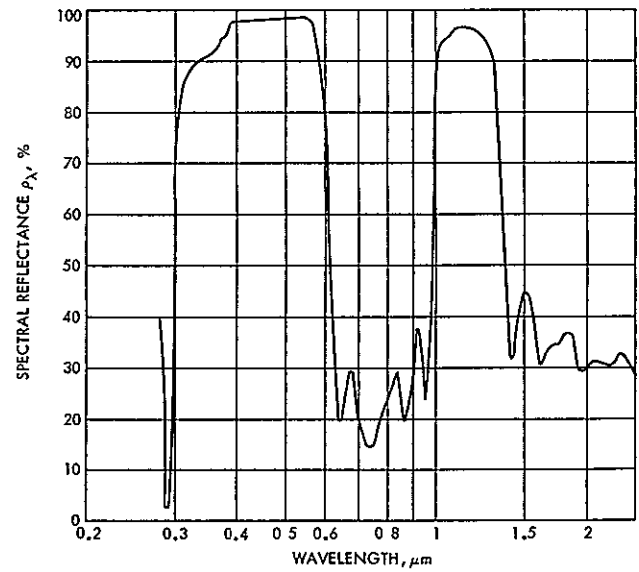


Fig. 115. Spectral reflectance of 4026 filter on 2 ohm-cm solar cell

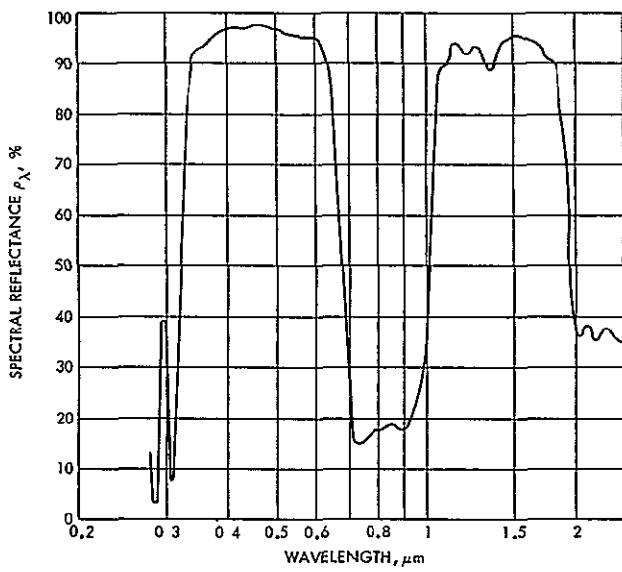


Fig. 116. Spectral reflectance of modified 4026 filter on 2 ohm-cm solar cell

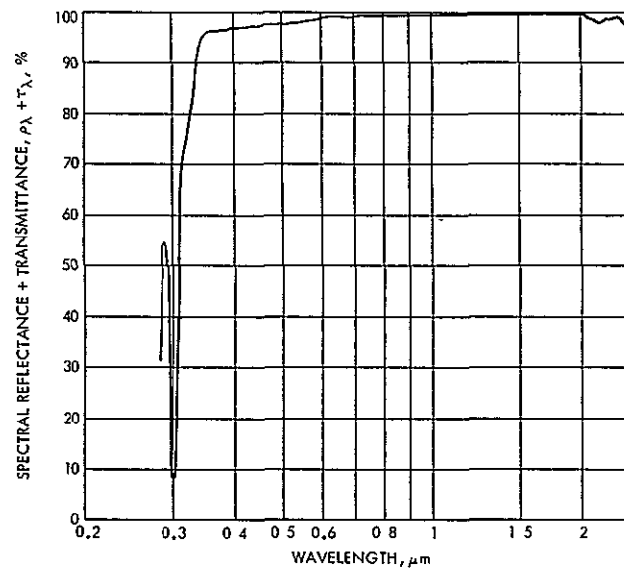


Fig. 118. Spectral reflectance plus transmittance of modified 4026 filter

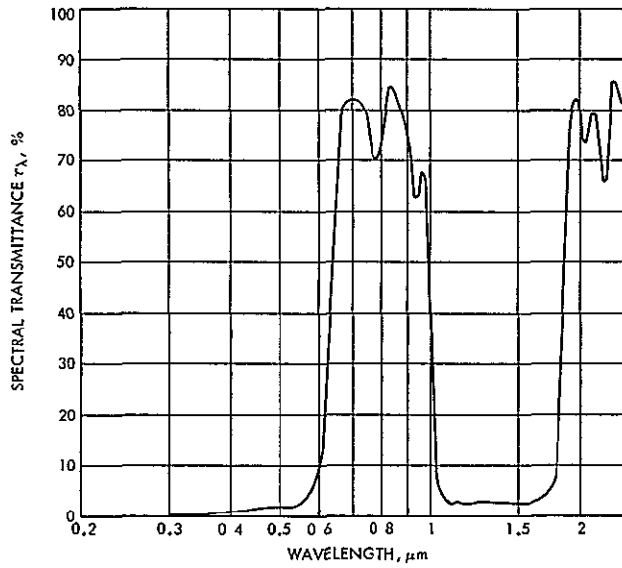


Fig. 117. Spectral transmittance of modified 4026 filter

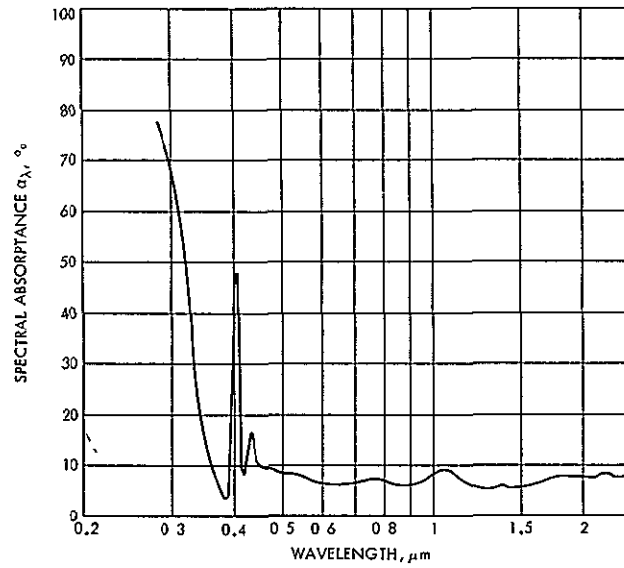


Fig. 119. Spectral absorptance of SI-100/blue filter mirror surface (sample A)

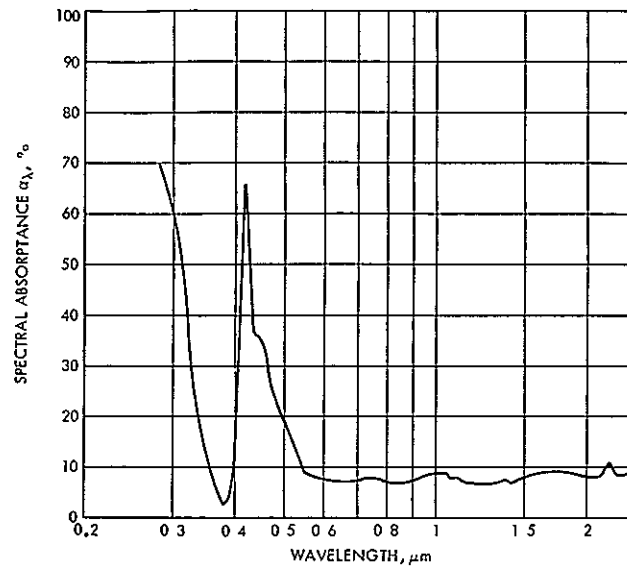


Fig. 120. Spectral absorptance of SI-100/blue filter mirror surface (sample B)

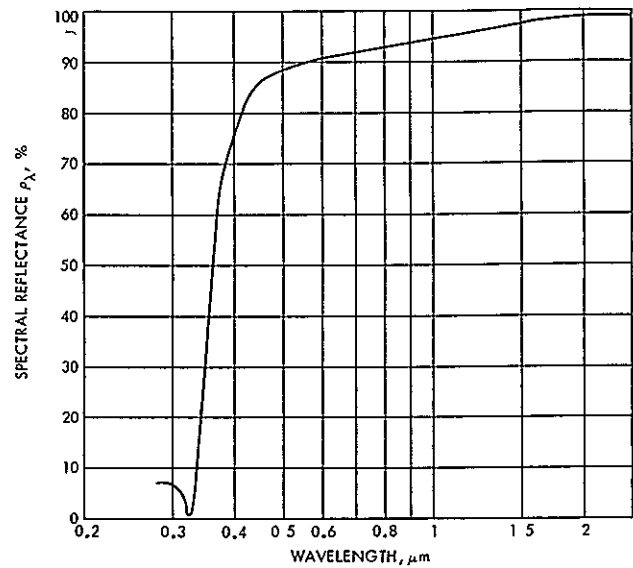


Fig. 122 Spectral reflectance of "wide grid" (Ti/Ag/SiO surface)

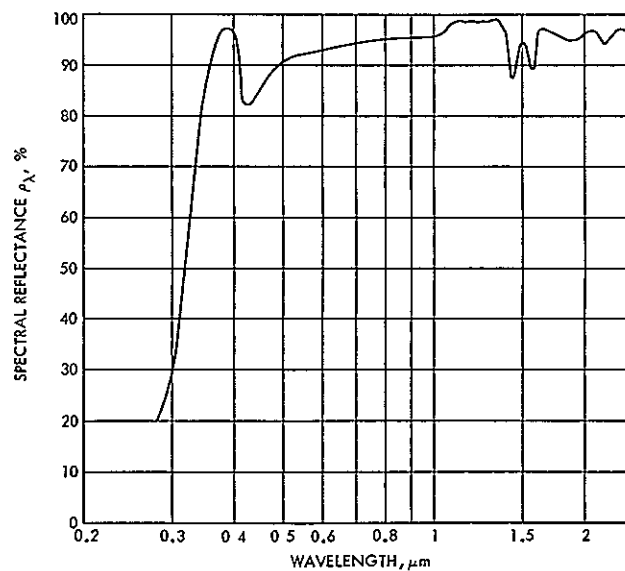


Fig. 121 Spectral reflectance of SI-100/blue-red filter mirror surface

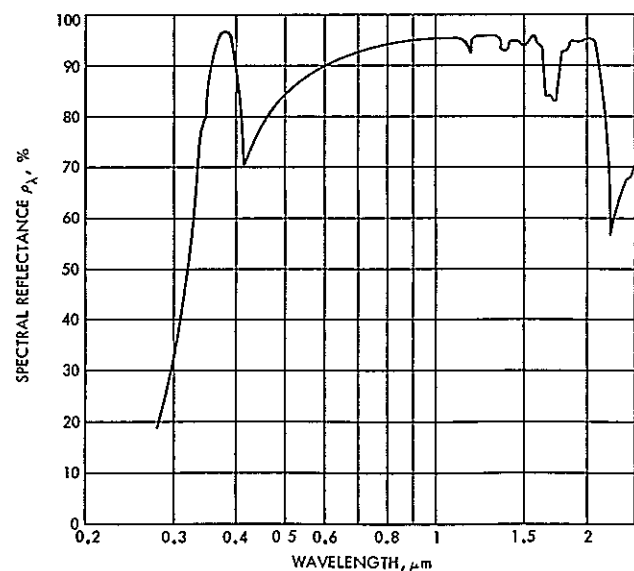


Fig. 123 Spectral reflectance of blue filter on "wide grid" (Ti/Ag/SiO surface)

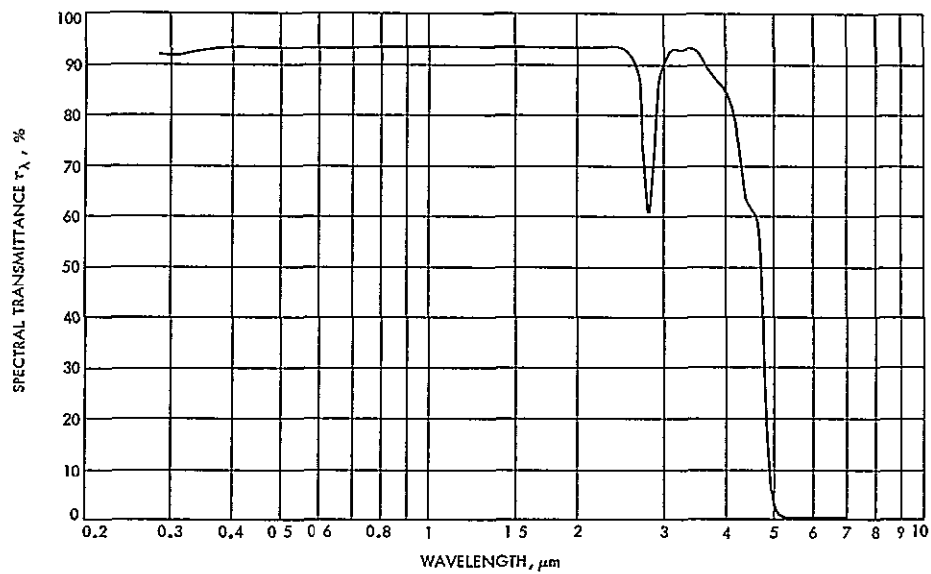


Fig. 124. Spectral transmittance of fused silica cover

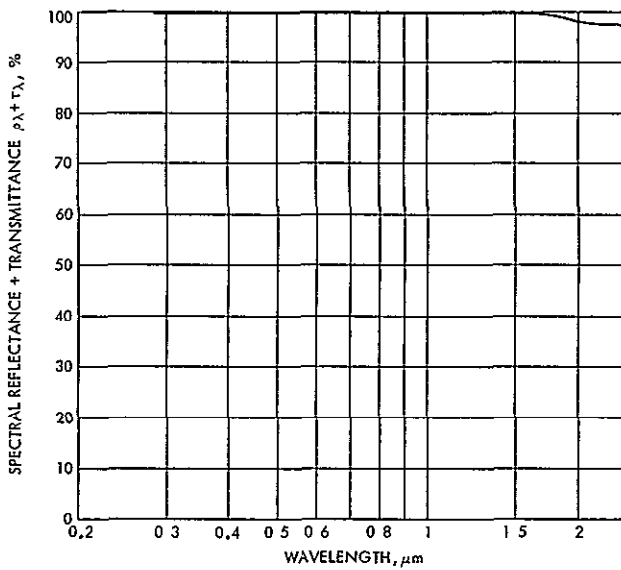


Fig. 125 Spectral reflectance plus transmittance of fused silica cover

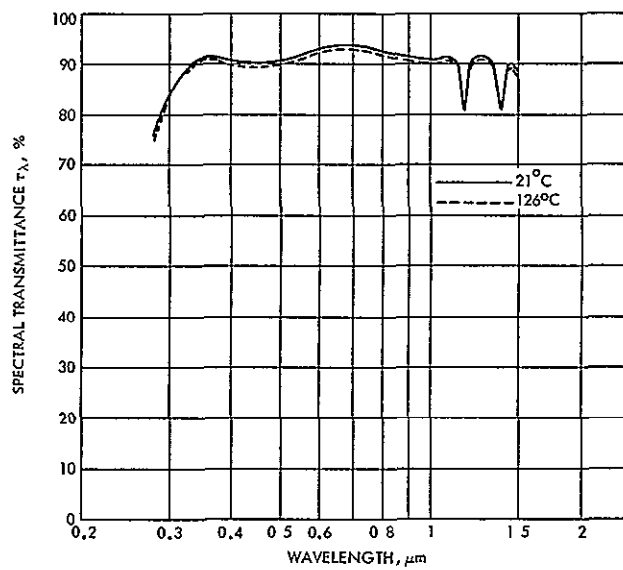


Fig. 126 Spectral transmittance of RTV-602 adhesive

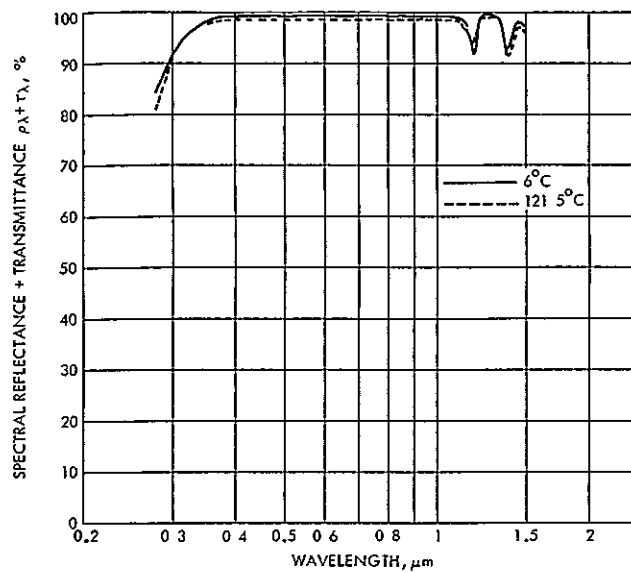


Fig. 127. Spectral reflectance plus transmittance of RTV-602 adhesive

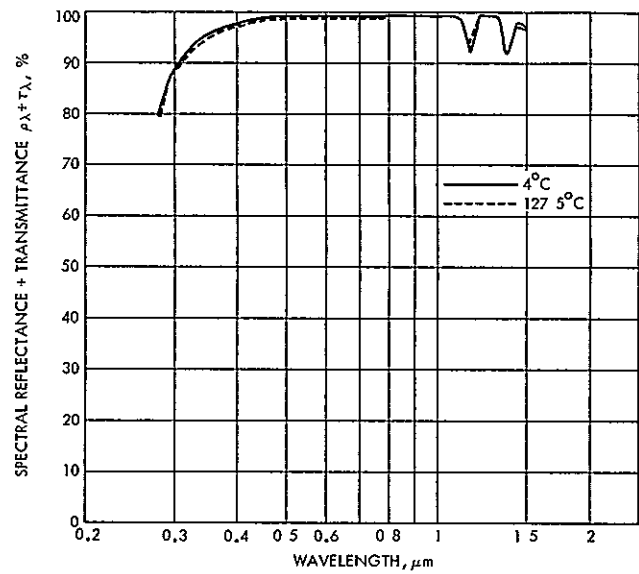


Fig. 129. Spectral reflectance plus transmittance of XR6-3489 adhesive

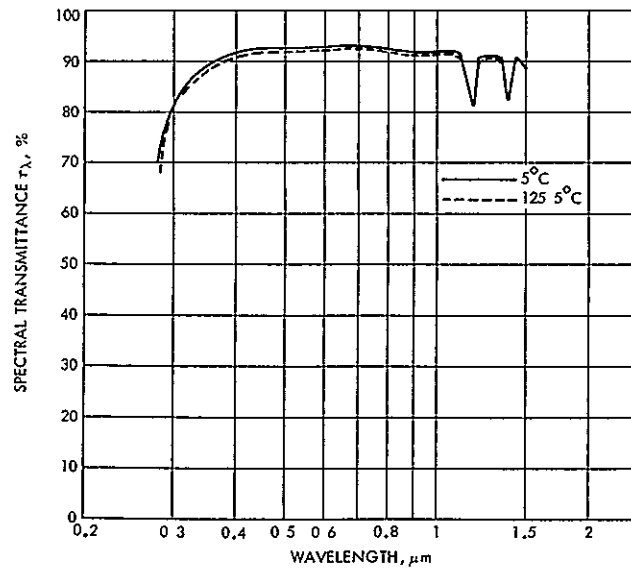


Fig. 128. Spectral transmittance of XR6-3489 adhesive

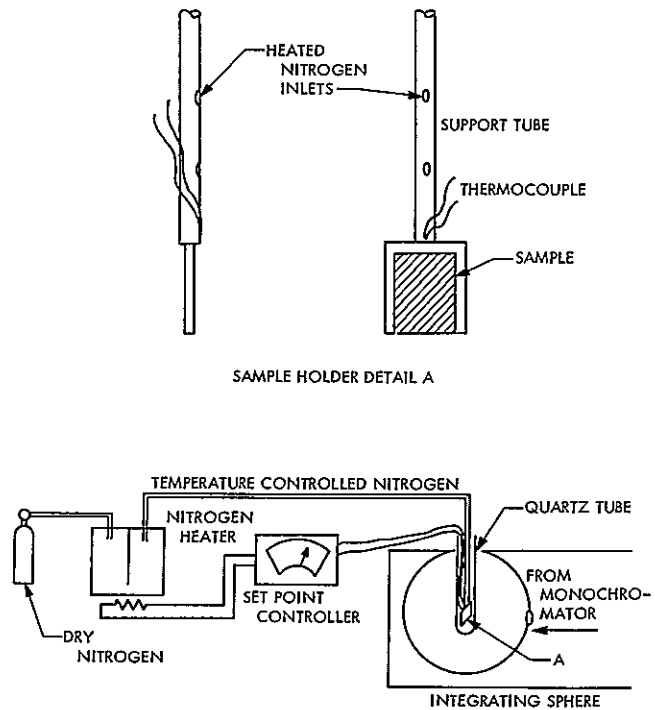


Fig. 130 Adhesive test schematic and sample holder detail

VII SOLAR CELL MODULE THERMAL RADIATION PROPERTIES

A Objective

Since solar cell modules are composite surfaces made up of filtered cells, metal ohmic contacts, and intercell spaces, their thermal radiative characteristics are represented by effective emittances and effective absorptances. For typical cell modules with blue filters, these effective properties are essentially the same as the filtered cell properties described in the previous section. The thermal properties of the electrical contact and intercell space areas are similar to those of the cell and thus do not affect the composite characteristics significantly. However, when cells with highly reflective coverglasses are used, the thermal properties of the contact and intercell space areas can contribute significantly to the effective properties of the solar cell module.

For this reason, one of the primary objectives of the calorimetric measurement program described in this section was to evaluate the thermal radiative characteristics of the ohmic contact and intercell space areas. In addition, the program was designed to provide hemispherical emittance data on the composite surfaces as a function of temperature and to check our ability to predict the effective solar absorptance of a composite solar cell module from the properties of its surface components.

Test specimens included cell modules with the standard blue and blue-red filters, one with the modified 4026 selective bandpass filter, one with partially mirrored coverglasses, and one made using multiple wide-grid cells with blue filters.

B Experimental Approach

Because conventional optical methods are not really suitable for determining effective surface

properties directly, calorimetric techniques were used to evaluate the effective hemispherical emittances and effective solar absorptances of the test modules. The calorimetric system consisted of a cold-wall vacuum chamber, heating devices, supporting structures, and the cell modules whose radiative properties were to be determined.

Using conventional calorimetric techniques, the test modules were suspended in the cold-wall vacuum environment and were heated using an electrical heater and (for absorptance measurements) a solar simulator. In order to establish a computable relationship between the radiative properties being measured and the modules' thermal behavior, the thermal characteristics of each component of the system were described in a thermal balance, and the heat exchanges between the surfaces of the components through conduction and radiation were specified in the boundary conditions. The thermal balance was implemented using an eleven-node mathematical model; seven nodes represented various parts of the test module, and four nodes represented the surrounding environment. The basic nodal energy balance relationship for each node is of the form

$$P_1 - \sum_{j=1}^{11} Q_{1j} + \alpha_1 S A_{S_1} = A_1 \epsilon_1 \left(\sigma T_1^4 - \sum_{j=1}^{11} G_{1j} \right) \quad (4)$$

where

P_1 = net energy input to node 1 through electrical heating

Q_{1j} = net conductive heat transfer to node 1 from node j

α_1 = integrated solar absorptance of node 1
 A_{S_1} = solar irradiated area associated with node 1
 A_1 = total surface area associated with node 1
 S = solar irradiation flux
 ϵ_1 = total hemispherical emittance of the surface associated with node 1
 G_{1j} = total infrared irradiation flux to node 1 from node j
 σ = Stefan-Boltzmann constant
 T_1 = nodal equilibrium temperature

For emittance measurements, the energy balance relationship noted by Eq. (4) reduces to the set of 11 equations

$$P_1 = \sum_{j=1}^{11} K_{1j}(T_1 - T_j) + A_1 \epsilon_1 \left(\sigma T_1^4 - \sum_{j=1}^{11} G_{1j} \right), \quad 1 = 1, 11 \quad (5)$$

where the symbols are defined as above except that

P_1 = electrical energy applied to node 1 minus the heat lost through power leads and thermocouple leads
 K_{1j} = thermal conductance between nodes 1 and j

After system calibration, the effective hemispherical emittance of the module is the only unknown in this set of equations, and it can thus be determined as the value required to make the calculated sample temperature match the experimentally measured value

The integrated solar absorptance measurement can be implemented using either of two calorimetric techniques: an indirect (α/ϵ) technique which is similar to the emittance measurement, or a direct technique. The indirect method requires a knowledge of both the solar intensity and all surface emittance involved in the system. For this approach, the absorbed solar energy replaces the electrical heating used in the emittance measurements and Eq. (5) reduces to

$$A_{S_1} \alpha_1 S = \sum_{j=1}^{11} K_{1j}(T_1 - T_j) + A_1 \epsilon_1 \left(\sigma T_1^4 - \sum_{j=1}^{11} G_{1j} \right), \quad 1 = 1, 11 \quad (6)$$

where the symbols are as before

The direct method, on the other hand, requires two separate measurements. In the first measurement, the test surface is illuminated with solar energy at intensity S . Additional electrical heating Q_e^I is applied to the sample, and the equilibrium temperature corresponds to the total heat input $Q_e^I + A_{S_1} \alpha_1 S$ and is recorded to be T_0 . In the second measurement, the solar simulator is turned off, and the sample is heated by the electrical heater alone to an equilibrium temperature matching the previous measurement, T_0 . In other words, the electrical heat input in the second measurement, Q_e^H , is exactly equal to that in the first run, $A_{S_1} \alpha_1 S + Q_e^I$. The solar absorptance can then be easily calculated from

$$\alpha_s = \frac{Q_e^H - Q_e^I}{A_{S_1} S} \quad (7)$$

Although both techniques were used in the current program, most of the data were obtained using the direct method in order to ensure that no inherent uncertainty was carried over from the emittance measurements.

C Test Apparatus

A general view of the experimental setup is shown in Fig. 131. The basic calorimetric system for the total hemispherical emittance measurements consisted of a BEMCO liquid-nitrogen-cooled chamber, a KAPCO voltage-regulated power supply, a DYMEC integrating digital voltmeter, a JOSEPH K 0°C reference junction, and auxiliary data acquisition systems, including an amplifier, a scanner, and a printer. For solar absorptance measurements, a spectrosun Model 25 MARK II solar simulator was used together with a set of standard solar cell test equipment.

Each solar cell test module consisted of a four-by-four array of 2-cm-square solar cell/coverglass assemblies bonded onto a 1.0-mm-thick substrate sheet with typical intercell spacing. The spaces parallel to the cell's ohmic contact were 0.53 mm (21 mils) in width, and the spaces between parallel cells were 0.30 mm (12 mils) in width. The back surface and the edges of the substrate were painted with Parson's optical black lacquer, the thermal properties of which were established as part of the system calibration discussed later.

The substrate sheet to which the cells were bonded consisted of a 76-mm (3-in.) square film heater (with Kapton insulation) sandwiched between two 0.40-mm (16-mil) aluminum plates and bonded together with EC 2216 adhesive. A thermocouple was embedded between the heater and the aluminum plate (denoted as the front plate) as shown in Fig. 132. This thermocouple position served as one node in the thermal model of the system, and its reading was related to solar cell temperatures and other module temperatures during the system calibration, which is described later.

The test module was suspended in the cold-wall chamber on 0.13-mm (5-mil) nylon threads which were attached to a 165-mm (6.5-in.) square

by 1.5-mm (60-mil) thick aluminum frame, which was in turn mounted to the chamber's end shroud as shown in Fig. 133. Besides holding the test module, the frame served to shield the end shroud from solar irradiation and held reference solar cells and thermocouples used to measure the solar intensity during solar absorptance measurements. The geometrical configuration between the sample and the rest of the chamber is shown in Fig. 134.

D. System Calibration

Before conducting the actual emittance and absorptance measurements, it was necessary to calibrate various parts of the calorimetric system. The calibration procedure is presented in four parts: (1) calibration of the test module temperature measurements, (2) calibration of the conductive heat losses from power and thermocouple leads, (3) calibration of the solar simulator, and (4) calibration of the thermal radiation properties of the painted surfaces of the cell modules.

1 Calibration of Test Module Temperature Measurements As a first step, the thermocouple wires used for the instrumentation of the modules were calibrated in order to achieve a resulting instrumentation accuracy of approximately $\pm 0.5^\circ\text{F}$ (0.3°C). Following the thermocouple calibration, a test module substrate was constructed with thermocouples embedded at three different locations in order to measure the temperature gradients in the plane of the substrate. The gradient between the center thermocouple location and the rim of the module substrate varied from less than 0.5°F (0.3°C) for module temperatures less than 100°F (38°C) to a maximum of 3°F (1.7°C) at 300°F (140°C). This information was used in defining the thermal conductance between the substrate thermocouple node and the node representing the edge of the substrate.

In order to measure the gradients through the substrate, identical thermocouples (36-gauge chromel-constantan wires with aluminized Mylar shieldings) were placed on the surface of the substrate as well as next to the heater. In this case, the embedded thermocouple reads the mean temperature of the heater and the substrate surface and should be higher than the actual surface temperature. The reading of the surface thermocouple should be slightly lower than the true surface temperature, because of conductive heat lost down the thermocouple leads. However, the difference between the two readings was found to be negligible when the substrate was kept below room temperature in the LN_2 chamber and was less than 0.3°C when the sample was heated to 150°C .

Because the effective emittance of the cell module is very sensitive to the surface or cell temperature measurement, an attempt was also made to relate actual cell and coverglass temperatures to the substrate's thermocouple reading. This was accomplished by installing three 40-gauge bare chromel-constantan thermocouples at various positions on the module's surface. The readings from these thermocouples were then compared with the reading of the 36-gauge chromel-constantan thermocouple embedded in the module substrate. All four thermocouples had identical readings at room temperature. However,

when the sample was heated to 150°C , a temperature difference of approximately 2°C developed between the substrate and cell surface. This information was used to define the thermal conductance between the substrate thermocouple node and the solar cell node in the thermal model of the system.

2 Calibration for Conductive Heat Loss. Conductive heat losses from power and thermocouple leads were also measured in the calibration procedure. In addition to the actual power and the thermocouple leads, pairs of dummy leads were embedded in the substrate in a similar fashion. Measurements of power inputs were then made before and after the dummy leads were removed. The difference in electrical power inputs required to maintain the substrate at the same temperature for the two measurements corresponds to the conductive heat loss due to the dummy leads at the specific temperature level. Heat losses for both the heater and thermocouple leads were so established over a broad range of module temperatures.

3 Calibration of the Solar Simulator During the solar absorptance measurements, a Spectrosun Model 25 Mark II solar simulator was used to irradiate the test modules. In order to allow continuous monitoring of the incident solar intensity at the position of the test module, four solar cells were mounted on the module-holding frame adjacent to and in the plane of the module. The short-circuit current produced by these cells is proportional to the intensity of illumination and was used to monitor the intensity level. The absolute energy intensity at the target plane was established using a primary absolute cavity radiometer (Refs. 11 and 12) with a reported accuracy of better than 0.3% and was directly correlated with the cell short-circuit current. Thus, following the initial calibration, the intensity irradiated on the module surface was readily obtained by measuring the short-circuit current output of the calibrated cells on the supporting frame.

a Uniformity of the illumination Uniformity of the simulated solar beam at the target plane was measured in ambient air using a scanning device. When a 26% neutral-density filter was placed in front of the lenticules, a maximum intensity variation of $\pm 3.5\%$ was measured across the 15-cm (6-in.) diameter beam. With 42 and 65% neutral density filters, the corresponding intensity variations were ± 2.4 and 2.6% respectively. When no filter was applied, the variation in intensity was $\pm 2.4\%$ for the full beam, and, within a 11-cm (4.5-in.) diameter circle, the intensity variation was only $\pm 1.5\%$.

b Spectral distribution Six bandpass filters were used to calibrate the energy distribution curve from $0.4 \mu\text{m}$ to $1.1 \mu\text{m}$. The filtered cells were mounted on a temperature-controlled plate (28°C), and the short-circuit current was compared with standard cell balloon flight test measurements. The relative spectral distribution, calculated on the basis of an equal energy match, is compared with the Air-Mass-Zero solar spectrum shown in Fig. 135.

4 Calibration of Painted Surfaces. As all the specimens prepared for the present testing

program were either fully or partially coated with certain reference paints, the total hemispherical emittance of the painted surfaces had to be measured first. This also served as a meaningful calibration for the whole system by allowing the emittances obtained in the present program to be compared with those published in the literature. Three paints were studied in this investigation: Parson's optical black, Cat-A-Lac flat black, and Cat-A-Lac white. Although platinum black is believed to be a better reference surface for calibration purposes, as it is "black" over a wide wavelength range, it was not used because of the complicated chemical application process it requires. In the current program, Parson's optical black was used for all calibrated surfaces because it appeared to be sufficiently stable in the temperature range of interest (-40°C to +170°C). The Cat-A-Lac paints were included primarily because of their extensive use on past JPL spacecraft.

The paint test samples were obtained by painting both sides of the cell module substrates with the selected paints. The emittances of the painted substrates were then determined using the techniques outlined in the experimental approach. Figure 136 shows the measured total hemispherical emittance of the Parson's black paint and Fig. 137 gives the total hemispherical emittance of the Cat-A-Lac paints.

The integrated solar absorptance was also determined for the Parson's optical black and Cat-A-Lac flat black paints. The values of 0.98 and 0.965, respectively, appear to be in good agreement with published data.

E Experimental Procedure

Following the system calibration, the total hemispherical emittance and integrated solar absorptance was determined for a number of solar cell modules. The test specimens included solar cell modules with standard blue and blue-red filters, one with the modified 4026 selective band-pass filter, one with partially mirrored cover-glasses, and one made using multiple wide-grid cells with blue filters. The partially mirrored cell module and the multiple wide-grid cell module are shown in Figs. 138 and 139, respectively. The 2 ohm-cm cell with blue filter module can be seen in the module-holding frame in Fig. 133.

During the measurements, the chamber was cooled with liquid nitrogen and the working pressure was reduced to less than 10^{-4} N/m² (10^{-6} torr). Besides the module and holding-frame thermocouples, six others were used to monitor the temperatures of various positions on the cold-wall shroud and chamber window. The cold shroud maintained an average temperature around -182°C (-295°F), and the inner window surface remained around 7°C (20°F).

For the emittance measurements, the samples were heated electrically via the 350-ohm heater in the module substrate. Heater current and voltage and the various temperatures were recorded automatically every 4 min. The equilibrium temperature was taken as the average of four consecutive readings where the module temperature had a rate of change of less than 0.002 mV/4 min or 0.4°C/h, and where the four readings contained at least one

local maximum and one local minimum. These measurements were repeated using various heater powers in order to obtain sample emittance as a function of temperature.

The thermal model used for evaluating the effective emittance of the cell modules consisted of eleven nodes: seven module nodes, two holding frame nodes, the chamber window, and the chamber wall. A sketch of the thermal model of the whole calorimetric system is shown in Fig. 140. Following the equilibrium temperature measurements, the thermal model was evaluated numerically on a digital computer, and the module's effective hemispherical emittance was determined by forcing the temperature of the thermocouple node (node 11 in Fig. 140) to equal the measured temperature.

The integrated solar absorptance of the sample could have been determined in a similar manner by heating the test module with the radiant flux from the solar simulator instead of with the substrate heater. However, in order to ensure that no inherent uncertainty was carried over from the emittance measurements, the direct method outlined in the experimental approach was used to determine the solar absorptance independent of the emittance measurement.

This technique required two separate equilibrium measurements for each absorptance determination. After the module's equilibrium temperature was measured for a given solar flux and electrical power input, a second measurement was made to determine the additional heater power required to maintain the same equilibrium temperature with the solar simulator turned off. Since both the electrical power and solar intensity were measurable, the effective solar absorptance could be calculated directly.

Using the measurement techniques described above, the apparent solar absorptance and emittance of the ohmic contact and intercell space areas was established by first determining the absorptance and emittance of a special module with typical contacts and intercell spaces but with the cells filtered with OCLI SI-100 mirrors. The contacts and spaces were then coated with Parson's optical black lacquer, and the absorptance and emittance of the module were re-evaluated. The apparent thermal radiation properties of the contact and intercell space areas were then deduced by comparing the emittances and absorptances of the painted and unpainted modules.

F Experimental Results and Discussion

1 Emittance Measurements. Since solar cell modules are composite surfaces of cell ensembles, metallic contact strips and intercell spaces, their thermal radiative characteristics are represented by effective emittances and effective solar absorptances. The effective total hemispherical emittances for the modules considered in this investigation are shown in Fig. 141 as a function of cell temperature. Because the module emittance is almost entirely determined by the properties of the quartz coverglass, the emittances of the various modules are very similar.

In order to estimate the expected error in the emittance measurements, a detailed error analysis of the entire calorimetric system was conducted. Based on this analysis, an error bound of $\pm 2.5\%$ was established for the measurements. The TRW data points for the blue filter module represent hemispherical emittance measurements conducted in TRW's calorimetric apparatus, using a similar module of their own design but fabricated using the same cells, filters, cell interconnections, and cell spacing as the JPL module. The TRW data points tend to confirm the accuracy of the results presented.

2 Apparent Absorptance of Contact and Intercell Space Areas. For the modules used in these tests, the intercell spaces and metallic contact strips covered 11.5% of the module's projected area at room temperature. Because of the extreme difference in thermal expansion coefficients of the coverglass and the aluminum substrate, the intercell space area ($\sim 6\%$ at room temperature) varied somewhat with temperature as shown in Fig. 142. As a result, the apparent absorptance and emittance of the intercell spaces, which are presented in Fig. 143, tend to increase with increasing temperature.

Although the emittance of the contact and intercell space areas plays a minor role in determining the effective emittance of a cell module,

the apparent solar absorptance of these areas can significantly increase the effective solar absorptance of a module made with highly reflective coverglasses.

3. Solar Absorptance Measurements The effective integrated solar absorptances for the modules measured in this study are presented in Table 4 along with the error bounds established for the measurements. The percentage uncertainty for the modified 4026 filter module is considerably higher than the others because the spectrally selective filter is quite sensitive to uncertainties in the spectral distribution of the solar simulator.

For comparison purposes, Table 4 also contains the effective solar absorptances calculated using the component absorptances presented in Section VI of this report, the area dimensions given in Section III, and the contact and intercell space properties given in Fig. 143. The spread in the calculated values reflects the effect of the measured variation in the solar absorptances of the component surfaces as presented in Table 3 in Section VI, but does not include the measurement uncertainty in the photometric measurements. The agreement between the measured effective absorptances and those derived from the photometric measurements is considered excellent and appears to be sufficient to ensure the accuracy of results presented.

Table 4. Effective solar absorptance of test modules fabricated using various solar cell/coverglass assemblies and typical cell spacing

Module type	Effective solar absorptance	
	Measured	Calculated
Blue filter on 2 ohm-cm cell	0.780 ±0.015	0.78
Blue-red filter on 2 ohm-cm cell	0.700 ±0.015	0.69 - 0.70
Modified 4026 filter on 2 ohm-cm cell	0.363 ±0.025	0.35 - 0.36
Blue filter on multiple wide grid cell	0.412 ±0.007	0.40 - 0.41
Blue filter with mirror bar opposite contact on 2 ohm-cm cell	0.380 ±0.007	0.37 - 0.39

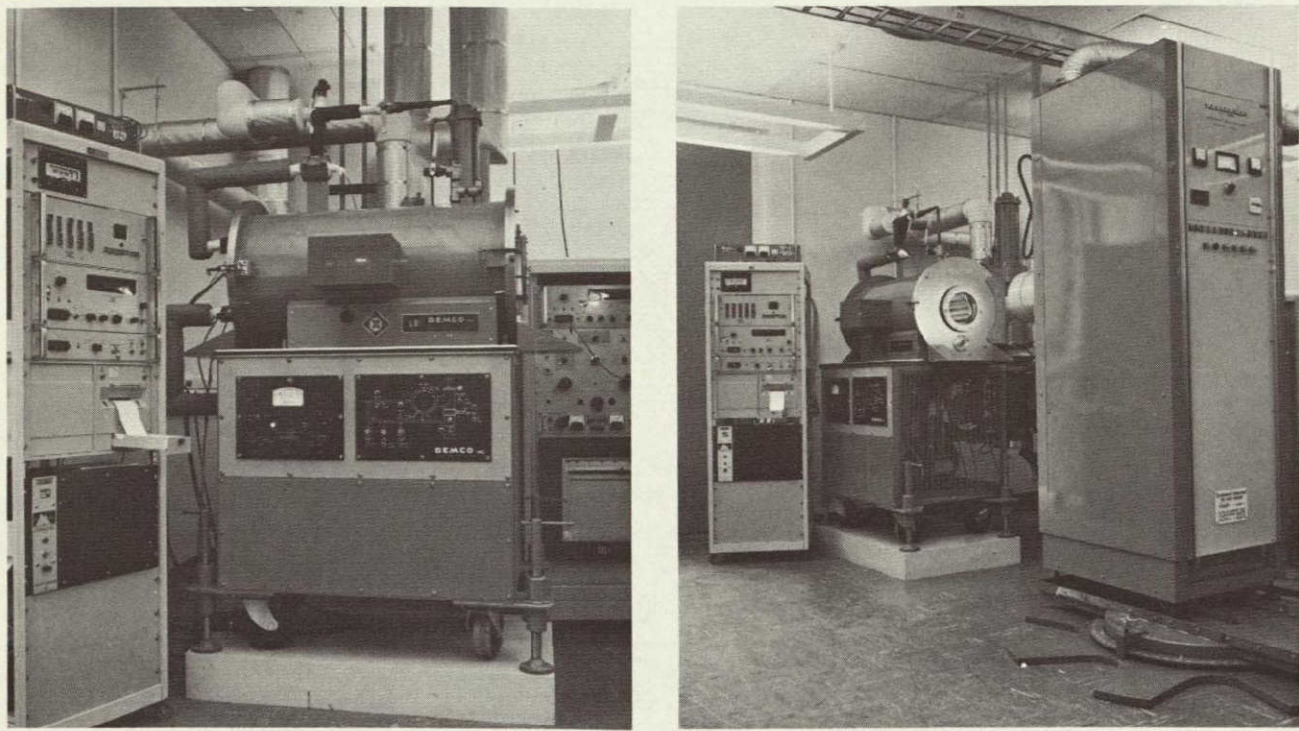


Fig. 131. Calorimetric test facility

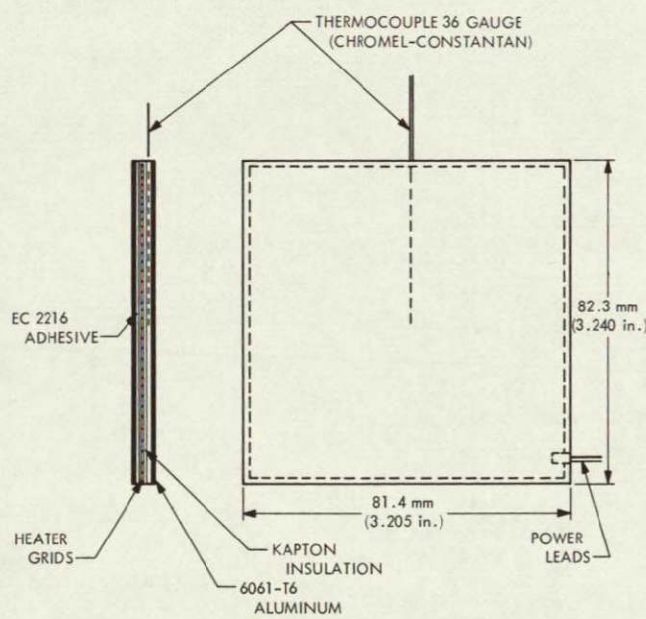


Fig. 132. Module substrate construction

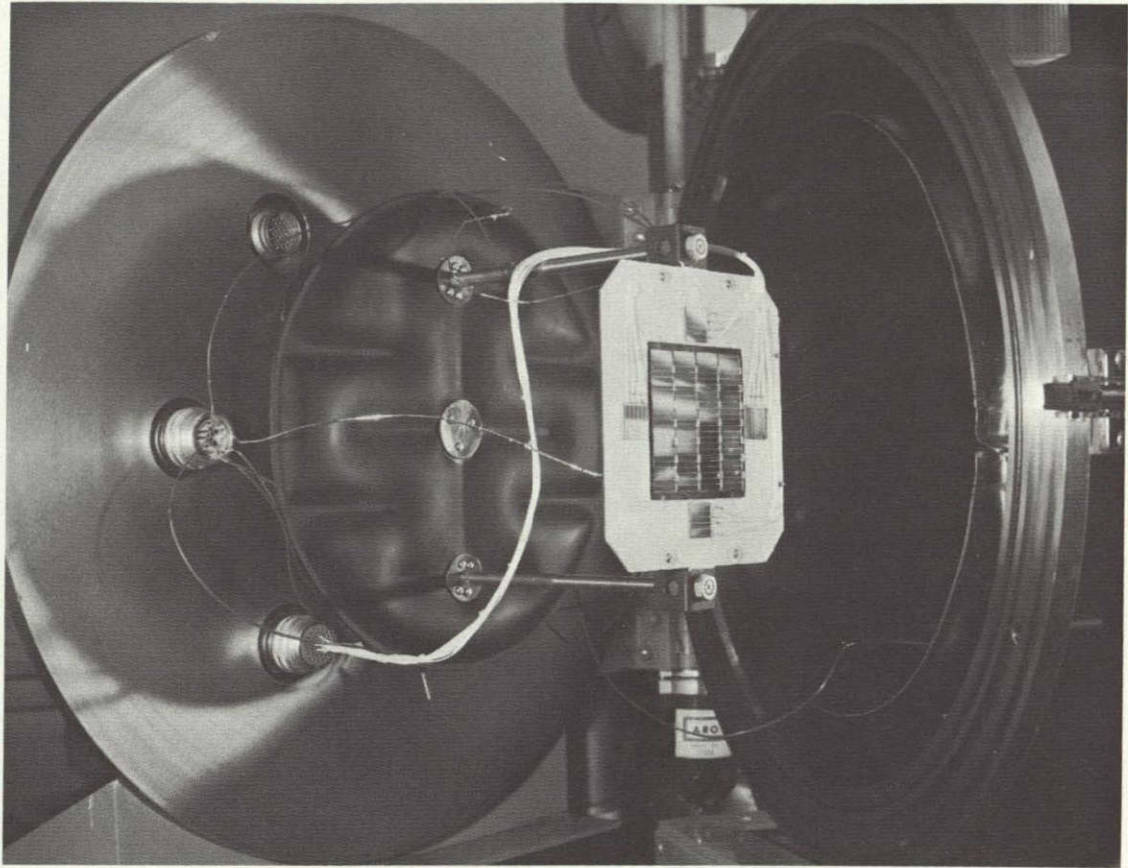


Fig. 133. Test module mounting assembly

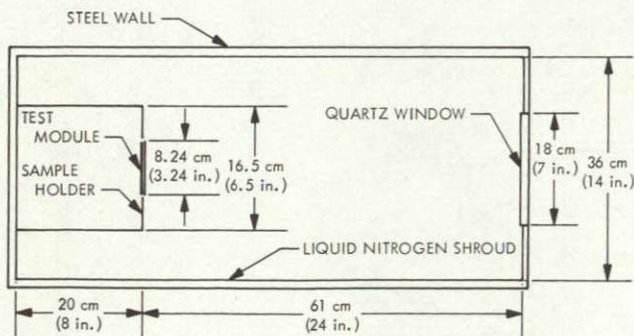


Fig. 134. Calorimetric system geometric configuration

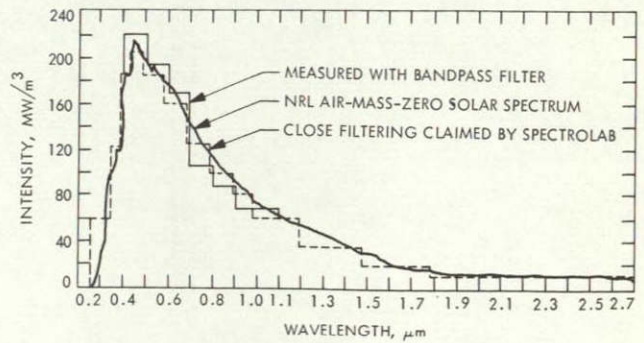


Fig. 135. Spectral distribution of solar simulator (adjusted for equal energy match)

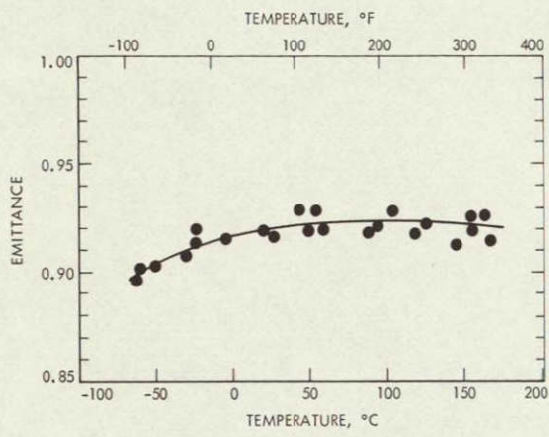


Fig. 136. Total hemispherical emittance of Parson's black paint

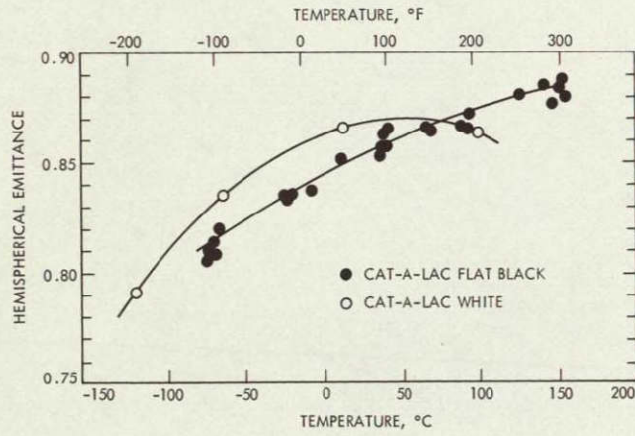


Fig. 137. Total hemispherical emittance of Cat-A-Lac paints

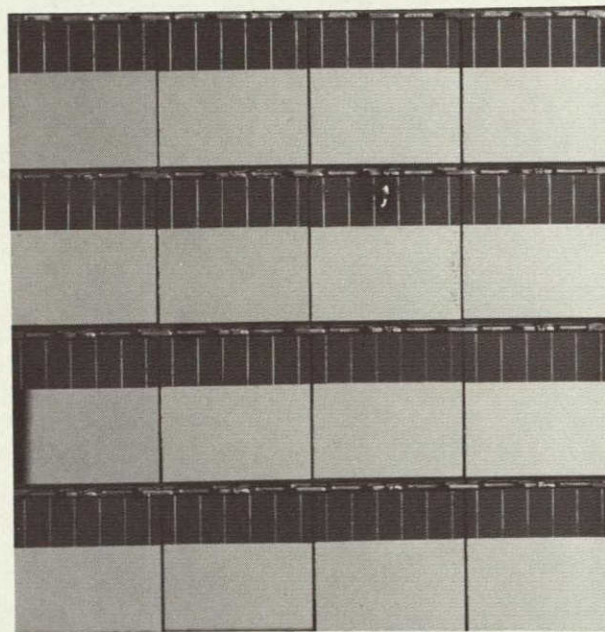


Fig. 138. Test module made using partially mirrored coverglasses on 2 ohm-cm cells

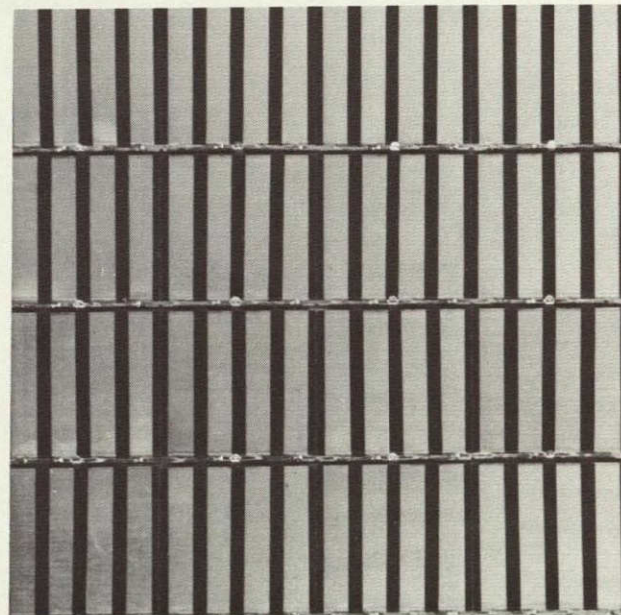


Fig. 139. Test module made using blue filters on multiple wide-grid cells

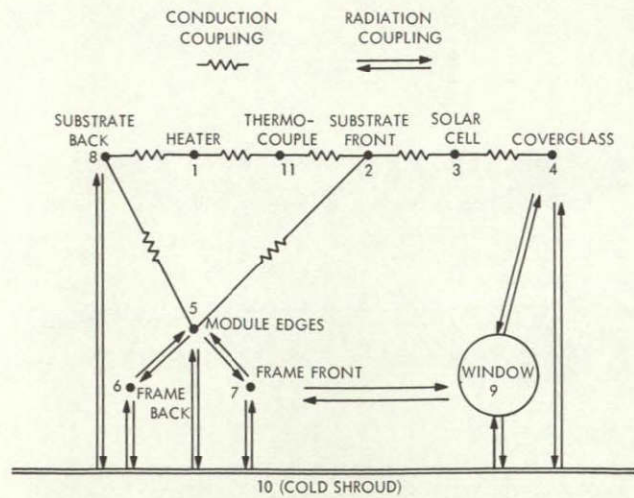


Fig. 140. Eleven-node thermal model of calorimetric system

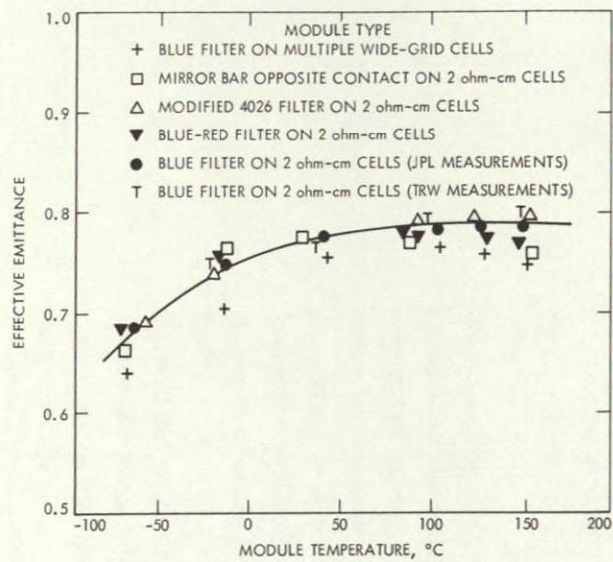


Fig. 141. Effective front surface emittance of test modules fabricated using various solar cell assemblies and typical cell spacing

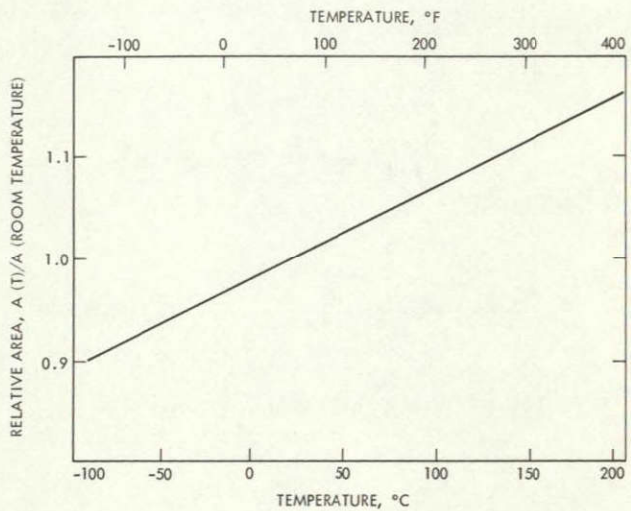


Fig. 142. Effect of module temperature on the relative size of the intercell spaces

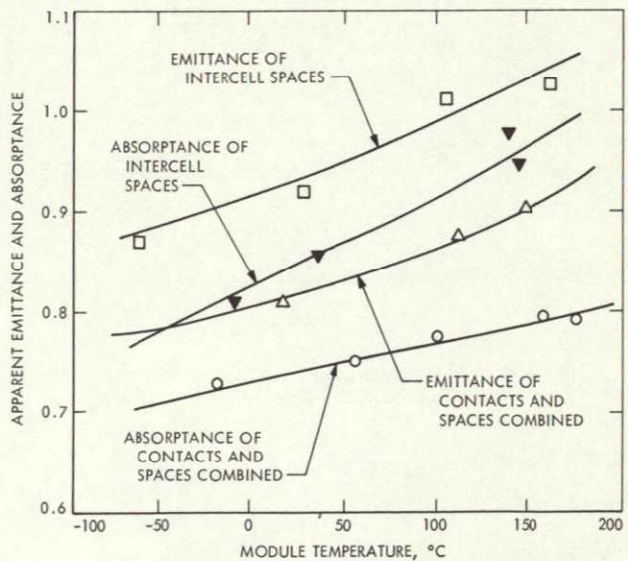


Fig. 143. Apparent emittance and solar absorptance of contact and intercell space areas based on the size of these areas at room temperature

VIII. IRRADIATION EFFECTS ON SOLAR CELL STACK THERMO-OPTICAL PROPERTIES

The irradiation effects measurements reported herein were conducted by Boeing Radiation Effects Laboratory, Seattle, Washington, under JPL Purchase Order No HF-525908

A Objective

To properly analyze the thermal behavior of solar array structures with regard to absorption or rejection of incident solar energy along the mission path, a fairly accurate knowledge of thermo-optical properties degradation due to the space environment is needed. This environment consists primarily of ultraviolet and particulate irradiation in the space vacuum. The particulate irradiation is composed predominantly of protons with a mixture of some alpha particles.

The objective of the testing was to provide information on solar cell thermo-optical properties degradation due to the varying irradiation fluxes along a Venus-Mercury trajectory. Of particular interest were the new cell assemblies and components considered in this study.

B Experimental Approach

The total time for a Venus-Mercury mission, including a period of 20 days past Mercury encounter, is approximately 4800 h. Because of the difficulties of running tests of this duration, a two-phase test program was devised: (1) a 500-h evaluation test at a constant sample temperature and flux intensity approximating the conditions in the neighborhood of Mercury, and (2) a 2400-h complete mission simulation test with sample temperature and flux intensities varying with time.

1. 500-h Evaluation Test. This test was conducted with the sample cells at a constant temperature of 140°C. The ultraviolet irradiation flux was equal

to five earth sun intensities and the equivalent solar wind (particulate matter) consisted of 3-KeV protons at a flux of approximately

$$1.2 \times 10^9 \frac{\text{particles}}{\text{cm}^2 \text{ sec}}$$

The particle dosage also included the proton equivalence of

$$3.75 \times 10^7 \frac{\text{particles}}{\text{cm}^2 \text{ sec}}$$

of alpha particles at the Mercury solar wind level (Refs. 13 and 14). In order to assess individual and combined effects of irradiation, three identical groups of samples were selected and were exposed to different types of irradiation: ultraviolet, proton, and combined proton-ultraviolet. The description of the six samples composing each group is given in Table 5.

2. 2400-h Mission Simulation Test Like the 500-h test, the 2400-h test consisted of exposing three identical groups of samples to ultraviolet, proton, and combined proton-ultraviolet irradiation. However, in this test the sample temperature and flux intensity were varied as shown in Figs. 144 and 145. The temperature profile was derived analytically, and represents a typical solar array temperature variation along the mission path. The temperature between Mercury and 20 days flight past Mercury was assumed (for test purposes) as constant and equal to 140°C. In order to achieve a total irradiance equal to the expected mission irradiance, the ultraviolet and

proton irradiation was maintained at twice the expected level. The actual proton flux can be obtained by multiplying the normalized intensity (suns) in Fig. 145 by 2.4×10^8 particles/cm² sec, which is the approximate proton flux in the solar wind near earth (1 sun intensity). The proton energy level, as in the 500-h test, was held at 3 keV.

For this test the sample size was increased from six to the nine sample types listed in Table 6. This allowed the addition of a bare fused silica sample, an unmounted blue-red filter, and a second coverglass adhesive sample (XR6-3489).

C. Test Apparatus

A description of the Boeing Radiation Effects Laboratory facility is given in Ref. 15, and more details of particular interest to this program can be found in Ref. 16. Basically, the facility consists of a combined radiation effects test chamber and a low-energy-particle accelerator.

The accelerator employs an Ortec 501 RF ion source capable of supplying hydrogen ions of several species. Magnetic deflection is used to analyze the ion output and separate the chosen component or specie (in this case protons) for injection into the chamber. An Einzel lens (in addition to a similar one employed at the ion source) is positioned along the beam axis and provides a measure of electrostatic defocusing for enlarging the proton beam size. The ultraviolet irradiation flux (up to 10-space-suns) is provided by a dual water-cooled long-arc xenon source. An in situ spectral monitoring of the xenon continuum (see Ref. 15) provides an intermittent analysis of the photon radiation level so that any lamp degradation can be compensated for by increasing or decreasing the arc current.

Particle dosimetry is performed by Faraday cups and copper discs. The arrangement allows monitoring of the particle beam profile prior to exposure and periodically during each exposure. Neutralization of the proton beam by means of "thermal" electrons was not considered for this program, as only very small effects could be anticipated from a careful study of the results presented in Ref. 16.

Figure 146 shows a general view of the combined radiation effects test chamber and low energy particle accelerator with its ion source and magnetic deflector in the foreground. The chamber-mounted sample wheel was specifically adapted to the test requirements of the solar cell assemblies and components. In addition, special nonstandard sample holders were procured.

Figure 147 shows the test samples for the 2400-h proton/ultraviolet radiation test, and the proton dosimetry array, mounted to the combined radiation effects test chamber door. With the door closed, samples are in their measurement position adjacent to the integrating sphere shown. In this same position, the proton dosimetry array is situated correctly to measure proton intensity across the exposure area. A 180-deg rotation brings the samples into proper position to begin sample exposure. At that time, "proton-only" samples are

adjacent to the UV-baffling channel seen projecting past the long-arc ultraviolet sources toward the chamber door.

Figure 148 shows more clearly the 2400-h test configuration. The samples near the bottom of the photograph (1- X 1-cm filters and 2- X 2-cm cells) are approaching the measurement position, where the transmission measurement light projects through the tube and each filter sample in turn. Reflectance measurements utilize the integrating sphere, shown in Fig. 147. The dosimetry array is likewise approaching the exposure position where the 21 cylindrical tabs map proton beam uniformity. At the center of the dosimetry array, the large aperture allows protons to enter the fixed Faraday cup to measure absolute beam intensity.

D. Presentation of Results

The test results, as presented herein, consist of integrated solar absorptances and transmittances (the latter for transparent samples) which, for the 500-h test, are given in Table 7, and for the 2400-h test in Table 8. The sample numbers are those listed in Tables 5 and 6. Also included are the spectral measurements from both tests; these are presented in a graphical form. To limit the number of graphs, the 500-h test spectral measurements of the effects due only to ultraviolet and proton fluxes have been deleted. However, a complete set of available graphical data, taken during the 2400-h test, is incorporated.

The photometric measurements of the thermo-optical properties were made in situ at the time intervals indicated in Tables 7 and 8. In the case of the 500-h test, the initial measurements were made at a room temperature of approximately $15 \pm 5^\circ\text{C}$, although subsequent measurements were made at 140°C . Likewise, data for the first 753 h of the 2400-h test were also obtained at room temperature, because the temperatures between 0° and 16°C , as specified by the temperature profile given in Fig. 144, were found difficult to control. For temperatures higher than room temperature, the profile given in Fig. 144 was followed very closely. The flux intensities were also closely represented by taking very small incremental steps as shown in Fig. 145.

The graphical data for both 500-h and 2400-h tests are organized in a manner allowing an easy comparison of irradiation effects. Because of this, the graphs are not in sequence with the sample number lists given in Tables 5 and 6.

Figures 149-156 present the spectral thermo-optical properties for the group of samples which was exposed to the combined proton-ultraviolet irradiation during the 500-h test. Each curve is identified by a number which indicates the time at which the measurement was taken. The times corresponding to the numbers are indicated in Table 7.

Figures 157-195 provide a complete set of the data obtained from the 2400-h test; i.e., in addition to combined proton-ultraviolet effects, the individual effects for ultraviolet and proton irradiation are also included. Identification similar

to that used in the 500-h test results is used for the superimposed curves. The actual measurement times are indicated in Table 8.

E Analysis and Discussion

Examination of the 500-h test spectral data indicates that samples tested experienced very little degradation of their thermo-optical properties. The results further indicate that the observed degradation is almost entirely caused by the ultraviolet radiation, the effects due to protons being very small. The integrated results given in Table 7 reveal no significant changes in either the absorptance or in the transmittance of the samples.

One interesting side product of the 500-h test was the damage to the modified 4026 filter, which is attributed to thermal effects. After the test the filter layer stacks exhibited mosaic-type cracks causing some increase in absorptance in the visible spectral band. Figure 196 shows the damage as seen through a microscope at 25X.

The 2400-h test spectral data tend to confirm the conclusions derived from the 500-h test. However, the degradation between 0.25 to 0.6 μm is considerably higher and appears to be consistently increasing with exposure time. The blue-red filter, in addition, suffered some degradation between 1.1 and 1.35 μm .

The fact that ultraviolet irradiation contributes most to the degradation is confirmed during this mission simulation test, proton irradiation effects are much smaller. By comparing

reflectance and transmittance data, it is seen that most of the degradation (due primarily to ultraviolet) takes place in the bandwidths which are not transmitted through the filter. This can also be inferred from the transmittance measurements seen in Figs. 187 and 189, where transmittance is decreased in the 0.25- to 0.6- μm region due to increased glass absorptance.

The data on adhesives show that both adhesives tested degrade considerably below 0.8 μm if unprotected by a proper filter (see Fig. 126, Section VI). The XR6-3480 adhesive appears to be more resistant to degradation than the RTV 602.

Inspection of the data given in Table 8 reveals only small changes for the integrated values of absorptance and transmittance, with the exception of the absorptance of the modified 4026 filter and the transmittance of the blue-red filter.*

Comparing 500-h test results with the 2400-h test measurements, it appears that sample temperature has some influence on the degree of degradation during exposure. Degradation tends to be higher on colder samples (room temperature) as opposed to those kept at elevated temperatures.

The physical appearance of the bonded (non-transparent) samples after the 2400-h test shows that ultraviolet irradiation (0.2-0.4 μm) penetrates the filter layers in all three types of filters tested and causes some degradation of the bond adhesive. This effect appears to be responsible for the absorptance increase in the visible spectral range.

*Some difficulties were experienced in providing a proper *in situ* arrangement for transmission measurements. In view of this, the transmission data for the modified 4026 filters, between 0.6 and 1 μm , are subject to further verification.

Table 5. Samples exposed to irradiation in 500-h test

Sample Description	Sample Numbers for Type of Exposure		
	Ultraviolet	Proton + Ultrav.	Proton
Blue filter on 2Ωcm cell	2035	2041	2047
Modified 4026 filter on 2Ωcm cell	2036	2042	2048
Blue-red filter-RTV602-polished aluminum	2037	2043	2049
Blue filter	2038	2044	2050
Modified 4026 filter	2039	2045	2051
Blue-red filter on 2Ωcm cell	2040	2046	2052

Table 6. Samples exposed to irradiation in 2400-h test

Sample Description	Sample Numbers for Type of Exposure		
	Ultraviolet	Proton + Ultrav.	Proton
Blue filter on 2Ωcm cell	2074	2083	2092
Modified 4026 filter on 2Ωcm cell	2075	2084	2093
Blue-red filter on 2Ωcm cell	2076	2085	2094
Blue filter	2077	2086	2095
Modified 4026 filter	2078	2087	2096
Blue-red filter	2079	2088	2097
Clear glass (7940 fused silica)	2080	2089	2098
Clear glass-RTV602-polished aluminum	2081	2090	2099
Clear glass-XR6-3489-polished aluminum	2082	2091	2100

Table 7. Integrated solar absorptance and transmittance, 500-h test

JPL Sample	Solar Absorptance (α s)						Remarks
	Pre-irrad. Room temp. (0)	Pre-irrad +140 °C (1)	After 53 hrs. (2)	After 140 hrs. (3)	After 317 hrs. (4)	After 500 hrs. (5)	
2035		0.78	0.79	0.79	0.79	0.79	
2036		0.30	0.30	0.30	0.30	0.30	
2037		0.20	0.21	0.21	0.22	0.22	Ultraviolet
2038*		0.08	0.07	0.05	0.04	0.03	
2039		0.05	0.05	0.05	0.06	0.06	
2040		0.69	0.69	0.68	0.69	0.68	
2041	0.78	0.78	0.79	0.79	0.79	0.79	
2042	0.30	0.30	0.31	0.31	0.30	0.31	
2043	0.21	0.20	0.21	0.21	0.22	0.22	Proton- ultraviolet
2044	0.01	0.02	0.03	0.02	0.03	0.03	
2045	0.05	0.05	0.05	0.05	0.06	0.06	
2046	0.69	0.69	0.68	0.68	0.68	0.68	
2047		0.78	0.78	0.78	0.78	0.78	
2048		0.29	0.29	0.30	0.29	0.30	
2049		0.21	0.20	0.20	0.21	0.21	Proton
2050		0.03	0.03	0.02	0.03	0.03	
2051		0.05	0.05	0.05	0.06	0.05	
2052		0.69	0.69	0.69	0.69	0.68	
Solar Transmittance (τ s)							
2038*		0.78	0.80	0.82	0.83	0.84	Ultraviolet
2039		0.26	0.27	0.27	0.26	0.26	
2044	0.86	0.85	0.84	0.85	0.84	0.84	Proton- ultraviolet
2045	0.27	0.26	0.27	0.27	0.26	0.26	
2050		0.84	0.84	0.85	0.84	0.83	Proton
2051		0.26	0.27	0.27	0.26	0.26	

* Results invalid (surface of the sample soiled).

Table 8. Integrated solar absorptance and transmittance, 2400-h test

JPL Sample	Solar Absorptance (α_s)					Remarks
	In vacuum before exposure (1)	After 222 hrs. exposure (2)	After 753 hrs. (3)	After 1573 hrs. (4)	After 2400 hrs. (5)	
2074	0.79	0.79	0.79	0.80	0.80	
2075	0.31	0.34	0.34	0.35	0.37	
2076	0.70	0.70	0.70	0.70	0.70	
2077	0.03	0.05	0.06	0.06	0.08	
2078	0.05	0.05	0.06	0.07	0.08	Ultraviolet
2079	0.06	0.07	0.07	0.08	0.09	
2080	0.01	0.01	0.02	0.04	0.05	
2081	0.25	0.32	0.36	0.46	0.54	
2082	0.22	0.27	0.28	0.33	0.48	
2083	0.78	0.79	0.79	0.78	0.79	
2084	0.31	0.34	0.36	0.41	0.44	
2085	0.70	0.71	0.71	0.70	0.70	
2086	0.04	0.04	0.05	0.06	0.07	Proton- ultraviolet
2087	0.05	0.06	0.07	0.11	0.12	
2088	0.06	0.07	0.08	0.09	0.11	
2089	0.01	0.01	0.02	0.04	0.05	
2090	0.22	0.26	0.29	0.36	0.46	
2091	0.22	0.26	0.28	0.34	0.47	
2092	0.77	0.78	0.78	0.77	0.79	
2093	0.30	0.32	0.32	0.32	0.34	
2094	0.70	0.70	0.70	0.70	0.70	
2095	0.04	0.03	0.04	0.05	0.06	
2096	0.05	0.05	0.06	0.06	0.06	Proton
2097	0.05	0.07	0.07	0.06	0.06	
2098	0.01	0.01	0.01	0.01	0.02	
2099	0.22	0.23	0.23	0.23	0.25	
2100	0.21	0.23	0.23	0.24	0.26	
Solar Transmittance (τ_s)						
2077	0.85	0.84	0.83	0.83	0.82	
2078	0.29	0.30	0.30	0.30	0.30	Ultraviolet
2079	0.71	0.70	0.70	0.70	0.69	
2080	0.92	0.92	0.91	0.89	0.88	
2086	0.84	0.84	0.84	0.82	0.82	
2087	0.29	0.29	0.29	0.29	0.29	Proton- ultraviolet
2088	0.71	0.70	0.69	0.68	0.66	
2089	0.92	0.92	0.91	0.89	0.88	
2095	0.84	0.86	0.85	0.84	0.83	
2096	0.29	0.30	0.29	0.29	0.30	Proton
2097	0.71	0.70	0.70	0.70	0.70	
2098	0.92	0.92	0.92	0.92	0.92	

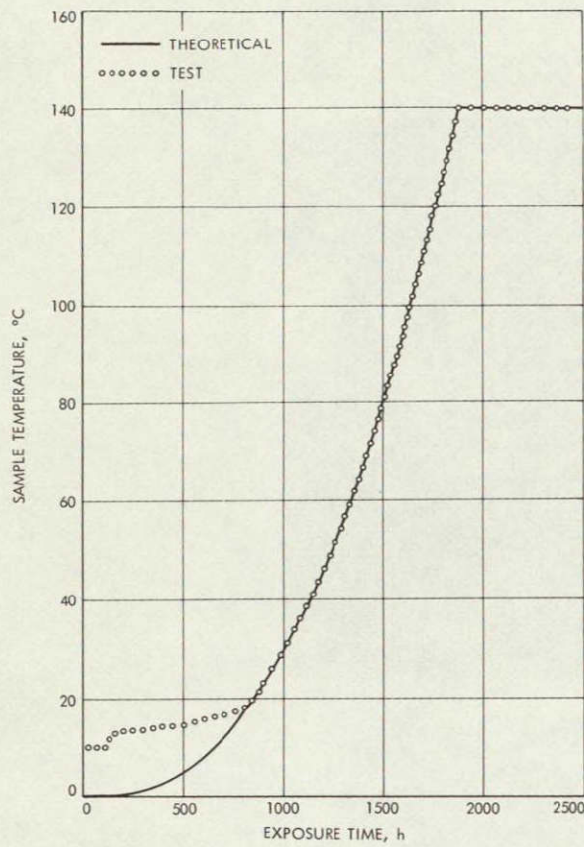


Fig. 144. Sample temperature, 2400-h test

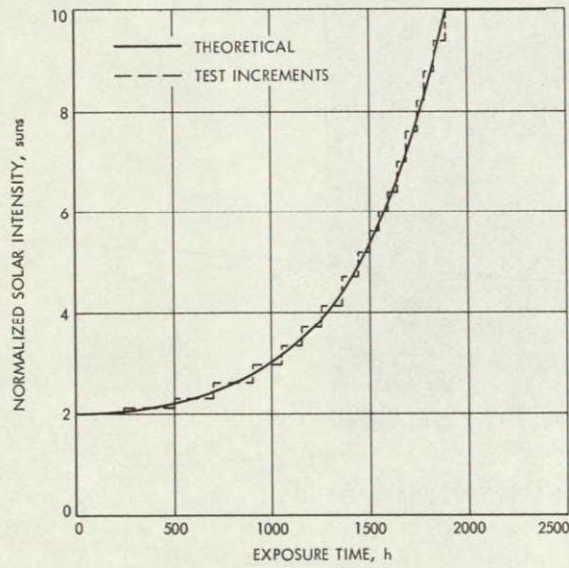


Fig. 145. Flux intensity, 2400-h test

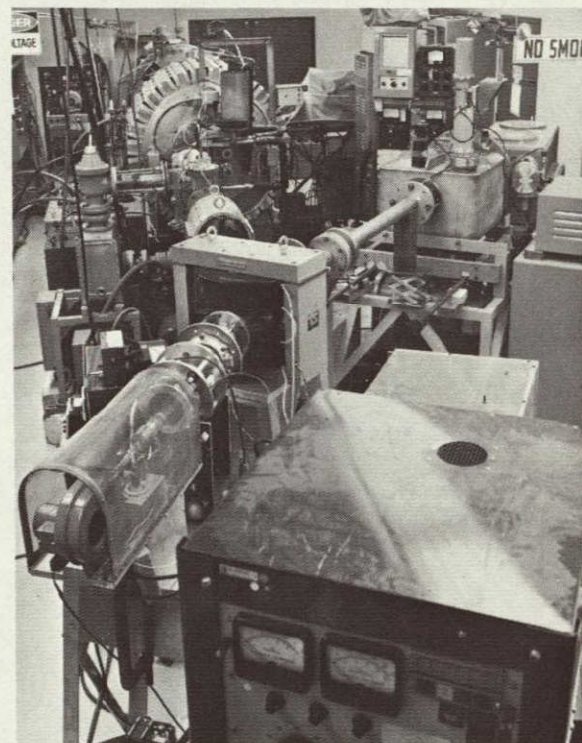


Fig. 146. Combined radiation effects test chamber and low-energy-particle accelerator

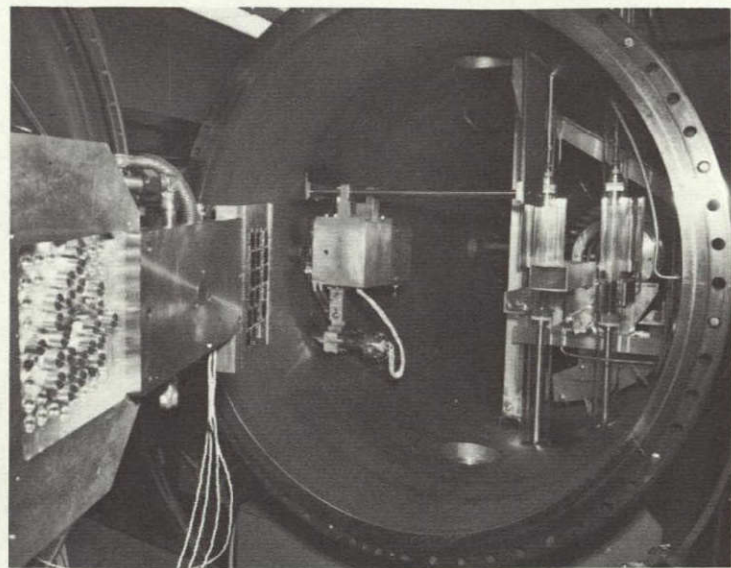


Fig. 147. Open chamber view of 2400-h test setup

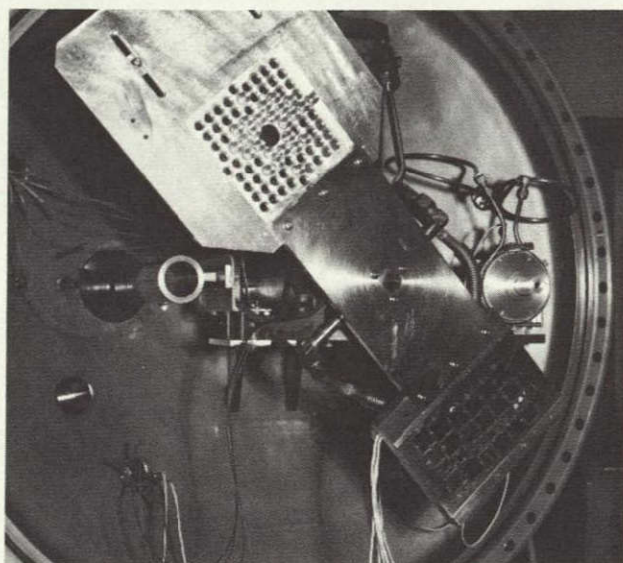


Fig. 148. Closeup view of samples and dosimetry tabs mounted on the chamber door wheel, 2400-h test

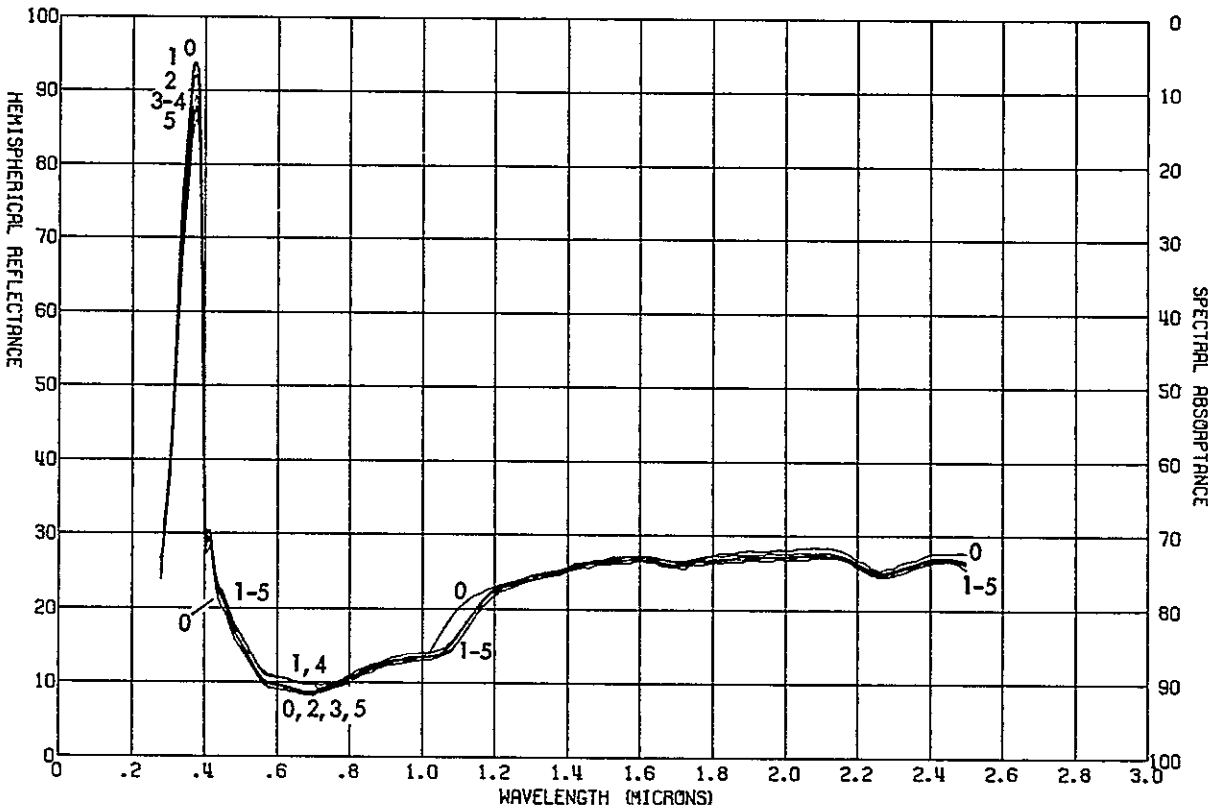


Fig. 149 Proton-ultraviolet effects on reflectance of sample 2041, blue filter on 2 ohm-cm cell, 500-h test

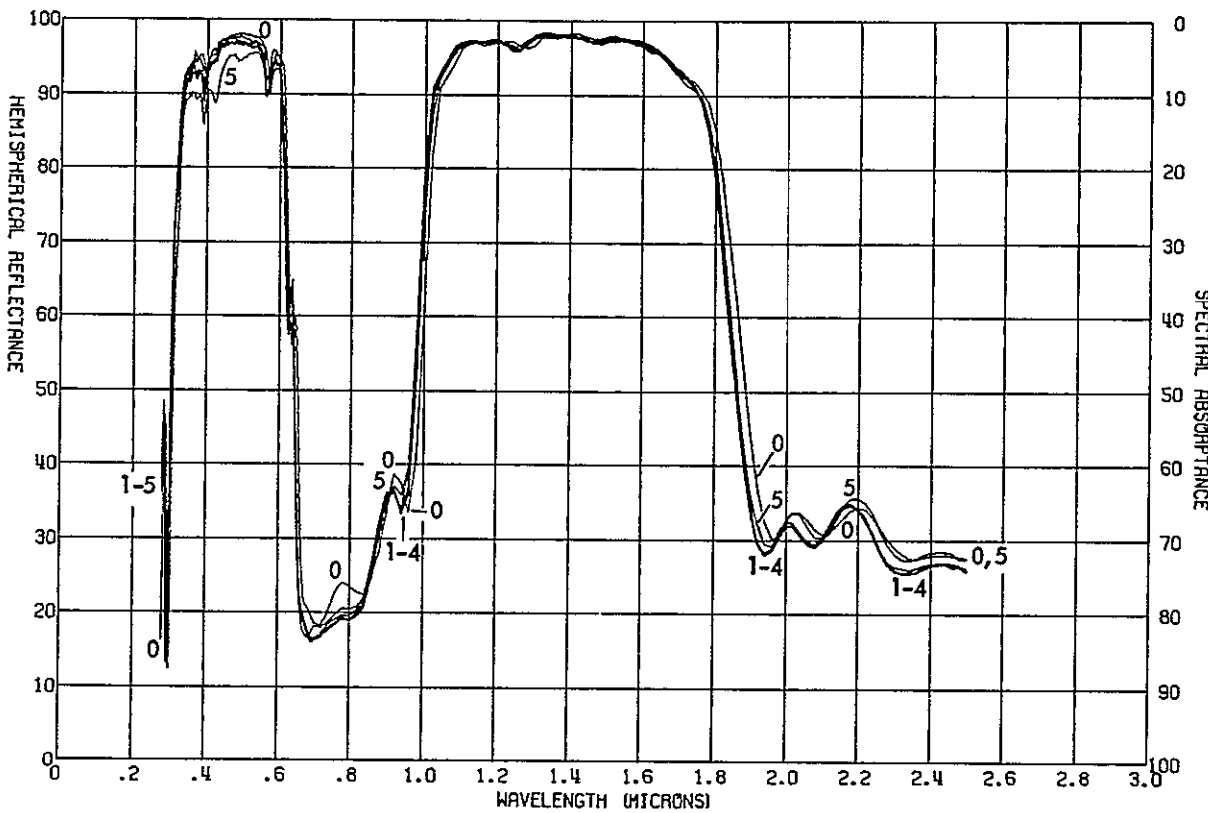


Fig. 150 Proton-ultraviolet effects on reflectance of sample 2042, modified 4026 filter on 2 ohm-cm cell, 500-h test

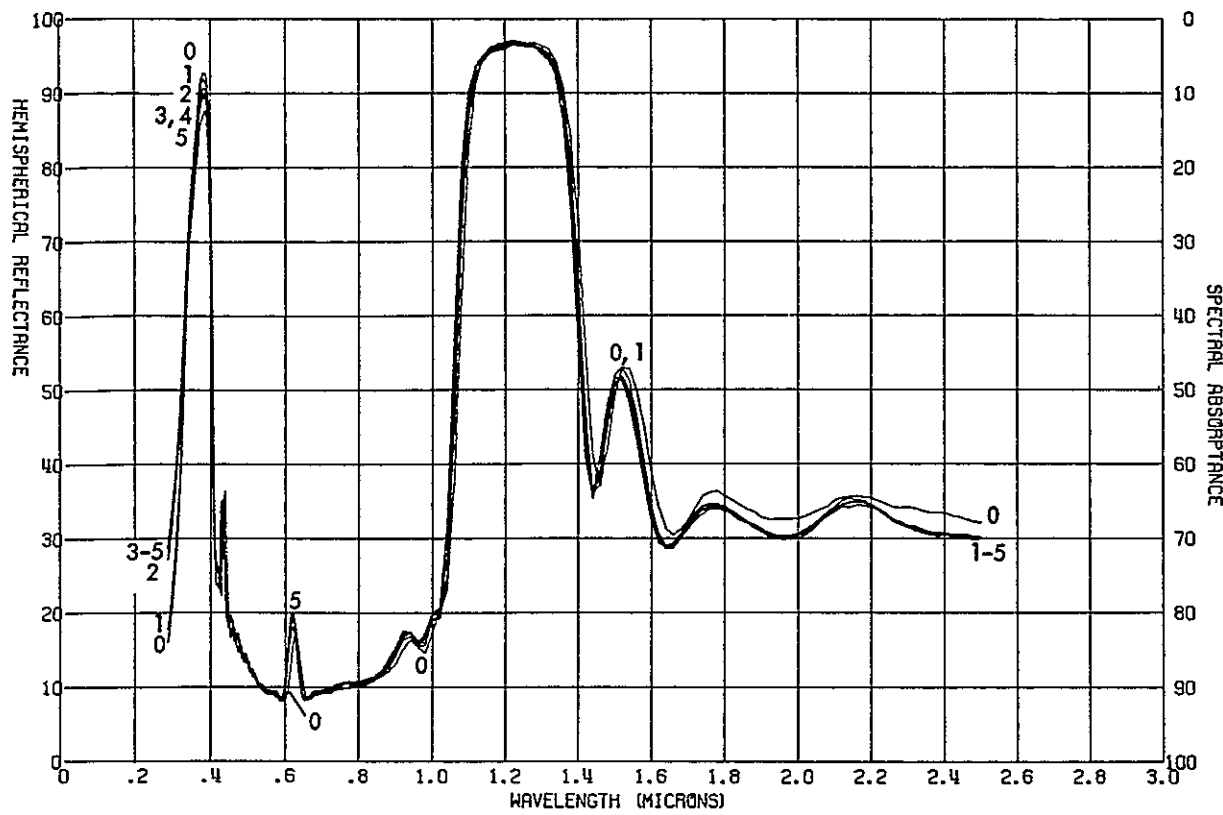


Fig. 151. Proton-ultraviolet effects on reflectance of sample 2046, blue-red filter on 2 ohm-cm cell, 500-h test

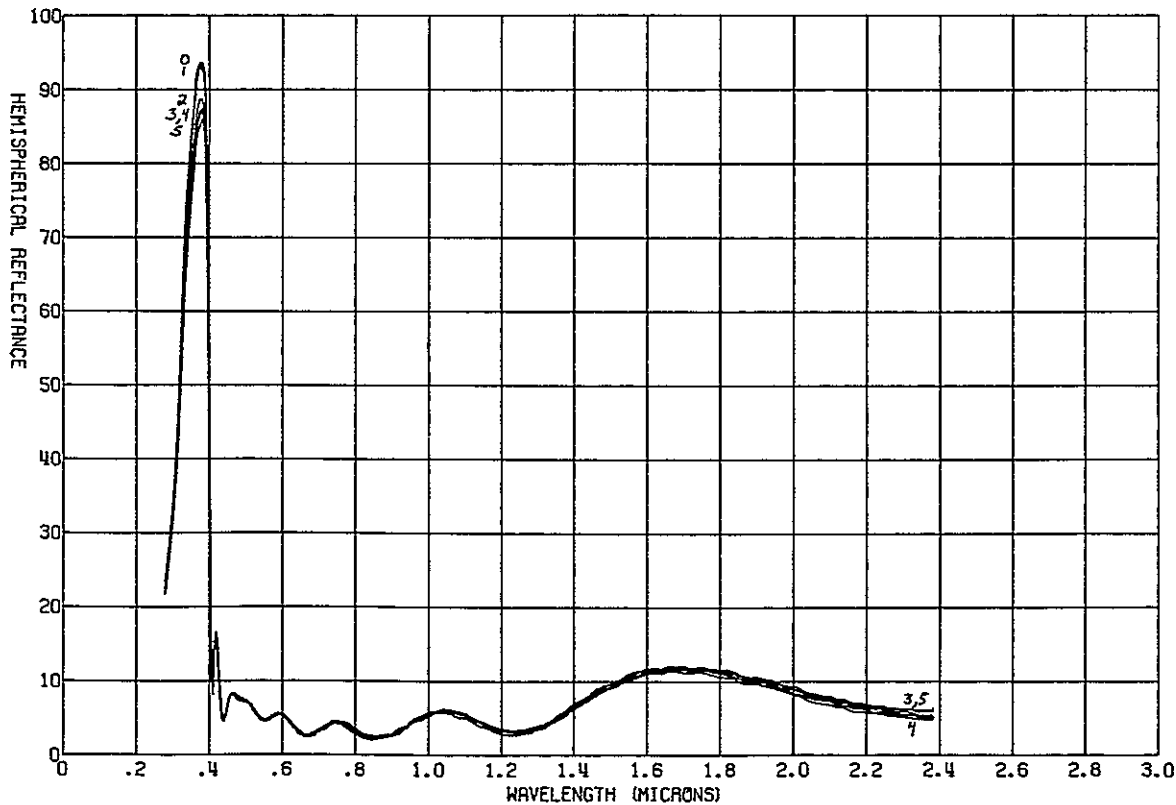


Fig. 152. Proton-ultraviolet effects on reflectance of sample 2044, blue filter, 500-h test

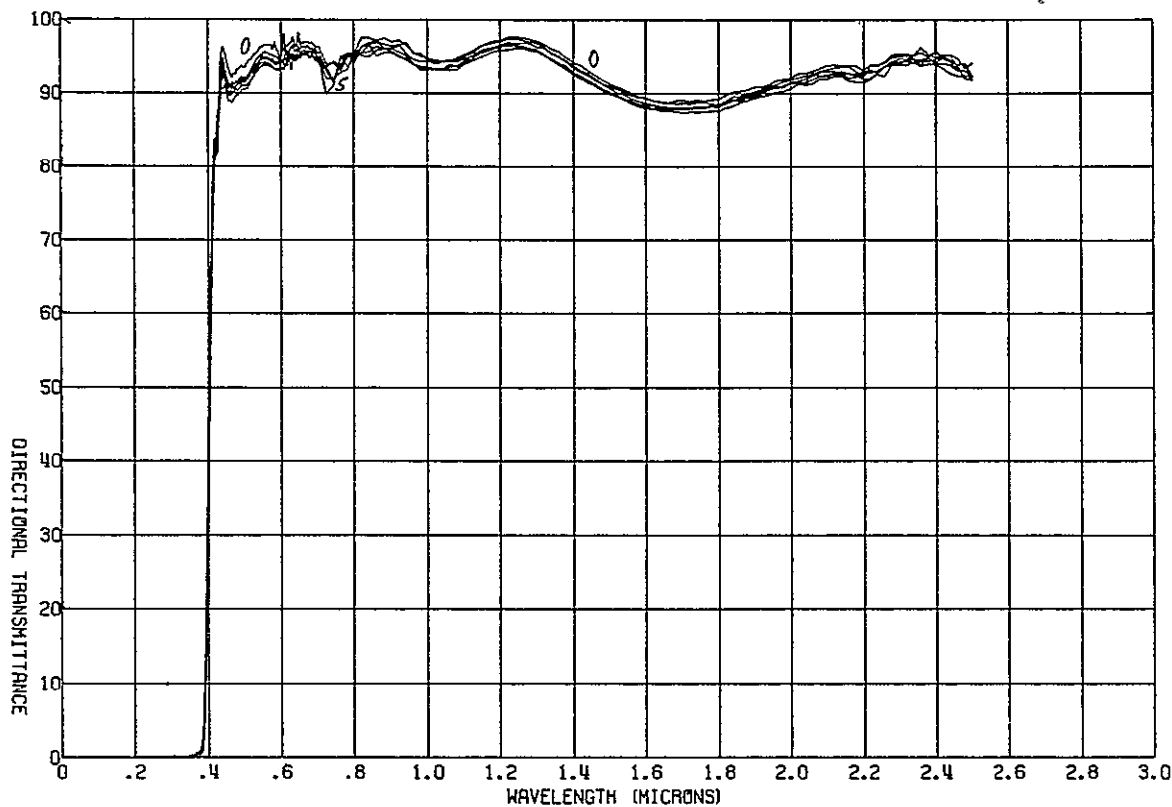


Fig. 153. Proton-ultraviolet effects on transmittance of sample 2044, blue filter, 500-h test

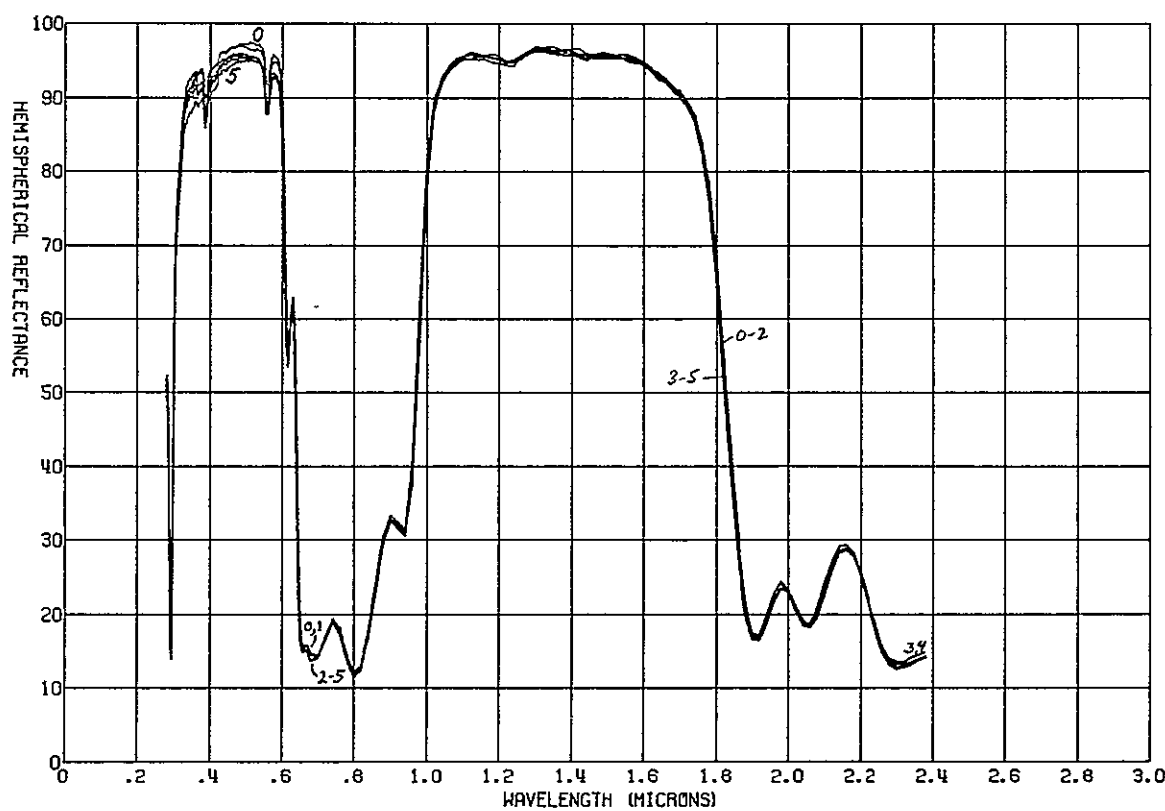


Fig. 154. Proton-ultraviolet effects on reflectance of sample 2045, modified 4026 filter, 500-h test

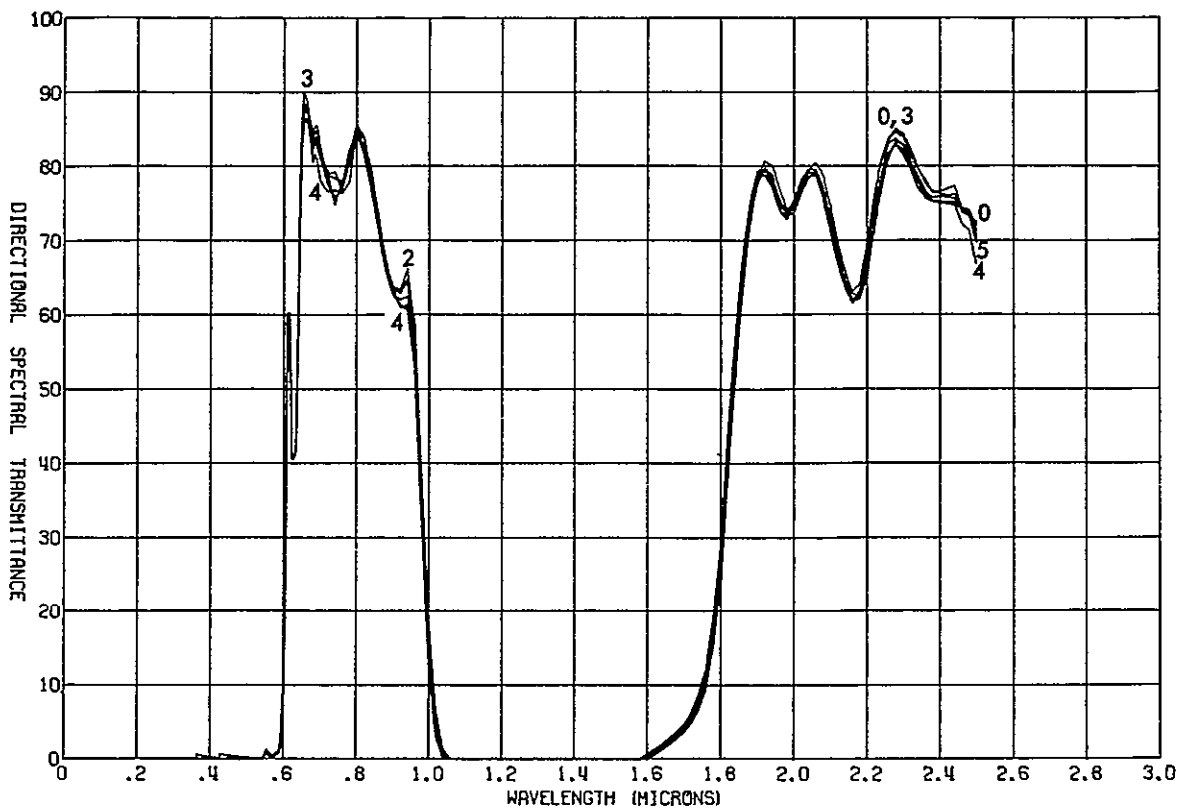


Fig. 155 Proton-ultraviolet effects on transmittance of sample 2045, modified 4026 filter, 500-h test

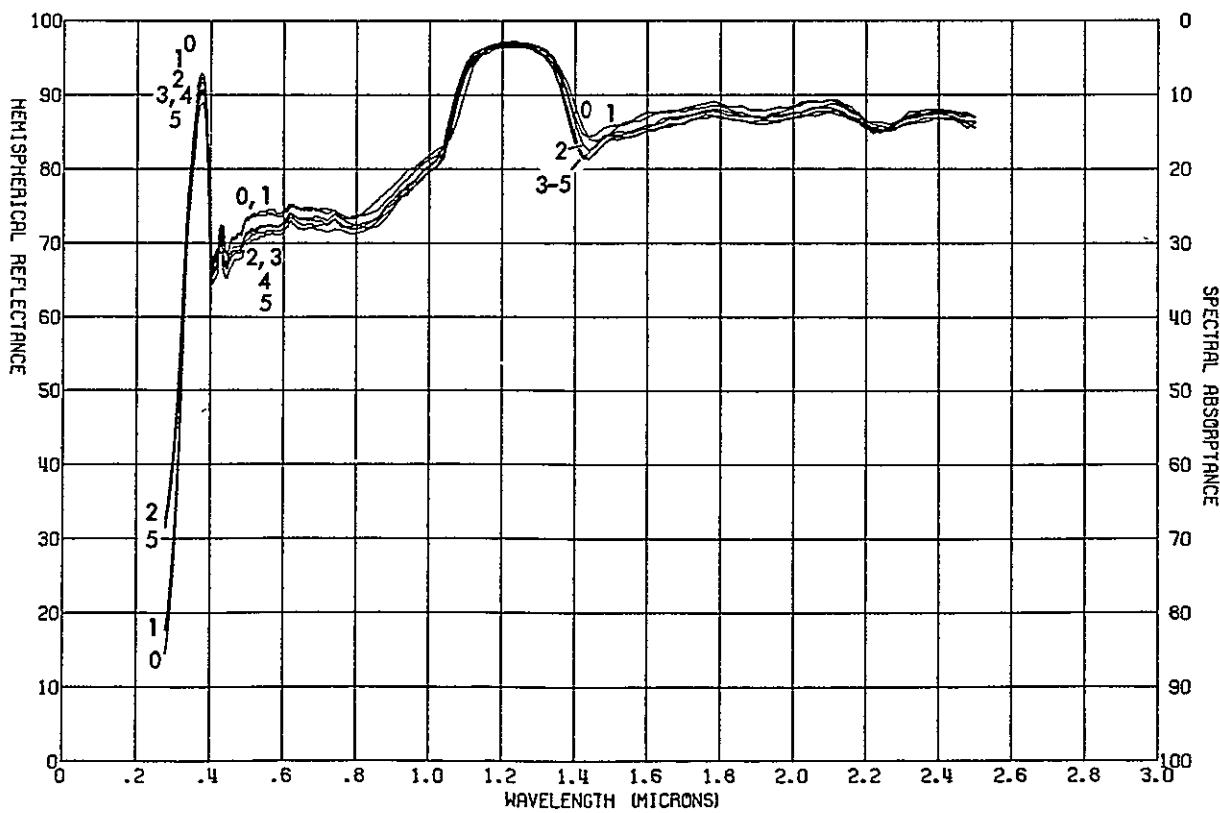


Fig. 156. Proton-ultraviolet effects on reflectance of sample, 2043, blue-red filter, RTV 602, polished aluminum, 500-h test

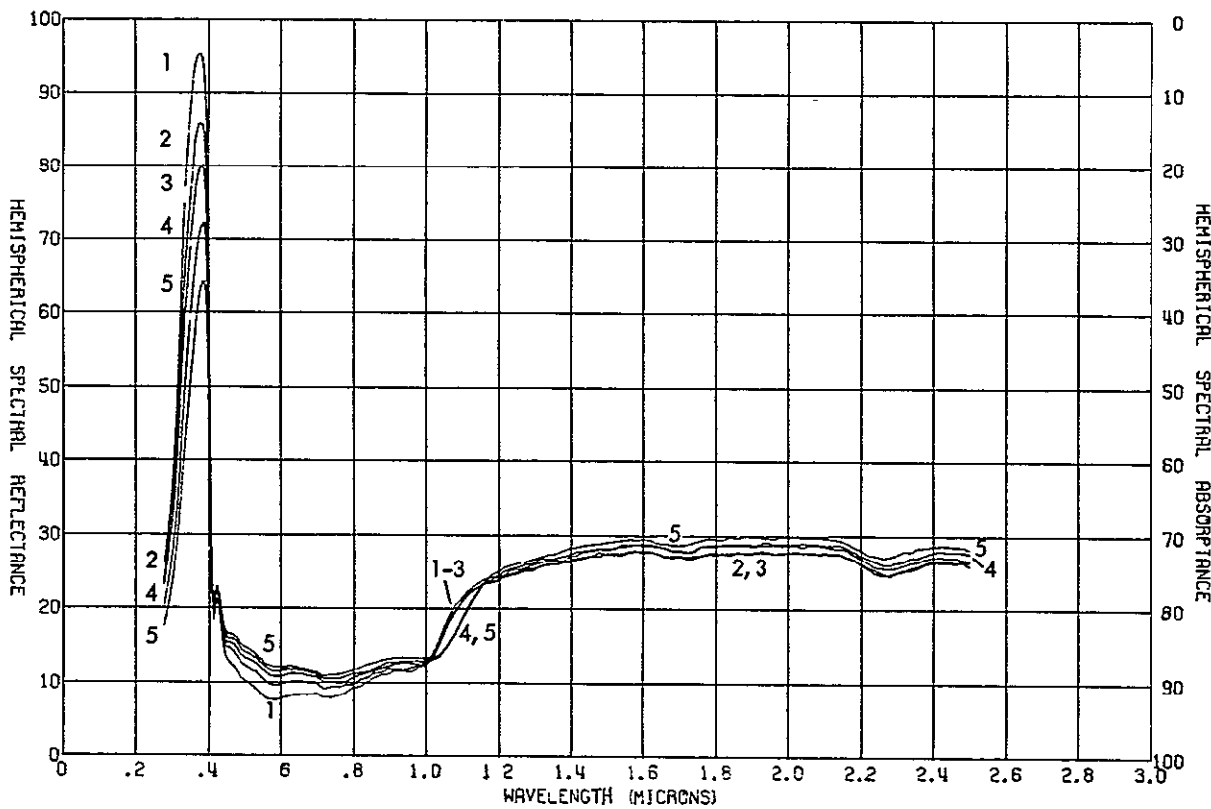


Fig 157 Ultraviolet effects on reflectance of sample 2074, blue filter on
2 ohm-cm cell, 2400-h test

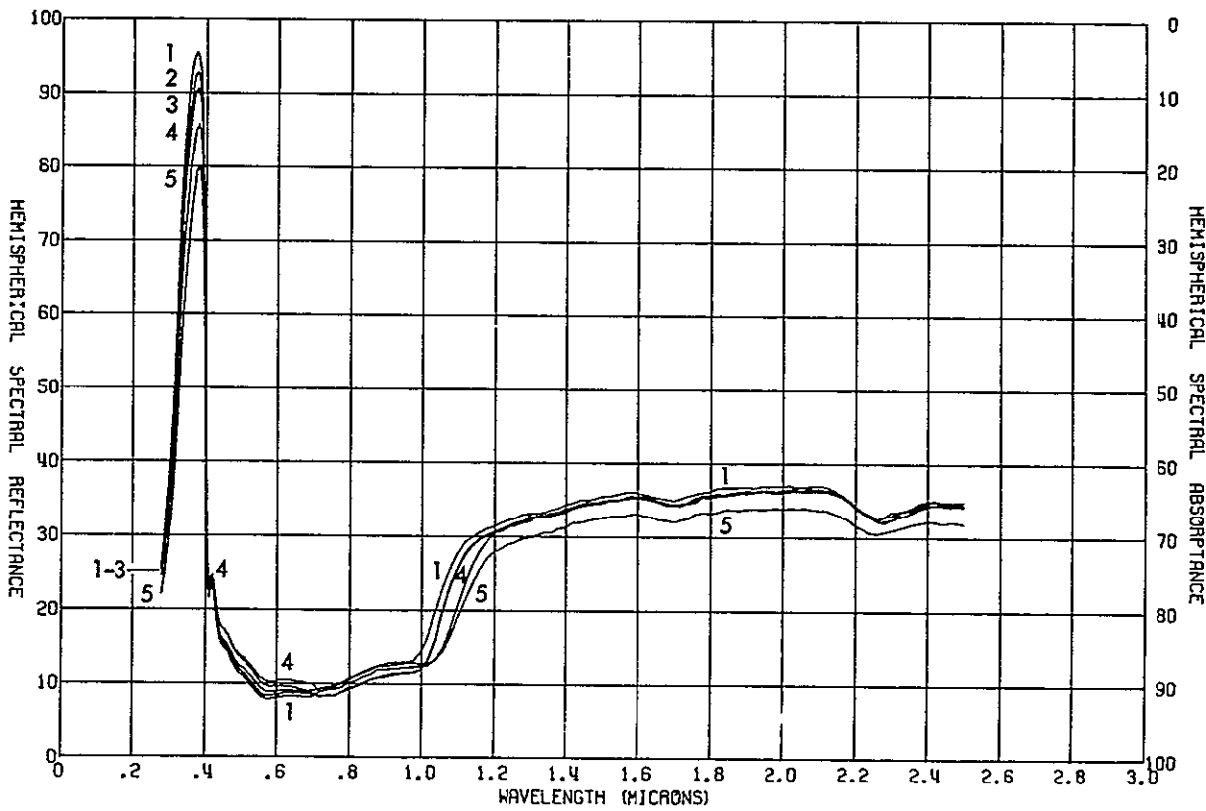


Fig 158. Proton effects on reflectance of sample 2092, blue filter on
2 ohm-cm cell, 2400-h test

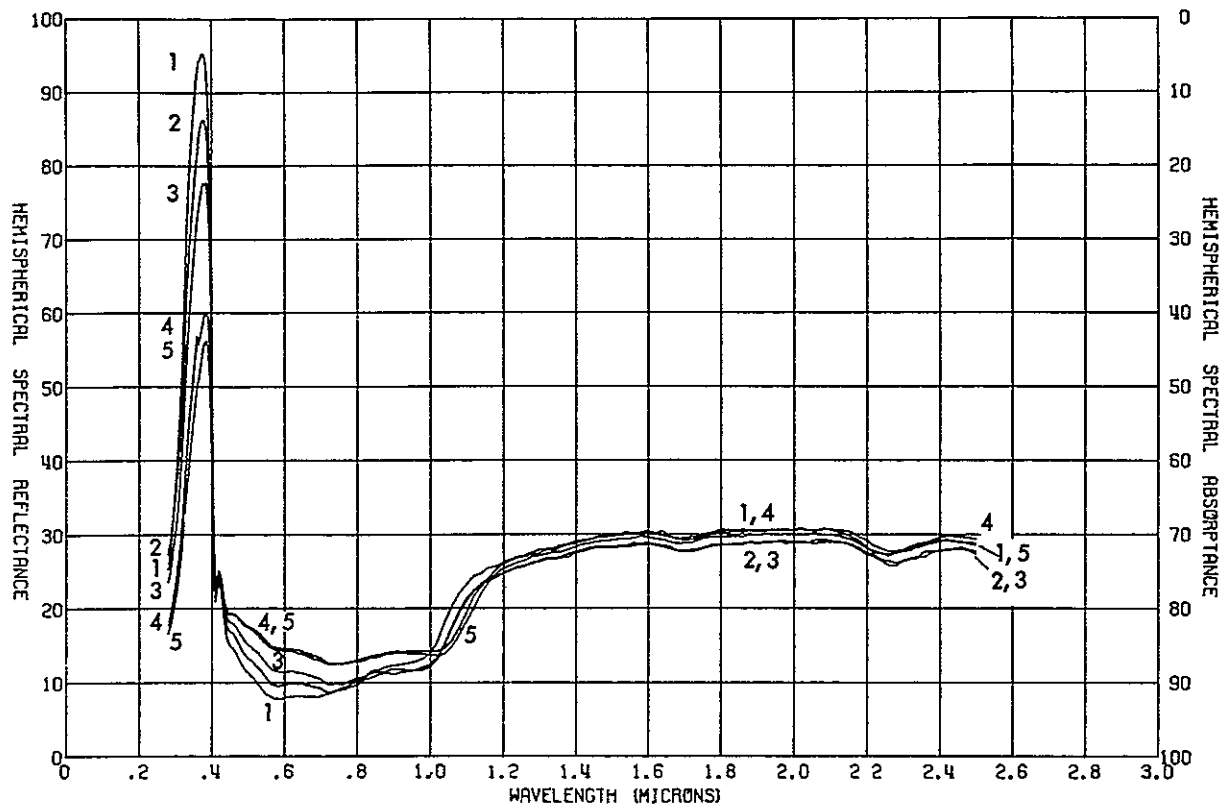


Fig. 159. Proton-ultraviolet effects on reflectance of sample 2083, blue filter on 2 ohm-cm cell, 2400-h test

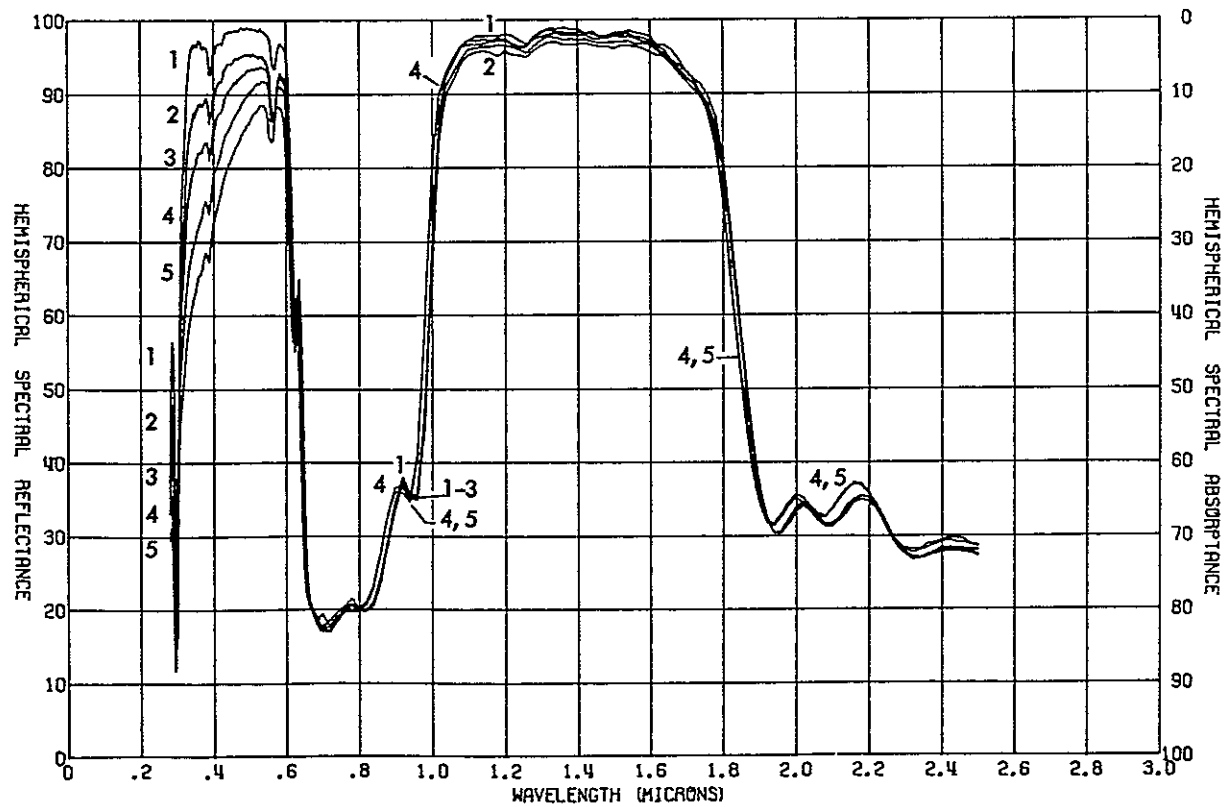


Fig. 160. Ultraviolet effects on reflectance of sample 2075, modified 4026 filter on 2 ohm-cm cell, 2400-h test

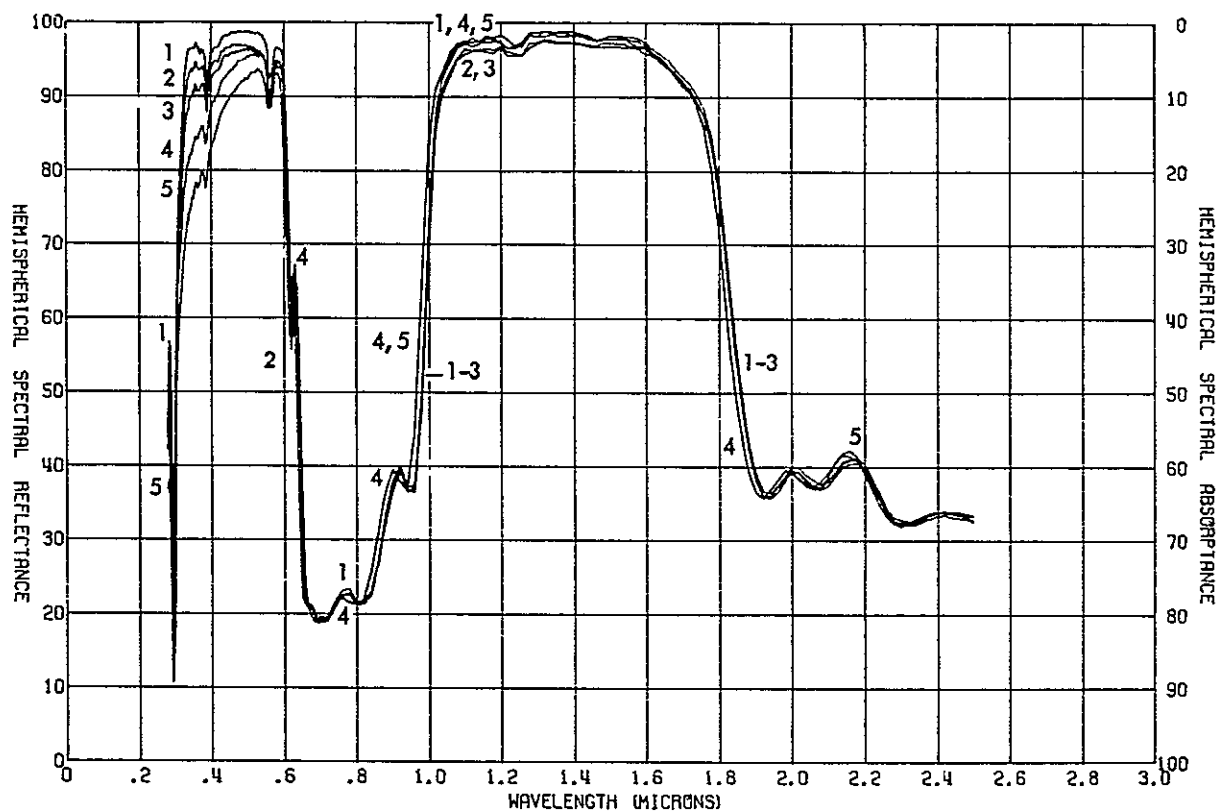


Fig. 161 Proton effects on reflectance of sample 2093, modified 4026 filter on 2 ohm-cm cell, 2400-h test

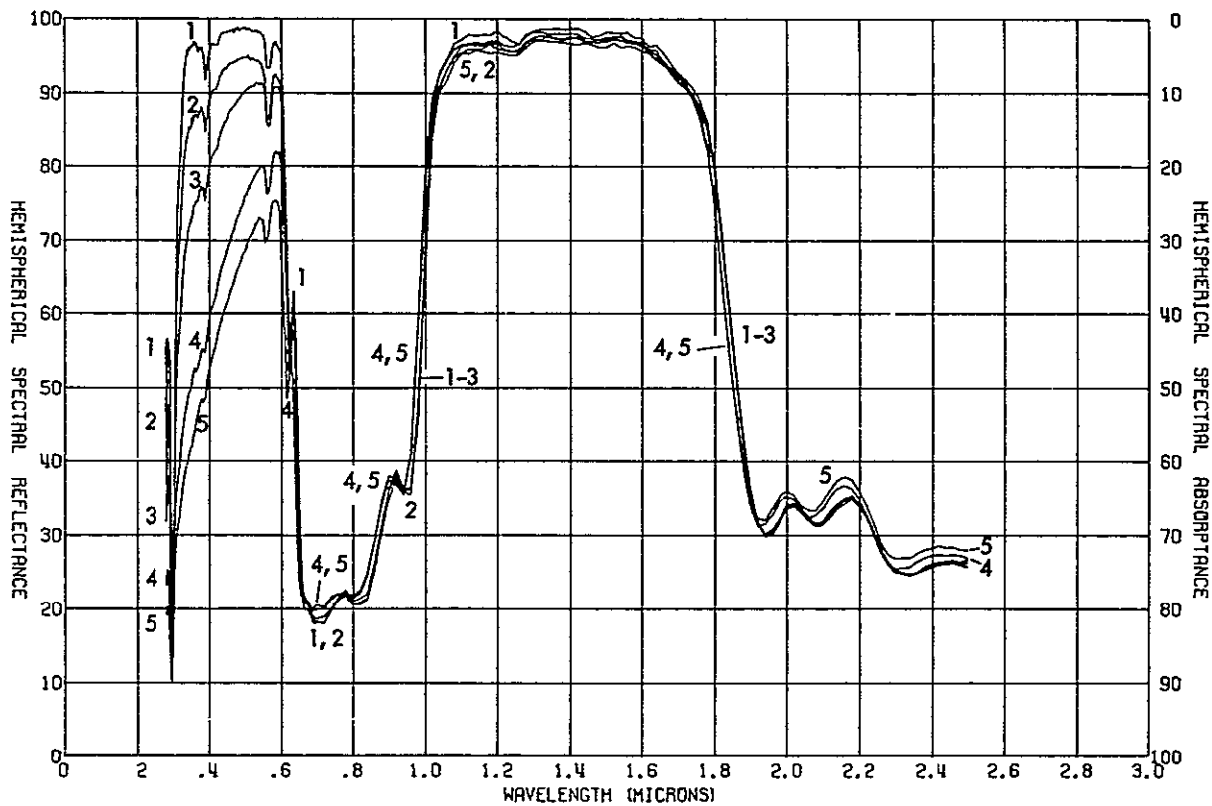


Fig. 162. Proton-ultraviolet effects on the reflectance of sample 2084, modified 4026 filter on 2 ohm-cm cell, 2400-h test

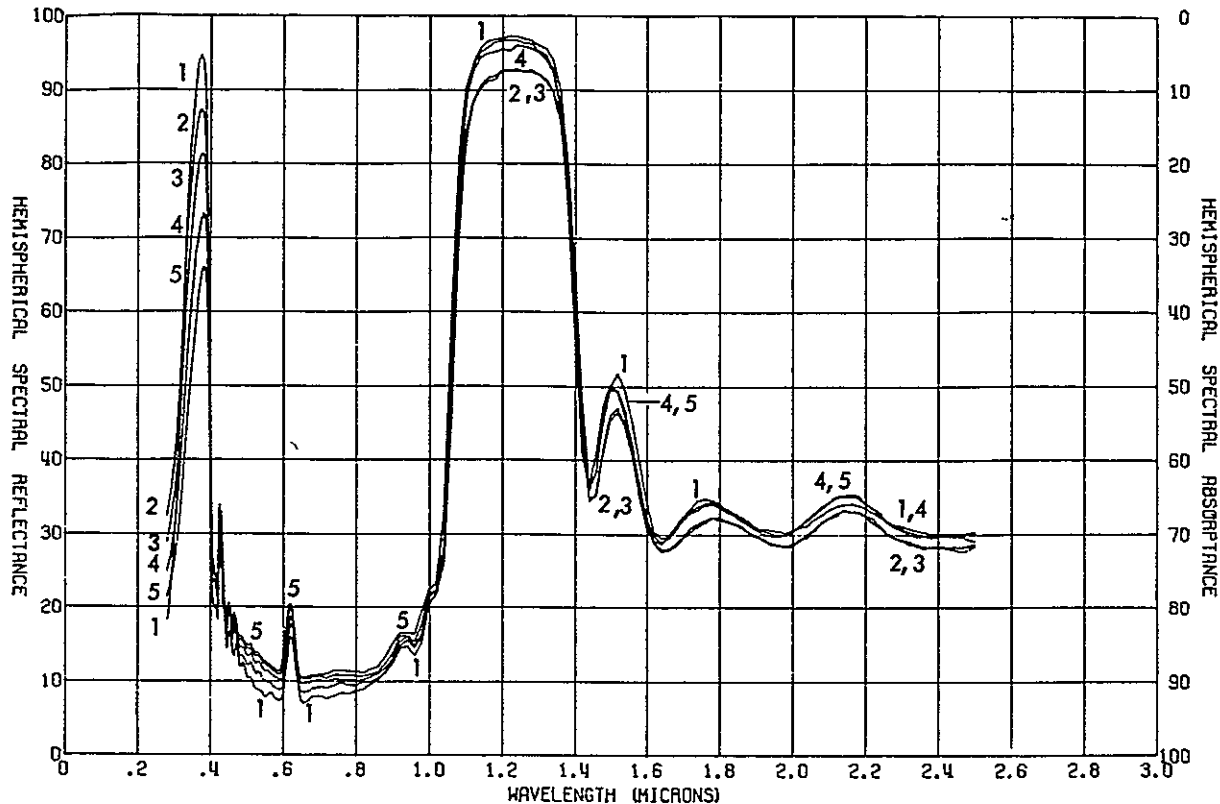


Fig. 163 Ultraviolet effects on reflectance of sample 2076, blue-red filter on 2 ohm-cm cell, 2400-h test

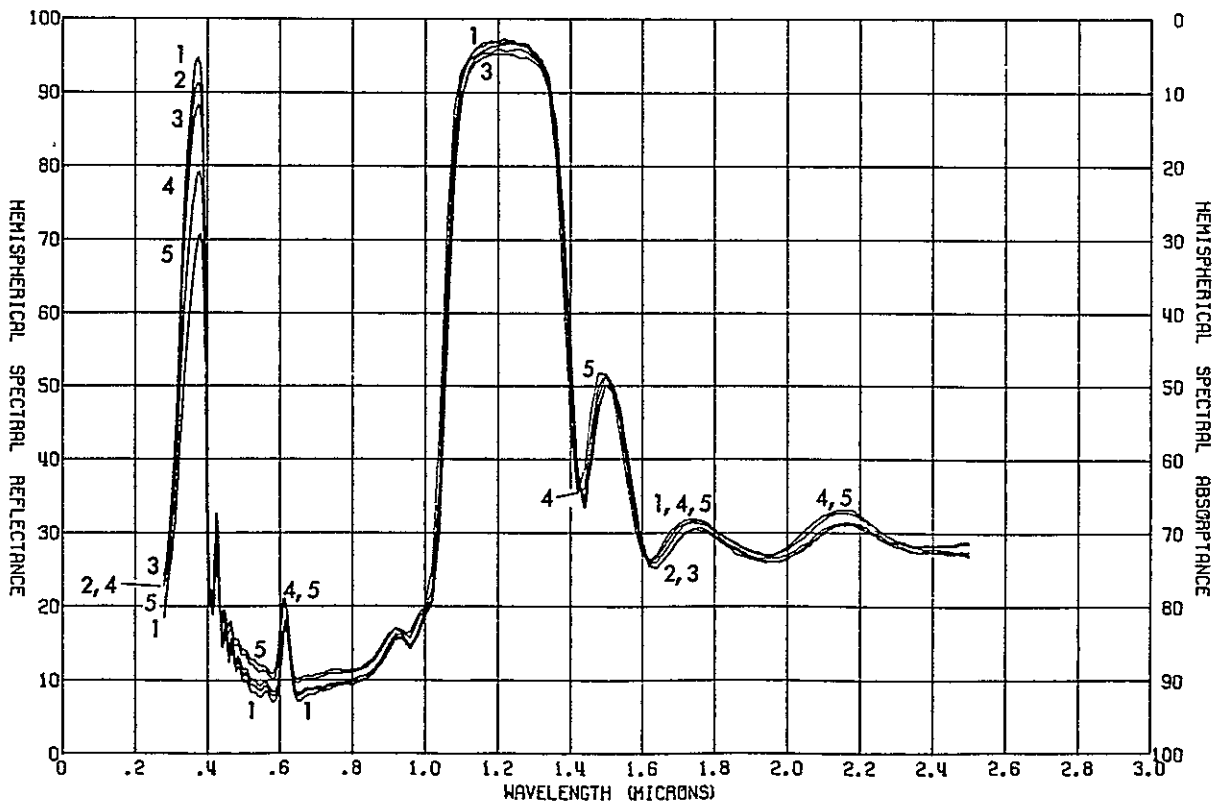


Fig. 164. Proton effects on reflectance of sample 2094, blue-red filter on 2 ohm-cm cell, 2400-h test

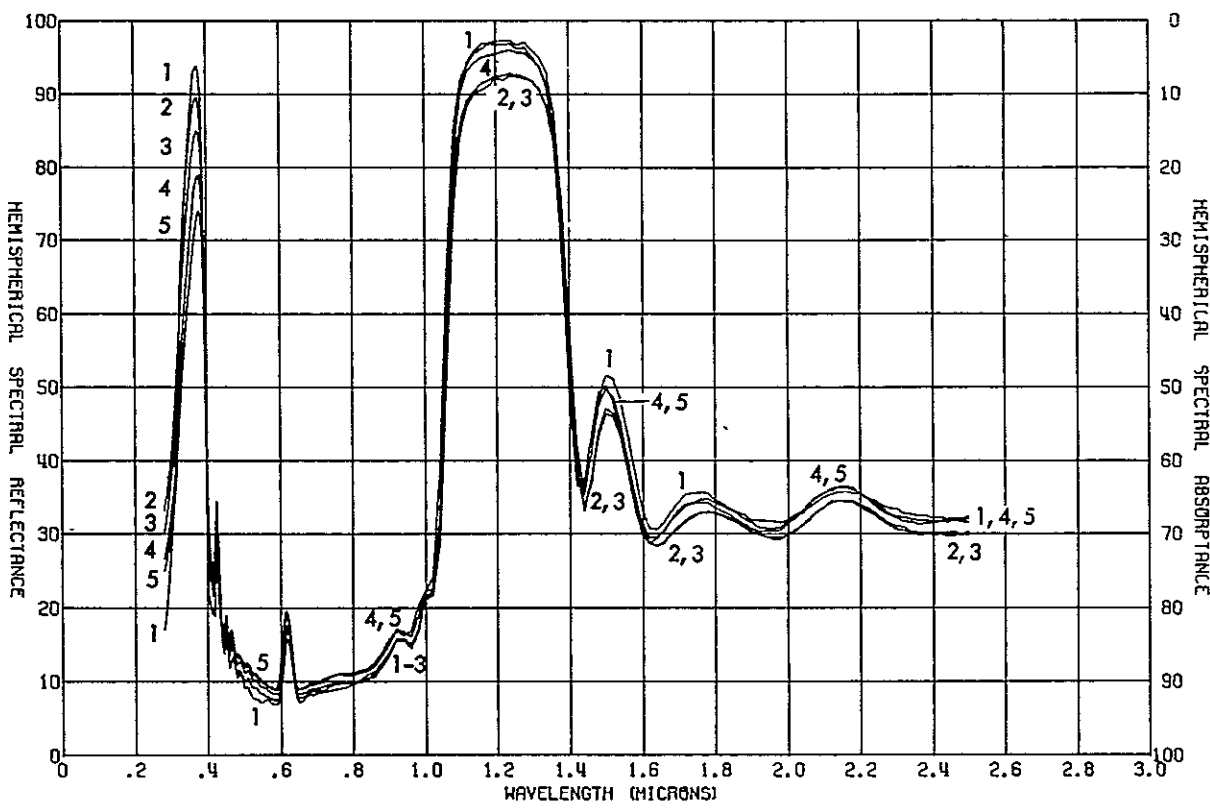


Fig 165 Proton-ultraviolet effects on reflectance of sample 2085, blue-red filter on 2 ohm-cm cell, 2400-h test

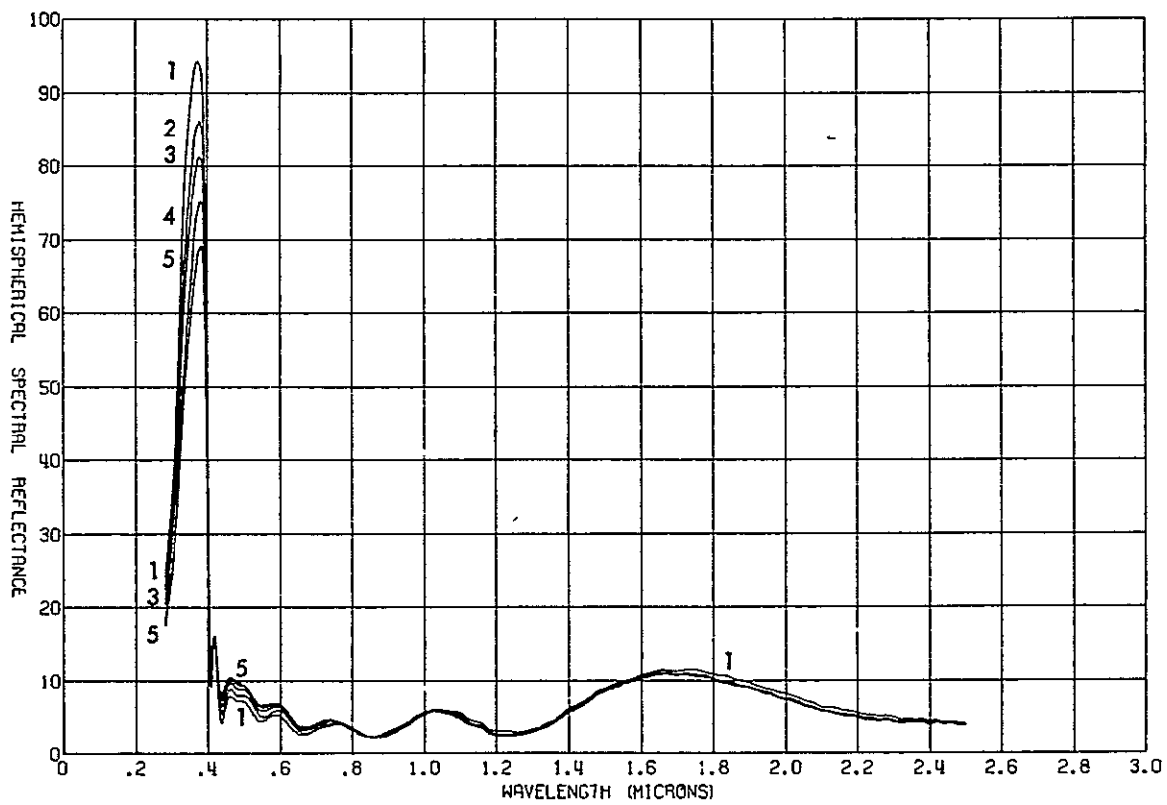


Fig 166. Ultraviolet effects on reflectance of sample 2077, blue filter, 2400-h test

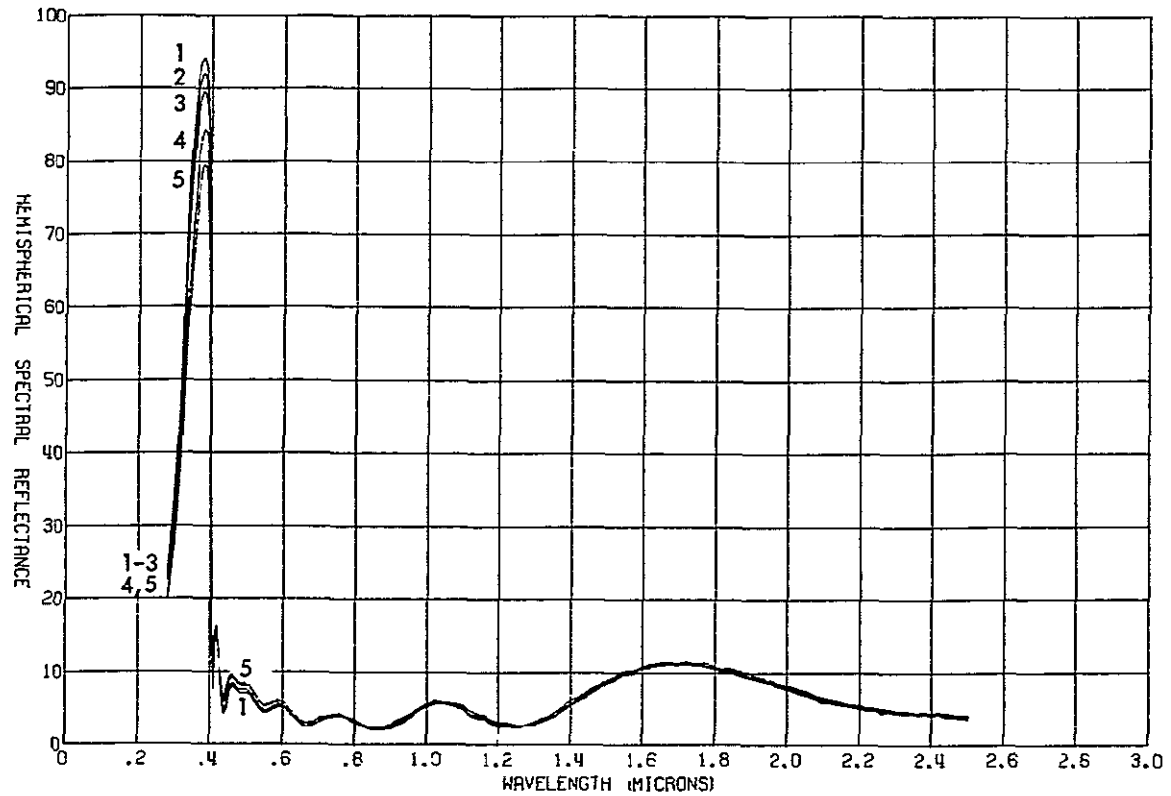


Fig. 167. Proton effects on reflectance of sample 2095, blue filter, 2400-h test

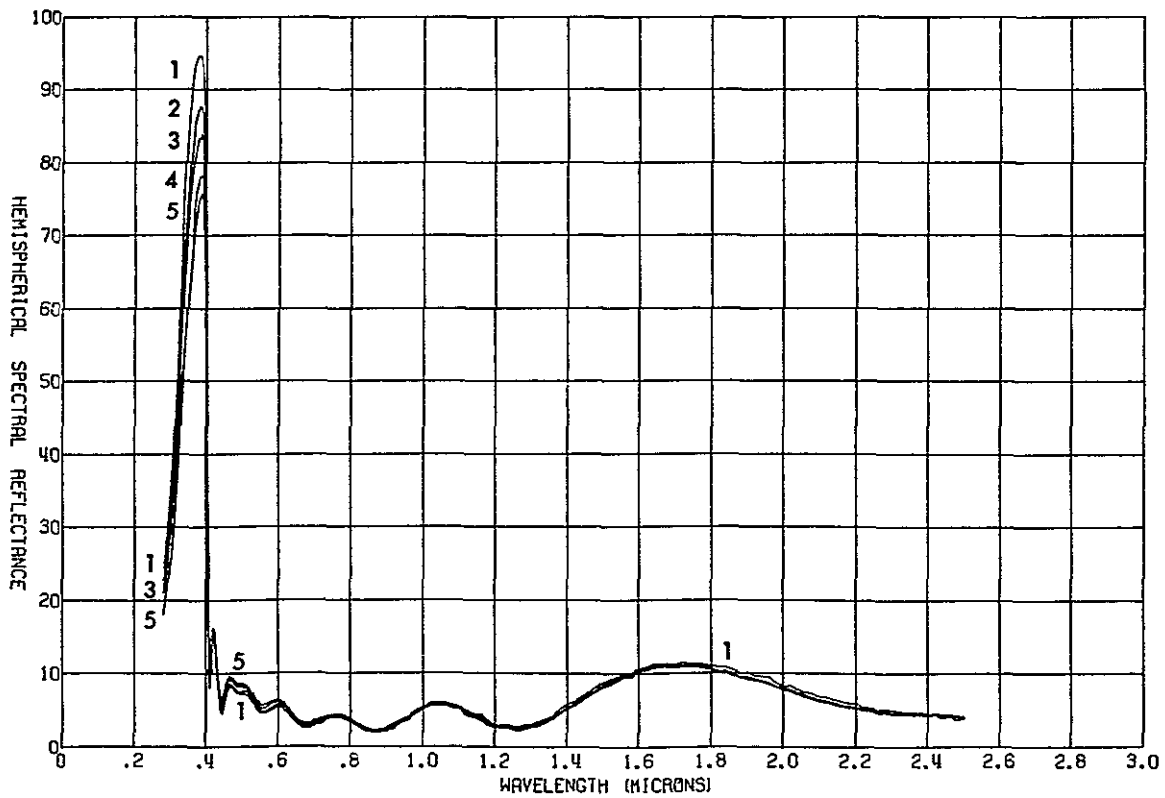


Fig. 168. Proton-ultraviolet effects on reflectance of sample 2086, blue filter, 2400-h test

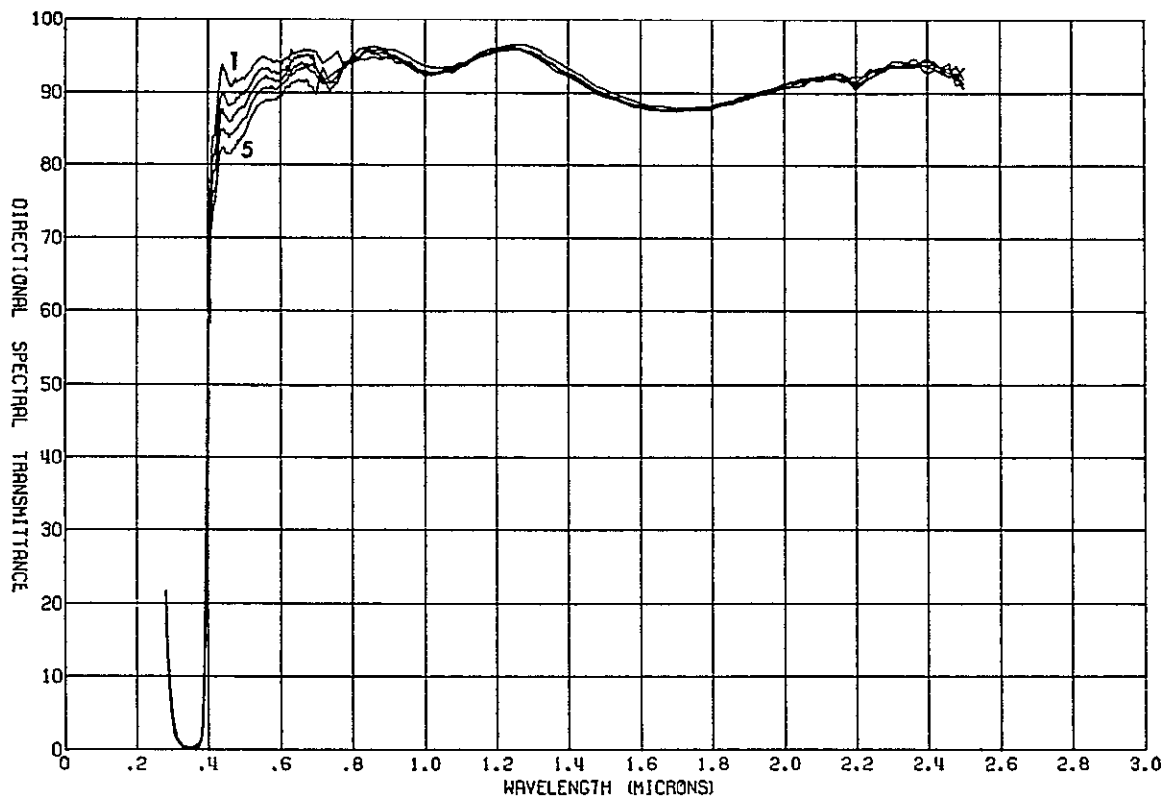


Fig. 169 Ultraviolet effects on transmittance of sample 2077, blue filter, 2400-h test

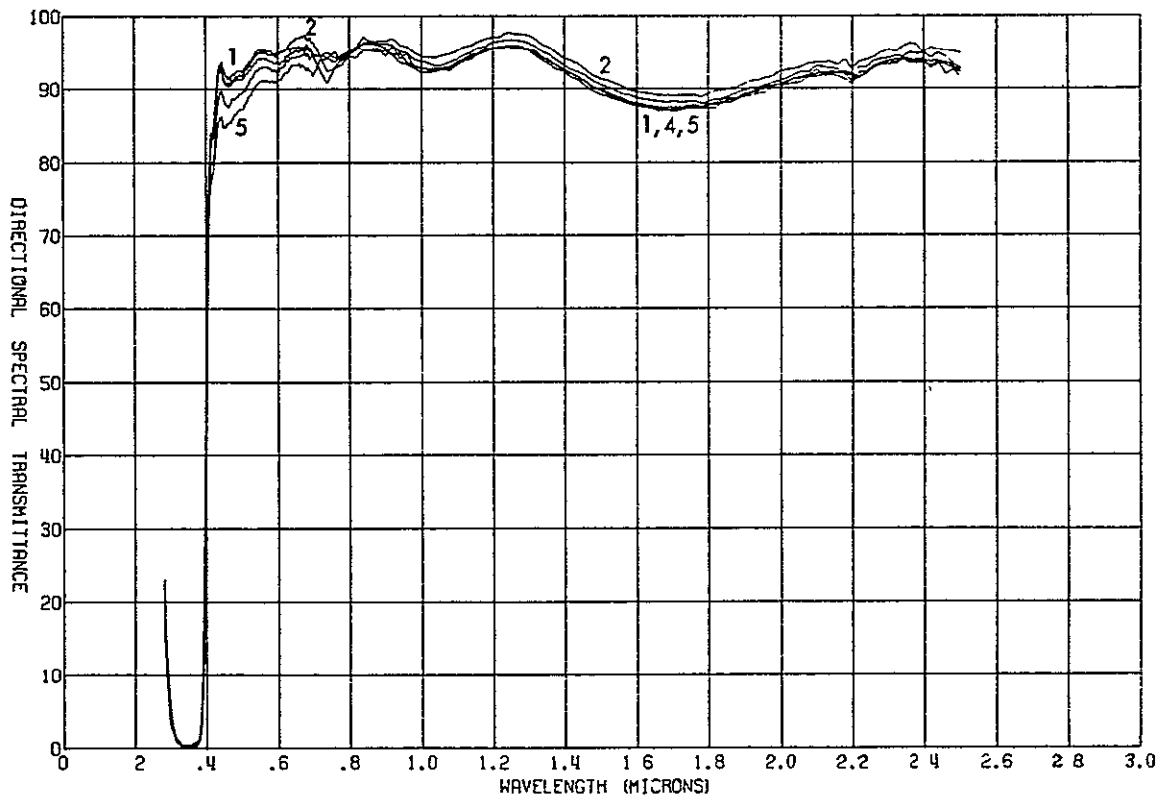


Fig. 170. Proton effects on transmittance of sample 2095, blue filter, 2400-h test

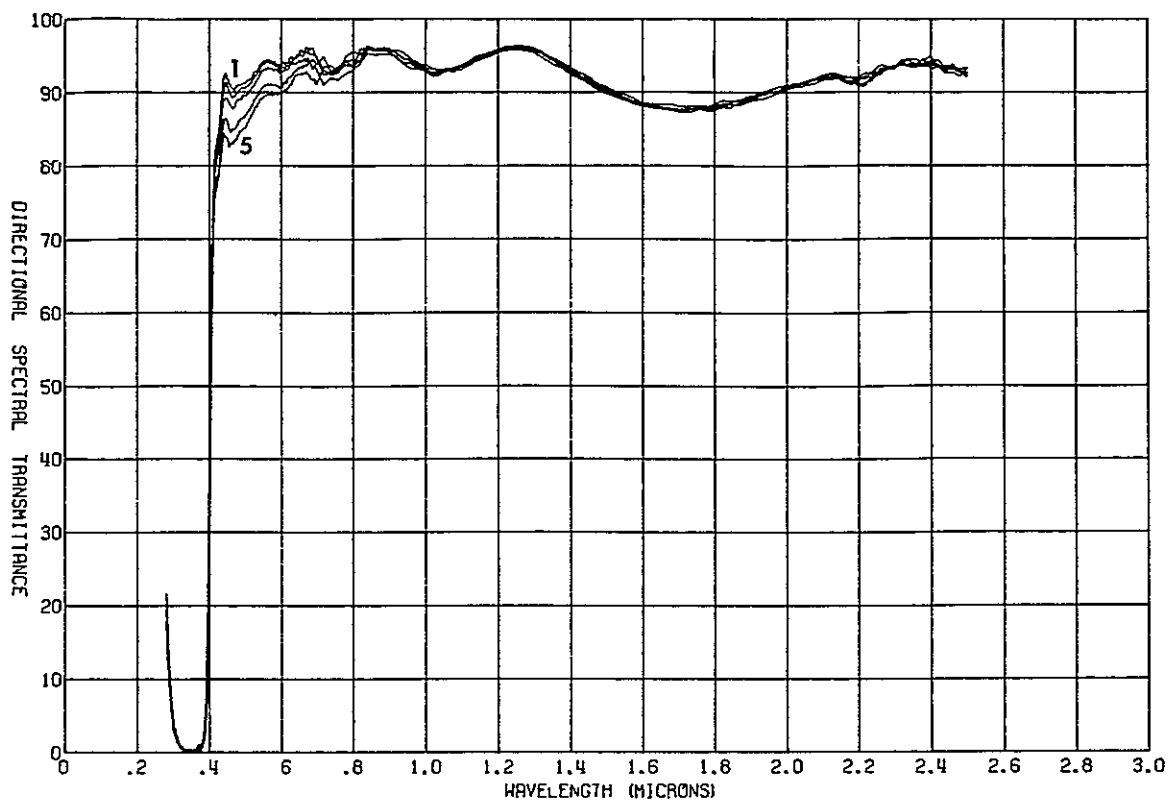


Fig. 171 Proton-ultraviolet effects on transmittance of sample 2086, blue filter, 2400-h test

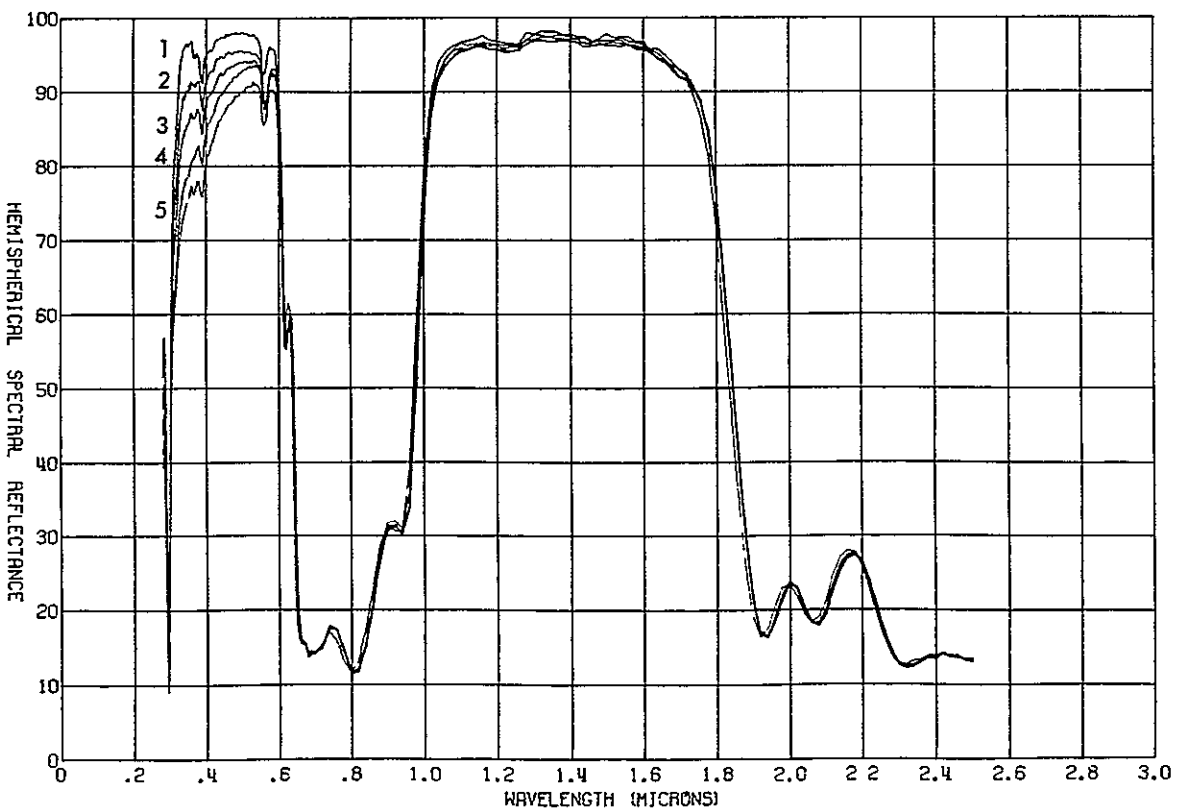


Fig. 172. Ultraviolet effects on reflectance of sample 2078, modified 4026 filter, 2400-h test

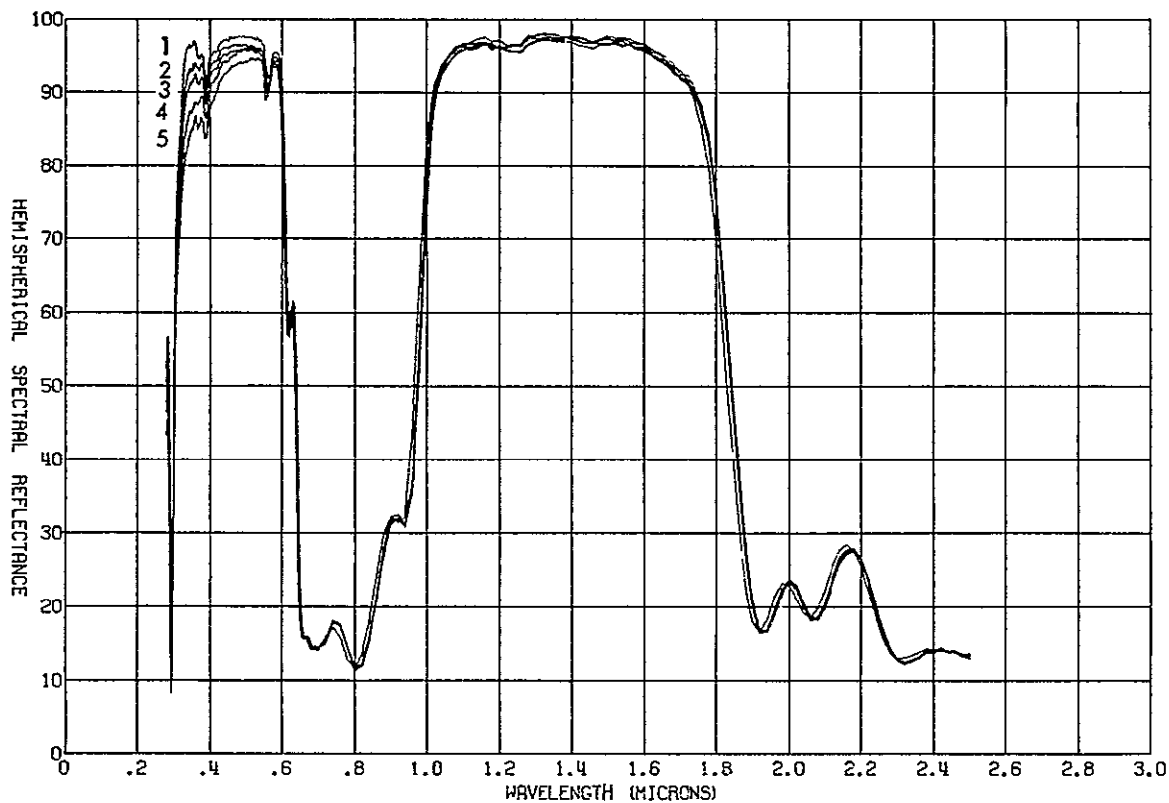


Fig. 173 Proton effects on reflectance of sample 2096, modified 4026 filter, 2400-h test

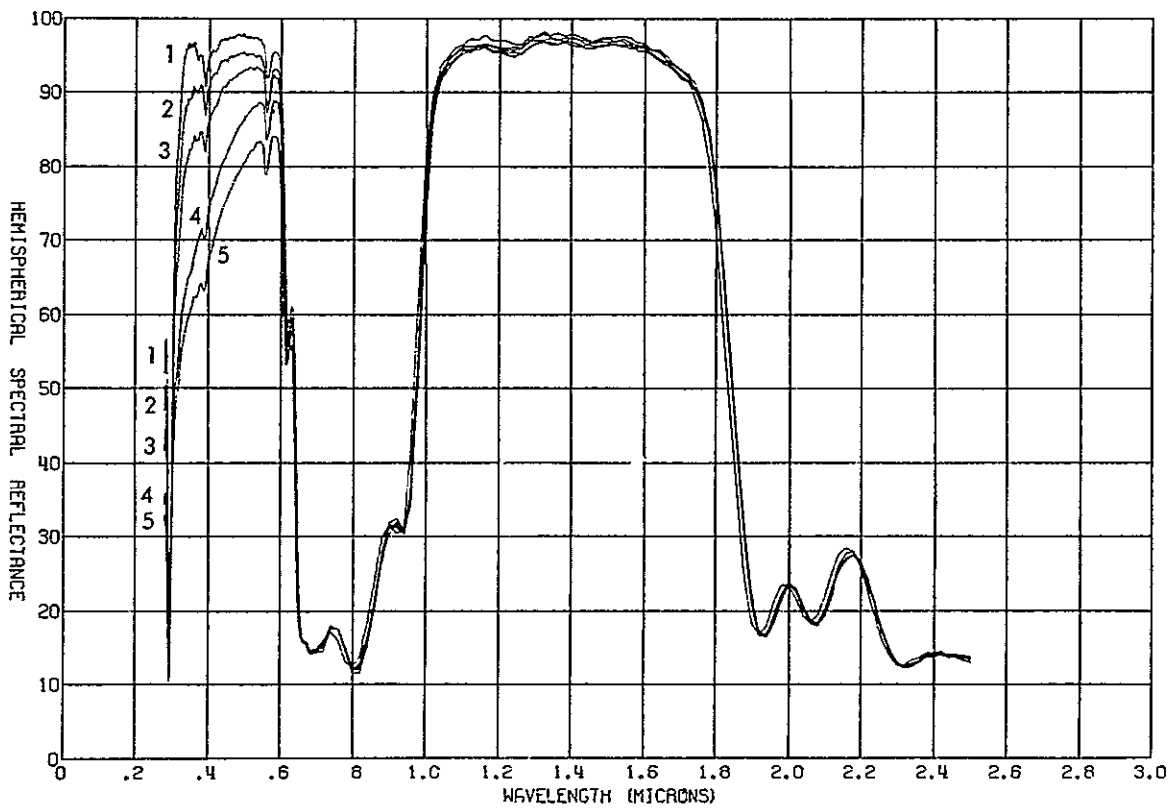


Fig. 174. Proton-ultraviolet effects on reflectance of sample 2087, modified 4026 filter, 2400-h test

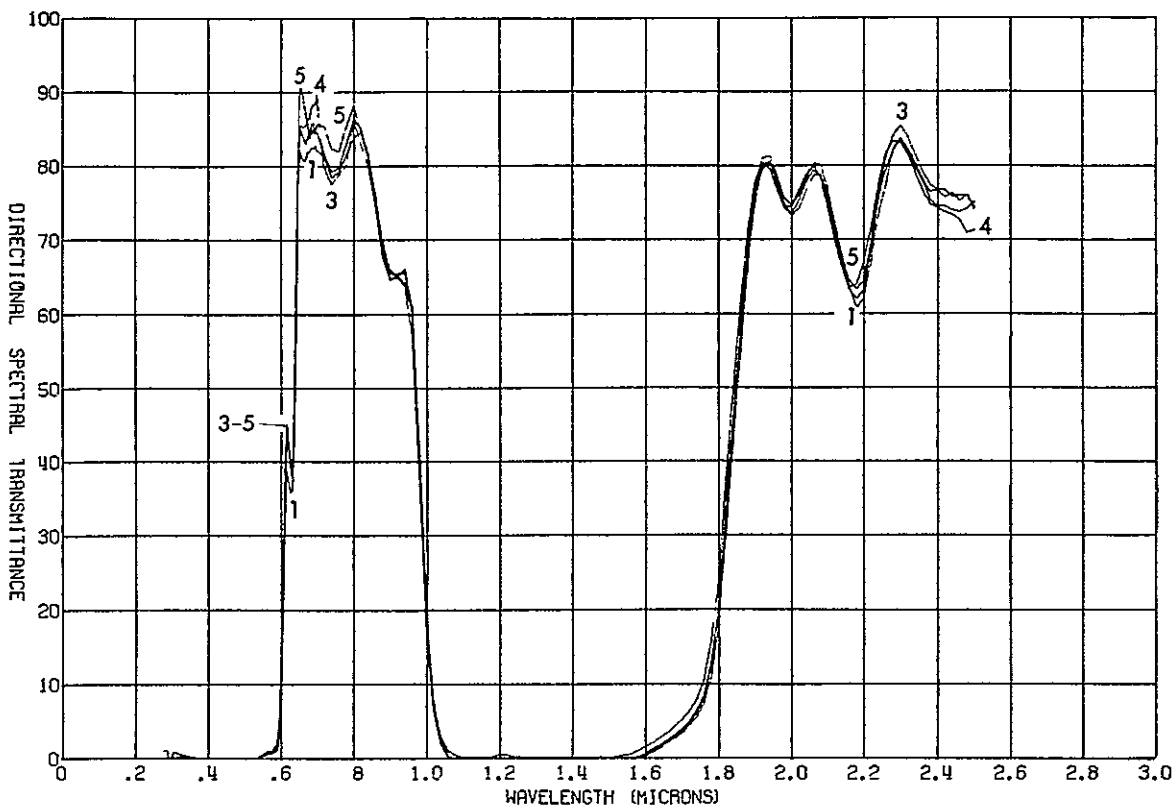


Fig. 175. Ultraviolet effects on transmittance of sample 2078, modified 4026 filter, 2400-h test

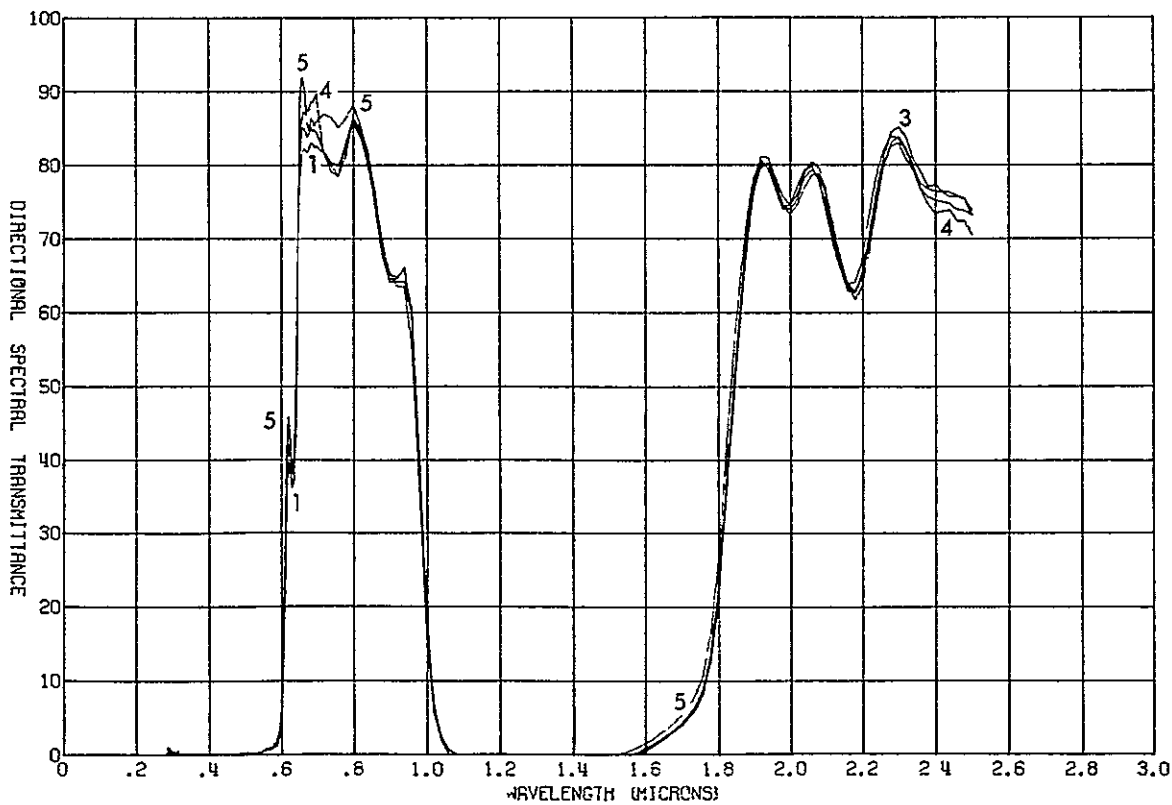


Fig. 176. Proton effects on transmittance of sample 2096, modified 4026 filter, 2400-h test

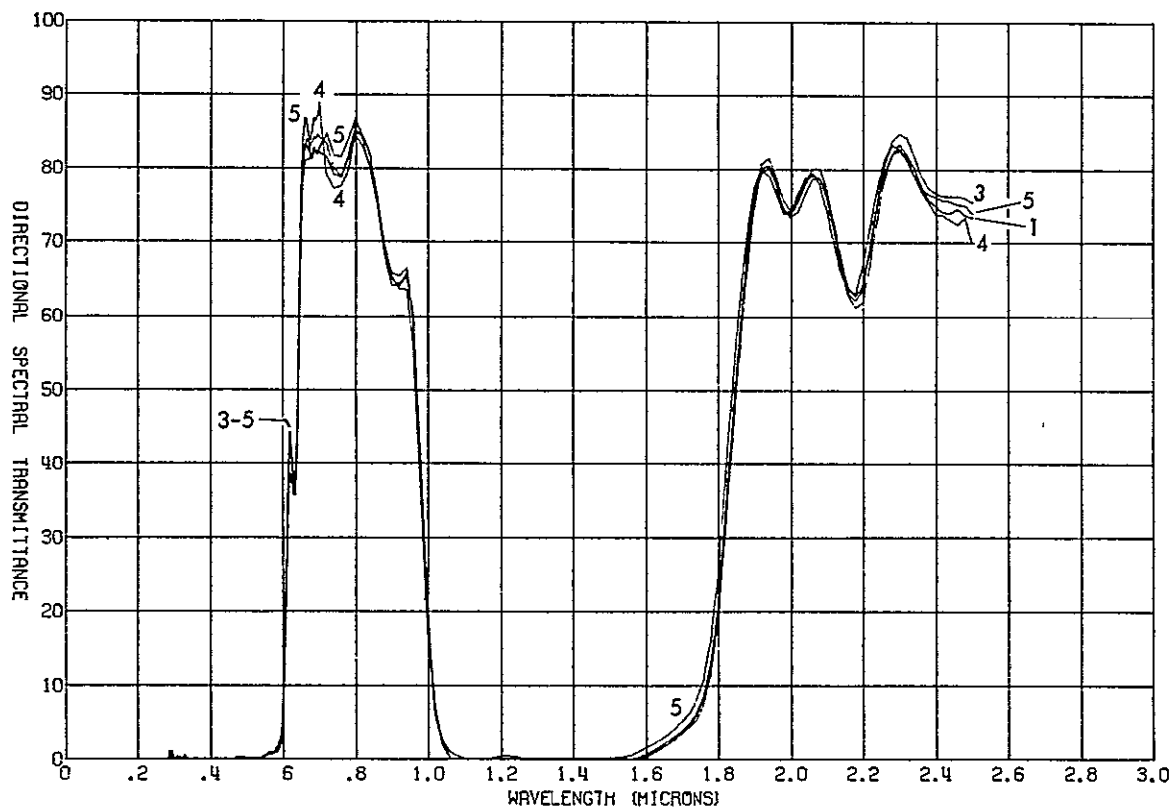


Fig. 177 Proton-ultraviolet effects on transmittance of sample 2087,
modified 4026 filter, 2400-h test

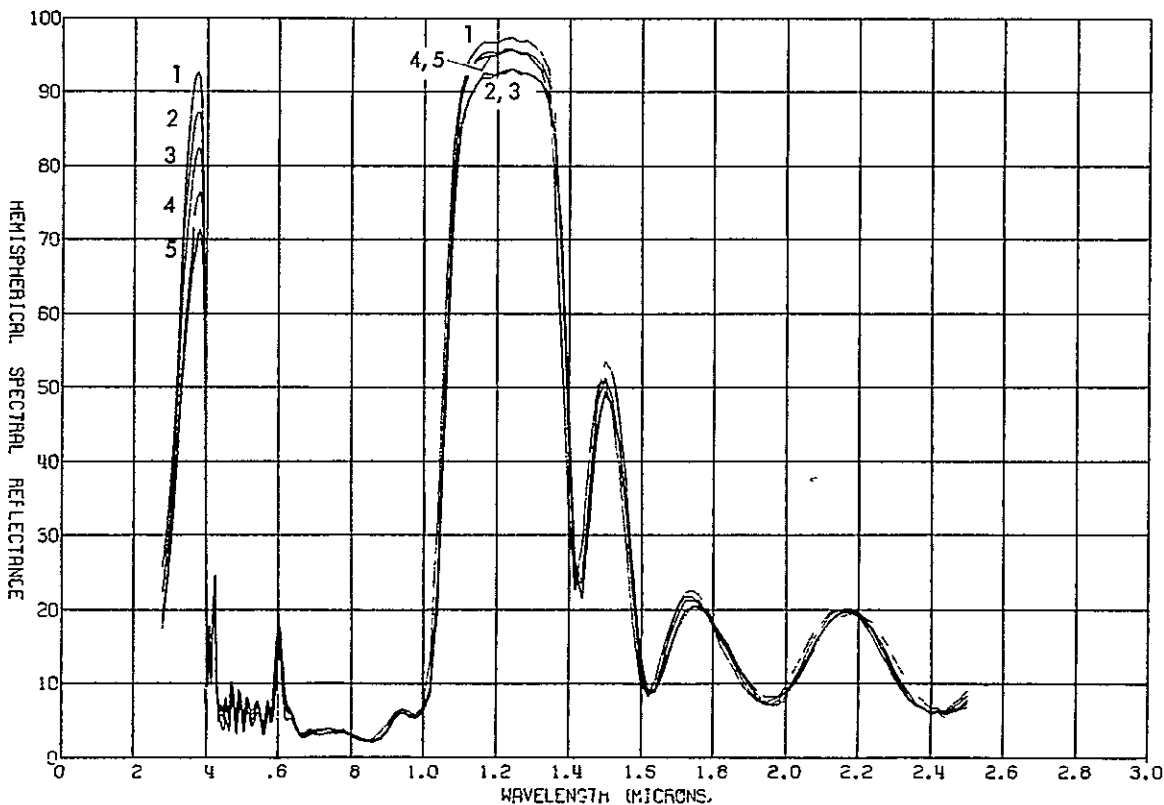


Fig. 178. Ultraviolet effects on reflectance of sample 2079, blue-red filter,
2400-h test

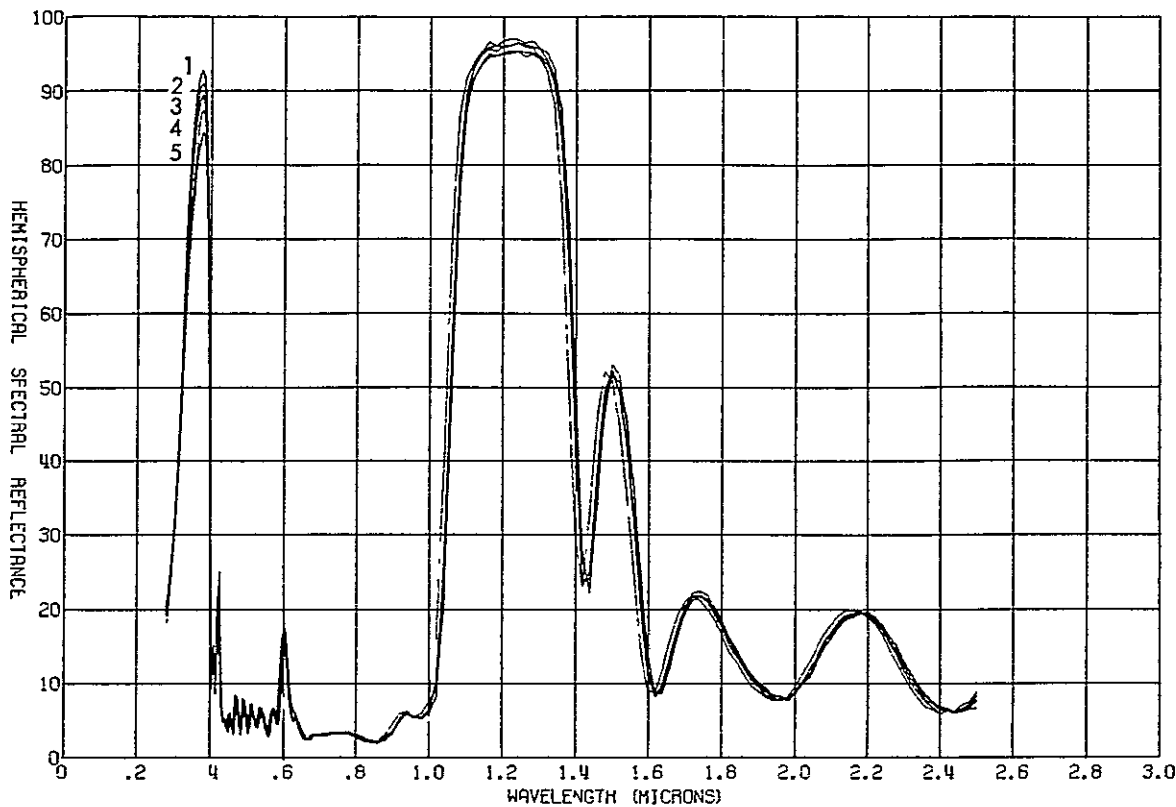


Fig. 179. Proton effects on reflectance of sample 2097, blue-red filter, 2400-h test

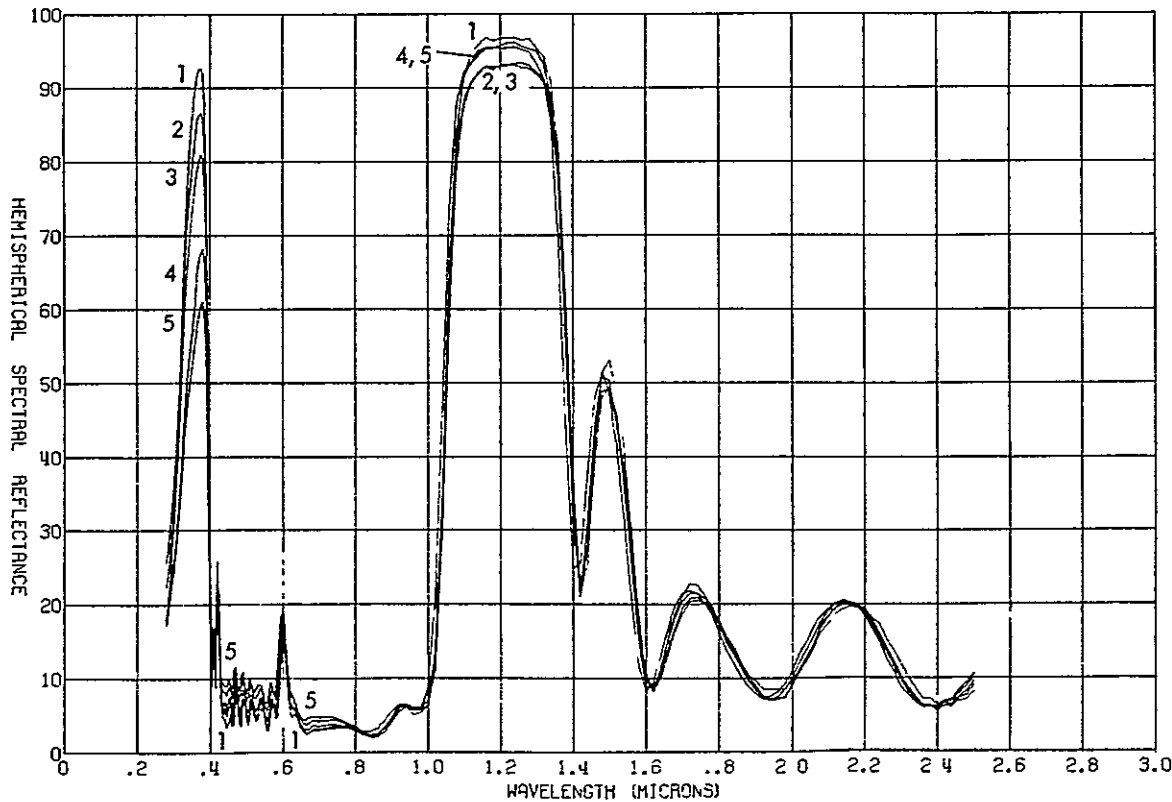


Fig. 180 Proton-ultraviolet effects on reflectance of sample 2088, blue-red filter, 2400-h test

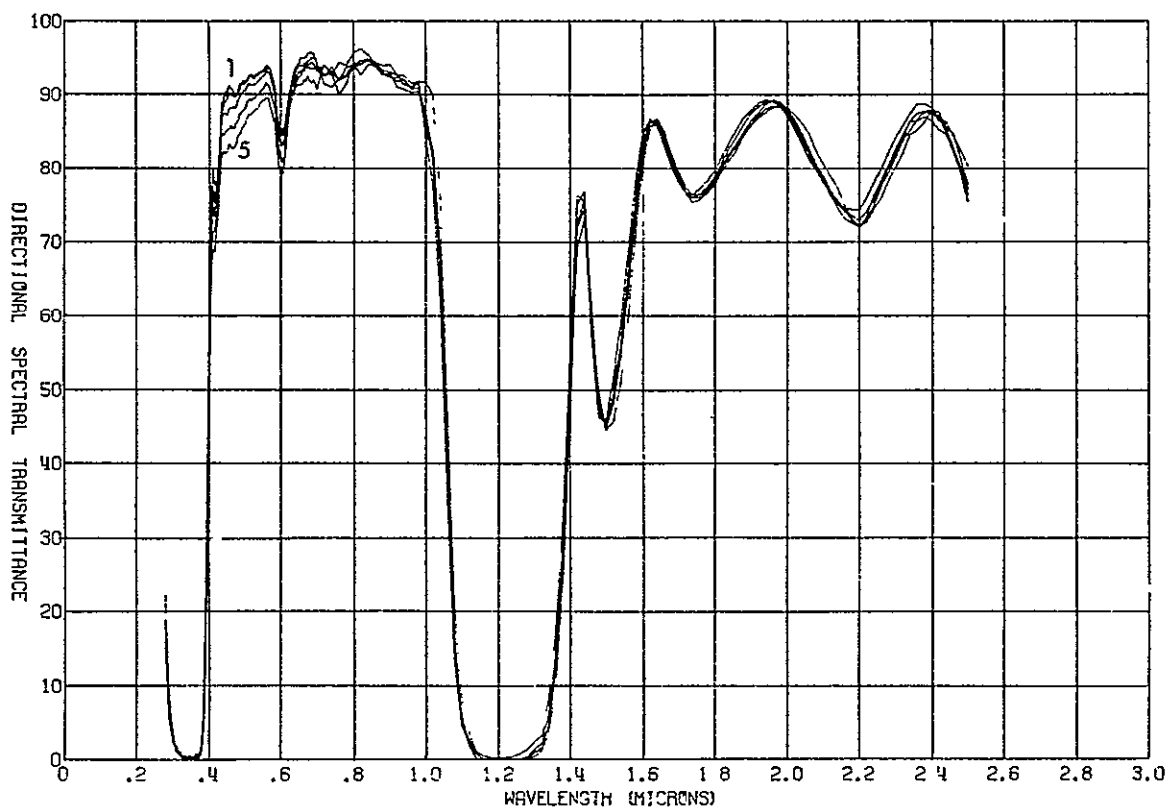


Fig. 181 Ultraviolet effects on transmittance of sample 2079, blue-red filter, 2400-h test

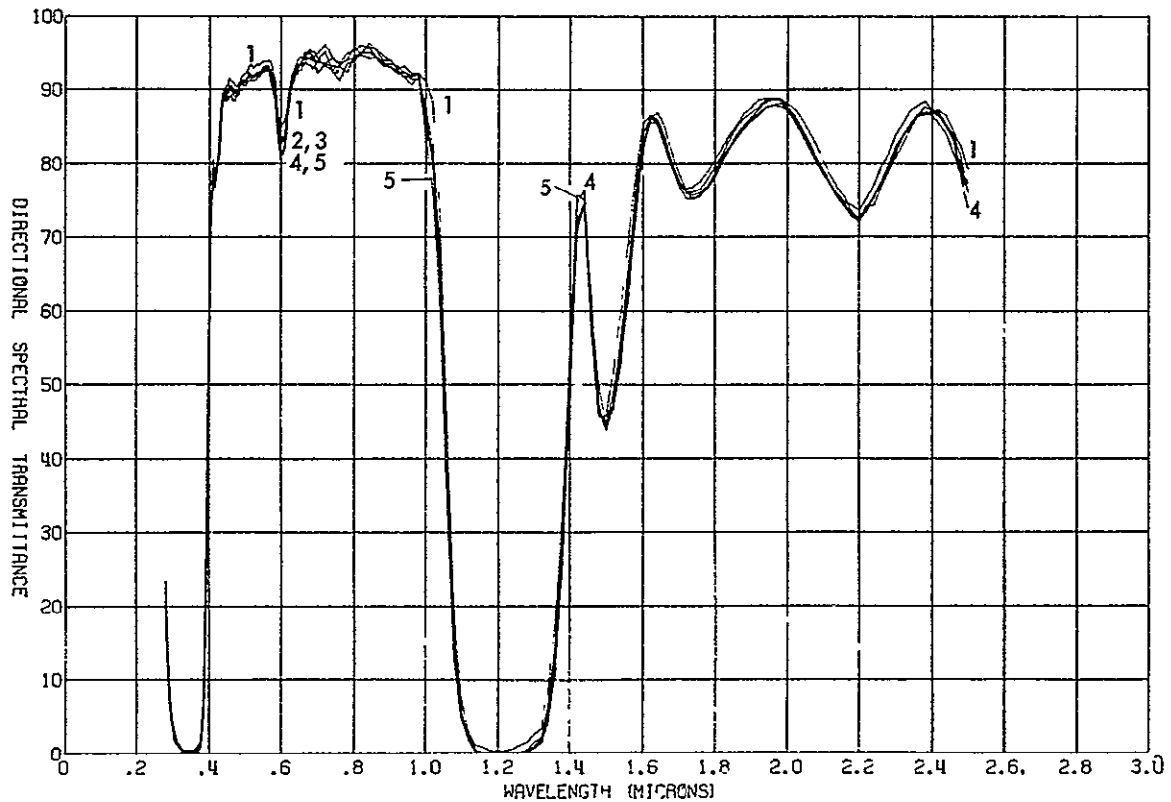


Fig. 182. Proton effects on transmittance of sample 2097, blue-red filter, 2400-h test

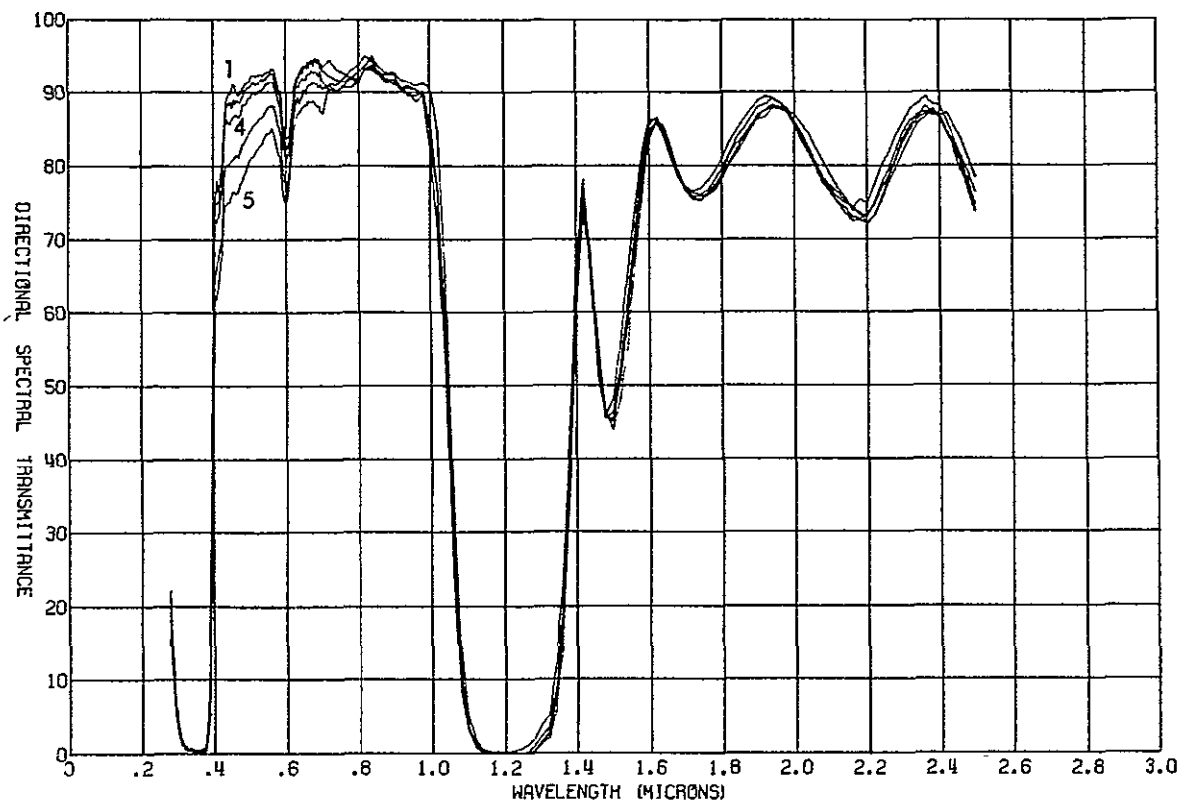


Fig 183. Proton-ultraviolet effects on transmittance of sample 2088, blue-red filter, 2400-h test

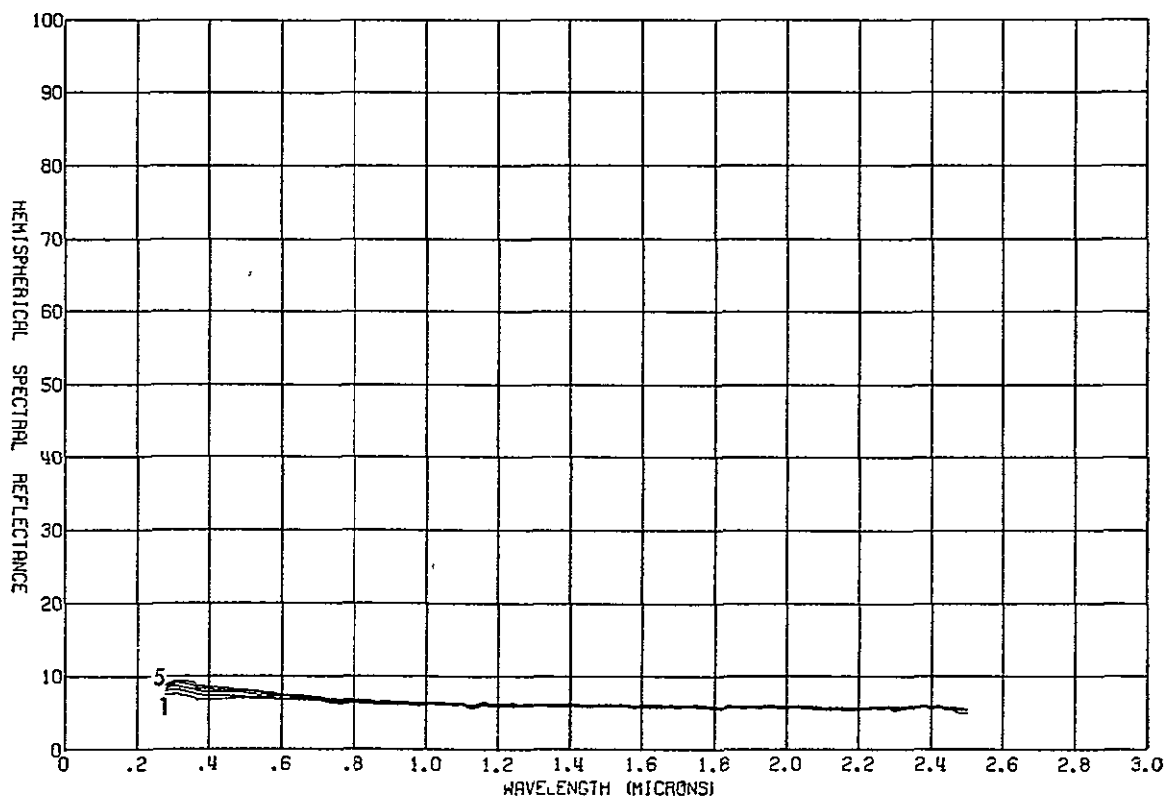


Fig 184. Ultraviolet effects on reflectance of sample 2080, clear glass (7940 fused silica), 2400-h test

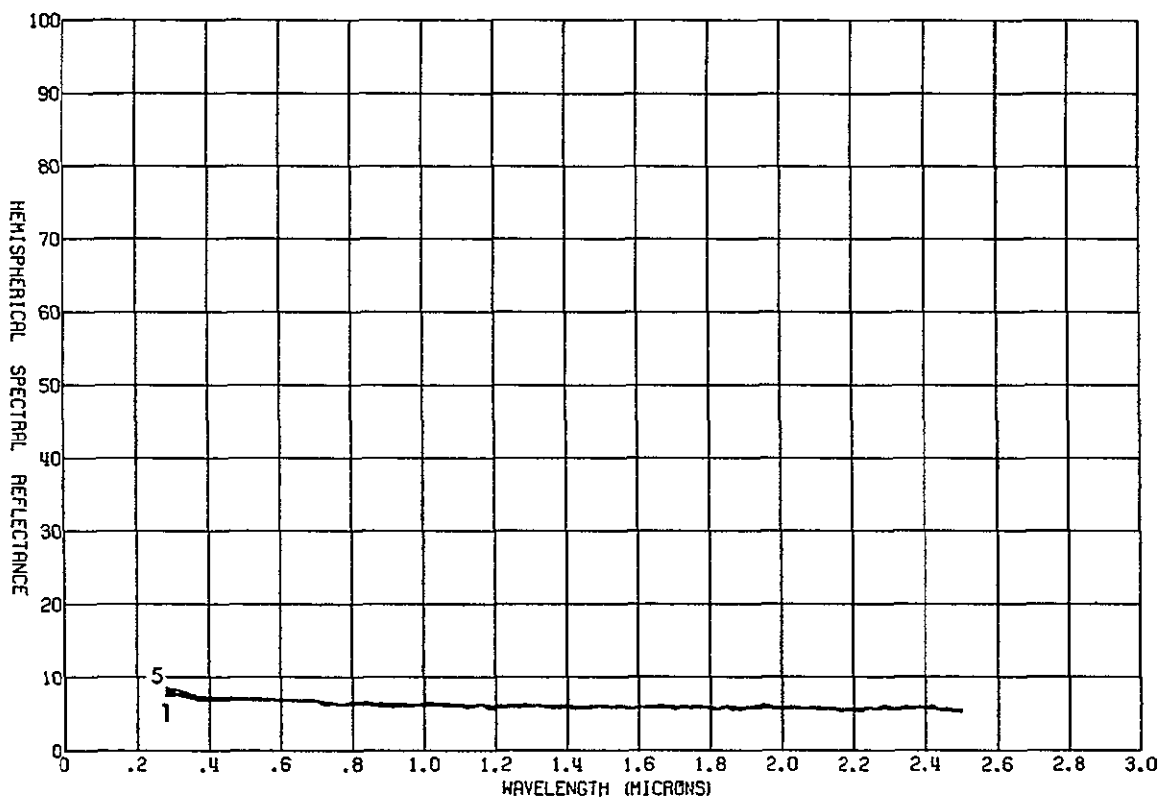


Fig. 185. Proton effects on reflectance of sample 2098, clear glass (7940 fused silica), 2400-h test

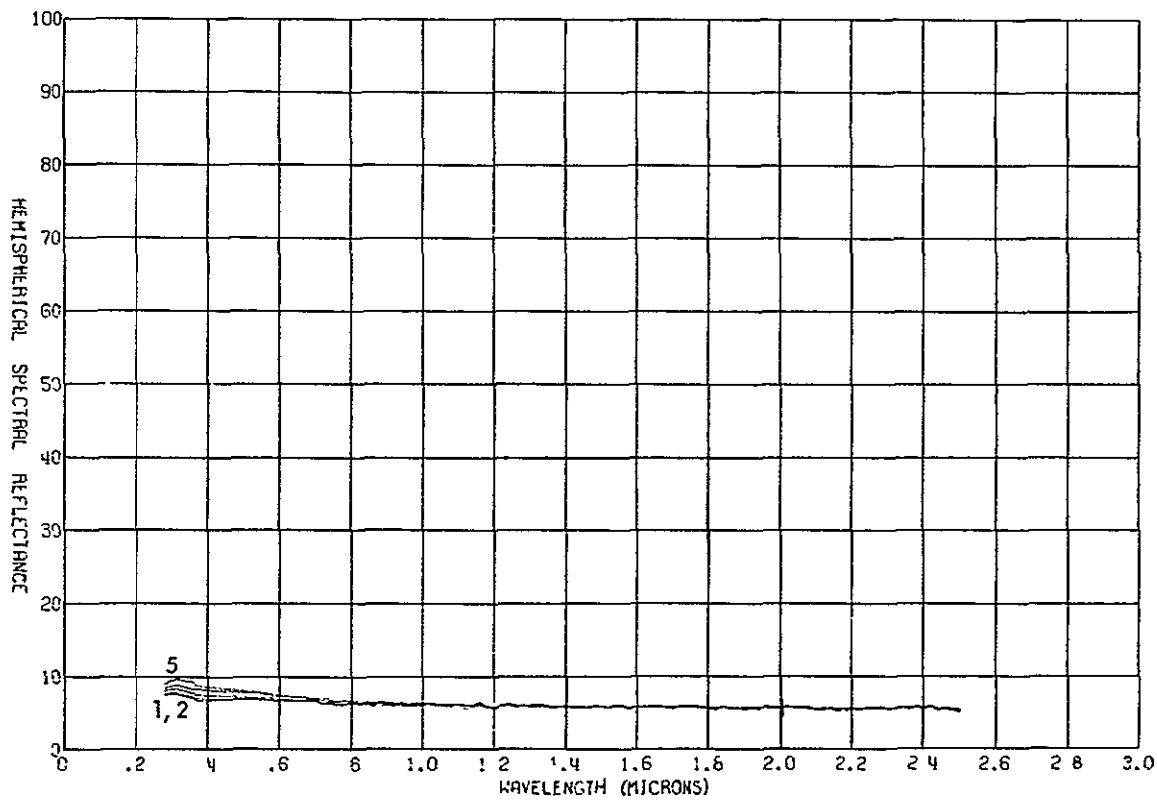


Fig. 186. Proton-ultraviolet effects on the reflectance of sample 2089, clear glass (7940 fused silica), 2400-h test

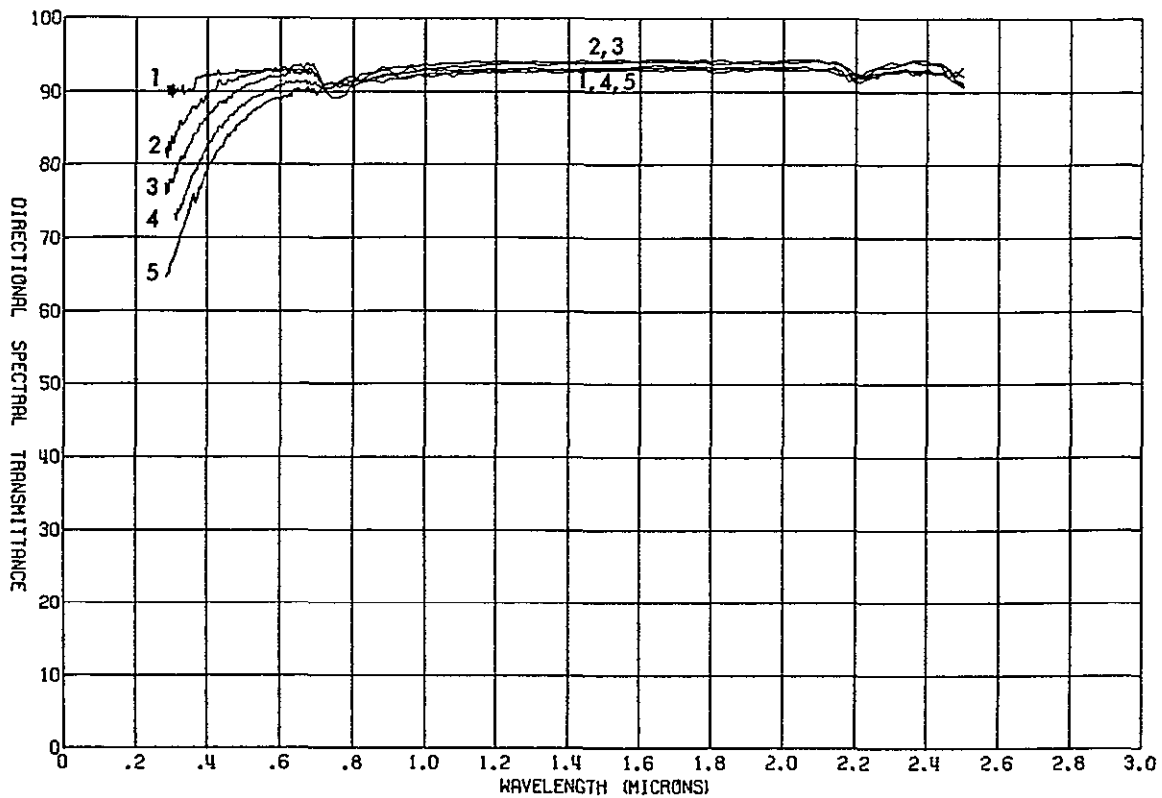


Fig. 187. Ultraviolet effects on transmittance of sample 2080, clear glass
(7940 fused silica), 2400-h test

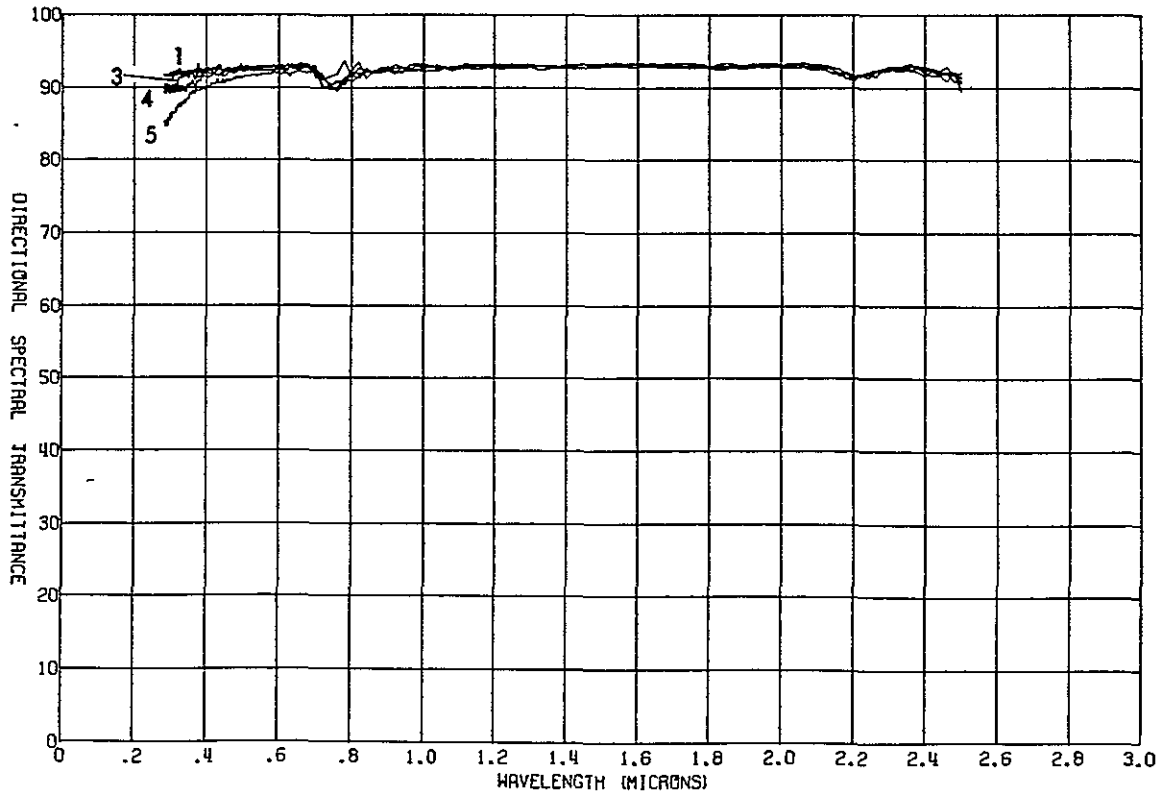


Fig. 188. Proton effects on transmittance of sample 2098, clear glass
(7940 fused silica), 2400-h test

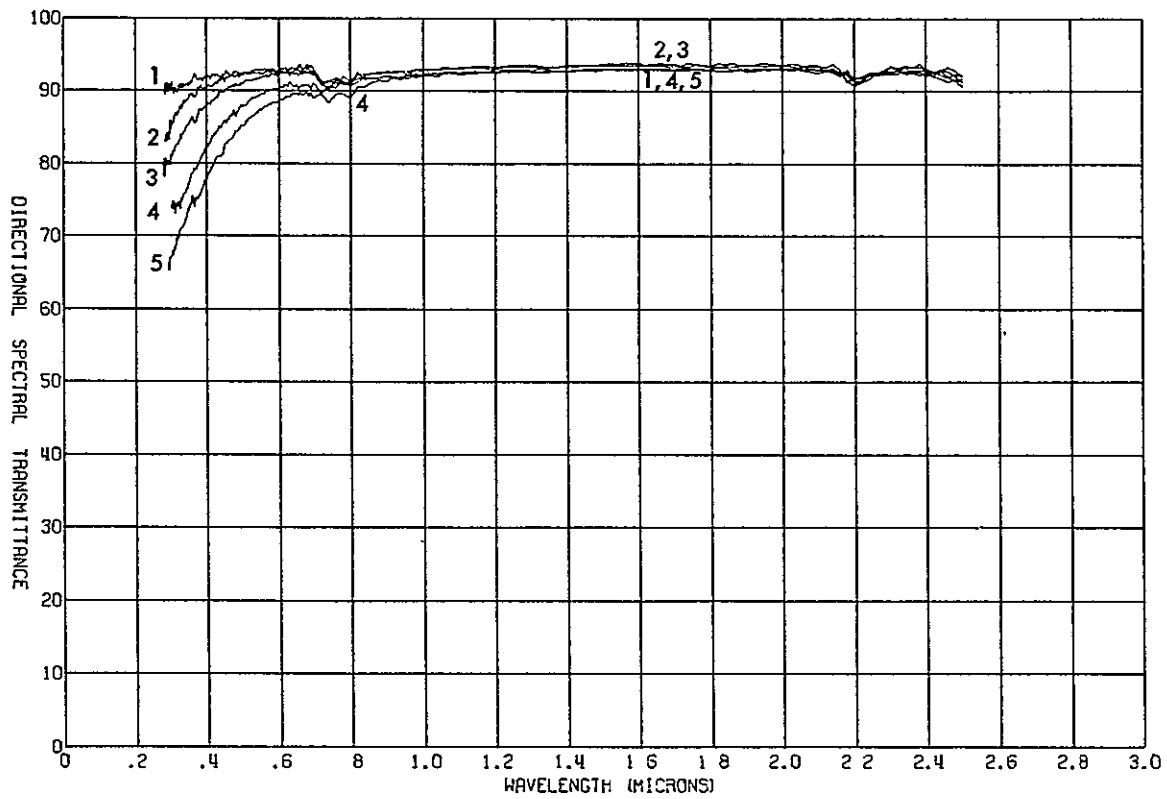


Fig. 189. Proton-ultraviolet effects on transmittance of sample 2089, clear glass (7940 fused silica), 2400-h test

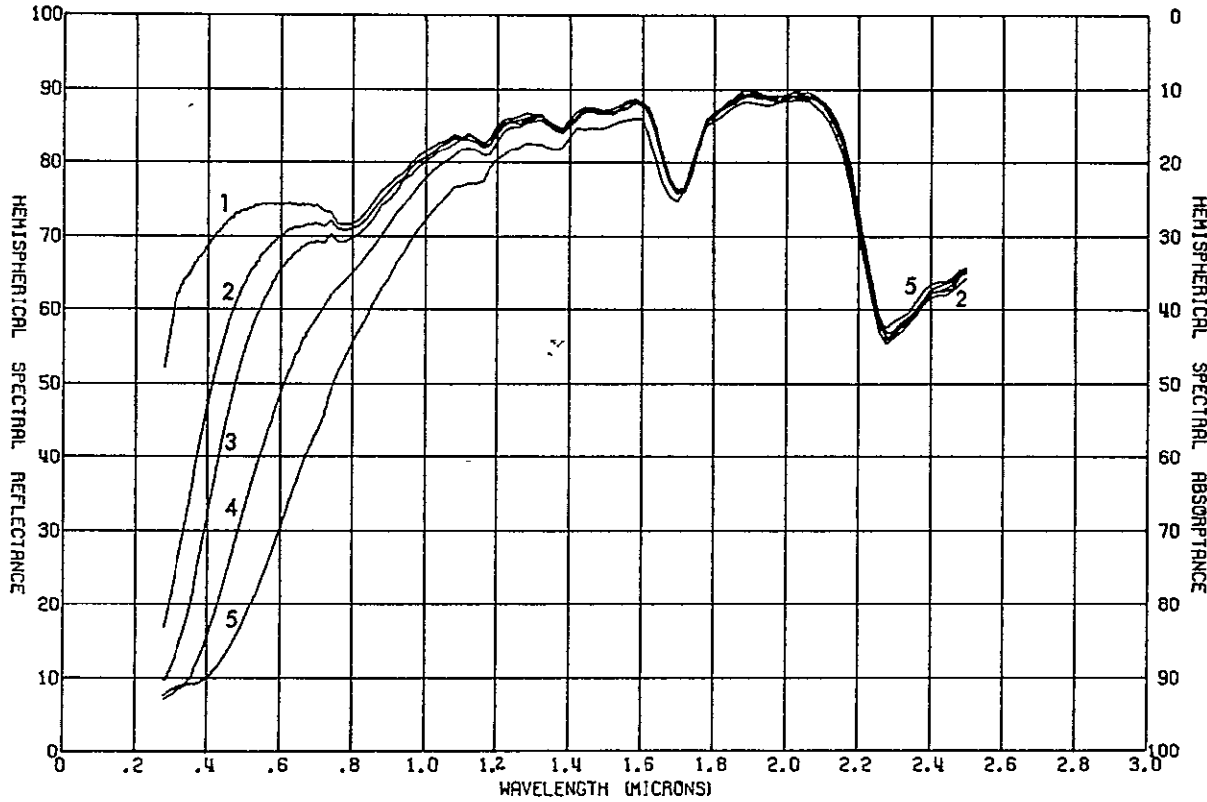


Fig. 190. Ultraviolet effects on reflectance of sample 2081, clear glass, RTV 602, polished aluminum, 2400-h test

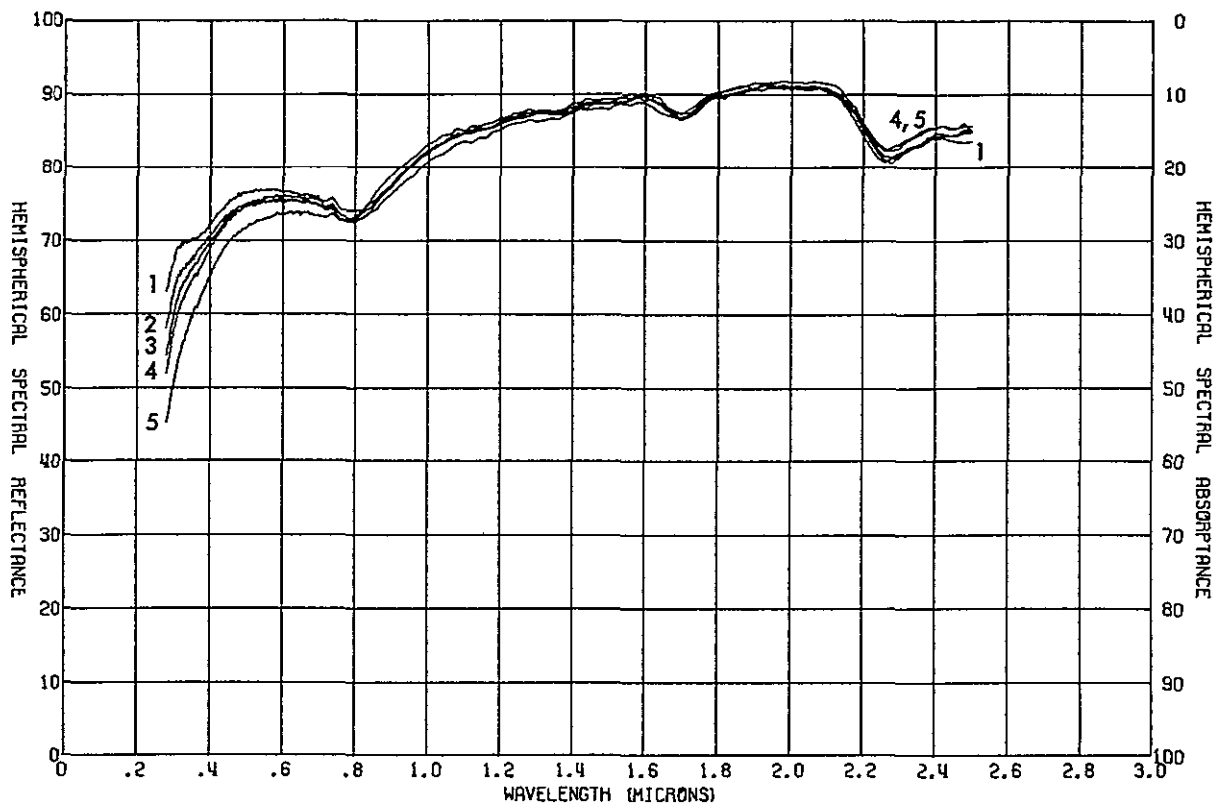


Fig. 191. Proton effects on reflectance of sample 2099, clear glass, RTV 602, polished aluminum, 2400-h test

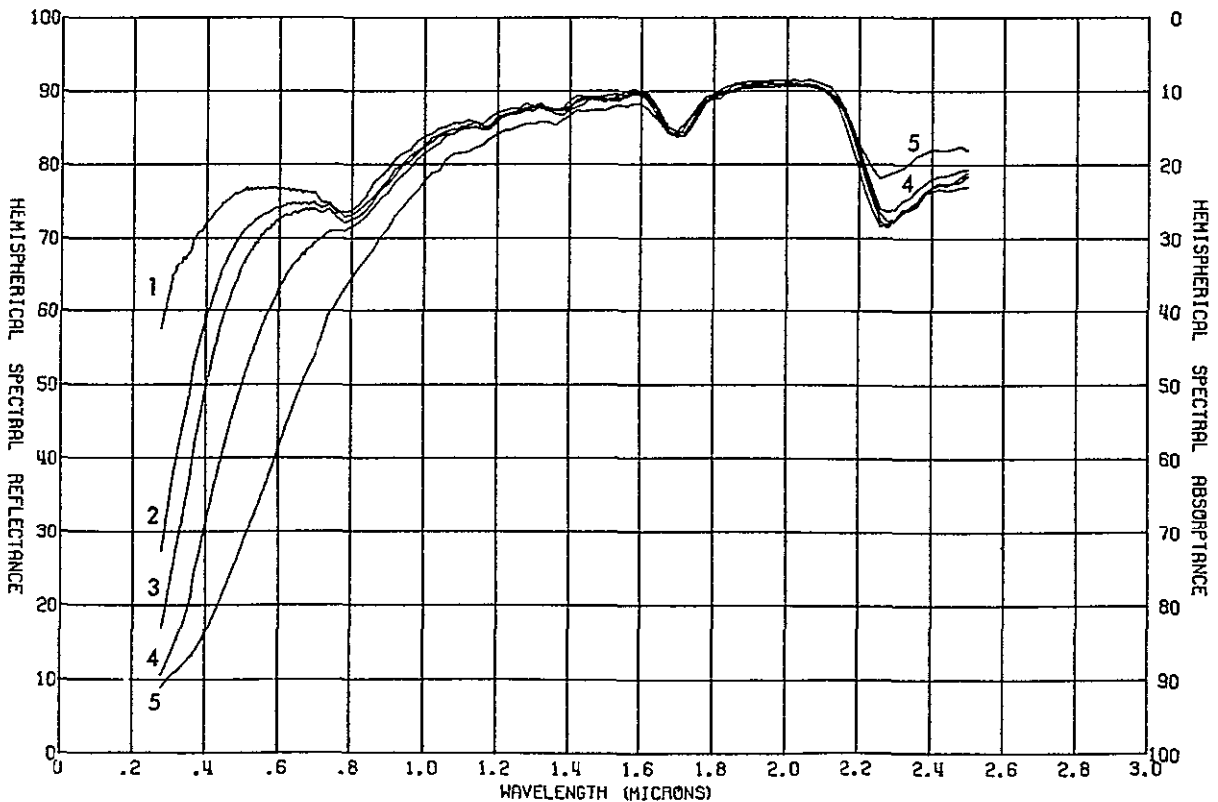


Fig. 192. Proton-ultraviolet effects on reflectance of sample 2090, clear glass, RTV 602, polished aluminum, 2400-h test

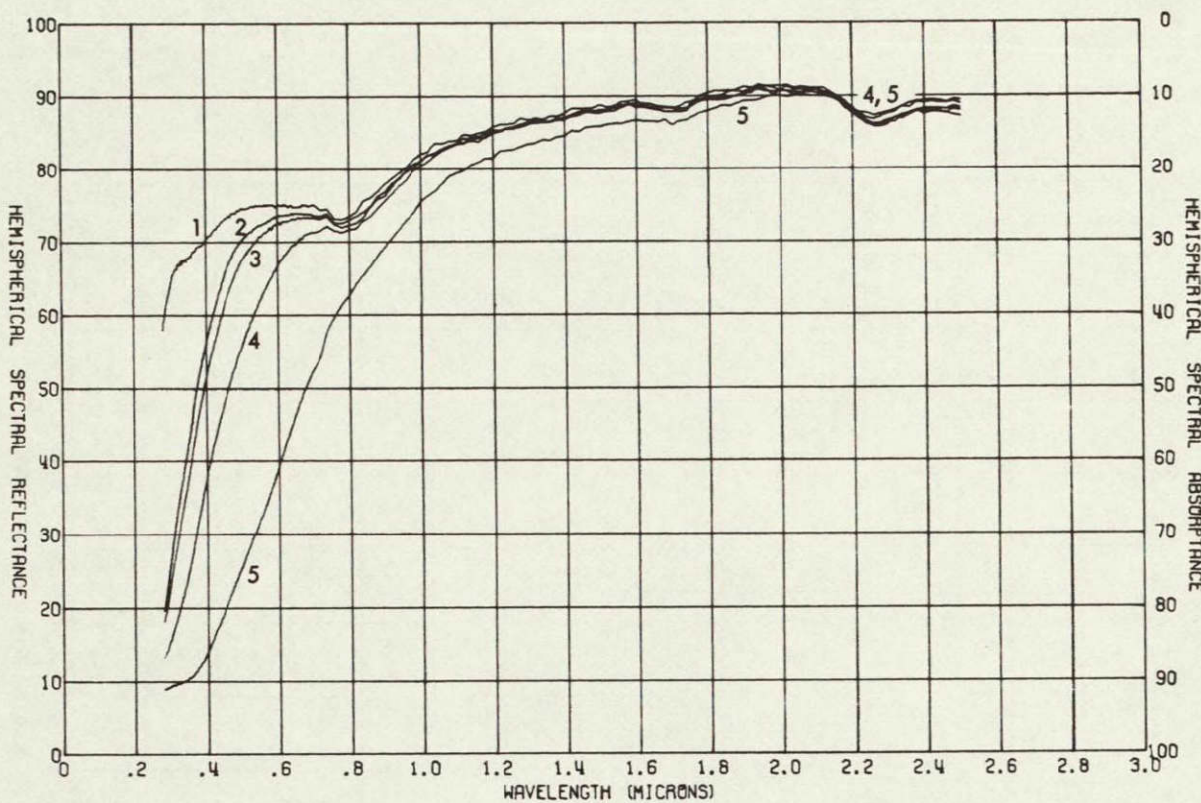


Fig. 193. Ultraviolet effects on reflectance of sample 2082, clear glass, XR6-3489, polished aluminum, 2400-h test

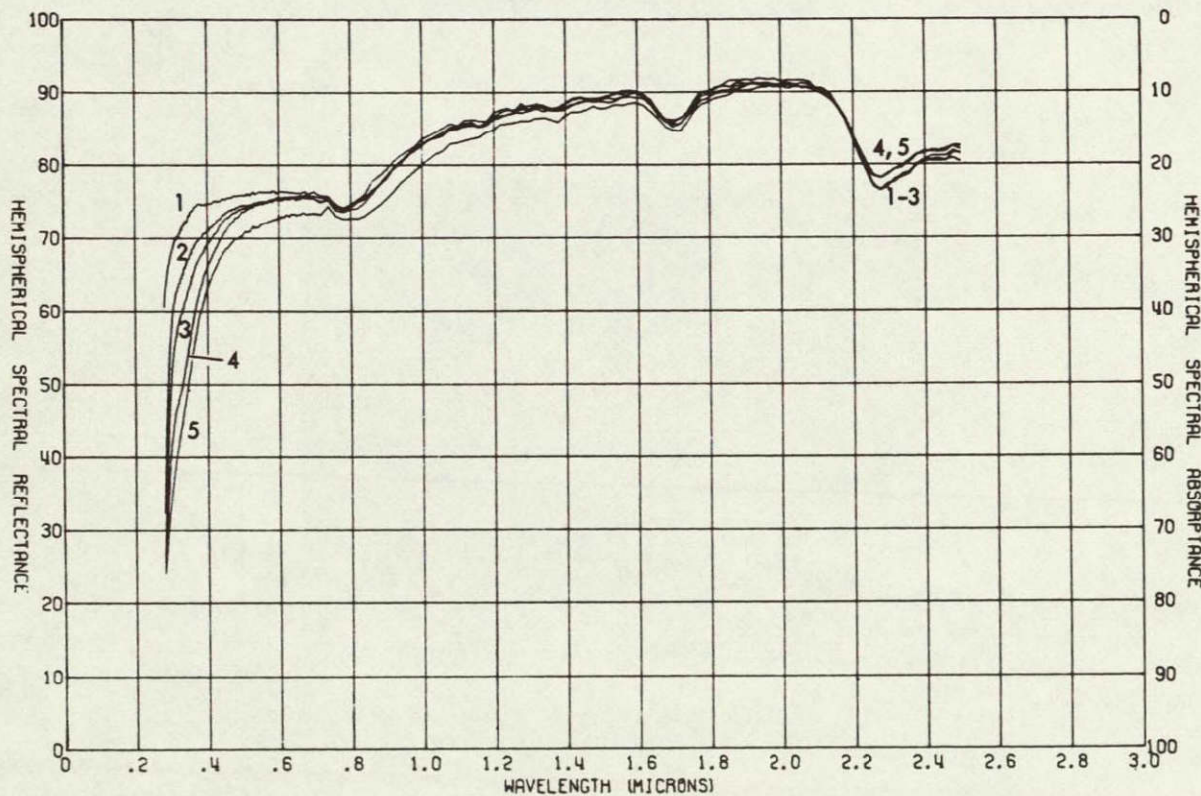


Fig. 194. Proton effects on reflectance of sample 2100, clear glass, XR6-3489, polished aluminum, 2400-h test

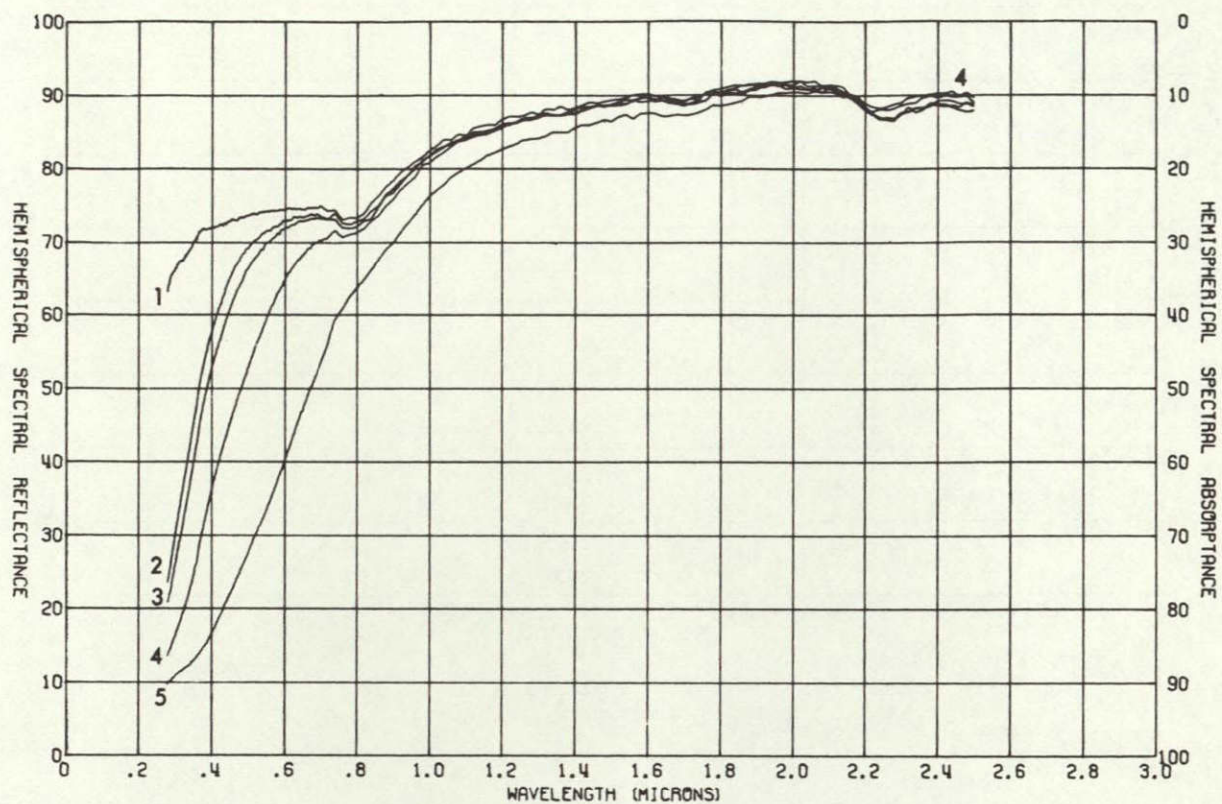


Fig. 195. Proton-ultraviolet effects on reflectance of sample 2091, clear glass, XR6-3489, polished aluminum, 2400-h test

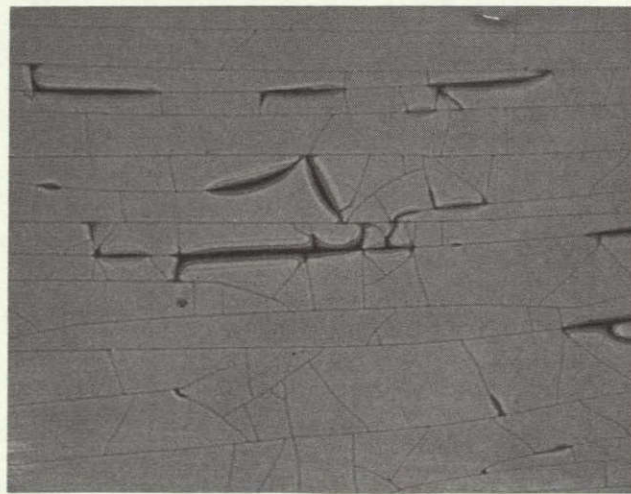


Fig. 196. Damage to filter layers sustained by modified 4026 filter on 2 ohm-cm cell during 500-h test

IX. SOLAR CELL ADHESIVE PROPERTIES

A. Objective

The solar cell adhesives discussed here are involved in two functional applications. The applications include those of bonding the coverglass to the solar cell and bonding the solar cell to the panel substrate.

During a nominal 200-day near-sun mission, the solar cell adhesives must function for extended periods of time with cell temperatures approaching 160°C and while subjected to thermal stresses induced by the overall combination of materials used in the solar panel. In order to prevent delamination, which would lead to increased thermal gradients and catastrophic overheating, the adhesives must have adequate long-term thermomechanical capabilities. In addition, their outgassing properties must be consistent with spacecraft requirements.

The objective of the work described here was to evaluate the thermomechanical and outgassing properties of a number of candidate solar cell adhesive systems. The long-term strengths of the adhesives were determined by subjecting lap shear specimens to a simulated space environment of 160°C and 10^{-4} N/m² (10^{-6} torr) for 1000 h. The outgassing properties were established with weight loss and volatile condensable matter (VCM) tests.

B. Selected Adhesives

The candidate adhesives considered in this program were selected as representative of those currently being used as solar cell adhesives and are presented in Table 9. In all cases, the selected adhesive systems are based on silicone resins and are well suited for service at the temperatures being considered. At the elevated temperature of

+160°C, all the adhesives are thermally stable and safe from the risk of depolymerization. In addition, all of the adhesives have brittle points lower than -40°C and, consequently, will avoid the danger of experiencing a second-order phase change with its decreased flexibility characteristics.

In general, the thermomechanical properties of the silicone adhesives candidates will vary, although basically they are the same class of material.

The three silicone resin systems selected for evaluation as coverglass adhesives must have optical transparency to the solar energy spectrum. Hence, for reasons of transparency, these candidates necessarily have unfilled resin systems. Categorically, unfilled resin systems compared with those of filled resin systems are more likely to have higher shrinkage, greater weight loss, lower inherent strength, and a higher absolute quantity of chemically unreacted or undesirable residual constituents. The three coverglass adhesive candidates evaluated in this program are influenced by these factors.

C. Experimental Procedures

1. Lap Shear Tests. Lap shear specimens were prepared for each of the eight candidate adhesive systems in accordance with ASTM designation D1002-64 and had a nominal 2.5-cm by 1 3-cm (1-in. by 1/2-in.) overlap adhesive bonded area. The substrate material was aluminum alloy 2024-T3 having a 1.6-mm (0.064-in.) nominal thickness. Each adhesive system was mixed, cured, and primer-coated, when applicable, in accordance with the manufacturers' recommendations. A summary of the adhesive preparations is as given in Table 10.

Ten specimens of each adhesive system were prepared, properly identified, and then randomly divided into two groups of five specimens. One group of five lap shear specimens was selected to act as control specimens, and the remaining five were designated as the active test specimen group, which was subjected for 1,000 h to a temperature of 160°C and a pressure of 10^{-4} N/m² (10^{-6} torr).

After the period of thermal vacuum exposure was completed, both the control and active groups were evaluated for mechanical shear strength characteristics. The shear strength tests were performed at the ambient room temperature of the test laboratory and were conducted in accordance with ASTM designation D1002-64. The crosshead separation rate of the testing machine was 0.02 mm/s (0.050 in./min.).

2. Weight-Loss and Volatile Condensable Matter Tests. The weight loss and volatile condensable matter were determined in the micro-VCM apparatus that was developed under JPL-sponsored work. The test procedure involved comminuting about 0.2 g of cured adhesive and subjecting the finely divided sample to 125°C at 10^{-4} N/m² (10^{-6} torr) for a 24-h period. During the course of the test, the volatile matter from the sample passed over a condenser plate maintained at a temperature of 25°C. Since configuration is not involved, the data represent a good estimate of the total weight of matter which is eventually available for emission from the adhesive in a space environment. In addition, an estimate is made regarding the amount of VCM which may adhere to cool surfaces of a spacecraft. The weight loss and VCM data are for the mixing ratios and cure times of the candidate adhesive systems.

D. Experimental Results and Discussion

The data for the lap shear tests are displayed in Fig. 197 and the outgassing data are compared in Fig. 198.

Considering the lap shear test results, it is apparent that the thermal vacuum exposure had no significant effect on the adhesives intended for making the cell to substrate bond. However, the identical exposure did significantly change the lap shear strengths of two of the filter cover adhesives; namely, XR 6-3489 and DC 93-500. Outgassing data on the subject adhesives reveal that only two adhesive systems had very low relative weight losses and volatile matter contents. The low outgassing systems were those of RTV-566 and DC 93-500, both of which are believed to have been subjected to molecular distillation by the manufacturers. Obviously, these are comparatively high-cost materials.

1. Filter Cover Adhesives. All of these shear test specimens had adhesive-type failures. This

is understandable because the filter cover adhesive systems contain no filler material and employ no substrate primer coating. With regard to curing temperatures, note that adhesive XR6-3489 requires an elevated temperature cure of 65°C for 4 h. The other systems, DC 93-500 and RTV-602, will crosslink and cure at 25°C.

After the thermal-vacuum exposure, the test specimens bonded with XR6-3489 had an average shear strength of 3.09 MN/m² (448 psi), which is significantly higher than the 1.56 MN/m² (226 psi) value of the control group specimens. This higher value is confirmed statistically at the 98% confidence level. Also, showing an increase in strength after thermal-vacuum exposure is the DC 93-500 system with a shear strength of 3.64 MN/m² (528 psi) compared to 2.79 MN/m² (404 psi) for the control group specimens. Again, the difference is statistically significant. The remaining system, RTV-602, showed no apparent change when exposed to the simulated space environment.

2. Solar Cell to Substrate Adhesives. All of the candidate adhesives intended for the solar cell to substrate application contain a filler material and will cure at 25°C, and all but one employ a primer coating to enhance adhesion. Although they exhibited various types of failure modes, these adhesives were not significantly affected by the thermal-vacuum environment. The lowest value of shear strength was for the system not employing a primer, RTV-8373, and it exhibited an adhesive-type failure mode. RTV-566 had the highest value of shear strength, with a 75/25 cohesive-adhesive failure mode; it also had the best outgassing characteristics. The only detriment associated with RTV-566 is its relatively high cost.

The RTV-40 adhesive, previously used by JPL for solar cell to substrate bonding, was not affected by the simulated space environment and had a relatively high shear strength of 3.69 MN/m² (534 psi). Of course, the outgassing characteristics of RTV-40 are considerably worse than those of RTV-566. Actually, an improved version of RTV-40, designated RTV-41, is available with the same general characteristics but with an improved uniformity of cure and a longer shelf life.

The other adhesives, namely, RTV-560 and the one-component system, DC 90-092, were the ones with the highest weight losses and VCM contents. The RTV-560 system exhibited half cohesive and half adhesive failure modes but had a respectable strength in the 3 MN/m² (400 psi) range. One of the oldest in-use adhesives, DC 90-092, showed complete cohesive failure modes, with strength values in the 1.5 MN/m² (200 psi) range.

The advantages and disadvantages of the various systems are summarized in Table 11.

Table 9. Solar cell adhesives subjected to thermal-mechanical
and outgassing tests

Literature reference No. ^a	Adhesive resin/hardener	Primer
Coverglass adhesive candidates primer		
17	XR63-489/R-3489	--
18	DC 93-500/93-500	--
19	RTV 602/SRC-05	--
Solar cell substrate adhesive candidates		
19	RTV-560/9930	SS 4044
20	RTV-8373/9858	(No primer)
21	DC 90-092 (one component)	PR 1902
22	RTV-566 A/B	SS 4155
19	RTV-40/Thermolite-12	SS 4004

^aSee reference section

Table 10. Summary of the adhesive preparations

Adhesive component				Primer component	
Resin	Curing agent	Cure agent mix ratio by weight, parts/100 resin	Cure	Designation	Cure
XR 6-3489	R-3489	10	4 h at 65°C	None	--
DC93-500	93-500	10	7 days at 25°C	None	--
RTV-602	SRC-05	0.25	36h at 25°C	None	--
RTV-40	Thermolite 12	0.5	7 days at 25°C	SS4004--Make light pink coat 10 to 20 µm thick	1 h at 25°C
RTV-560	9930	10	3 days at 25°C	SS4044--Make uniform clear coat 10 to 20 µm thick	1 h at 25°C
RTV-566	A/B	0.1	7 days at 25°C	SS4155--Make uniform blue coat 10 to 20 µm thick	1 h at 25°C
RTV-8373	9858	3	3 days at 25°C	None	--
DC90-092	None	--	7 days at 25°C	PR1902--Make uniform blue coat approximately 10-µm thick	1 h at 25°C

Table 11. Advantages and disadvantages of adhesive systems tested

Adhesive system	Advantages	Disadvantages
For bonding filter covers		
1. DC 93-500/93-500	High strength: 3.5 MN/m ² (500 psi) Low outgassing: 0.2% weight loss and 0.02% VCM content	High Cost After thermal-vacuum exposure exhibited increase in shear strength
2. XR6-3489/R-3489	High strength: 2.8 MN/m ² (400 psi)	Requires elevated temperature cure. After thermal-vacuum exposure exhibited increase in shear strength. Outgassing: 1.4% weight loss and 0.6% VCM content
3 RTV 602/SRC-05	Low strength: 1.0 MN/m ² (100 psi)	Outgassing 3% weight loss and 1% VCM content
For bonding solar cells		
1. RTV-566 A/B Use SS 4155 primer	High strength: 5.5 MN/m ² (800 psi) Low outgassing: 0.3% weight loss and 0.01% VCM content	High Cost
2. RTV-41 (RTV-40)/T-12 Use SS 4004 primer	Good strength: 3.5 MN/m ² (500 psi)	Outgassing: 2% weight loss and 0.5% VCM content.
3 RTV-560/9930 Use SS 4044 primer	Good strength: 2.8 MN/m ² (400 psi)	Outgassing: 3% weight loss and 0.5% VCM content

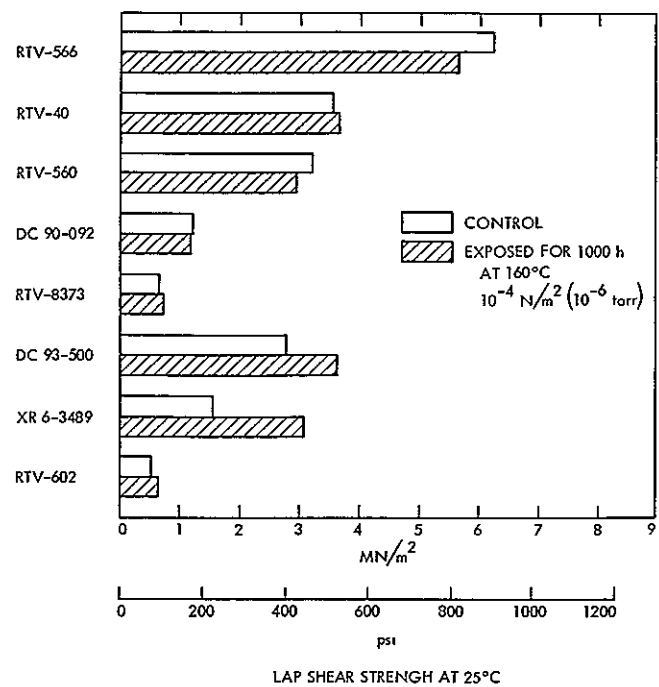


Fig. 197 Effect of 1000-h vacuum soak at 160 °C on the lap shear strength of selected adhesives

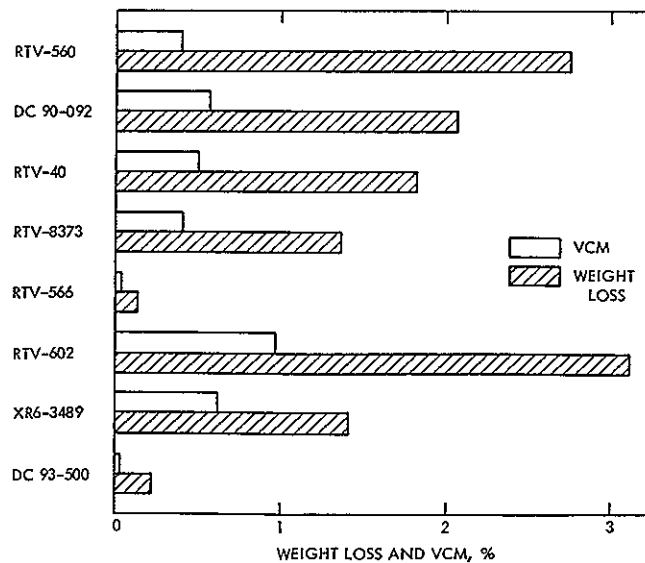


Fig. 198. Weight loss and volatile condensable matter content of selected adhesives

X PERFORMANCE COMPARISONS

Because the various solar cell assembly types considered in this study have different thermal characteristics, comparisons of their electrical performances must take into account the difference in their operating temperatures. In addition, since the relative performance of the designs varies in different ways with incident intensity, the comparisons must be made on a mission performance basis, where performance is described as a function of solar intensity. To satisfy these requirements, a computer program was generated to plot the predicted temperature and maximum power performance of the various solar cell assembly types as a function of solar intensity from 1 to 6 suns. In addition to handling both normal and tilted panels, the program also had provisions for comparing different cell types on an equal thermal performance basis. This was accomplished by adjusting the amount of mirror area on the mirrored coverglass and wide-grid cell types so as to achieve the desired operating temperature characteristics.

In order to calculate the maximum power output of the various designs, the maximum power per cell was first determined by interpolating within the matrices of maximum power measurements presented in Section IV. The total power per unit area was subsequently obtained by multiplying the cell power by an assumed 2260 cells/m² (210 cells/ft²) and then scaling the resulting power by a fixed amount. The scaling factor was chosen as the value required to give a 1 sun, 55°C power of 100 W/m² (9.3 W/ft²) for a flat panel utilizing the baseline 2 ohm-cm cell with blue filter. The resulting scale factor of 0.856 was used with all cell assembly types to make the results comparable. When the percentage of mirror area on mirrored coverglass and wide-grid cells was changed, the power of the altered cell was

extrapolated assuming the power was linearly proportional to the percentage of active area. All of the mirrored coverglass and wide grid cell performance profiles given here have been so adjusted.

In order to calculate equilibrium temperature versus intensity for the various panel configurations, a one-node (isothermal) model was constructed using the absorptivities and emissivities presented in Sections VI and VII for the cell assembly components and for the intercell space and cell contact areas which make up the panel's front surface. A 90% packing factor was used, based on 5% intercell spaces and 5% cell ohmic contact areas. The emittance of the rear surface was chosen as the value required to give the base line array using 2 ohm-cm cells with blue filters an equilibrium temperature of 55°C at 1 AU. Though the effect of the electrical power output on the panel temperature was included, the result of thermal interaction with the spacecraft bus or between panels was neglected.

The following subsections compare the relative performance of the various solar cell thermal approaches considered in this study.

A Variable Angle of Incidence Designs

In order to compare the thermal and electrical performance of tilttable panels utilizing different solar cell assemblies, the above-described computer program was used to generate temperature and maximum-power profiles for angles of inclination ranging from 0 deg (normal to the sun) to 70 deg. Two profiles were generated for each tilt angle, one assuming that the effective solar intensity varies according to the cosine of the angle of incidence, and the second including the additional

decrease in the effective intensity caused by the variation in cell stack reflectance described in Section V. Though the latter represents the expected behavior and provides a more conservative estimate of available power, the cosine relationship is included to provide a more conservative estimate of solar array temperature.

Figures 199-201 describe the relative performance of three solar cell assembly types: the baseline 2 ohm-cm cell with blue filter, the same cell with blue-red filter, and a 10 ohm-cm cell with blue-red filter. Recall that the power and thermal characteristics of the designs have been scaled to force the baseline 2 ohm-cm cell with blue filter to operate at a power of 100 W/m² and a temperature of 55°C at 1 AU. From the figures it is clear that the 2 ohm-cm cell offers a considerable power advantage over the 10 ohm-cm cell. This is because of the higher resistance of the 10 ohm-cm and its higher temperature dependence. Note also that, although the 2 ohm-cm cells with blue and blue-red filters have essentially the same power output when tilted equally, the blue-red filtered cell operates about 15°C cooler. As a result an array utilizing blue-red filters will require slightly less tilt and may offer slightly more power than the same array with blue filters when forced to meet the same temperature requirements.

B Mirror Mosaic Approaches

In order to compare the electrical performance of the various partially mirrored coverglass and wide-grid cell designs, it was necessary to force all of the designs to have equal thermal performance characteristics. This was done by adjusting the percentage of mirror area on each configuration so as to achieve an array operating temperature of 140°C at a solar intensity of 5 suns. The power output was then scaled proportionally.

Figure 202 compares the relative performance of the various mirror mosaic approaches. Of significant interest is the excellent performance of the multiple wide-grid cells in comparison with the partially mirrored coverglass configurations.

Apparently the decreased series resistance due to the increased grid area more than compensates for the higher solar absorptance of the Ag-Ti mirror surface*. This is substantiated by the rather poor performance of the single wide-grid cell which has two large active areas with no grid collectors.

As with the wide-grid cells, the position and shape of the mirror on the partially mirrored coverglass approaches also has an effect on cell performance at high solar intensities. Note that when the cell's series resistance is minimized by placing the mirrored area opposite the cell's ohmic contact, a 30% increase in maximum power is achieved at 6 suns.

C Selective Bandpass Filter Designs

In order to compare the electrical performance of the various selective filter configurations with the performance of the mirror mosaic approaches, it was again necessary to force all of the designs to have equal thermal performance characteristics. Since adding mirror area to the selective filters was considered unrealistic, the mirror fraction of the mirror mosaic designs was adjusted so that each exhibited the same operating temperature characteristics as the reference selective filter design.

Figures 203-205 compare the performance of the 4025, 4026, and modified 4026 filters with the wide-grid, mirrored coverglass, and tilted panel approaches. From these figures it is clear that although the 4025 and 4026 filters exhibit somewhat more power at 1 sun, they are quite comparable to the mirror mosaic approaches at high solar intensities. The modified 4026 filter, on the other hand, exhibits a considerable power advantage over the mirror mosaic approaches.

One must note, however, that this advantage is somewhat academic at this time because of the extensive degradation obtained when the selective bandpass filters were subjected to low-energy proton and ultraviolet radiation as described in Section VIII.

*The curves in Fig. 202 are based on an assumed solar absorptance of 0.10 for the mirrored coverglass areas and 0.13 for the wide-grid mirror areas.

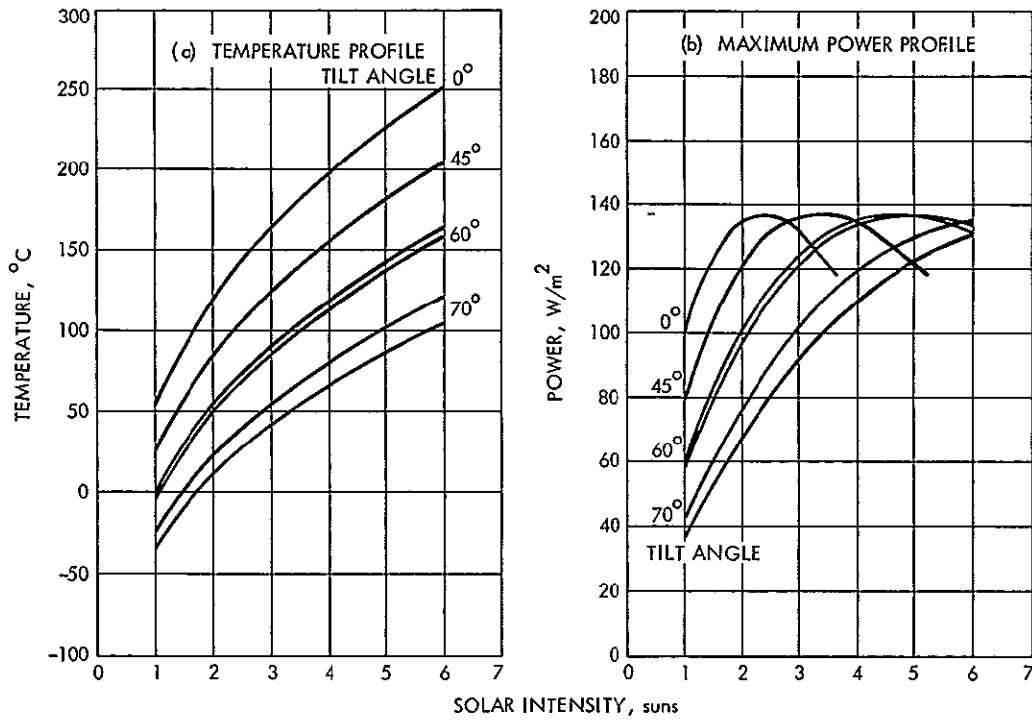


Fig. 199. Temperature-power performance of a tiltable panel using 2 ohm-cm cells with blue filters. The upper curve for each tilt angle is based on the effective intensity varying according to the cosine of the angle of incidence; the lower curve includes the additional decrease in intensity caused by the increase in cell stack reflectance.

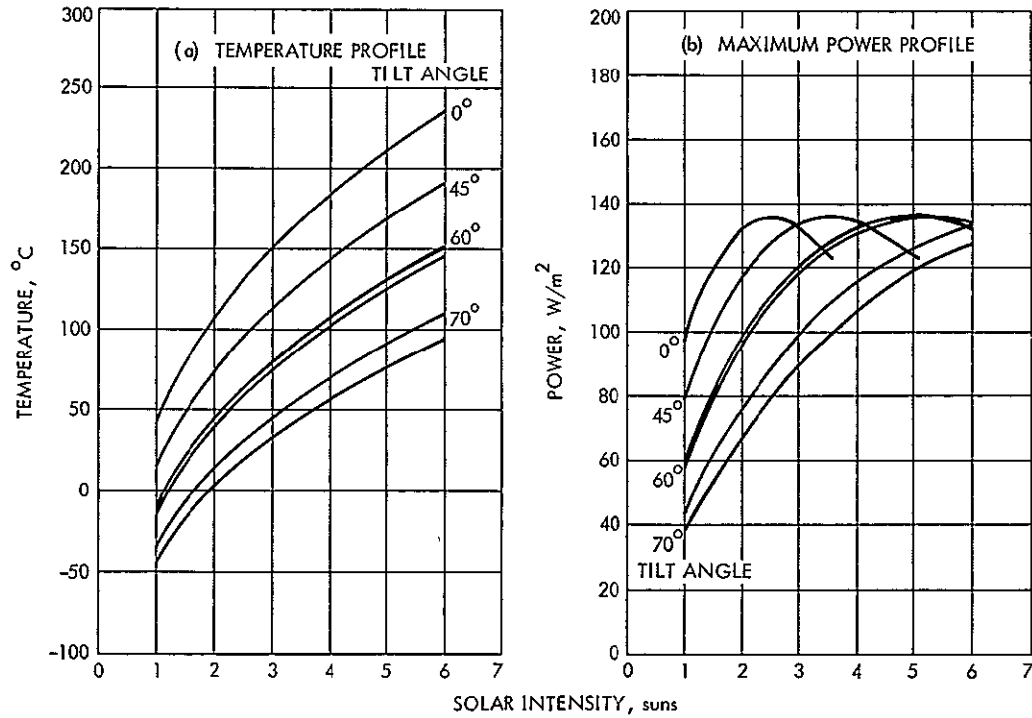


Fig. 200 Temperature-power performance of a tiltable panel using 2 ohm-cm cells with blue-red filters. The upper curve for each tilt angle is based on the effective intensity varying according to the cosine of the angle of incidence; the lower curve includes the additional decrease in intensity caused by the increase in cell stack reflectance.

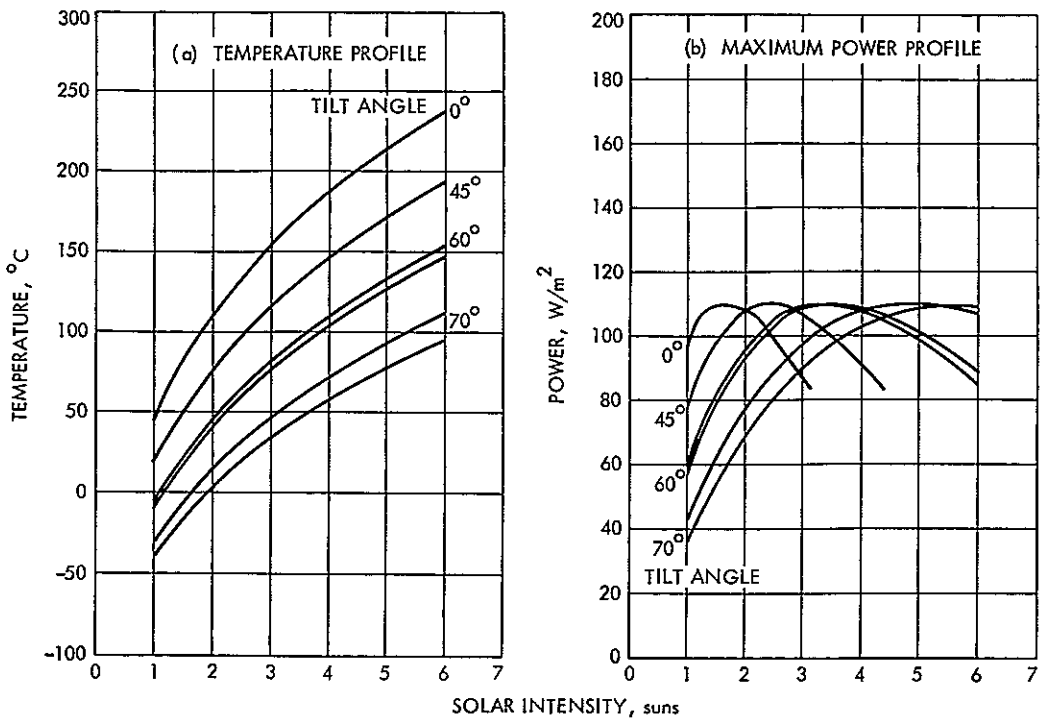


Fig. 201. Temperature-power performance of a tilttable panel using 10 ohm-cm cells with blue-red filters. The upper curve for each tilt angle is based on the effective intensity varying according to the cosine of the angle of incidence; the lower curve includes the additional decrease in intensity caused by the increase in cell stack reflectance

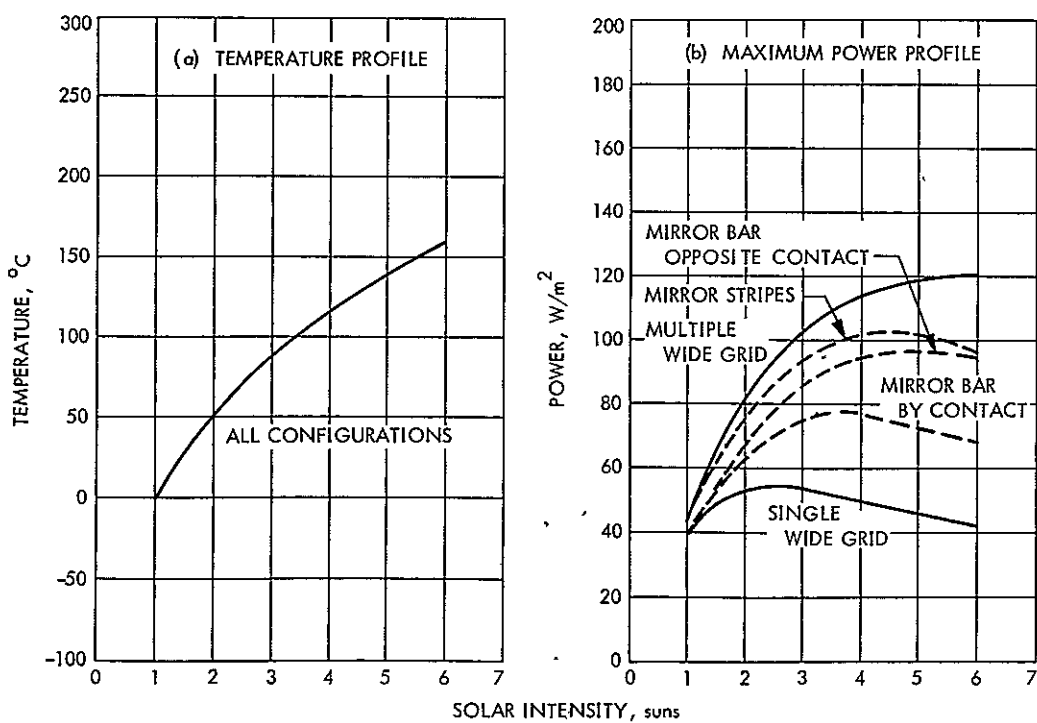


Fig. 202. Comparison of the temperature-power performance of various mirror mosaic configurations using 2 ohm-cm cells

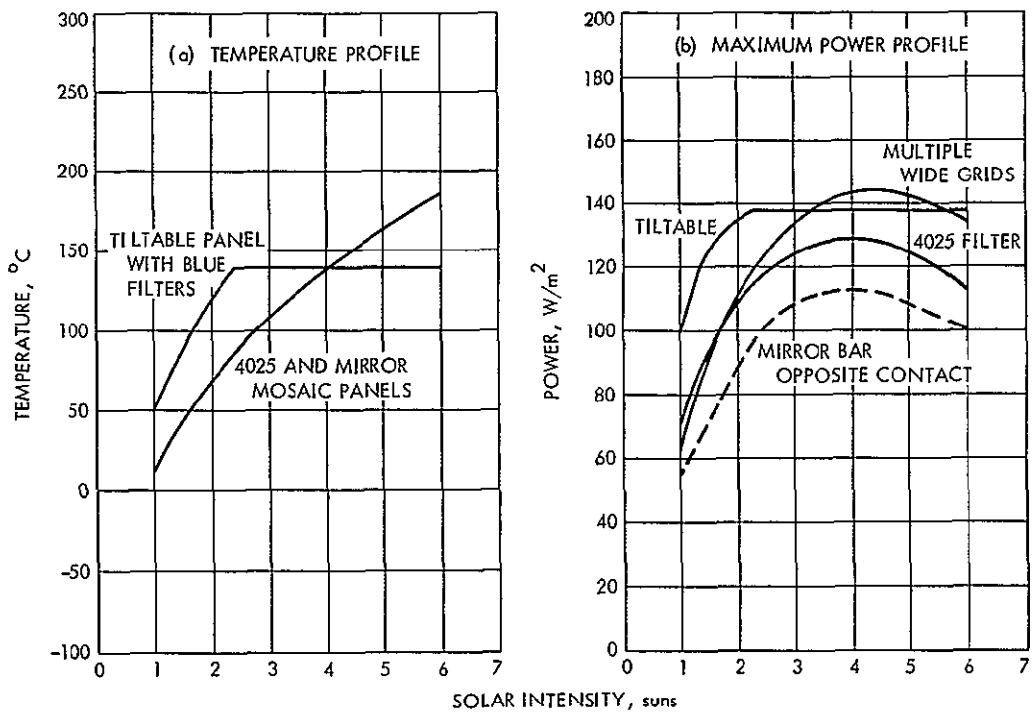


Fig. 203. Comparison of the temperature-power performance of 4025 selective bandpass filters on 2 ohm-cm cells with that of tiltable and mirror mosaic 2 ohm-cm cell arrays

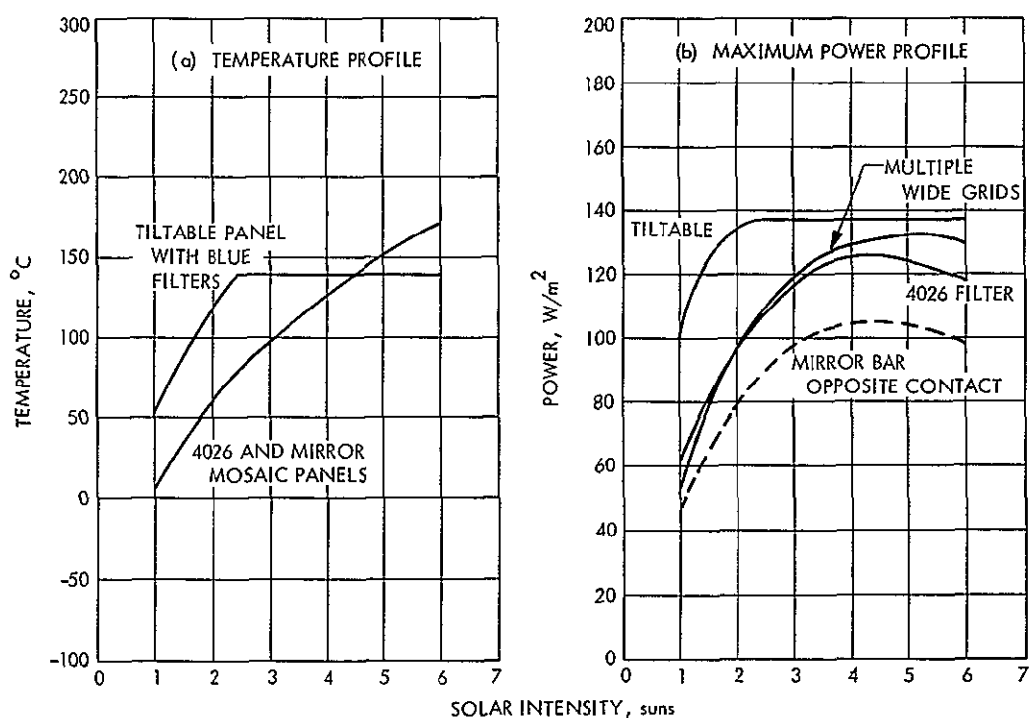


Fig. 204. Comparison of the temperature-power performance of 4026 selective bandpass filters on 2 ohm-cm cells with that of tiltable and mirror mosaic 2 ohm-cm cell arrays

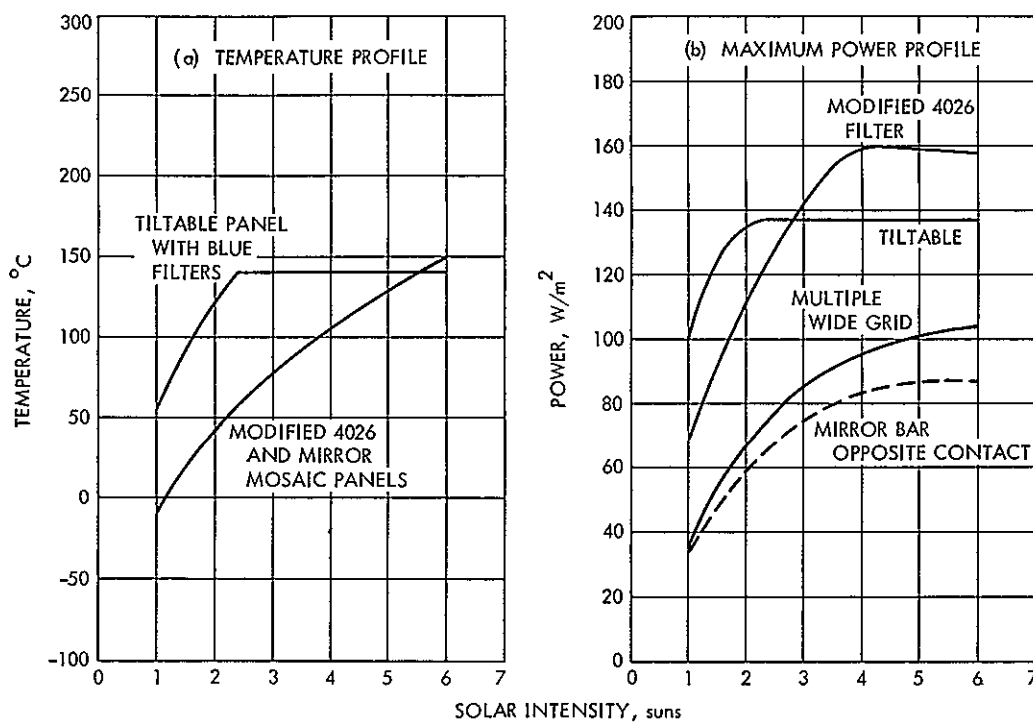


Fig 205. Comparison of the temperature-power performance of modified 4026 filters on 2 ohm-cm cells with that of tilttable and mirror mosaic 2 ohm-cm cell arrays

REFERENCES

1. Greenwood, R. F., Results of the 1968 Balloon Flight Solar Cell Standardization Program, Technical Report 32-1426 Jet Propulsion Laboratory, Pasadena, Calif., Dec. 1, 1969
2. Yasui, R. K., and Schmidt, L. W., "Performance Characteristics of Ti-Ag Contact N/P and P/N Silicon Solar Cells," presented at IEEE 8th Photovoltaics Specialist Conference, Seattle, Wash., Aug. 5, 1970
3. Ross, R. G., Jr., "Solar Panel Approaches for a Venus-Mercury Flyby," ASME Paper 70-Av/Sp T-29, presented at the Space Technology and Heat Transfer Conference, Los Angeles, Calif., June 21-24, 1970, sponsored by the American Society of Mechanical Engineers
4. Johnson, P. A., Laboratory Experiments on the Performance of Silicon Solar Cells at High Solar Intensities and Temperatures, NASA TN D-2733. Ames Research Center, Moffett Field, California, 1965
5. Sears, F. W., Optics, Addison-Wesley Publishing Co., 1949, p. 174.
6. Thermophysical Property Measurements, Facilities and Service Available for Aerospace Applications, TRW Systems document 09990-6011-TU00. TRW Space Systems, One Space Park, Redondo Beach, Calif., July 1966
7. Edwards, D. K., et al, "Integrating Sphere for Imperfectly Diffuse Samples," J. Opt. Soc. Am., Vol. 51, pp. 1279-88, Nov 1961
8. Cahn, L., and Henderson, B. D., "Performance of the Beckman DK Spectrophotometer," J. Opt. Soc. Am., Vol. 48, pp. 380-387, June 1958.
9. Dunkle, R. V., et al, "Heated Cavity Reflectometer for Angular Measurements," in Progress in International Research on Thermodynamics and Transport Properties, Symposium on Thermophysical Properties, Ind., 1962, pp. 541-562. ASME and Academic Press, New York, 1962.
10. Johnson, F. S., "The Solar Constant," J. Meteorol., Vol. 11, pp. 431-439, Dec. 1954.
11. Kendall, J. M., Sr., and Berdahl, C. M., "Two Blackbody Radiometers of High Accuracy," Appl. Opt., Vol. 9, pp. 1082-1091, May 1970.
12. Kendall, J. M., Sr., Primary Absolute Cavity Radiometer, TR-32-1396. Jet Propulsion Laboratory, Pasadena, Calif., July 15, 1969
13. King, H. J., and Tuccaro, D. E., Solar Wind Simulation Techniques, Final Report, Hughes Research Laboratories, NASA CR-73443, Contract NAS 2-5585. The Boeing Company Aerospace Group, Seattle, Wash., Apr 1970.
14. Buhler, F., et al, "Apollo 11 Solar Wind Composition Experiment: First Results," Science, Vol. 166, pp. 1502-03, Dec. 19, 1969.
15. Fogdall, L. B., et al., "In Situ Electron, Proton, and Ultraviolet Radiation Effects on Thermal Control Coatings," Final Report for NASA Goddard Contract NAS 5-9650, Boeing Document D2-84118-9. The Boeing Company Aerospace Group, Seattle, Wash., Jan 1969.

16. Fogdall, L. B., et al., "Experimental Study of Effects of Simulated Neutralized Solar Wind on White-Pigment Thermal Control Coatings," NASA CR-73389, Contract NAS 2-5343. The Boeing Company Aerospace Group, Seattle, Wash., Oct. 1969.
17. Dow Corning XR 63-488 Resin and Dow Corning XR 63-489 Resin (For Optical Applications), brochure. Dow Corning Corp., Jan 1967.
18. Dow Corning 93-500 Space Grade Encapsulant, brochure Dow Corning Corp., Mar. 1968
19. RTV Silicone Rubber, Technical Data Book S-3C, General Electric Corp., undated.
20. Silicone Rubber RTV Compounds, Technical Data Book S-3C-1B. General Electric Corp., undated.
21. Dow Corning 90-092 Aerospace Sealant, brochure. Dow Corning Corp., Aug. 1964
22. Preliminary Product Data--RTV 566, brochure. General Electric Corp., Mar. 1969

APPENDIX A
SOLAR CELL SPECIFICATIONS

Solar cells are to comply with the requirements listed below.

A. Electrical Requirements

- (1) The cells shall be shallow-diffused n/p.
- (2) The base resistivity shall be 0.7-3 ohm-cm.
- (3) The cells delivered under this requirement shall have an electrical output of 125 ± 5 mA at 485 mV measured under a filtered xenon solar simulator.
- (4) The intensity of the xenon light source shall be adjusted by use of a calibrated cell, or cells, traceable to a balloon-flown standard cell so that the I_{SC} , measured in air-mass-zero sunlight (139.6 mW/cm^2) is equal. The uniformity of light over the entire cell test area, measured with a 0.5-cm^2 cell at 1.0-ohm load, shall not vary more than 1%. The optical lens system of the xenon light source shall be free from contamination and cleaned at frequent intervals as determined by measurements of uniformity and spectral quality. Any electrical, mechanical, or optical changes in the xenon source shall be recorded, and, upon request, records shall be made available at JPL.
- (5) The electrical requirements of the cell shall be measured at a cell temperature of $28 \pm 1^\circ\text{C}$.

B. Mechanical Requirements

- (1) Configuration: The solar cell configuration shall conform to JPL Drawing DS-116 (Fig. A-3).
- (2) Weight: Maximum cell weight shall be 0.50 g before solder dipping.
- (3) Contacts: The solar cell contacts shall be sintered silver titanium. The grid lines shall be considered as part of the n contact.
- (4) The cells shall be of good appearance and free from defects such as surface scratches, crystal joints, chips, and cracks, except that edge chips shall be no larger than 0.5 mm deep by 4 mm long, and corner chips shall have a hypotenuse less than 1.5 mm in length.

C. Solder

- (1) The cells shall be supplied with soldered n and p contacts.
- (2) The free-form height of the grid lines and n-layer collector strip shall be no greater than 0.05 mm above the cell surface. The rear surface contact shall be complete and free of voids and shall be flat within 0.13 mm. The contacts shall have a minimum solder coverage of 95% of the available contact area.

D. Packaging

- (1) There shall be a maximum of 100 cells per plastic carton.
- (2) Cells shall be kept separate by individual pouches.

Fig. A-1 Specification for 2 ohm-cm solar cell

Solar cells are to comply with the requirements listed below.

A. Electrical Requirements

- (1) The cells shall be shallow-diffused n/p.
- (2) The base resistivity shall be 7-13 ohm cm.
- (3) The cells delivered under this requirement shall have an electrical output of 139 mA minimum at 400 mV measured under a filtered xenon solar simulator.
- (4) The intensity of the xenon light source shall be adjusted by use of a calibrated cell, or cells, traceable to a balloon-flown standard cell so that the I_{sc} , measured in air-mass-zero sunlight (139.6 mW/cm^2) is equal. The uniformity of light over the entire cell test area, measured with a 0.5-cm² cell at a 1.0-ohm load, shall not vary more than 2%. The optical lens system of the xenon light source shall be free from contamination and cleaned at frequent intervals as determined by measurements of uniformity and spectral quality. Any electrical, mechanical, or optical changes in the xenon source shall be recorded, and, upon request, records shall be made available to JPL.
- (5) The electrical requirements of the cell shall be measured at a cell temperature of $28 \pm 1^\circ\text{C}$.

B. Mechanical Requirements

- (1) Configuration: The solar cells shall be $20.00 \pm 0.13 \text{ mm} \times 20.00 \pm 0.13 \text{ mm}$. The corner angles and overall configuration of the cell shall be defined by the contractor, subject to the approval of JPL.
- (2) Weight: The weight minimum of the cell shall be 0.360 g before solder dipping.
- (3) Thickness: Minimum overall thickness shall be 0.46 mm.
- (4) Contacts: The solar cell contacts shall be sintered silver titanium.
- (5) The cells shall be of good appearance and free from defects such as surface scratches, crystal joints, chips, and cracks, except that edge chips shall be no larger than 0.5 mm deep by 4 mm long, and corner chips shall have a hypotenuse less than 1.5 mm in length.

C. Solder

- (1) The cells shall be supplied with soldered n and p contacts. The grid lines shall be considered as part of the n contact.
- (2) The free-form height of the grid lines and n-layer collector strip shall be no greater than 0.05 mm above the cell surface. The rear surface contact shall be complete and free of solder voids and shall be flat within 0.13 mm. The contacts shall have a minimum solder coverage of 90% of the available contact area.

D. Packaging

- (1) There shall be a maximum of 100 cells per plastic carton.
- (2) Cells shall be kept separate by individual pouches.

Fig. A-2. Specification for 10 ohm-cm solar cell

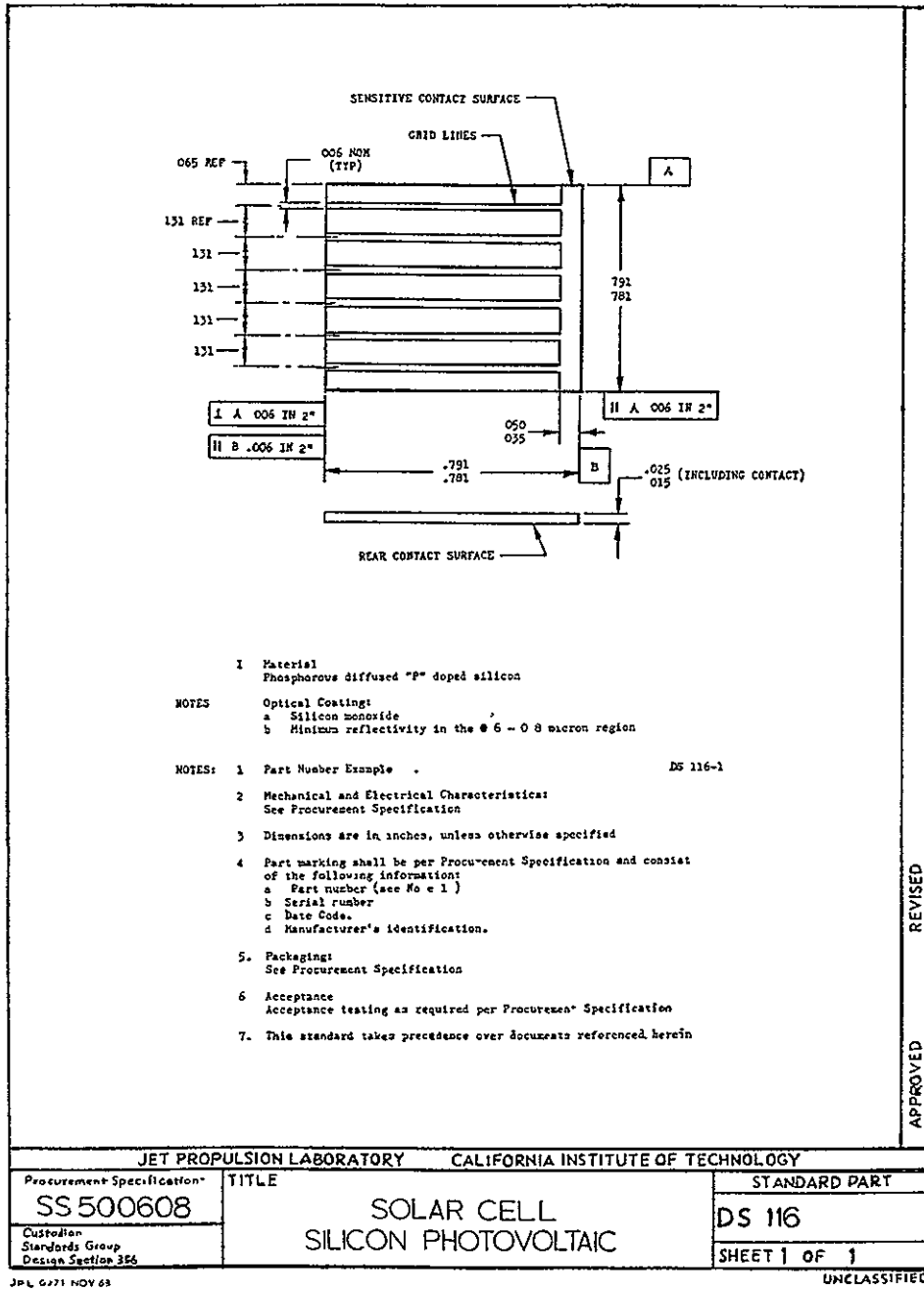
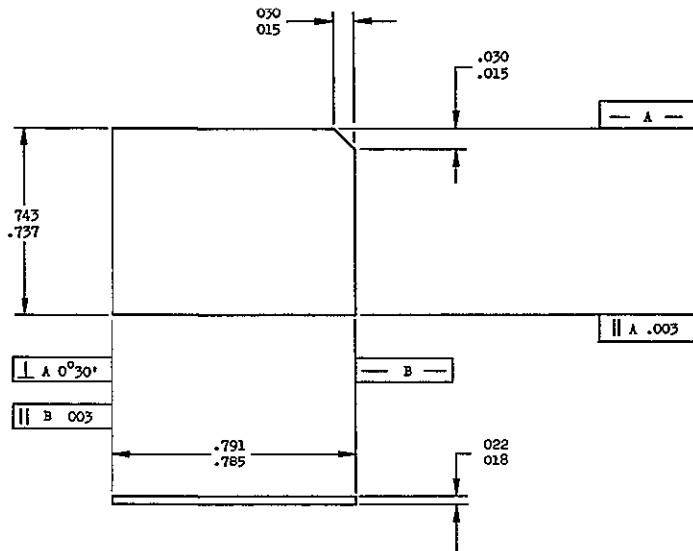
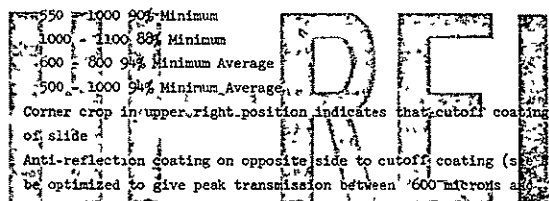


Fig. A-3. Silicon photovoltaic solar cell specification



- NOTES
- Material 7940 "Industrial Grade" fused silica
 - Inspection Criteria (Unless otherwise specified, all dimensions are in inches)
 - Maximum diameter bubbles allowable shall be 0.010, not more than six bubbles per coverglass. Bubbles less than 0.005 in diameter shall be discounted
 - Surface quality shall be 80-50
 - Maximum allowable chip dimensions
 - Edge chips 0.010 projection into face, 0.030 length
 - Corner chips 0.010 projection into face, 0.030 length
 - Coating quality There shall be no visible evidence of pinholes, lint marks or jig marks on either surface of the coated filter
 - Coating continuity There shall be no uncoated areas
 - Spectral characteristics per cent transmission for radiation normal to surface
 - Transmission characteristics (Wavelength μ)

300 - 370	Less than 1% average
395 - 425	50% Absolute
500 - 550	85% Minimum
550 - 1000	99% Minimum
1000 - 1100	88% Minimum
1100 - 1200	94% Minimum Average
1200 - 1300	94% Minimum Average
 - Corner crop in upper right position indicates that cutoff coating is on bottom of slide
 - Anti-reflection coating on opposite side to cutoff coating (see note 5) should be optimized to give peak transmission between 600 microns and 800 microns
- (NOTES CONTINUED ON SHEET 2)



JET PROPULSION LABORATORY		CALIFORNIA INSTITUTE OF TECHNOLOGY
Procurement Specification: NONE	TITLE: SOLAR CELL FILTER (2cm X 2cm NOMINAL CELL)	STANDARD PART DS 119
Custodian, Standards Group Design Section 356	SUPERSEDES:	SHEET 1 OF 2

UNCLASSIFIED JPL 0971 FEB 63

REVISED: (A) 2-8-66 (B) 2-7-17 (C) 6-29-67

APPROVED: 3-3-64

Fig. A-4 Solar cell filter specification

STANDARD PART DRAWING - ADDITIONAL SHEET

NOTES (CONTINUED)

- 7 Environmental requirements
- a Abrasion resistance; The filter shall be subject to eraser abrasion resistance test of 20 complete cycles with a pressure of 2 to 2 1/2 pounds (Ref Mil-C-675, Paragraph 4 6 11)
 - b Vendor to submit a certification stating that the cover slips, when cemented to the cell, and the assembly is tested per JPL Specification SS500608 Para 4 5 3, 4 5 4, 4 5 5 and 4 5 9, shall remain within the specification Vendor to perform environmental tests in accordance with paragraph 4 of OCLI General Spec Guide for Solar Cell Covers, dated 1/1/66, except that the abrasion test will not be repeated.
 - c All units must be capable of meeting optical and mechanical requirements upon completion of environmental tests.
- 8 This Standard takes precedence over documents referenced herein

HI-REL

JET PROPULSION LABORATORY		CALIFORNIA INSTITUTE OF TECHNOLOGY	
DS 119	REV C	TITLE:	
		SOLAR CELL FILTER (2 cm X 2 cm NOMINAL CELL)	REV
SHEET 2			SHEET

JPL09713 APR 65

UNCLASSIFIED

Fig A-4. (Contd)

APPENDIX B
SOLAR CELL ELECTRICAL PROPERTIES DATA

Table B-1. Maximum power, blue filter on 2 ohm-cm cell

MAXIMUM POWER (P_{MAX}, MW)

SOLAR INTENSITY (MW/CM ^{**2})	5.00	25.00	50.00	100.00	140.00	250.00	400.00	550.00	700.00	850.00
CELL TEMP. (DEG. C)										
-160.00	1.90	.00	.00	.76	.00	.00	.00	.00	.00	.00
-140.00	1.87	10.68	.00	.00	.00	.00	.00	.00	.00	.00
-120.00	1.78	10.55	23.06	.00	.00	.00	.00	.00	.00	.00
-100.00	1.80	10.67	23.48	46.79	.00	.00	.00	.00	.00	.00
-80.00	1.80	10.94	23.57	48.38	70.69	.00	.00	.00	.00	.00
-60.00	1.78	10.90	23.75	49.79	72.28	130.37	.00	.00	.00	.00
-40.00	1.73	10.65	23.26	49.55	73.06	132.26	.00	.00	.00	.00
-20.00	1.66	10.10	22.18	47.36	70.85	129.06	.00	.00	.00	.00
0.00	1.52	9.73	20.81	45.46	66.50	122.61	.00	.00	.00	.00
20.00	1.35	9.08	19.47	42.25	62.83	115.01	.00	.00	.00	.00
40.00	1.26	8.18	17.94	38.54	57.30	103.68	.00	.00	.00	.00
60.00	1.09	7.33	16.10	35.04	50.99	93.72	144.53	196.20	248.40	298.34
80.00	.00	.00	.00	.00	45.49	83.56	127.81	174.42	218.28	263.80
100.00	.00	.00	.00	.00	38.78	73.37	112.13	152.47	190.29	229.34
120.00	.00	.00	.00	.00	33.16	62.32	97.80	129.43	163.27	196.02
140.00	.00	.00	.00	.00	27.73	52.51	83.29	111.07	136.71	163.73
160.00	.00	.00	.00	.00	.00	42.99	68.73	90.56	112.28	134.51

Table B-2 Maximum-power voltage, blue filter on 2 ohm-cm cell

AVERAGE MAXIMUM POWER VOLTAGE (V_{MP}, MV)

SOLAR INTENSITY (MW/CM ^{**2})	5.00	25.00	50.00	100.00	140.00	250.00	400.00	550.00	700.00	850.00
CELL TEMP. (DEG. C)										
-160.00	604.27	.00	.00	.00	.00	.00	.00	.00	.00	.00
-140.00	589.38	665.15	.00	.00	.00	.00	.00	.00	.00	.00
-120.00	585.58	652.92	686.69	.00	.00	.00	.00	.00	.00	.00
-100.00	578.35	639.54	678.96	687.46	.00	.00	.00	.00	.00	.00
-80.00	551.73	625.54	657.23	674.00	682.81	.00	.00	.00	.00	.00
-60.00	519.98	604.08	636.46	654.14	659.31	657.23	.00	.00	.00	.00
-40.00	482.46	570.95	601.46	622.00	637.54	633.46	.00	.00	.00	.00
-20.00	442.38	527.23	565.85	581.77	597.69	601.85	.00	.00	.00	.00
0.00	403.69	486.27	522.54	541.77	548.85	560.62	.00	.00	.00	.00
20.00	361.85	440.69	472.96	495.12	512.54	519.00	.00	.00	.00	.00
40.00	315.19	398.62	430.77	450.08	463.92	473.54	.00	.00	.00	.00
60.00	276.46	357.31	388.35	405.58	419.38	426.62	427.46	425.85	419.46	413.19
80.00	.00	.00	.00	.00	373.08	381.69	384.46	380.42	379.42	375.08
100.00	.00	.00	.00	.00	327.08	337.15	344.73	341.42	339.15	336.27
120.00	.00	.00	.00	.00	282.85	293.69	302.04	296.31	300.19	296.88
140.00	.00	.00	.00	.00	237.92	251.85	261.31	257.15	261.23	258.42
160.00	.00	.00	.00	.00	.00	212.46	222.46	220.62	225.00	223.67

Table B-3. Maximum-power current, blue filter on 2 ohm-cm cell

AVERAGE MAXIMUM POWER CURRENT (IMP. MA)										
SOLAR INTENSITY TWH/CM ²	5.00	25.00	50.00	100.00	140.00	250.00	400.00	550.00	700.00	850.00
CELL TEMP. (DEG. C)										
-160.00	3.11	.00	.00	.00	.00	.00	.00	.00	.00	.00
-140.00	3.15	16.02	.00	.00	.00	.00	.00	.00	.00	.00
-120.00	3.01	16.13	33.52	.00	.00	.00	.00	.00	.00	.00
-100.00	3.11	16.66	34.75	68.02	.00	.00	.00	.00	.00	.00
-80.00	3.24	17.48	35.83	71.73	103.45	.00	.00	.00	.00	.00
-60.00	3.43	18.03	37.30	76.10	109.59	198.31	.00	.00	.00	.00
-40.00	3.59	18.65	38.66	79.65	114.57	208.73	.00	.00	.00	.00
-20.00	3.74	19.16	39.20	81.42	118.55	214.42	.00	.00	.00	.00
+00	3.76	20.01	39.83	83.91	121.17	218.69	.00	.00	.00	.00
20.00	3.73	20.59	41.17	85.33	122.59	221.62	.00	.00	.00	.00
40.00	4.01	20.52	41.65	85.62	123.52	218.96	.00	.00	.00	.00
60.00	3.94	20.51	41.45	85.40	121.80	219.81	338.13	460.81	592.12	721.69
80.00	.00	.00	.00	121.94	218.96	332.45	458.52	575.15	702.92	
100.00	.00	.00	.00	118.60	217.62	325.27	446.42	560.81	681.38	
120.00	.00	.00	.00	117.27	212.15	323.76	436.73	543.54	659.54	
140.00	.00	.00	.00	116.59	208.54	318.69	431.96	522.85	633.00	
160.00	.00	.00	.00	.00	202.38	308.80	410.19	496.15	600.77	

NOT REPRODUCIBLE

Table B-4. Open-circuit voltage, blue filter on 2 ohm-cm cell

AVERAGE OPEN CIRCUIT VOLTAGE (VOC. MV)										
SOLAR INTENSITY TWH/CM ²	5.00	25.00	50.00	100.00	140.00	250.00	400.00	550.00	700.00	850.00
CELL TEMP. (DEG. C)										
-160.00	934.48	.00	.00	.00	.00	.00	.00	.00	.00	.00
-140.00	801.05	866.82	.00	.00	.00	.00	.00	.00	.00	.00
-120.00	772.26	837.71	849.79	.00	.00	.00	.00	.00	.00	.00
-100.00	735.09	805.89	824.37	830.75	.00	.00	.00	.00	.00	.00
-80.00	693.93	765.08	785.50	800.18	808.45	.00	.00	.00	.00	.00
-60.00	653.18	725.24	746.55	765.28	771.95	786.66	.00	.00	.00	.00
-40.00	608.94	681.56	705.83	724.30	737.19	752.17	.00	.00	.00	.00
-20.00	565.64	637.40	661.98	682.20	696.16	713.61	.00	.00	.00	.00
+00	519.85	591.68	617.92	640.62	653.12	671.95	.00	.00	.00	.00
20.00	473.01	547.15	572.38	596.75	609.85	629.41	.00	.00	.00	.00
40.00	427.12	500.85	526.35	549.89	564.43	585.13	.00	.00	.00	.00
60.00	378.13	453.61	480.29	504.73	518.80	541.20	553.63	564.43	572.46	580.38
80.00	.00	.00	.00	.00	471.67	495.48	509.54	519.92	529.52	537.30
100.00	.00	.00	.00	.00	425.38	449.98	466.34	477.19	486.61	493.28
120.00	.00	.00	.00	.00	379.29	403.94	422.49	432.59	442.65	450.24
140.00	.00	.00	.00	.00	333.72	357.35	378.30	389.32	398.93	406.40
160.00	.00	.00	.00	.00	.00	312.08	333.28	344.88	354.88	362.48

Table B-5 Short-circuit current, blue filter on 2 ohm-cm cell

AVERAGE SHORT CIRCUIT CURRENT (ISC, MA)										
SOLAR INTENSITY (MW/CM**2)	5.00	25.00	50.00	100.00	140.00	250.00	400.00	550.00	700.00	850.00
CELL TEMP. (DEG. C)										
-160.00	3.62	.00	.00	.00	.00	.00	.00	.00	.00	.00
-140.00	3.67	17.72	.00	.00	.00	.00	.00	.00	.00	.00
-120.00	3.53	17.87	36.69	.00	.00	.00	.00	.00	.00	.00
-100.00	3.62	18.29	37.63	73.79	.00	.00	.00	.00	.00	.00
-80.00	3.77	19.18	38.75	77.18	109.62	.00	.00	.00	.00	.00
-60.00	3.95	19.81	40.48	81.93	116.12	209.25	.00	.00	.00	.00
-40.00	4.13	20.79	42.16	85.51	121.98	221.10	.00	.00	.00	.00
-20.00	4.33	21.25	93.16	88.30	126.05	228.45	.00	.00	.00	.00
-0.00	4.41	22.39	43.91	91.96	129.33	234.35	.00	.00	.00	.00
20.00	4.46	23.23	45.39	93.45	133.09	239.20	.00	.00	.00	.00
40.00	4.86	23.55	46.51	94.93	134.85	239.11	.00	.00	.00	.00
60.00	4.90	23.83	47.17	95.77	134.16	292.15	374.47	514.25	672.31	835.33
80.00	.00	.00	.00	.00	136.29	245.89	377.79	521.71	672.77	842.89
100.00	.00	.00	.00	.00	136.02	249.67	378.58	525.68	676.17	850.05
120.00	.00	.00	.00	.00	137.28	249.62	387.15	526.78	683.42	856.10
140.00	.00	.00	.00	.00	139.15	252.56	395.12	537.79	679.29	857.11
160.00	.00	.00	.00	.00	.00	255.21	398.19	532.66	685.62	860.26

Table B-6. Maximum power, blue-red filter on 2 ohm-cm cell

AVERAGE MAXIMUM POWER (PMAX, MW)						
SOLAR INTENSITY (MW/CM**2)	140.00	265.70	400.00	550.00	700.00	850.00
CELL TEMP. (DEG. C)						
-40.00	69.46	.00	.00	.00	.00	.00
-20.00	65.38	.00	.00	.00	.00	.00
-0.00	62.19	117.45	.00	.00	.00	.00
20.00	57.06	178.35	.00	.00	.00	.00
40.00	51.29	97.92	147.77	.00	.00	.00
60.00	.00	89.30	135.24	181.57	.00	.00
80.00	.00	.00	110.32	160.10	194.78	.00
100.00	.00	.00	104.15	139.03	167.52	.00
120.00	.00	.00	.00	118.36	141.11	168.41
140.00	.00	.00	.00	.00	118.34	140.97
160.00	.00	.00	.00	.00	94.81	112.84

Table B-7. Maximum-power voltage, blue-red filter on 2 ohm-cm cell

AVERAGE MAXIMUM POWER VOLTAGE (VMPP, MV)						
SOLAR INTENSITY (MW/CM**2)	140.00	265.70	400.00	550.00	700.00	850.00
CELL TEMP. (DEG. C)						
-40.00	543.00	.00	.00	.00	.00	.00
-20.00	593.37	.00	.00	.00	.00	.00
-0.00	544.75	550.75	.00	.00	.00	.00
20.00	503.12	510.75	.00	.00	.00	.00
40.00	453.75	457.00	456.00	.00	.00	.00
60.00	.00	415.50	415.62	410.50	.00	.00
80.00	.00	.00	359.00	366.13	363.31	.00
100.00	.00	.00	320.56	326.00	327.50	.00
120.00	.00	.00	.00	297.00	287.06	285.44
140.00	.00	.00	.00	.00	248.50	249.31
160.00	.00	.00	.00	.00	208.75	210.63

Table B-8. Maximum-power current, blue-red filter on 2 ohm-cm cell

AVERAGE MAXIMUM POWER CURRENT (IMP·MA)						
SOLAR INTENSITY (MW/CM**2)	140.00	265.70	400.00	550.00	700.00	850.00
CELL TEMP. (DEG. C)						
-40.00	108.01	.00	.00	.00	.00	.00
-20.00	110.19	.00	.00	.00	.00	.00
.00	114.16	213.25	.00	.00	.00	.00
20.00	113.41	212.13	.00	.00	.00	.00
40.00	113.04	214.25	324.00	.00	.00	.00
60.00	.00	212.50	325.31	442.75	.00	.00
80.00	.00	.00	323.29	437.13	535.75	.00
100.00	.00	.00	317.13	426.25	511.12	.00
120.00	.00	.00	.00	412.12	491.00	589.31
140.00	.00	.00	.00	.00	475.88	565.00
160.00	.00	.00	.00	.00	453.88	534.87

Table B-9 Open-circuit voltage, blue-red filter on 2 ohm-cm cell

AVERAGE OPEN CIRCUIT VOLTAGE (VOC·MV)						
SOLAR INTENSITY (MW/CM**2)	140.00	265.70	400.00	550.00	700.00	850.00
CELL TEMP. (DEG. C)						
-40.00	735.70	.00	.00	.00	.00	.00
-20.00	592.84	.00	.00	.00	.00	.00
.00	549.42	667.94	.00	.00	.00	.00
20.00	505.72	624.74	.00	.00	.00	.00
40.00	558.74	580.02	592.86	.00	.00	.00
60.00	.00	535.87	550.90	561.21	.00	.00
80.00	.00	.00	505.47	517.87	525.71	.00
100.00	.00	.00	461.76	473.39	482.21	.00
120.00	.00	.00	.00	427.31	436.35	443.84
140.00	.00	.00	.00	.00	391.39	400.17
160.00	.00	.00	.00	.00	346.01	353.71

Table B-10. Short-circuit current, blue-red filter on 2 ohm-cm cell

AVERAGE SHORT CIRCUIT CURRENT (ISC·MA)						
SOLAR INTENSITY (MW/CM**2)	140.00	265.70	400.00	550.00	700.00	850.00
CELL TEMP. (DEG. C)						
-40.00	114.71	.00	.00	.00	.00	.00
-20.00	116.40	.00	.00	.00	.00	.00
.00	120.74	226.36	.00	.00	.00	.00
20.00	122.37	229.66	.00	.00	.00	.00
40.00	123.12	231.96	359.72	.00	.00	.00
60.00	.00	233.74	352.99	505.25	.00	.00
80.00	.00	.00	365.87	508.51	635.27	.00
100.00	.00	.00	368.21	511.99	636.49	.00
120.00	.00	.00	.00	512.95	636.89	730.16
140.00	.00	.00	.00	.00	540.24	786.92
160.00	.00	.00	.00	.00	633.00	772.31

Table B-11. Maximum power, blue-red filter on 10 ohm-cm cell

AVERAGE MAXIMUM POWER (P _{MAX} , MW)						
SOLAR INTENSITY (MW/CM**2)	140.00	265.70	400.00	550.00	700.00	850.00
CELL TEMP. (DEG. C)						
-40.00	67.65	.00	.00	.00	.00	.00
-20.00	64.95	.00	.00	.00	.00	.00
.00	62.19	113.82	.00	.00	.00	.00
20.00	56.86	105.00	.00	.00	.00	.00
40.00	50.87	94.88	135.19	.00	.00	.00
60.00	.00	83.56	120.71	155.24	.00	.00
80.00	.00	.00	103.06	132.27	155.36	.00
100.00	.00	.00	85.07	109.65	129.05	.00
120.00	.00	.00	.00	87.97	101.99	116.63
140.00	.00	.00	.00	.00	78.65	90.27
160.00	.00	.00	.00	.00	58.16	66.38

Table B-12. Maximum-power voltage, blue-red filter on 10 ohm-cm cell

AVERAGE MAXIMUM POWER VOLTAGE (V _{MP} , MV)						
SOLAR INTENSITY (MW/CM**2)	140.00	265.70	400.00	550.00	700.00	850.00
CELL TEMP. (DEG. C)						
-40.00	582.20	.00	.00	.00	.00	.00
-20.00	547.40	.00	.00	.00	.00	.00
.00	507.50	498.10	.00	.00	.00	.00
20.00	462.00	453.80	.00	.00	.00	.00
40.00	412.00	410.10	401.20	.00	.00	.00
60.00	.00	352.40	355.20	345.20	.00	.00
80.00	.00	.00	314.90	303.40	306.40	.00
100.00	.00	.00	259.40	252.00	255.30	.00
120.00	.00	.00	.00	231.40	230.00	227.90
140.00	.00	.00	.00	.00	193.70	191.40
160.00	.00	.00	.00	.00	158.00	161.50

Table B-13. Maximum-power current, blue-red filter on 10 ohm-cm cell

AVERAGE MAXIMUM POWER CURRENT (I _{MP} , MA)						
SOLAR INTENSITY (MW/CM**2)	140.00	265.70	400.00	550.00	700.00	850.00
CELL TEMP. (DEG. C)						
-40.00	116.24	.00	.00	.00	.00	.00
-20.00	118.66	.00	.00	.00	.00	.00
.00	122.56	228.52	.00	.00	.00	.00
20.00	123.08	231.40	.00	.00	.00	.00
40.00	123.38	231.40	327.00	.00	.00	.00
60.00	.00	230.60	337.80	448.40	.00	.00
80.00	.00	.00	327.30	436.00	507.00	.00
100.00	.00	.00	315.80	418.60	486.60	.00
120.00	.00	.00	.00	380.00	443.40	511.80
140.00	.00	.00	.00	.00	406.00	471.80
160.00	.00	.00	.00	.00	368.00	411.20

Table B-14. Open-circuit voltage, blue-red filter on 10 ohm-cm cell

AVERAGE OPEN CIRCUIT VOLTAGE (VOC, MV)						
SOLAR INTENSITY (MW/CM**2)	140.00	265.70	400.00	550.00	700.00	850.00
<hr/>						
CELL TEMP. (DEG. C)						
-40.00	599.28	.00	.00	.00	.00	.00
-20.00	562.02	.00	.00	.00	.00	.00
.00	518.78	631.78	.00	.00	.00	.00
20.00	573.92	589.18	.00	.00	.00	.07
40.00	525.39	543.00	552.06	.00	.00	.00
50.00	.00	496.00	507.30	515.28	.00	.00
80.00	.00	.00	459.50	468.50	475.44	.00
100.00	.00	.00	411.96	420.96	429.22	.00
120.00	.00	.00	.00	371.76	778.92	384.44
140.00	.00	.00	.00	.00	330.34	337.06
160.00	.00	.00	.00	.00	281.28	287.30

Table B-15. Short-circuit current, blue-red filter on 10 ohm-cm cell

AVERAGE SHORT CIRCUIT CURRENT (ISC, MA)						
SOLAR INTENSITY (MW/CM**2)	140.00	265.70	400.00	550.00	700.00	850.00
<hr/>						
CELL TEMP. (DEG. C)						
-40.00	125.68	.00	.00	.00	.00	.00
-20.00	127.94	.00	.00	.00	.00	.00
.00	132.72	250.97	.00	.00	.00	.00
20.00	134.45	255.12	.00	.00	.00	.00
40.00	135.50	257.78	389.52	.00	.00	.00
50.00	.00	260.22	399.10	557.44	.00	.00
80.00	.00	.00	402.80	559.48	695.56	.00
100.00	.00	.00	403.38	558.52	688.94	.00
120.00	.00	.00	.00	553.02	674.14	805.88
140.00	.00	.00	.00	.00	549.70	765.18
160.00	.00	.00	.00	.00	605.54	698.00

NOT REPRODUCIBLE

Table B-16. Maximum power, 4024 filter on 2 ohm-cm cell

AVERAGE MAXIMUM POWER (PMAX, MW)						
SOLAR INTENSITY (MW/CM**2)	140.00	250.00	400.00	550.00	700.00	850.00
<hr/>						
CELL TEMP. (DEG. C)						
-40.00	50.04	.00	.00	.00	.00	.00
-20.00	47.45	.00	.00	.00	.00	.00
.00	44.02	81.34	.00	.00	.00	.00
20.00	41.00	75.23	.00	.00	.00	.00
40.00	37.52	68.09	102.15	.00	.00	.00
50.00	.00	60.68	91.93	125.24	.00	.00
80.00	.00	.00	80.03	112.76	139.17	.00
100.00	.00	.00	71.91	97.22	122.40	.00
120.00	.00	.00	.00	93.39	163.64	125.49
140.00	.00	.00	.00	.00	82.28	105.33
160.00	.00	.00	.00	.00	71.29	94.41

Table B-17. Maximum-power voltage, 4024 filter on 2 ohm-cm cell

AVERAGF MAXIMUM POWER VOLTAGE (VMP,MV)						
SOLAR INTENSITY (MW/CM**2)	140.00	250.00	400.00	550.00	700.00	850.00
CELL TEMP. (DEG. C)						
-40.00	630.17	.00	.00	.00	.00	.00
-20.00	588.25	.00	.00	.00	.00	.00
.00	542.00	549.63	.00	.00	.00	.00
20.00	493.53	509.50	.00	.00	.00	.00
40.00	445.08	447.75	464.38	.00	.00	.00
60.00	.00	410.50	410.25	410.50	.00	.00
80.00	.00	.00	371.25	376.50	368.75	.00
100.00	.00	.00	329.37	329.01	332.50	.00
120.00	.00	.00	.00	284.00	292.00	287.00
140.00	.00	.00	.00	.00	253.75	251.38
160.00	.00	.00	.00	.00	206.50	210.75

Table B-18. Maximum-power current, 4024 filter on 2 ohm-cm cell

AVERAGF MAXIMUM POWER CURRENT (IMP,MA)						
SOLAR INTENSITY (MW/CM**2)	140.00	250.00	400.00	550.00	700.00	850.00
CELL TEMP. (DEG. C)						
-40.00	79.40	.00	.00	.00	.00	.00
-20.00	80.80	.00	.00	.00	.00	.00
.00	82.95	149.00	.00	.00	.00	.00
20.00	83.22	147.25	.00	.00	.00	.00
40.00	84.17	152.25	220.00	.00	.00	.00
60.00	.00	147.95	210.25	300.00	.00	.00
80.00	.00	.00	210.00	297.75	377.50	.00
100.00	.00	.00	215.63	295.50	368.25	.00
120.00	.00	.00	.00	293.83	355.30	437.25
140.00	.00	.00	.00	.00	348.00	419.25
160.00	.00	.00	.00	.00	245.50	400.50

Table B-19. Open-circuit voltage, 4024 filter on 2 ohm-cm cell

AVERAGF OPEN CIRCUIT VOLTAGE (VOC,MV)						
SOLAR INTENSITY (MW/CM**2)	140.00	250.00	400.00	550.00	700.00	850.00
CELL TEMP. (DEG. C)						
-40.00	727.67	.00	.00	.00	.00	.00
-20.00	584.85	.00	.00	.00	.00	.00
.00	640.32	656.90	.00	.00	.00	.00
20.00	594.25	612.40	.00	.00	.00	.00
40.00	550.20	566.55	582.07	.00	.00	.00
60.00	.00	521.72	538.67	550.97	.00	.00
80.00	.00	.00	493.30	506.10	513.55	.00
100.00	.00	.00	448.17	463.00	470.83	.00
120.00	.00	.00	.00	415.17	424.58	434.12
140.00	.00	.00	.00	.00	384.08	390.42
160.00	.00	.00	.00	.00	336.95	343.47

Table B-20. Short-circuit current, 4024 filter on 2 ohm-cm cell

AVERAGE SHORT CIRCUIT CURRENT (ISC, MA)						
SOLAR INTENSITY (MW/CM**2)	140.00	250.00	400.00	550.00	700.00	850.00
CELL TEMP. (DEG. C)						
-40.00	87.60	.00	.00	.00	.00	.00
-20.00	88.70	.00	.00	.00	.00	.00
.00	89.50	159.47	.00	.00	.00	.00
-20.00	90.42	151.02	.00	.00	.00	.00
40.00	91.57	162.70	241.45	.00	.00	.00
60.00	.00	163.35	247.50	337.15	.00	.00
80.00	.00	.00	243.80	339.77	436.22	.00
100.00	.00	.00	246.40	342.65	441.10	.00
120.00	.00	.00	.00	348.97	441.55	545.52
140.00	.00	.00	.00	.00	448.85	547.75
160.00	.00	.00	.00	.00	450.00	545.52

Table B-21. Maximum power, 4025 filter on 2 ohm-cm cell

AVERAGE MAXIMUM POWER (P _{MAX} , MW)						
SOLAR INTENSITY (MW/CM**2)	140.00	250.00	400.00	550.00	700.00	850.00
CELL TEMP. (DEG. C)						
-40.00	44.56	.00	.00	.00	.00	.00
-20.00	41.45	.00	.00	.00	.00	.00
.00	39.80	78.18	.00	.00	.00	.00
20.00	35.50	64.73	.00	.00	.00	.00
40.00	32.79	59.10	89.91	.00	.00	.00
60.00	.00	52.57	81.72	112.74	.00	.00
80.00	.00	.00	72.18	100.70	125.65	.00
100.00	.00	.00	63.15	87.65	110.74	.00
120.00	.00	.00	.00	75.60	95.02	114.63
140.00	.00	.00	.00	.00	80.77	96.91
160.00	.00	.00	.00	.00	66.76	78.44

Table B-22. Maximum-power voltage, 4025 filter on 2 ohm-cm cell

AVERAGE MAXIMUM POWER VOLTAGE (V _{MP} , MV)						
SOLAR INTENSITY (MW/CM**2)	140.00	250.00	400.00	550.00	700.00	850.00
CELL TEMP. (DEG. C)						
-40.00	523.25	.00	.00	.00	.00	.00
-20.00	582.87	.00	.00	.00	.00	.00
.00	531.00	552.12	.00	.00	.00	.00
20.00	493.53	502.25	.00	.00	.00	.00
40.00	446.75	460.12	458.50	.00	.00	.00
60.00	.00	404.00	415.75	417.50	.00	.00
80.00	.00	.00	377.75	376.63	378.75	.00
100.00	.00	.00	332.75	333.13	340.50	.00
120.00	.00	.00	.00	292.87	294.75	294.50
140.00	.00	.00	.00	.00	258.75	256.50
160.00	.00	.00	.00	.00	224.12	213.75

Table B-23. Maximum-power current, 4025 filter on 2 ohm-cm cell

AVERAGE MAXIMUM POWER CURRENT (IMP, MA)						
SOLAR INTENSITY (MW/CM**2)	140.00	250.00	400.00	550.00	700.00	850.00
CELL TEMP. (DEG. C)						
-40.00	71.50	.00	.00	.00	.00	.00
-20.00	71.15	.00	.00	.00	.00	.00
.00	73.07	127.12	.00	.00	.00	.00
20.00	71.92	128.90	.00	.00	.00	.00
40.00	72.50	128.42	196.00	.00	.00	.00
60.00	.00	130.18	196.50	269.87	.00	.00
80.00	.00	.00	191.00	267.25	331.50	.00
100.00	.00	.00	189.75	263.50	325.00	.00
120.00	.00	.00	.00	258.00	322.00	389.00
140.00	.00	.00	.00	.00	311.75	377.50
160.00	.00	.00	.00	.00	297.50	367.50

Table B-24. Open-circuit voltage, 4025 filter on 2 ohm-cm cell

AVERAGE OPEN CIRCUIT VOLTAGE (VOC, MV)						
SOLAR INTENSITY (MW/CM**2)	140.00	250.00	400.00	550.00	700.00	850.00
CELL TEMP. (DEG. C)						
-40.00	724.25	.00	.00	.00	.00	.00
-20.00	581.22	.00	.00	.00	.00	.00
.00	535.90	651.32	.00	.00	.00	.00
20.00	590.55	607.27	.00	.00	.00	.00
40.00	546.05	562.57	576.67	.00	.00	.00
60.00	.00	515.12	534.70	546.32	.00	.00
80.00	.00	.00	489.45	501.90	507.80	.00
100.00	.00	.00	444.50	457.60	464.82	.00
120.00	.00	.00	.00	410.35	419.72	427.97
140.00	.00	.00	.00	.00	378.67	386.20
160.00	.00	.00	.00	.00	332.70	337.15

Table B-25. Short-circuit current, 4025 filter on 2 ohm-cm cell

AVERAGE SHORT CIRCUIT CURRENT (ISC, MA)						
SOLAR INTENSITY (MW/CM**2)	140.00	250.00	400.00	550.00	700.00	850.00
CELL TEMP. (DEG. C)						
-40.00	74.25	.00	.00	.00	.00	.00
-20.00	75.52	.00	.00	.00	.00	.00
.00	76.47	135.97	.00	.00	.00	.00
20.00	77.60	137.72	.00	.00	.00	.00
40.00	78.52	139.33	214.20	.00	.00	.00
60.00	.00	140.30	216.27	300.60	.00	.00
80.00	.00	.00	217.12	303.47	386.85	.00
100.00	.00	.00	219.35	305.92	391.55	.00
120.00	.00	.00	.00	309.40	394.55	480.62
140.00	.00	.00	.00	.00	395.70	483.18
160.00	.00	.00	.00	.00	397.27	483.13

Table B-26. Maximum power, 4026 filter on 2 ohm-cm cell

AVERAGE MAXIMUM POWER (P _{MAX} , MW)						
SOLAR INTENSITY (MW/CM**2)	140.00	250.00	400.00	550.00	700.00	850.00
CELL TEMP. (DEG. C)						
-40.00	37.03	.00	.00	.00	.00	.00
-20.00	35.25	.00	.00	.00	.00	.00
.00	33.10	59.77	.00	.00	.00	.00
20.00	32.47	55.76	.00	.00	.00	.00
40.00	27.69	50.69	31.07	.00	.00	.00
60.00	.00	44.52	72.96	101.45	.00	.00
80.00	.00	.00	64.85	89.69	113.11	.00
100.00	.00	.00	56.08	79.17	99.00	.00
120.00	.00	.00	.00	57.45	84.18	103.56
140.00	.00	.00	.00	.00	71.64	87.89
160.00	.00	.00	.00	.00	59.74	69.99

Table B-27 Maximum-power voltage, 4026 filter on 2 ohm-cm cell

AVERAGE MAXIMUM POWER VOLTAGE (V _{MP} , MV)						
SOLAR INTENSITY (MW/CM**2)	140.00	250.00	400.00	550.00	700.00	850.00
CELL TEMP. (DEG. C)						
					NOT REPRODUCIBLE	
-40.00	627.77	.00	.00	.00	.00	.00
-20.00	592.75	.00	.00	.00	.00	.00
.00	541.52	548.12	.00	.00	.00	.00
20.00	487.50	439.75	.00	.00	.00	.00
40.00	443.17	454.75	464.50	.00	.00	.00
60.00	.00	406.53	420.00	423.50	.00	.00
80.00	.00	.00	379.25	374.88	383.00	.00
100.00	.00	.00	332.00	334.77	333.00	.00
120.00	.00	.00	.00	290.12	290.50	297.13
140.00	.00	.00	.00	.00	255.50	255.63
160.00	.00	.00	.00	.00	219.25	211.25

Table B-28 Maximum-power current, 4026 filter on 2 ohm-cm cell

AVERAGE MAXIMUM POWER CURRENT (I _{MP} , MA)						
SOLAR INTENSITY (MW/CM**2)	140.00	250.00	400.00	550.00	700.00	850.00
CELL TEMP. (DEG. C)						
-40.00	59.02	.00	.00	.00	.00	.00
-20.00	59.50	.00	.00	.00	.00	.00
.00	61.25	109.05	.00	.00	.00	.00
20.00	62.52	111.50	.00	.00	.00	.00
40.00	62.50	111.47	174.50	.00	.00	.00
60.00	.00	109.75	177.75	239.62	.00	.00
80.00	.00	.00	171.00	239.25	295.25	.00
100.00	.00	.00	162.88	237.00	297.25	.00
120.00	.00	.00	.00	232.50	289.75	353.25
140.00	.00	.00	.00	.00	280.50	343.75
160.00	.00	.00	.00	.00	273.75	331.38

Table B-29. Open-circuit voltage, 4026 filter on 2 ohm-cm cell

AVERAGE OPEN CIRCUIT VOLTAGE (VOC, MV)						
SOLAR INTENSITY (MW/CM**2)	140.00	250.00	400.00	550.00	700.00	850.00
CELL TEMP. (DEG. C.)						
-40.00	720.27	.00	.00	.00	.00	.00
-20.00	577.40	.00	.00	.00	.00	.00
0.00	531.92	647.37	.00	.00	.00	.00
20.00	585.47	603.87	.00	.00	.00	.00
40.00	540.97	557.85	573.22	.00	.00	.00
60.00	.00	509.72	520.47	543.07	.00	.00
80.00	.00	.00	483.82	497.63	504.42	.00
100.00	.00	.00	439.77	453.72	460.65	.00
120.00	.00	.00	.00	405.90	415.95	423.68
140.00	.00	.00	.00	.00	373.15	382.62
160.00	.00	.00	.00	.00	328.42	333.47

Table B-30. Short-circuit current, 4026 filter on 2 ohm-cm cell

AVERAGE SHORT CIRCUIT CURRENT (ISC, MA)						
SOLAR INTENSITY (MW/CM**2)	140.00	250.00	400.00	550.00	700.00	850.00
CELL TEMP. (DEG. C.)						
-40.00	63.27	.00	.00	.00	.00	.00
-20.00	64.52	.00	.00	.00	.00	.00
0.00	65.50	115.72	.00	.00	.00	.00
20.00	56.57	117.35	.00	.00	.00	.00
40.00	67.40	118.72	189.17	.00	.00	.00
60.00	.00	119.25	191.28	264.85	.00	.00
80.00	.00	.00	192.55	267.77	341.40	.00
100.00	.00	.00	194.12	263.63	344.37	.00
120.00	.00	.00	.00	272.87	347.27	427.50
140.00	.00	.00	.00	.00	251.52	434.45
160.00	.00	.00	.00	.00	355.32	429.88

Table B-31. Maximum power, modified 4026 filter on 2 ohm-cm cell

AVERAGE MAXIMUM POWER (PMAX, MW)						
SOLAR INTENSITY (MW/CM**2)	140.00	250.00	400.00	550.00	700.00	850.00
CELL TEMP. (DEG. C.)						
-40.00	37.96	.00	.00	.00	.00	.00
-20.00	35.86	.00	.00	.00	.00	.00
0.00	33.61	62.09	.00	.00	.00	.00
20.00	30.89	57.12	.00	.00	.00	.00
40.00	28.17	52.02	85.45	.00	.00	.00
60.00	.00	46.79	77.25	108.53	.00	.00
80.00	.00	.00	67.81	96.24	118.98	.00
100.00	.00	.00	59.44	84.37	105.04	.00
120.00	.00	.00	.00	72.45	89.12	109.03
140.00	.00	.00	.00	.00	74.30	90.65
160.00	.00	.00	.00	.00	60.73	74.20

Table B-32. Maximum-power voltage, modified 4026 filter on 2 ohm-cm cell

AVERAGE MAXIMUM POWER VOLTAGE (VMP, MV)						
SOLAR INTENSITY (MW/CM**2)	140.00	250.00	400.00	550.00	700.00	850.00
CELL TEMP. (DEG. C)						
-40.00	633.75	.00	.00	.00	.00	.00
-20.00	584.87	.00	.00	.00	.00	.00
.00	542.50	551.50	.00	.00	.00	.00
20.00	488.25	504.75	.00	.00	.00	.00
40.00	445.00	459.25	469.13	.00	.00	.00
60.00	.00	413.50	425.37	425.63	.00	.00
80.00	.00	.00	377.63	383.63	381.00	.00
100.00	.00	.00	336.50	342.12	342.12	.00
120.00	.00	.00	.00	297.38	293.50	295.75
140.00	.00	.00	.00	.00	250.75	258.87
160.00	.00	.00	.00	.00	212.88	217.75

Table B-33. Maximum-power current, modified 4026 filter on 2 ohm-cm cell

AVERAGE MAXIMUM POWER CURRENT (IMP, MA)						
SOLAR INTENSITY (MW/CM**2)	140.00	250.00	400.00	550.00	700.00	850.00
CELL TEMP. (DEG. C)						
-40.00	59.90	.00	.00	.00	.00	.00
-20.00	61.32	.00	.00	.00	.00	.00
.00	61.95	112.60	.00	.00	.00	.00
20.00	63.27	113.17	.00	.00	.00	.00
40.00	63.30	113.27	182.15	.00	.00	.00
60.00	.00	113.17	181.63	255.00	.00	.00
80.00	.00	.00	179.57	250.88	312.25	.00
100.00	.00	.00	176.62	246.62	307.00	.00
120.00	.00	.00	.00	243.63	303.63	368.63
140.00	.00	.00	.00	.00	296.37	350.12
160.00	.00	.00	.00	.00	285.25	340.75

Table B-34. Open-circuit voltage, modified 4026 filter on 2 ohm-cm cell

AVERAGE OPEN CIRCUIT VOLTAGE (VOC, MV)						
SOLAR INTENSITY (MW/CM**2)	140.00	250.00	400.00	550.00	700.00	850.00
CELL TEMP. (DEG. C)						
-40.00	722.65	.00	.00	.00	.00	.00
-20.00	678.55	.00	.00	.00	.00	.00
.00	633.97	652.45	.00	.00	.00	.00
20.00	587.05	607.17	.00	.00	.00	.01
40.00	541.90	562.17	578.60	.00	.00	.00
60.00	.00	515.87	534.15	547.12	.00	.00
80.00	.00	.00	487.30	501.62	510.35	.00
100.00	.00	.00	441.47	456.37	465.42	.00
120.00	.00	.00	.00	409.90	418.30	428.47
140.00	.00	.00	.00	.00	372.45	382.40
160.00	.00	.00	.00	.00	326.45	336.35

Table B-35. Short-circuit current, modified 4026 filter on 2 ohm-cm cell

AVERAGE SHORT CIRCUIT CURRENT (ISC, MA)						
SOLAR INTENSITY (MW/CM**2)	140.00	250.00	400.00	550.00	700.00	850.00
CELL TEMP. (DEG. C)						
-40.00	63.92	.00	.00	.00	.00	.00
-20.00	65.50	.00	.00	.00	.00	.00
0.00	66.77	119.67	.00	.00	.00	.00
20.00	67.87	121.67	.00	.00	.00	.00
40.00	68.87	123.27	198.27	.00	.00	.00
60.00	.00	125.15	200.45	280.12	.00	.00
80.00	.00	.00	202.07	283.05	350.52	.00
100.00	.00	.00	204.22	286.10	354.17	.00
120.00	.00	.00	.00	289.42	357.67	438.63
140.00	.00	.00	.00	.00	358.97	440.91
160.00	.00	.00	.00	.00	359.88	441.28

Table B-36. Maximum power, blue filter with mirror stripes on 2 ohm-cm cell

AVERAGE MAXIMUM POWER (PMAX, MW)						
SOLAR INTENSITY (MW/CM**2)	140.00	250.00	400.00	550.00	700.00	850.00
CELL TEMP. (DEG. C)						
-40.00	22.21	.00	.00	.00	.00	.00
-20.00	20.98	.00	.00	.00	.00	.00
0.00	20.04	38.00	.00	.00	.00	.00
20.00	18.23	34.76	.00	.00	.00	.00
40.00	16.43	31.43	51.45	.00	.00	.00
60.00	.00	28.35	46.54	63.76	.00	.00
80.00	.00	.00	41.30	56.67	70.86	.00
100.00	.00	.00	36.98	49.90	61.97	.00
120.00	.00	.00	.00	42.56	52.36	65.51
140.00	.00	.00	.00	.00	43.93	54.59
160.00	.00	.00	.00	.00	34.98	43.26

Table B-37. Maximum-power voltage, blue filter with mirror stripes on 2 ohm-cm cell

AVERAGE MAXIMUM POWER VOLTAGE (VMPP, MV)						
SOLAR INTENSITY (MW/CM**2)	140.00	250.00	400.00	550.00	700.00	850.00
CELL TEMP. (DEG. C)						
-40.00	608.40	.00	.00	.00	.00	.00
-20.00	571.50	.00	.00	.00	.00	.00
0.00	525.10	541.30	.00	.00	.00	.00
20.00	477.10	492.70	.00	.00	.00	.00
40.00	427.60	446.60	458.90	.00	.00	.00
60.00	.00	398.30	410.90	417.00	.00	.00
80.00	.00	.00	363.70	370.90	375.70	.00
100.00	.00	.00	320.00	324.90	328.80	.00
120.00	.00	.00	.00	287.20	284.40	282.70
140.00	.00	.00	.00	.00	243.80	241.00
160.00	.00	.00	.00	.00	202.40	203.10

Table B-38. Maximum-power current, blue filter with mirror stripes on 2 ohm-cm cell

AVERAGE MAXIMUM POWER CURRENT (IMP·MA)						
SOLAR INTENSITY (MW/CM**2)	140.00	250.00	400.00	550.00	700.00	850.00
CELL TEMP. (DEG. C)						
-40.00	36.50	.00	.00	.00	.00	.00
-20.00	36.70	.00	.00	.00	.00	.00
0.00	38.16	70.20	.00	.00	.00	.00
20.00	38.20	70.54	.00	.00	.00	.00
40.00	38.42	70.38	112.12	.00	.00	.00
60.00	.00	71.16	113.26	152.90	.00	.00
80.00	.00	.00	113.56	152.80	188.60	.00
100.00	.00	.00	113.88	153.60	188.50	.00
120.00	.00	.00	.00	148.20	184.10	231.70
140.00	.00	.00	.00	.00	180.20	226.50
160.00	.00	.00	.00	.00	172.80	213.00

Table B-39. Open-circuit voltage, blue filter with mirror stripes on 2 ohm-cm cell

AVERAGE OPEN CIRCUIT VOLTAGE (VOC·MV)						
SOLAR INTENSITY (MW/CM**2)	140.00	250.00	400.00	550.00	700.00	850.00
CELL TEMP. (DEG. C)						
-40.00	705.02	.00	.00	.00	.00	.00
-20.00	660.10	.00	.00	.00	.00	.00
0.00	615.26	633.48	.00	.00	.00	.00
20.00	569.68	588.82	.00	.00	.00	.00
40.00	521.92	542.16	558.22	.00	.00	.00
60.00	.00	496.26	513.00	522.80	.00	.00
80.00	.00	.00	465.38	477.60	484.94	.00
100.00	.00	.00	420.34	431.20	439.86	.00
120.00	.00	.00	.00	385.84	392.84	401.78
140.00	.00	.00	.00	.00	347.90	357.06
160.00	.00	.00	.00	.00	301.54	310.28

Table B-40. Short-circuit current, blue filter with mirror stripes on 2 ohm-cm cell

AVERAGE SHORT CIRCUIT CURRENT (ISC·MA)						
SOLAR INTENSITY (MW/CM**2)	140.00	250.00	400.00	550.00	700.00	850.00
CELL TEMP. (DEG. C)						
-40.00	38.46	.00	.00	.00	.00	.00
-20.00	39.24	.00	.00	.00	.00	.00
0.00	41.04	75.12	.00	.00	.00	.00
20.00	41.46	76.00	.00	.00	.00	.00
40.00	41.78	76.72	122.12	.00	.00	.00
60.00	.00	77.82	123.72	168.64	.00	.00
80.00	.00	.00	126.10	170.74	214.00	.00
100.00	.00	.00	128.64	174.52	216.22	.00
120.00	.00	.00	.00	176.14	218.42	274.74
140.00	.00	.00	.00	.00	220.72	277.78
160.00	.00	.00	.00	.00	222.84	277.10

Table B-41. Maximum power, blue filter with mirror bar by contact on 2 ohm-cm cell

AVERAGE MAXIMUM POWER (P _{MAX} , W)						
SOLAR INTENSITY (MW/CM**2)	140.00	250.00	400.00	550.00	700.00	850.00
CELL TEMP. (DEG. C)						
-40.00	22.69	.00	.00	.00	.36	.00
-20.00	21.72	.00	.00	.00	.36	.00
0.00	20.67	78.99	.00	.00	.36	.00
20.00	18.90	75.59	.00	.00	.36	.00
40.00	17.10	32.39	51.26	.00	.36	.00
60.00	.00	28.87	46.00	61.05	.36	.00
80.00	.00	.00	42.57	53.81	65.65	.00
100.00	.00	.00	35.18	47.15	56.46	.00
120.00	.00	.00	.00	48.07	47.29	56.36
140.00	.00	.00	.00	.00	39.02	47.25
160.00	.00	.00	.00	.00	30.84	36.85

Table B-42. Maximum-power voltage, blue filter with mirror bar by contact on 2 ohm-cm cell

AVERAGE MAXIMUM POWER VOLTAGE (V _{MP} , MV)						
SOLAR INTENSITY (MW/CM**2)	140.00	250.00	400.00	550.00	700.00	850.00
CELL TEMP. (DEG. C)						
-40.00	603.75	.00	.00	.00	.00	.00
-20.00	559.00	.00	.00	.00	.38	.00
0.00	519.87	534.37	.00	.00	.00	.00
20.00	473.63	483.00	.00	.00	.00	.00
40.00	423.00	438.12	437.13	.00	.00	.00
60.00	.00	327.67	392.50	395.87	.00	.00
80.00	.00	.00	347.75	353.00	356.62	.00
100.00	.00	.00	307.25	310.50	312.38	.00
120.00	.00	.00	.00	273.87	272.25	267.00
140.00	.00	.00	.00	.00	230.98	231.88
160.00	.00	.00	.00	.00	194.00	194.25

Table B-43. Maximum-power current, blue filter with mirror bar by contact on 2 ohm-cm cell

AVERAGE MAXIMUM POWER CURRENT (I _{MP} , MA)						
SOLAR INTENSITY (MW/CM**2)	140.00	250.00	400.00	550.00	700.00	850.00
CELL TEMP. (DEG. C)						
-40.00	37.55	.00	.00	.00	.00	.00
-20.00	38.17	.00	.00	.00	.00	.00
0.00	33.75	72.95	.00	.00	.00	.00
20.00	39.93	73.67	.00	.00	.00	.00
40.00	40.42	73.90	117.20	.00	.00	.00
60.00	.00	74.40	117.12	154.00	.00	.00
80.00	.00	.00	116.55	152.13	183.62	.00
100.00	.00	.00	114.37	151.50	179.88	.00
120.00	.00	.00	.00	146.00	173.12	212.50
140.00	.00	.00	.00	.00	168.50	202.88
160.00	.00	.00	.00	.00	158.38	189.00

Table B-44. Open-circuit voltage, blue filter with mirror bar by contact on 2 ohm-cm cell

AVERAGE OPEN CIRCUIT VOLTAGE (VOC, MV)						
SOLAR INTENSITY (MW/CM**2)	140.00	250.00	400.00	550.00	700.00	850.00
<hr/>						
CELL TEMP. (DEG. C)						
-40.00	705.80	.00	.00	.00	.00	.00
-20.00	661.50	.00	.00	.00	.00	.00
.00	617.42	634.57	.00	.00	.00	.00
20.00	571.42	589.70	.00	.00	.00	.00
40.00	523.32	544.12	558.25	.00	.00	.00
60.00	.00	497.22	512.30	522.27	.00	.00
80.00	.00	.00	465.50	475.67	484.85	.00
100.00	.00	.00	419.77	430.70	438.52	.00
120.00	.00	.00	.00	385.22	391.30	400.40
140.00	.00	.00	.00	.00	345.67	355.20
160.00	.00	.00	.00	.00	300.35	307.47

Table B-45. Short-circuit current, blue filter with mirror bar by contact on 2 ohm-cm cell

AVERAGE SHORT CIRCUIT CURRENT (ISC, MA)						
SOLAR INTENSITY (MW/CM**2)	140.00	250.00	400.00	550.00	700.00	850.00
<hr/>						
CELL TEMP. (DEG. C)						
					NOT REPRODUCIBLE	
-40.00	41.10	.00	.00	.00	.00	.00
-20.00	42.00	.00	.00	.00	.70	.00
.00	43.70	79.65	.00	.00	.30	.00
20.00	44.07	80.57	.00	.00	.70	.00
40.00	44.52	91.55	129.92	.00	.00	.00
60.00	.00	92.72	131.50	179.50	.00	.00
80.00	.00	.00	134.35	182.05	223.10	.00
100.00	.00	.00	136.92	186.30	229.65	.00
120.00	.00	.00	.00	188.70	230.50	287.70
140.00	.00	.00	.00	.00	229.82	285.15
160.00	.00	.00	.00	.00	228.40	277.37

Table B-46. Maximum power, blue filter with mirror bar opposite contact on 2 ohm-cm cell

AVERAGE MAXIMUM DCWFP (PMAX, MW)						
SOLAR INTENSITY (MW/CM**2)	140.00	250.00	400.00	550.00	700.00	850.00
<hr/>						
CELL TEMP. (DEG. C)						
-40.00	22.66	.00	.00	.00	.00	.00
-20.00	21.61	.00	.00	.00	.00	.00
.00	20.64	38.62	.00	.00	.00	.00
20.00	18.95	35.65	.00	.00	.00	.00
40.00	17.16	32.46	54.66	.00	.00	.00
60.00	.00	29.35	49.58	58.13	.00	.00
80.00	.00	.00	44.22	60.89	76.85	.00
100.00	.00	.00	39.19	53.62	66.91	.00
120.00	.00	.00	.00	46.23	57.10	71.91
140.00	.00	.00	.00	.00	48.15	60.53
160.00	.00	.00	.00	.00	39.24	48.85

Table B-47. Maximum-power voltage, blue filter with mirror bar opposite contact on 2 ohm-cm cell

AVERAGE MAXIMUM POWER VOLTAGE (V _{MP} , MV)						
SOLAR INTENSITY (MW/CM ^{**2})	140.00	250.00	400.00	550.00	700.00	850.00
CELL TEMP. (DEG. C)						
-40.00	613.75	.00	.00	.00	.00	.00
-20.00	568.50	.00	.00	.00	.00	.00
.00	528.50	544.87	.00	.00	.00	.00
20.00	481.38	498.75	.00	.00	.00	.00
40.00	432.50	450.00	465.25	.00	.00	.00
60.00	.00	477.63	417.50	424.50	.00	.00
80.00	.00	.00	374.75	383.88	387.13	.00
100.00	.00	.00	330.25	327.75	345.13	.00
120.00	.00	.00	.00	294.00	296.00	293.50
140.00	.00	.00	.00	.00	255.13	255.13
160.00	.00	.00	.00	.00	210.25	215.63

Table B-48. Maximum-power current, blue filter with mirror bar opposite contact on 2 ohm-cm cell

AVERAGE MAXIMUM POWER CURRENT (I _{MP} , MA)						
SOLAR INTENSITY (MW/CM ^{**2})	140.00	250.00	400.00	550.00	700.00	850.00
CELL TEMP. (DEG. C)						
-40.00	36.00	.00	.00	.00	.00	.00
-20.00	38.00	.00	.00	.00	.00	.00
.00	39.55	70.87	.00	.00	.00	.00
20.00	39.35	71.47	.00	.00	.00	.00
40.00	39.57	72.12	117.47	.00	.00	.00
60.00	.00	72.00	119.00	160.50	.00	.00
80.00	.00	.00	119.00	158.02	198.50	.00
100.00	.00	.00	118.57	153.75	193.97	.00
120.00	.00	.00	.00	157.25	192.87	245.00
140.00	.00	.00	.00	.00	188.00	237.25
160.00	.00	.00	.00	.00	186.63	225.50

Table B-49. Open-circuit voltage, blue filter with mirror bar opposite contact on 2 ohm-cm cell

AVERAGE OPEN CIRCUIT VOLTAGE (V _{OC} , MV)						
SOLAR INTENSITY (MW/CM ^{**2})	140.00	250.00	400.00	550.00	700.00	850.00
CELL TEMP. (DEG. C)						
-40.00	710.25	.00	.00	.00	.00	.00
-20.00	665.10	.00	.00	.00	.00	.00
.00	621.27	638.95	.00	.00	.00	.00
20.00	575.17	595.52	.00	.00	.00	.00
40.00	528.10	549.45	567.32	.00	.00	.00
60.00	.00	503.32	522.85	532.97	.00	.00
80.00	.00	.00	475.45	487.77	497.20	.00
100.00	.00	.00	431.15	441.55	452.10	.00
120.00	.00	.00	.00	397.37	406.40	414.60
140.00	.00	.00	.00	.00	360.85	370.37
160.00	.00	.00	.00	.00	314.65	323.27

Table B-50. Short-circuit current, blue filter with mirror bar opposite contact on 2 ohm-cm cell

AVERAGE SHORT CIRCUIT CURRENT (ISC, mA)						
SOLAR INTENSITY (MW/CM**2)	140.00	250.00	400.00	550.00	700.00	850.00
CELL TEMP. (DEG. C)						
-40.00	40.57	.90	.30	.00	.00	.00
-20.00	41.30	.00	.90	.00	.00	.00
.00	42.97	76.85	.70	.00	.00	.00
20.00	43.35	77.55	.00	.00	.00	.00
40.00	43.87	78.30	127.55	.00	.00	.00
60.00	.00	79.47	129.12	175.25	.00	.00
80.00	.00	.00	131.43	178.02	222.90	.00
100.00	.00	.00	134.00	181.42	225.02	.00
120.00	.00	.00	.00	182.40	226.82	287.62
140.00	.00	.00	.00	.00	229.23	289.65
160.00	.00	.00	.00	.00	233.50	289.72

Table B-51. Maximum power, blue-red filter on 2 ohm-cm multiple wide-grid cell

AVERAGE MAXIMUM POWER (PMP, mW)						
SOLAR INTENSITY (MW/CM**2)	140.00	250.00	400.00	550.00	700.00	850.00
CELL TEMP. (DEG. C)						
-40.00	23.72	.00	.00	.00	.00	.00
-20.00	23.28	.00	.00	.00	.00	.00
.00	22.13	44.53	.00	.00	.00	.00
20.00	20.82	41.76	.00	.00	.00	.00
40.00	19.22	38.24	62.85	.00	.00	.00
60.00	.00	34.54	57.05	79.68	.00	.00
80.00	.00	.00	51.34	71.95	91.37	.00
100.00	.00	.00	44.94	62.36	80.57	.00
120.00	.00	.00	.00	54.12	69.61	85.85
140.00	.00	.00	.00	.00	59.16	72.99
160.00	.00	.00	.00	.00	48.81	61.13

Table B-52. Maximum-power voltage, blue-red filter on 2 ohm-cm multiple wide-grid cell

AVERAGE MAXIMUM POWER VOLTAGE (VMP, mV)						
SOLAR INTENSITY (MW/CM**2)	140.00	250.00	400.00	550.00	700.00	850.00
CELL TEMP. (DEG. C)						
-40.00	620.58	.00	.00	.00	.00	.00
-20.00	580.33	.00	.00	.00	.30	.00
.00	539.50	558.33	.00	.00	.00	.00
20.00	493.23	514.25	.00	.00	.00	.00
40.00	445.92	466.25	479.00	.00	.70	.00
60.00	.00	419.83	432.08	438.83	.00	.00
80.00	.00	.00	396.17	394.42	403.08	.00
100.00	.00	.00	340.75	349.17	360.08	.00
120.00	.00	.00	.00	307.17	313.92	318.67
140.00	.00	.00	.00	.00	269.67	277.75
160.00	.00	.00	.00	.00	231.00	237.17

Table B-53. Maximum-power current, blue-red filter on 2 ohm-cm multiple wide-grid cell

AVERAGE MAXIMUM POWER CURRENT (TMD, MA)						
SOLAR INTENSITY (MW/CM**2)	140.00	250.00	400.00	550.00	700.00	850.00
CELL TEMP. (DEG. C)						
-40.00	38.22	.00	.00	.00	.00	.00
-20.00	40.12	.00	.00	.00	.00	.00
.00	41.02	79.75	.00	.00	.00	.00
20.00	42.15	81.20	.00	.00	.00	.00
40.00	43.10	82.03	131.22	.00	.00	.00
60.00	.00	82.28	132.02	181.58	.00	.00
80.00	.00	.00	132.95	182.42	226.57	.00
100.00	.00	.00	131.88	178.53	223.75	.00
120.00	.00	.00	.00	176.17	221.75	269.42
140.00	.00	.00	.00	.00	219.33	262.83
160.00	.00	.00	.00	.00	211.25	257.75

Table B-54. Open-circuit voltage, blue-red filter on 2 ohm-cm multiple wide-grid cell

AVERAGE OPEN CIRCUIT VOLTAGE (VOC, MV)						
SOLAR INTENSITY (MW/CM**2)	140.00	250.00	400.00	550.00	700.00	850.00
CELL TEMP. (DEG. C)						
-40.00	710.52	.00	.00	.00	.00	.00
-20.00	663.27	.00	.00	.00	.00	.00
.00	624.78	644.80	.00	.00	.00	.00
20.00	578.90	600.10	.00	.00	.00	.00
40.00	531.25	553.97	570.17	.00	.00	.00
60.00	.00	508.52	524.83	535.78	.00	.00
80.00	.00	.00	478.12	490.60	499.95	.00
100.00	.00	.00	432.98	444.52	455.37	.00
120.00	.00	.00	.00	398.77	409.37	417.80
140.00	.00	.00	.00	.00	364.22	371.65
160.00	.00	.00	.00	.00	318.48	326.70

Table B-55. Short-circuit current, blue-red filter on 2 ohm-cm multiple wide-grid cell

AVERAGE SHORT CIRCUIT CURRENT (ISC, MA)						
SOLAR INTENSITY (MW/CM**2)	140.00	250.00	400.00	550.00	700.00	850.00
CELL TEMP. (DEG. C)						
-40.00	44.62	.00	.00	.00	.00	.00
-20.00	45.77	.00	.00	.00	.00	.00
.00	46.40	87.03	.00	.00	.00	.00
20.00	47.22	88.78	.00	.00	.00	.00
40.00	48.27	89.85	142.28	.00	.00	.00
60.00	.00	90.87	144.15	197.12	.00	.00
80.00	.00	.00	146.42	200.22	249.33	.00
100.00	.00	.00	147.57	200.53	251.65	.00
120.00	.00	.00	.00	202.60	253.33	307.05
140.00	.00	.00	.00	.00	255.08	309.42
160.00	.00	.00	.00	.00	255.90	310.93

Table B-56. Maximum power, blue-red filter on 2 ohm-cm single wide-grid cell

AVERAGE MAXIMUM POWER (P _{MAX} , MW)						
SOLAR INTENSITY (MW/CM ^{**2})	140.00	250.00	400.00	550.00	700.00	850.00
<hr/>						
CELL TEMP. (DEG. C)						
-40.00	23.09	.00	.00	.00	.00	.00
-20.00	22.07	.00	.00	.00	.00	.00
.00	20.82	33.75	.00	.00	.00	.00
20.00	19.29	31.04	.00	.00	.00	.00
40.00	17.37	27.90	38.21	.00	.00	.00
60.00	.00	24.61	33.70	41.28	.00	.00
80.00	.00	.00	29.30	35.59	41.70	.00
100.00	.00	.00	24.93	30.22	35.84	.00
120.00	.00	.00	.00	25.27	29.75	33.91
140.00	.00	.00	.00	.00	24.42	27.83
160.00	.00	.00	.00	.00	18.88	22.25

Table B-57 Maximum-power voltage, blue-red filter on 2 ohm-cm single wide-grid cell

AVERAGE MAXIMUM POWER VOLTAGE (V _{MP} , MV)						
SOLAR INTENSITY (MW/CM ^{**2})	140.00	250.00	400.00	550.00	700.00	850.00
<hr/>						
CELL TEMP. (DEG. C)					NOT REPRODUCIBLE	
-40.00	529.06	.00	.00	.00	.00	.00
-20.00	505.00	.00	.00	.00	.00	.00
.00	472.25	451.42	.00	.00	.00	.00
20.00	432.83	415.17	.00	.00	.00	.00
40.00	389.83	386.08	382.33	.00	.00	.00
60.00	.00	348.75	351.50	357.92	.00	.00
80.00	.00	.00	319.75	326.33	329.00	.00
100.00	.00	.00	278.92	290.17	300.67	.00
120.00	.00	.00	.00	253.83	261.92	267.50
140.00	.00	.00	.00	.00	229.08	232.33
160.00	.00	.00	.00	.00	189.25	197.17

Table B-58. Maximum-power current, blue-red filter on 2 ohm-cm single wide-grid cell

AVERAGE MAXIMUM POWER CURRENT (I _{MP} , MA)						
SOLAR INTENSITY (MW/CM ^{**2})	140.00	250.00	400.00	550.00	700.00	850.00
<hr/>						
CELL TEMP. (DEG. C)						
-40.00	43.67	.00	.00	.00	.00	.00
-20.00	43.73	.00	.00	.00	.00	.00
.00	44.10	74.75	.00	.00	.00	.00
20.00	44.57	74.75	.00	.00	.00	.00
40.00	44.57	72.25	99.93	.00	.00	.00
60.00	.00	70.58	95.88	115.33	.00	.00
80.00	.00	.00	91.63	109.02	126.75	.00
100.00	.00	.00	89.40	104.17	119.25	.00
120.00	.00	.00	.00	99.52	113.58	126.75
140.00	.00	.00	.00	.00	106.58	120.00
160.00	.00	.00	.00	.00	99.75	112.83

Table B-59. Open-circuit voltage, blue-red filter on 2 ohm-cm single wide-grid cell

AVERAGE OPEN CIRCUIT VOLTAGE (VOC, MV)						
SOLAR INTENSITY (MW/CM**2)	140.00	250.00	400.00	550.00	700.00	850.00
CELL TEMP. (DEG. C)						
-40.00	692.10	.00	.00	.00	.00	.00
-20.00	652.13	.00	.00	.00	.00	.00
.00	610.25	622.45	.00	.00	.00	.00
20.00	565.43	579.25	.00	.00	.00	.00
40.00	517.57	534.02	545.03	.00	.00	.00
60.00	.00	487.00	493.40	507.15	.00	.00
80.00	.00	.00	452.25	461.27	469.40	.00
100.00	.00	.00	405.92	414.72	424.82	.00
120.00	.00	.00	.00	368.58	376.75	383.52
140.00	.00	.00	.00	.00	331.08	336.85
160.00	.00	.00	.00	.00	284.97	291.27

Table B-60. Short-circuit current, blue-red filter on 2 ohm-cm single wide-grid cell

AVERAGE SHORT CIRCUIT CURRENT (ISC, MA)						
SOLAR INTENSITY (MW/CM**2)	140.00	250.00	400.00	550.00	700.00	850.00
CELL TEMP. (DEG. C)						
-40.00	49.13	.00	.00	.00	.00	.00
-20.00	49.88	.00	.00	.00	.00	.00
.00	50.55	92.70	.00	.00	.00	.00
20.00	51.77	94.57	.00	.00	.00	.00
40.00	52.72	95.50	150.98	.00	.00	.00
60.00	.00	96.30	149.98	189.67	.00	.00
80.00	.00	.00	147.10	181.25	212.58	.00
100.00	.00	.00	141.77	172.57	200.70	.00
120.00	.00	.00	.00	165.07	189.80	214.08
140.00	.00	.00	.00	.00	178.10	200.80
160.00	.00	.00	.00	.00	165.67	187.12

Table B-61. Maximum power, blue-red filter on 10 ohm-cm multiple wide-grid cell

AVERAGE MAXIMUM POWER (PMAX, MW)						
SOLAR INTENSITY (MW/CM**2)	140.00	250.00	400.00	550.00	700.00	850.00
CELL TEMP, (DEG. C)						
-40.00	25.84	.00	.00	.00	.00	.00
-20.00	24.75	.00	.00	.00	.00	.00
.00	22.98	42.83	.00	.00	.00	.00
20.00	21.17	39.08	.00	.00	.00	.00
40.00	19.02	35.06	59.26	.00	.00	.00
60.00	.00	31.09	52.01	73.36	.00	.00
80.00	.00	.00	44.95	63.27	79.85	.00
100.00	.00	.00	37.93	54.20	67.10	.00
120.00	.00	.00	.00	44.44	55.51	69.86
140.00	.00	.00	.00	.00	43.76	54.80
160.00	.00	.00	.00	.00	33.34	41.29

Table B-62. Maximum-power voltage, blue-red filter on 10 ohm-cm multiple wide-grid cell

AVERAGE MAXIMUM POWER VOLTAGE (VMP, MV)						
SOLAR INTENSITY (MW/CM**2)	140.00	250.00	400.00	550.00	700.00	850.00
CELL TEMP. (DEG. C)						
-40.00	594.00	.00	.00	.00	.00	.00
-20.00	554.25	.00	.00	.00	.00	.00
.00	511.25	524.12	.00	.00	.00	.00
20.00	460.63	475.88	.00	.00	.00	.00
40.00	412.62	427.63	434.00	.00	.00	.00
60.00	.00	383.12	387.50	395.87	.00	.00
80.00	.00	.00	343.87	350.87	352.25	.00
100.00	.00	.00	294.38	304.50	304.38	.00
120.00	.00	.00	.00	257.12	257.75	261.62
140.00	.00	.00	.00	.00	211.75	216.88
160.00	.00	.00	.00	.00	173.88	177.00

Table B-63. Maximum-power current, blue-red filter on 10 ohm-cm multiple wide-grid cell

AVERAGE MAXIMUM POWER CURRENT (IMP, MA)						
SOLAR INTENSITY (MW/CM**2)	140.00	250.00	400.00	550.00	700.00	850.00
CELL TEMP. (DEG. C)						
-40.00	43.50	.00	.00	.00	.00	.00
-20.00	44.65	.00	.00	.00	.00	.00
.00	44.95	81.72	.00	.00	.00	.00
20.00	45.95	82.12	.00	.00	.00	.00
40.00	46.10	81.97	136.52	.00	.00	.00
60.00	.00	81.12	134.22	185.25	.00	.00
80.00	.00	.00	130.67	180.25	226.63	.00
100.00	.00	.00	128.80	176.75	220.38	.00
120.00	.00	.00	.00	172.75	215.25	266.87
140.00	.00	.00	.00	.00	206.50	252.50
160.00	.00	.00	.00	.00	191.50	233.00

Table B-64 Open-circuit voltage, blue-red filter on 10 ohm-cm multiple wide-grid cell

AVERAGE OPEN CIRCUIT VOLTAGE (VOC, MV)						
SOLAR INTENSITY (MW/CM**2)	140.00	250.00	400.00	550.00	700.00	850.00
CELL TEMP. (DEG. C)						
-40.00	684.20	.00	.00	.00	.00	.00
-20.00	642.27	.00	.00	.00	.00	.00
.00	597.97	612.52	.00	.00	.00	.00
20.00	549.40	566.82	.00	.00	.00	.00
40.00	501.62	518.67	532.62	.00	.00	.00
60.00	.00	469.67	485.15	494.55	.00	.00
80.00	.00	.00	436.32	447.22	452.92	.00
100.00	.00	.00	384.25	398.80	406.25	.00
120.00	.00	.00	.00	348.70	355.55	364.45
140.00	.00	.00	.00	.00	305.90	314.53
160.00	.00	.00	.00	.00	255.95	264.78

Table B-65 Short-circuit current, blue-red filter on 10 ohm-cm multiple wide-grid cell

AVERAGE SHORT CIRCUIT CURRENT (ISC,MA)

SOLAR INTENSITY (MW/CM ²)	140.00	250.00	400.00	550.00	700.00	850.00
CELL TEMP. (DEG. C)						
-40.00	47.92	.00	.00	.00	.00	.00
-20.00	48.95	.00	.00	.00	.00	.00
0.00	49.57	88.35	.00	.00	.00	.00
20.00	50.42	90.17	.00	.00	.00	.00
40.00	50.82	91.07	149.15	.00	.00	.00
60.00	.00	91.62	150.33	210.97	.00	.00
80.00	.00	.00	150.57	212.25	267.07	.00
100.00	.00	.00	151.65	213.45	265.92	.00
120.00	.00	.00	.00	213.50	265.60	333.22
140.00	.00	.00	.00	.00	262.80	325.75
160.00	.00	.00	.00	.00	257.93	319.42

Table B-66 Maximum power, blue-red filter on 10 ohm-cm single wide-grid cell

AVERAGE MAXIMUM POWER (PMAX,MW)

SOLAR INTENSITY (MW/CM ²)	140.00	250.00	400.00	550.00	700.00	850.00
CELL TEMP. (DEG. C)						
-40.00	23.42	.00	.00	.00	.00	.00
-20.00	21.83	.00	.00	.00	.00	.00
0.00	20.01	31.36	.00	.00	.00	.00
20.00	17.93	28.00	.00	.00	.00	.00
40.00	15.78	24.52	33.84	.00	.00	.00
60.00	.00	21.11	29.08	35.28	.00	.00
80.00	.00	.00	24.04	29.30	34.00	.00
100.00	.00	.00	19.71	24.14	27.96	.00
120.00	.00	.00	.00	19.23	21.93	25.59
140.00	.00	.00	.00	.00	16.67	19.36
160.00	.00	.00	.00	.00	11.95	13.87

Table B-67. Maximum-power voltage, blue-red filter on 10 ohm-cm single wide-grid cell

AVERAGE MAXIMUM POWER VOLTAGE (VMP,HV)

SOLAR INTENSITY (MW/CM ²)	140.00	250.00	400.00	550.00	700.00	850.00
CELL TEMP. (DEG. C)						
-40.00	542.00	.00	.00	.00	.00	.00
-20.00	498.00	.00	.00	.00	.00	.00
0.00	454.50	426.13	.00	.00	.00	.00
20.00	409.00	395.50	.00	.00	.00	.00
40.00	364.88	357.63	359.13	.00	.00	.00
60.00	.00	323.00	317.13	333.63	.00	.00
80.00	.00	.00	282.25	290.88	293.13	.00
100.00	.00	.00	250.25	252.88	258.63	.00
120.00	.00	.00	.00	215.13	215.75	225.25
140.00	.00	.00	.00	.00	176.62	183.25
160.00	.00	.00	.00	.00	143.50	146.62

Table B-68. Maximum-power current, blue-red filter on 10 ohm-cm single wide-grid cell

AVERAGE MAXIMUM POWER CURRENT (IMP, MA)

SOLAR INTENSITY (MW/CM ²)	140.00	250.00	400.00	550.00	700.00	850.00
CELL TEMP. (DEG. C)						
-40.00	43.22	.00	.00	.00	.00	.00
-20.00	43.85	.00	.00	.00	.00	.00
.00	44.02	73.60	.00	.00	.00	.00
20.00	43.85	70.80	.00	.00	.00	.00
40.00	43.25	68.57	94.22	.00	.00	.00
60.00	.00	65.37	91.70	105.75	.00	.00
80.00	.00	.00	85.20	100.75	116.00	.00
100.00	.00	.00	78.75	95.50	108.12	.00
120.00	.00	.00	.00	89.37	101.62	113.62
140.00	.00	.00	.00	.00	94.37	105.62
160.00	.00	.00	.00	.00	83.25	94.62

Table B-69. Open-circuit voltage, blue-red filter on 10 ohm-cm single wide-grid cell

AVERAGE OPEN CIRCUIT VOLTAGE (VOC, MV)

SOLAR INTENSITY (MW/CM ²)	140.00	250.00	400.00	550.00	700.00	850.00
CELL TEMP. (DEG. C)						
-40.00	681.27	.00	.00	.00	.00	.00
-20.00	633.97	.00	.00	.00	.00	.00
.00	587.17	598.90	.00	.00	.00	.00
20.00	537.10	550.32	.00	.00	.00	.00
40.00	488.17	501.45	511.42	.00	.00	.00
60.00	.00	450.93	463.07	470.62	.00	.00
80.00	.00	.00	411.75	421.27	426.45	.00
100.00	.00	.00	361.52	371.37	377.85	.00
120.00	.00	.00	.00	320.65	325.55	333.20
140.00	.00	.00	.00	.00	274.45	242.05
160.00	.00	.00	.00	.00	224.00	231.07

Table B-70. Short-circuit current, blue-red filter on 10 ohm-cm single wide-grid cell

AVERAGE SHORT CIRCUIT CURRENT (ISC, mA)

SOLAR INTENSITY (MW/CM ²)	140.00	250.00	400.00	550.00	700.00	850.00
CELL TEMP. (DEG. C)						
-40.00	46.95	.00	.00	.00	.00	.00
-20.00	47.85	.00	.00	.00	.00	.00
.00	48.70	88.15	.00	.00	.00	.00
20.00	49.55	89.87	.00	.00	.00	.00
40.00	50.05	90.82	146.55	.00	.00	.00
60.00	.00	91.35	143.78	180.57	.00	.00
80.00	.00	.00	137.55	171.07	196.40	.00
100.00	.00	.00	130.25	160.98	184.33	.00
120.00	.00	.00	.00	149.55	170.35	194.10
140.00	.00	.00	.00	.00	155.75	177.65
160.00	.00	.00	.00	.00	140.20	159.52